TOWARDS SUPRAMOLECULAR MULTIFUNCTIONAL ARCHITECTURES

A Dissertation
Presented to
The Academic Faculty

By

Warren William Gerhardt

In Partial Fulfillment
Of the Requirements for the Degree
Doctor of Philosophy in Chemistry

Georgia Institute of Technology

May, 2007

SUPRAMOLECULAR MULTIFUNCTIONAL ASSEMBLIES

Dr. Marcus Weck
Chemistry and Biochemistry
Georgia Institute of Technology

Dr. Julia M. Kubanek
Biology
Georgia Institute of Technology

Dr. Uwe H. F. Bunz
Chemistry and Biochemistry
Georgia Institute of Technology

Dr. David M. Collard
Chemistry and Biochemistry
Georgia Institute of Technology

Dr. Nicholas V. Hud
Chemistry and Biochemistry
Georgia Institute of Technology

Date Approved: 2/20/2007

I am turned into a sort of machine for observing facts and grinding out conclusions.

Charles Darwin

ACKNOWLEDGEMENTS

I would first like to thank my boss, Marcus you are the idea man, at least in the beginning, and I was just a pair of hands. You did a wonderful job trying to keep me positive, motivated and sane during numerous synthetic roadblocks. Thank you for sharing your experience, wisdom and departmental gossip during our many years together.

I would like to thank colleagues and friends in a particular order.

Elders and Peers:

Dr. Joel Pollino and Dr. Joe Carlise, you guys were wonderful friends and made what is supposed to be a dismal and grueling experience a little brighter, I loved all the nonchemistry activities we did in lab in the late hours to stave off boredom and/or suicide. Despite what people think you guys are also quite intelligent and helped me out a lot over the years.

Dr. Amy Meyers and Matija Ćrne, thank you both for good conversations and help in lab. Mary Nell Higley, you were awesome, my advice to others is to establish a relationship like we had it makes coming into lab a much more pleasant experience.

Soon to be Dr. Will Sommer, I don't know how you managed your crazy schedule and still volunteered with me virtually every weekend. I hope your thesis and defense go well

and all our hard work at AWARE will help contribute to Georgia wildlife for years to come.

Postdocs Dr. Michael Holbach, Dr. Ludger Paul Stubbs and Dr. Rob Kriegel, the three wisemen. You guys put up with so much of my crap. Thank you for answering all of my many questions with well thought out, intelligent responses and dealing so well with my physical abuse and taunting.

Dr. Kurt Knoblock, you deserve mention, although in another group our conversations and research discussions were helpful and important to my success.

New Students:

Clint South, you are one of the most thorough scientists I have ever worked with, and also an extremely obnoxious redneck, I still love you though (in an ambiguous way).

Kim Arrowood, you are the best and brightest of the new class, quite fit to carry on my research, and just like my research your reactions give you hell at every step. Keep persevering and lean on the postdocs, that's what Marcus pays them for.

Finally, I would like to thank those in my family who made my long and grueling journey a little smoother. So thanks and love go to my mother, my father, my stepmom Rae, my uncle Pete and aunt Betsy, my squeaky voiced little sister, and my grandfather Pete, they were supportive and inquisitive about what I did down here for the better part of my 20's. And for those who didn't make this whole trip with me, but always told me

how proud they were: my granddad Bill, he fortunately had the chance to give me a final thought by which to live by, and my Claira (AKA: Mimi)- I tried to be by your side and this stupid labwork kept me away- that was a sad reminder of the real priorities in life.

Finally, I will never forget Honey, the greatest dog of all time, she patiently waited for me when I came home late from lab every night, she was my best friend who cheered me up everyday and was in my arms to the very end.

As a final parting thought, I don't plan on getting any more Ph.D.s, it was truly hard work and only the second time in my life I have truly felt challenged.

TABLE OF CONTENTS

LIST OF TABLES

LIST OF FIGURES

LIST OF SCHEMES

ABBREVIATIONS

Bpy	bipyridine
CP	coordination polymer
DAP	diaminopyridine
DCC	dicyclohexyl carbodiimide
DCU	dicyclohexyl urea
DNA	deoxyribonucleic acid
EI	electron impact
ES	electrospray
H-bond	hydrogen bonding
HATU	2-(1H-7-azabenzotriazol-1-yl)--1,1,3,3-tetramethyl uronium hexafluorophosphate
HBTU	2-(1H-benzotriazol-1-yl)-1,1,3,3-tetramethyluronium hexafluorophosphate
HCTU	2-(6-Chloro-1H-benzotriazole-1-yl)-1,1,3,3-tetramethyluronium hexafluorophosphate
HOBt	1-hydroxybenzotriazole
HOAt	1-hydroxy-7-azabenzotriazole
ITC	isothermal titration calorimetry
K_a	association constant
K_{diss}	dissociation constant
Mebip	2,6-bis(1'-methylbenzimidazolyl)-pyridine
MLCT	metal to ligand charge transfer
MS	mass spectrometry

MSOA	multistage open association
OPV	oligo(*p*-phenylene vinylene)
PEO	poly(ethylene oxide)
PPE	poly(*p*-phenylene ethynylene)
PPV	poly(*p*-phenylene vinylene)
PVP	poly(vinylpyridine)
PyBOP	benzotriazole-1-yl-oxy-tris-pyrrolidino-phosphonium hexafluorophosphate
PyAOP	7-benzotriazole-1-yl-oxy-tris-pyrrolidino-phosphonium hexafluorophosphate
RNA	ribonucleic acid
SAM	self-assembled monolayer
SEC	size exclusion chromatography
SP	supramolecular polymer
TMV	tobaccoMosaic
Tpy	terpyridine
UPy	2-ureido-4-pyrimidone
WLA	weak link approach

SUMMARY

This thesis begins with the introduction of supramolecular chemistry and an explanation of why this synthetic strategy is aptly suited for the creation of increasingly larger and more complex structures, beyond the limits of traditional covalent synthesis. An extensive definition of self-assembly and the building blocks used by biological systems to create its functional supramolecular architectures is given. A review of novel synthetic finite and infinite supramolecular architectures is provided; despite these accomplishments there are few reports of biologically relevant synthetic architectures, as well as functional architectures. This thesis hypothesizes that new currently unattainable architectures can be achieved by using established metal-ligand interactions tethered to unique functional synthons.

The first supramolecular synthon is a functionalized cyclic peptide. Cyclic peptides can vertically self-assemble via H-bonds into well-defined organic nanotubes with useful inclusion and transport properties, which can be readily tuned to suit a potential application via a range of synthetic modifications. By adding a pyridyl ligand to the periphery the cycle is imbued with a horizontal metal-coordination self-assembly mode that may facilitate supramolecular membrane formation.

Our second supramolecular synthon has an "X-shaped" cruciform molecule terminated with two pyridyl ligand. Cruciform molecules have outstanding optical properties with potential electro-optical applications. A polymeric cruciform system may be well suited for device fabrications owing to the ease of solution processing. Therefore

we investigated a supramolecular polymeric strategy, to rapidly create a set of functional and solution processable coordination polymers.

The metal recognition unit chosen was a bimetallic "pincer" complex. This rigid, linear ditopic complex has a fast and quantitative coordination to pyridyl units, which were exploited to rapidly grow our supramolecular architectures.

Synthesis of our cyclic peptide ligand is completed and preliminary coordination studies confirm quantitative formation of primitive membrane architectures. The next phases of this research along with long-term future directions are outlined. Finally, several synthetic solutions are given to overcome the current limitations of our first generation of cruciform coordination polymers.

CHAPTER 1

Supramolecular Chemistry: Self-Assembled Architectures

1.1 Abstract

In this chapter the concept of supramolecular chemistry is introduced and its use for the creation of complex molecular architectures is explained. Supramolecular chemistry is a young field which focuses on the interactions of reversible and weak forces as opposed to traditional covalent forces. Self-assembly is an area of supramolecular chemistry that incorporates these weak interactions into small building blocks, which can then spontaneously create larger and complex structures with functions beyond the sum of the individual components. These large suprastructures may be placed into different architectural categories, finite architectures and infinite polymeric architectures. A review of these two supramolecular classes is given, and the goals of this thesis research in advancing these two areas of supramolecular self-assembly are stated.

1.2 Why Supramolecular Chemistry?

A complex synthetic target may be a cancer therapeutic,[1-4] or an attractive natural product.[5] For over a hundred years the challenge of synthesizing an organic molecular structure has relied on the making and breaking of covalent bonds. Scientist have successfully been manipulating and bringing together atoms and smaller molecular components into increasing larger and more complex structures using covalent synthesis.

Covalency is the sharing of electrons between nuclei through atomic orbital overlap. The molecular product held together by a covalent bond, which is the newly formed

molecular orbital defined by the shared electrons localized within it. The covalent bond formed is a strong, essentially irreversible linkage between atoms that has been synthetically exploited, forming one bond at a time, methodically building larger and larger covalent structures from smaller molecular starting materials. This has been the only available method to produce a molecule of a desired shape and function, with common molecular targets having less than 100 covalent bonds and molecular weights of several hundred Daltons.[6] Some of the largest structures synthesized at the upper limits of covalent synthesis, palytoxins, have molecular weights of several thousand Daltons and lengths of around one nm.[7, 8] However, these massive synthetic feats are on the small end when compared to biologically synthesized and microfabricated structures such as those found in Figure 1.1.

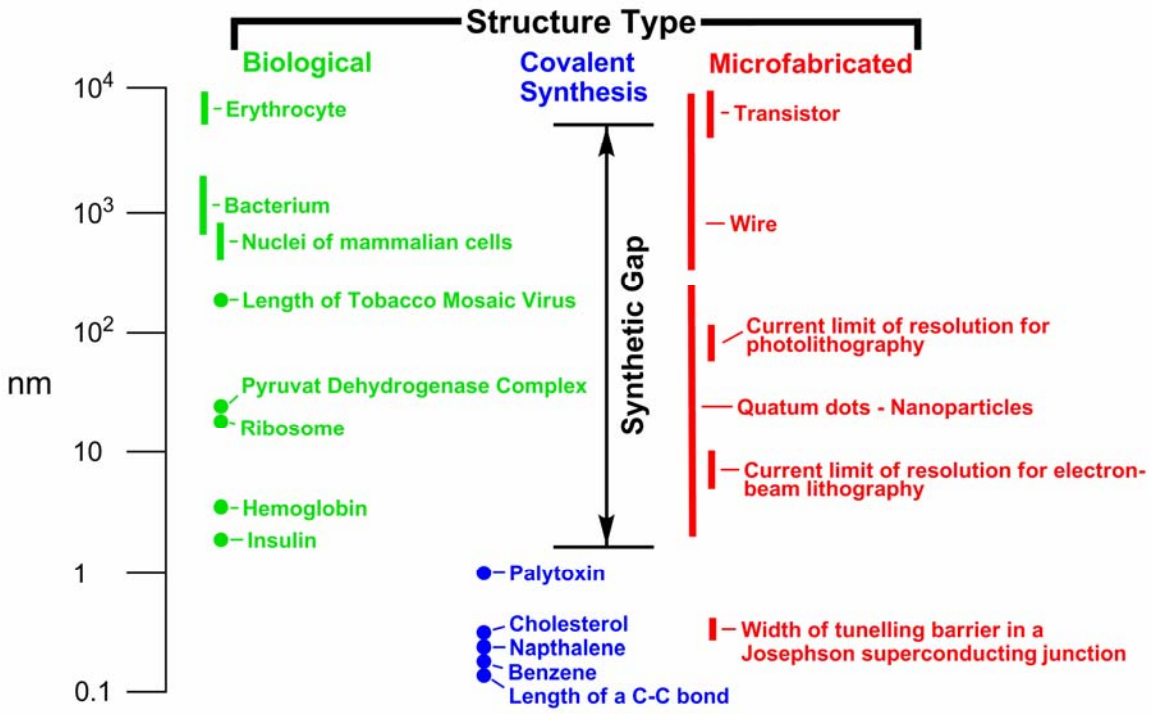

Figure 1.1 Relative size of structures generated in biology, covalent synthetic chemistry and microfabrication along a logarithmic scale. Only biology and microfabrication provide large nanoscopic structures.[8]

A current challenge for synthetic chemistry is to synthesize well-defined architectures and materials between 1-100 nm, known as nanostructures.[9] Synthetic nanostructures are expected to have potential applications in a range of technologies from medicine to electronics, and the synthetic challenges may require a paradigm shift away from covalent methodologies towards a more efficient strategy.[9-11]

This synthetic challenge has spawned an entire new field of research known as nanotechnology.[11] The synthesis of nanosize architectures can have either a "bottom-up" synthetic approach or "top-down" microfabrication approach,[11-15] Both of the current manufacturing approaches are reaching their respective upper and lower limits, where resources, time and cost are becoming prohibitive. In order to synthesize well-defined nanostructures a more efficient synthetic methodology is required.

Over the last several decades, a new synthetic methodology has been brought to the forefront. It uses the same assembly strategies that living organisms employ to facilitate the creation of anything from a virus to a multicellular organism.[16] It is hoped that this methodology will permit the synthesis of structures between 1 to 10^3 nm,[8] by relying on the interactions of reversible weak labile forces as opposed to static and strong covalent bonds. These weak labile interactions, chosen to be tolerant to one another and organized within synthetically practical small covalent building blocks may then undergo a spontaneous productive assembly to form a structurally larger and functionally more complex system.[16, 17] The building blocks are preprogrammed to assemble.[18] Guided by their attractive forces, the covalently inaccessible architecture builds itself.

Supramolecular chemistry, chemistry beyond the molecule,[16] is the domain of these weaker labile interactions. Lehn described supramolecular chemistry as the chemistry of intermolecular bonds giving molecular assemblies,[16, 19] the common weak interactions used to form these intermolecular bonds are hydrogen bonding, metal-coordination, electrostatic attractions, hydrophobic forces, van der Waals, cation-π and π-π interactions.[19]

Life has already figured out that a supramolecular strategy relying on these attractive forces is the most efficient way to build and maintain every organism. Following suit there has been a major research thrust to elucidate, understand and control supramolecular synthesis.[11, 14] Towards this goal, this thesis will discuss the use of labile metal-coordination interactions for the synthesis of new architectures with the ultimate goal of synthesizing innovative and functional supramolecular materials. Chapter One will introduce new concepts and highlight supramolecular milestones. Chapter Two will introduce and review a class of transition metal complexes, the metallated pincer complexes, which will be used to assemble new supramolecular materials. Chapters Three will detail the preliminary design, synthesis and investigation of the metal-ligand interactions between linear peptide ligands for the metallated pincer complex. These linear ligand studies will serve as model studies for cyclic peptide ligands. Chapter Four will detail the synthesis of a new unnatural cyclic peptide acting as a functional ligand coordinated to metallated pincer complexes. The ultimate goal of this research will be to supramolecularly synthesize well-defined nanoporous membranes. Chapter Five will introduce the synthesis of well-defined organometallic coordination polymers formed from ditopic fluorescent cruciform molecules coordinated through metallated pincer

complexes. This research will set the stage for the synthesis of multilayered hierarchical devices. Finally, Chapters Six and Seven will recapitulate the salient accomplishments of this thesis research and propose future directions.

1.3 Supramolecular Self-Assembly

Molecular recognition is binding with a purpose, it implies a structurally well-defined pattern of intermolecular interactions.[20] A molecule binding another molecule through these interactions produces a 'host-guest' complex or *supramolecule*.[20-22]

An autonomous assembly of supramolecular components into patterns, and systems without external intervention giving a suprastructure is the concept of self-assembly, as defined by Whitesides.[11] However a very broad interpretation of the term self-assembly has led Whitesides to proclaim after his initial definition "*…the definition of self-assembly is limitlessly elastic, as a result the term has been overused to the point of cliché.*"[11]

Perhaps one of the most cited definitions is given by Lehn, who shared the 1987 Nobel Prize for research into the supramolecular interactions of host-guest complexes.[23, 24] He states that "*…the spontaneous association of either a few or many components, resulting in the generation for either discrete oligomolecular supermolecules or of extended polymolecular assemblies.*"[16] He later calls self-assembly "*…a simple collection and aggregation of components in a confined entity.*"[18] By most definitions a minimal amount of necessary features can be gleaned to have a self-assembled system on a molecular scale.

1) The reliance on weak non-covalent complementary interactions

2) Organization of these interactions within a mobile component

3) Thermodynamically stable structures formed under equilibrium conditions

For this thesis self-assembly shall be defined *as a molecular recognition event of pre-programmed building blocks via weak labile interactions under equilibrium conditions, which leads to the formation of thermodynamically stable higher ordered suprastructures and architectures*. These pre-programmed building blocks have two parts: 1) a recognition component, which is electronically and structurally complementary to a recognition element on another building block, 2) a functional component endowed with unique features or properties tethered to the building block.

For this research the recognition components will be the coordination between a ligand and a transition metal complex. The functional tethers will be either a cyclic peptide for the formation of supramolecular porous membranes or a ditopic fluorescent cruciform molecule for the assembly of organometallic coordination polymers.

1.3.1 Weak Labile Interactions

Before introducing some of the myriad self-assembled suprastructures that have been created, a greater introduction into the concept of weak labile interactions is required. The strength or bond dissociation energy of C-C and C-H covalent bonds, the primary skeletal components of any covalent molecule average 83 and 99 Kcal/mol, respectively.[25] Overall typical covalent bonds range in strength from about 50-100 Kcal/mol.[26] Weak labile interactions are usually much weaker than this, as shown in Figure 1.2.

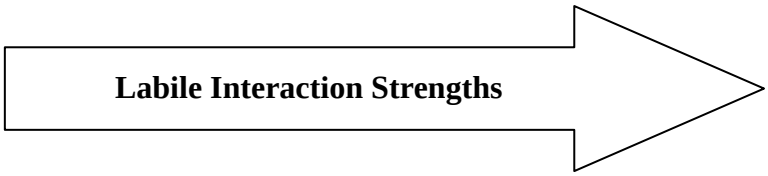

Weak (0-15 Kcal/mol)	Medium (15-60 Kcal/mol)	Strong (>60 Kcal/mol)
H-Bonding	concerted H-bonds	Ionic
π-π	Metal-coordination	Metal-coordination
Dipole-dipole	Ion-dipole	
Van der Waals		

Figure 1.2 Weak labile interactions categorized by strength of bond dissociation energies.

Ionic interactions are non-directional but are generally considered the strongest of these forces. Ionic interactions are electrostatic interactions along with the weaker ion-dipole and weakest dipole-dipole interactions all being Coulombic attractions of opposite charges, shown in Figure 1.3. A caveat for forces that are electrostatic in nature is that there association strengths are very susceptible to outside influences such as solvent and temperature effects, and the listed strengths are under optimum conditions.

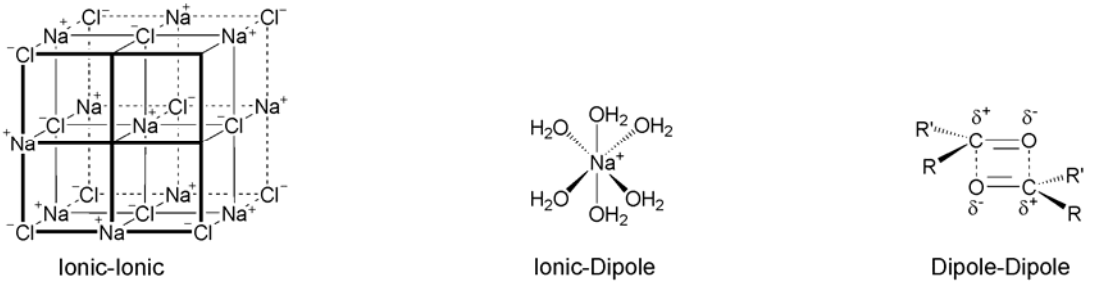

Figure 1.3 Ionic-ionic, ionic-dipole and dipole-dipole interactions are progressively weaker Coulombic forces.

A hydrogen bond (H-bond) is a special type of directional dipole-dipole interaction formed between a relatively acidic H atom and an electronegative atom(s) (most often O or N). They have been called the 'masterkey interaction in supramolecular chemistry' because they can be synthetically arranged with excellent precision, with arrays binding in a concerted manner leading to a dramatic increase of their cumulative binding strength, much like the multiple teeth of a zipper give a strong seam, as shown in Figure 1.4.[27]

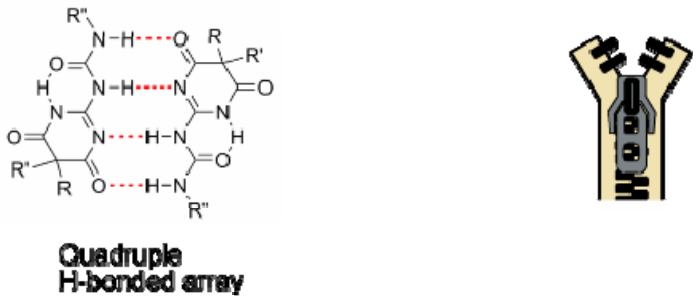

Figure 1.4 Hydrogen bonded array having a high cumulative strength, a principle similar to a zipper.

The most synthetically accessible of the remaining weakest forces are π-π interactions. These attractive forces between aromatic systems, believed to be electrostatic in nature,[27] are readily incorporated into aromatic supramolecular building blocks. Other weaker noncovalent interactions are not as well-defined and range in strength from < 1 Kcal/mol for van der Waals forces due to temporary electron cloud polarizations and cation-π (1-20 Kcal/mol) π-electron systems with positive or partial positive charges.[19, 27]

Metal-ligand coordination interactions, which will dominate later chapters of this thesis also play an important role in biological and synthetic supramolecular assemblies.[28] Owing to the wide range electronic structures throughout the metal ions these interactions

can ambiguously be ionic to somewhat covalent depending on the extent of orbital overlap.[27] Only transition metal-ligand interactions will be considered for this thesis research. They are geometrically specific, thermodynamically stable interactions which have varying degrees of kinetic lability. These geometric and stable interactions have permitted the creation of geometrically precise architectures.[29, 30] Shown in Figure 1.5 is a ruthenium-trisbipyridine (bpy) complex having an octahedral coordination sphere.[31] The metal-ligand spheres may also have interesting electro-optical properties which may be transferred or enhanced to the supramolecular structure making these interactions multifunctional.[32, 33]

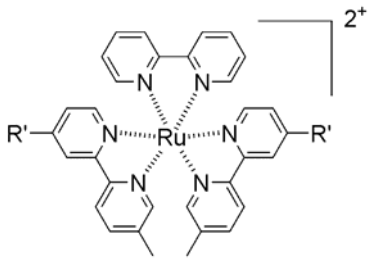

Ru-tris(bipyridine)

Figure 1.5 Metal-coordination, represented by an octahedral geometry of ruthenium tris(bipyridine).[34]

All of these interactions are dependent to different degrees on their surroundings, prevalent factors being temperature, concentration and solvent effects. This is best illustrated by H-bond arrays, which can form large robust assemblies in apolar solvents where their electrostatic interactions are not well solvated. H-bonded assemblies are much weaker in water and other protic polar solvents, which compete for the H-bonds and are present in much larger concentrations.[35]

Many factors must be taken into consideration before choosing the appropriate interaction(s) holding together a supramolecular assembly, *e.g.* solution and/or solid-state stabilities, cost, synthetic time and final properties such as mechanical strength or toxicity. Are the interactions passive or active, *i.e.* do they simply act as silent cohesive agents for tethered functionalities[36] or do they play a role in its final properties?[34] This is specifically relevant for transition metal complexes, which have important catalytic, electrical and/or optical properties.[37-39]

1.3.2 Self-assembled Functionalization

Lehn describes basic supramolecular functions as "*…molecular recognition, translocation, and transformation…*"[20]

For this thesis, function in self-assembly can be viewed as i) the basic transformation of a molecule via self-assembly, ii) the formation of a complex supramolecular architecture using self-assembly, or iii) the formation of a fully functional material for a specific application by self-assembly. The first rudimentary classification of function is when the self-assembly step itself imparts function. An example of this functionalization is the formation of acid dimers *via* self-assembly.[19] The second definition is based on the spontaneous generation of a larger and often more complex structure, *i.e.* a supramolecule with well-defined pockets or pores for molecular recognition, arranging molecules for catalysis or detection of analytes. The third class of self-assembled functionalization can be viewed as the endowment of a specific function or the creation of a material with a well-defined function, *i.e*. a device, using self-assembly.[40]

A device may result from the interplay of several binding subunits in polymolecular assemblies acting across interfaces. A stimuli responsive system having multiple components with feedback may be cross-catalytic or autocatalytic taking on tasks such as cooperativity, allostery, regulation and communication or signal transfer,[20] so far these features are only truly found in biological systems.[39, 41] These three classifications of function by self-assembly are not exclusive and can often go hand in hand giving multifunctional suprastructures.

Supramolecular chemists are farther behind and the current challenge is to develop greater functions and applications.[37] Most examples in the literature on the formation of functional materials *via* self-assembly rely on a single recognition unit motif. Examples include the formation of supramolecular polymers with visco-elastic control, block co-polymers, liquid crystalline systems, hybrid materials, and micellar structures.[17, 18, 42-48]

Using multiple recognition units is a direct route to greater complexity in functional systems.[36, 49, 50] A caveat for this strategy is that the multiple recognition motifs must be orthogonal; they must bind to their partner with a high fidelity in the presence of other different recognition motifs occurring simultaneously.[36, 51] Supramolecular systems from Stoddart use external stimuli to switch the preference of multiple interactions from repulsive to attractive within mechanically interlocked molecules creating molecular motion powering molecular shuttles, elevators and switches supporting the idea of molecular circuitry, computation and machines.[52-58]

1.3.3 Supramolecular Architectures

The building blocks, which contain all the necessary information to form vast infinite assemblies have been called supramolecular synthons[59] or tectons,[60] assembling via a molecular program.[61]

A supramolecular architecture is the final physical product of this programmed self-assembly. Whether an infinite polymer chain or membrane, a finite 2-D shape or 3-D structure,[14] or a molecular machine[57] they all began as a disordered stew of building blocks. Because of the reversible nature of weak labile interactions, a desired architecture may be in dynamic equilibrium with several other rapidly exchanging structures,[35, 62] also known as supramolecular isomerism.[16, 63] Nature overcomes this dynamic equilibrium by using very high molecular weight self-assembled aggregates; the sheer number of weak interactions assures that the structural integrity of the architecture is preserved. In synthetic systems keeping the equilibrium to the right maintains the architectures in solution. The choice, arrangement and number of weak interactions along with the solvent system will all help to stabilize the final architecture.[64]

Observing the structure-activity relationship,[28] the function of a supramolecular system is dictated by its architecture. To perform tasks, spatial placement of functional units in the architecture must be precise. Correct spatial placement of units is governed by thermodynamic stability, which statistically creates some imperfections. Post-self-assembly damage of either a mechanical, thermal, or radiative nature is certain to occur to a final functional architecture. Living systems have overcome these obstacles efficiently templating diverse architectures and large networks in a cooperative fashion; the function arising from a precise spatial structure maintained by an elaborate and energy intensive

repair-recycling-error checking system.[12] These elaborate biomechanical techniques are currently unfeasible for synthetic systems.

To achieve greater levels of function from supramolecular architectures, control over factors beyond just the assembly pattern will be required, layers of information laden sequences much like that found in nucleic acids and proteins may be necessary. This is a hierarchical approach to achieve complexity. Hierarchical self-assembly is the formation of organized structures through different and distinct levels of self-assembly processes that decrease in assembly strength, giving a supramolecular architecture having important macroscopic properties that are not the mere sum of its individual parts.[65]

Paying close attention to life's blueprints and masterful designs and following these loose guidelines supramolecular scientist are ardently working to increase the functional performance and complexity of supramolecular architectures.

1.4 Supramolecular Architectures in Living Systems

Supramolecular self-assembly is best appreciated by observing it in living systems, where it operates at its highest level of performance, and following the survival of the fittest principle all biological systems are functionally optimized. Biological self-assembly has evolved over three and a half billion years into many complex systems derived from an inherent simplicity.[30] This streamlined elegance is accomplished through a hierarchical assembly which ultimately creates enormous, complex structures from a very small class of mundane building blocks. A precise positioning of functionalities and dynamic structural rearrangements allows the final assemblies to perform as storage devices of genetic and molecular information, molecular machines

and selective catalysts.[37] The shining examples of biological self-assembled architectures are the two prevalent multifunctional biopolymers: nucleic acids and proteins.

1.4.1 Nucleic Acids

Nucleic acids come in two primary forms i) deoxyribonucleic acid (DNA) and ii) ribonucleic acid (RNA) both are biopolymers made up of four nucleotide monomers. Post polymerization DNA biopolymers self-assemble with complementary strands into supramolecular double helix architectures, [66, 67] as shown in Figure 1.6 A.

DNAs double helix architecture functions as an efficient and robust storage device for all of an organism's genetic information;[67] this genetic information is transcribed into RNA.

RNA prefers to exist predominantly as a single stranded species, however extensive blocks of complementary base pairs along the single strand can readily assemble folding over and forming secondary structures beyond the primary base pair sequence such as stems and loops giving hairpin architectures, as shown in Figure 1.6 B.

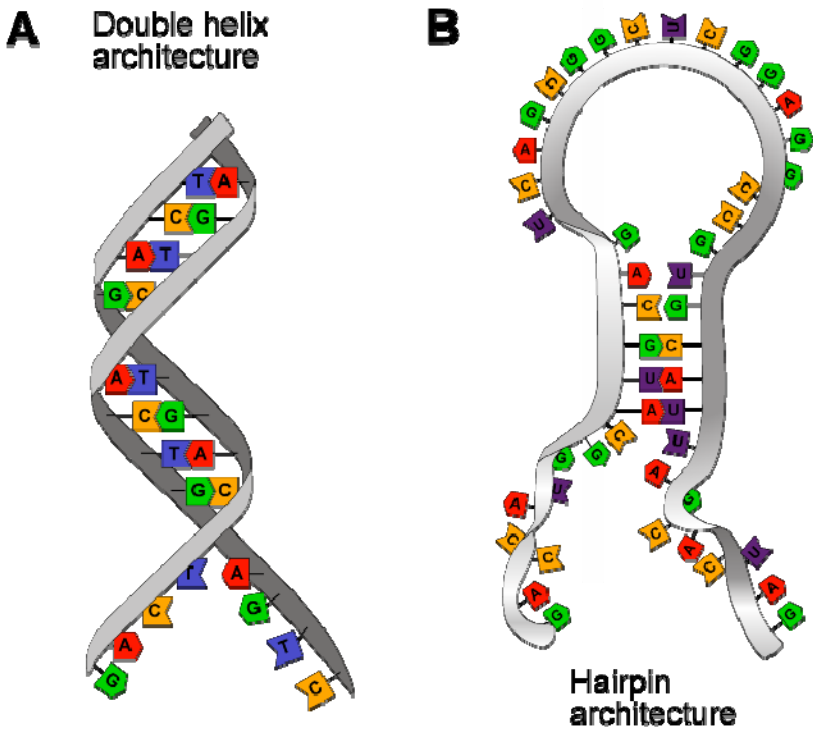

Figure 1.6 A) Double helix supramolecular architecture; B) supramolecular RNA hairpin architecture. Both formed through H-bonding of complimentary nucleotide base pairs.

RNAs surpramolecular architecture is multifunctional, it acts as a protective barrier between the sensitive genetic information and the harsh cellular environment, imparts hierarchical structural features reminiscent of enzymes,[68, 69] and translates the original DNA genetic information into proteins.[28]

1.4.2 Proteins and Peptides

The second class of biopolymers, proteins, is commonly polymerized from 20 chiral amino acid building blocks into a linear polyamide, peptide chain, called the primary structure, as shown in Figure 1.7.

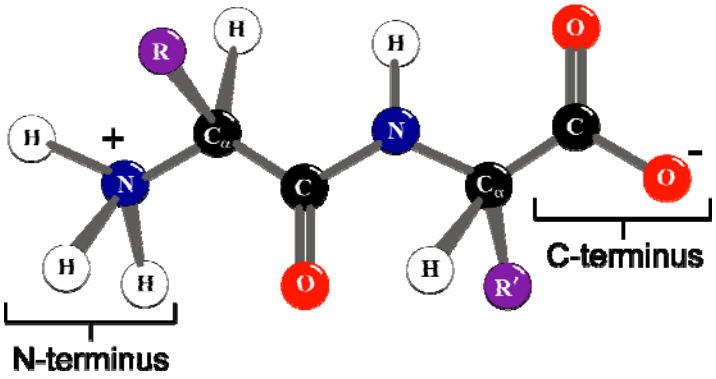

Figure 1.7 Zwitterionic dipeptide chain, with protonated N-terminus and deprotonated C-terminus; C_α are the amino acid stereogenic centers in an L-configuration; R is an amino acid side-chain and R′ is a different amino acid side-chain.

Using all the weak interactions permitted by the functional groups in the amino acid side-chains and the peptide backbone (amide nitrogens and oxygens), a peptide chain folds intra- and intermolecularly into a thermodynamically stable supramolecular architecture.[70] These suprastructures have a 3-D shape, which dictates their function while at the same time minimizing exposure of reactive components to the cellular environment.

There are approximately 25,000 proteins in the human body, with a multitude of different functional architectures.[71] They are the quintessential multifunctional machines involved in every aspect of our physiology and development.[28]

The hierarchical self-assembly of a protein begins with the folding of its primary structure into the secondary structures, the common motifs being α-helices and β-sheets, shown in Figures 1.8 and 1.9, respectively. These two conformationally stable structures are formed through H-bonding interactions of the backbone amide protons to the amide carboxyl oxygens.

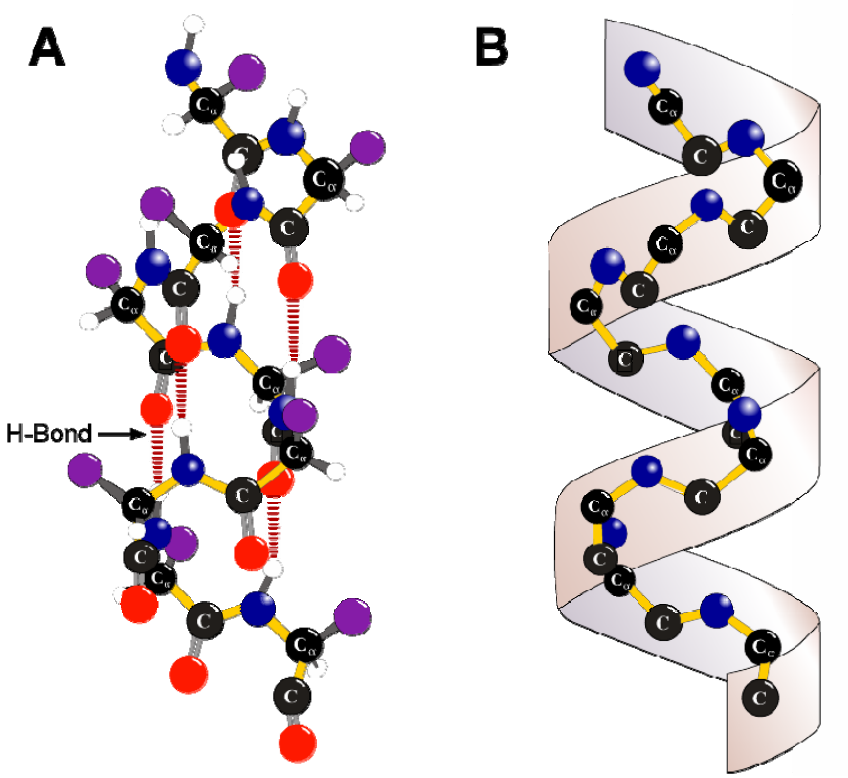

Figure 1.8 A) Peptide chain forming an α-helix through intramolecular H-bonds of amide protons with carbonyl amide oxygens; B) helical ribbon structure of peptide backbone, substituent atoms and side-chains removed for clarity.

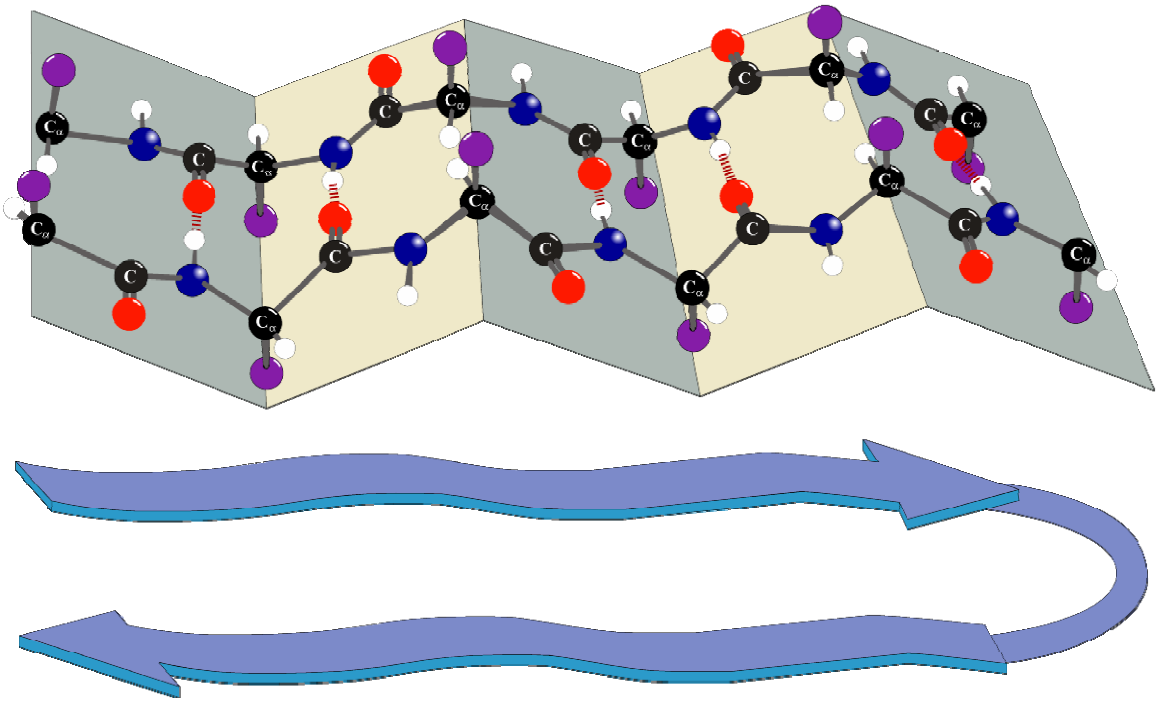

Figure 1.9 Two peptide chains H-bond to form an antiparallel β-sheet; ● are amino acid side-chains which alternately extend to opposite sides of the sheet are in register on adjacent chains. Ribbon arrows show direction of the antiparallel strands and connection between them.

Individual amino acid and particular sequences have a propensity for one secondary structure over the other,[72, 73] depending on how accepting the side-chains are of the restricted conformations and through further stabilization of the secondary structure via additional noncovalent interactions such as π–π or dipole interactions.[74, 75]

The next level of self-assembly gives the functional and 3-D tertiary structure. The hierarchy finally extends to a quaternary structures, which is a larger supramolecular structure composed of tertiary subunits.[28]

Enzymes, catalytic proteins, are wonderful examples of the structure-activity relationship. All of the weak interactions between amino acid residues act as structural

buttresses and reactive centers in the overall functional architecture. Hydrophilic residues are usually found on exposed surfaces, hydrophobic residues are in the interior creating areas of high organic content capable of solubilizing and binding reactive substrates with a high affinity. A small number of residues form the "active site", which binds and position the substrate(s) putting reactive species in close proximity. This increase of effective molarity along with other contributing catalytic factors leads to a 10^6 to 10^{12} acceleration of reaction rates under mild physiological conditions compared to the same uncatalyzed reactions.[76] If the 3-D supramolecular architecture regulating an enzymes function is disrupted its activity quickly falls off.[28]

Enzymes are currently known to perform about 4,000 biochemical reactions,[77] usually converting substrates to products in assembly line fashion within metabolic cycles.[28] These supramolecular machines may perform simultaneous reactions at multiple sites, undergo conformational changes to signal and alter future reactions and perform different types of catalysis under different conditions.[28, 78] Shown in Figure 1.10 is the crystal structure of α-chymotrypsin, a hydrolytic digestive enzyme.[79]

Figure 1.10 The crystal structure of α-chymotrypsin, a serine protease with a peptide in the cleft of its active site.[79]

Apart from enzymes, proteins have many other key functions, such as roles in structural rigidification of cellular structures and transport of vital molecules through the cellular fortifications they have built up.[28] Each different function generally requiring a new architecture. Life has figured out through evolutionary trial and error that these massive structures are simply too large and complex to assemble through covalent strategies. Over billions of years, the most efficient route found has been to covalently synthesize polymers from preprogrammed building blocks, which self-assemble into the functional structure, thus saving the organism time and energy.

This strategy is now clear to supramolecular chemist, with the next section reviewing some of their synthetic accomplishments over the last 40 years.

1.5 Supramolecular Architectures in Synthetic Systems

A striking example of the ability to self-assemble a hierarchical complex functional architecture from a limited number of simple and limited building blocks is the tobacco mosaic virus (TMV). It can assemble via noncovalent interactions *in vitro* from its single RNA strand (6402 bases) and 2134 protein subunits (each 158 amino acid residues) into an active infectious virus. The proteins form a hollow columnar coat protecting the RNA coiled in the center.[27] While synthetic systems of this magnitude are far off, the goal of mimicking biological devices and developing new functional molecules will still require a high degree of complexity.[37]

Synthetic systems have evolved over the last few decades from single host-guest interactions,[21] to aesthetically appealing and geometrically complex assemblies, currently functional systems with viable applications are the primary goals of supramolecular chemistry.[37, 39, 80]

The following examination of supramolecular architectures will be divided into two classes: 1) self-assembled finite molecular assemblies having a controlled termination step; 2) infinite self-assemblies lacking a controlled termination step giving polymeric architectures.

1.5.1 Finite Molecular Architectures

Early work in synthetic supramolecular chemistry began as 'host-guest' complexations. The host was a molecular entity having convergent binding sites, the guest with complimentary divergent binding sites.[19] The two formed a complex through a unique stereoelectronic structural relationship of weak electrostatic forces, such as the self-assembly between a macrocyclic ligand and a cation, see Figure 1.11.[21]

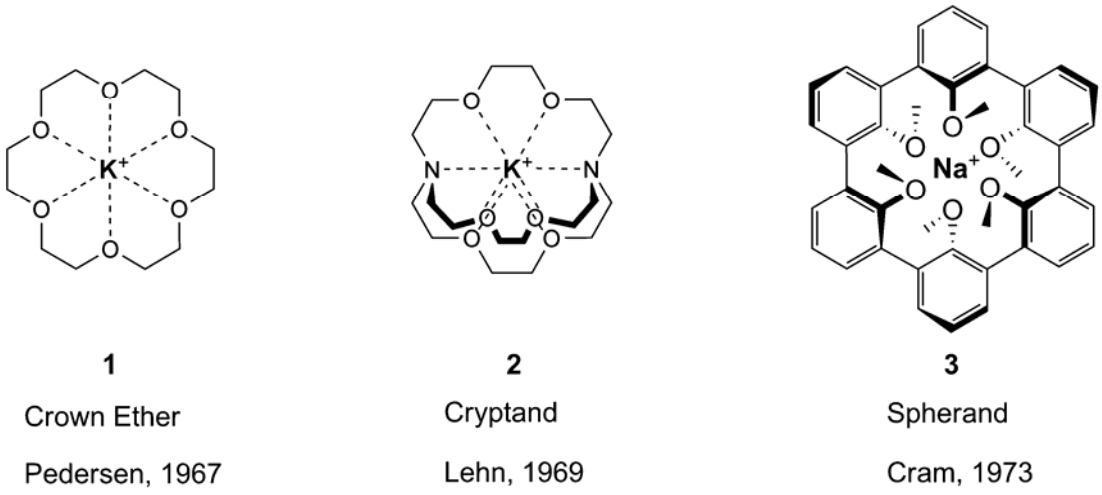

Figure 1.11 Representative 'host-guest' molecular recognition complexes synthesized and self-assembled by the 1987 Nobel Laureates.[23, 24, 81-84]

The complexes in Figure 1.11 and their respective analogs form strong, specific complexes with selected metal and organic cations through an all encompassing sphere of properly positioned weak interactions.[23, 24, 81-84] For the first time this demonstrated not only binding but recognition, via size selection.[85] Spherand **3** was shown to have the strongest binding owing to its pre-complexation shape, which does not have to sacrifice the free energy of reorganization to accommodate the cation guest. These structures besides being the groundswell for supramolecular chemistry, have found uses in

molecular and ion transport, separation and sequestration, medical imaging and anion activation.[20-22, 86] In more elaborate academic pursuits, Cram covalently built an enzyme mimic that bound a substrate and catalyzed the desired reaction with a 10^{11} rate acceleration.[87]

However, host-guest complexes **1**-**3** and their derivatives still relied on synthetically complex covalent host architectures. Beginning in the 1980's, weak labile interactions were used to self-assemble host like structures with well-defined cavities.[88] By using well-designed synthons that prefer macrocyclization over infinite polymer assemblies this strategy has been used for the self-assembly of other highly organized architectures.

Much like the spherand macrocyclic ligand, transition-metal macrocycles can form rigid structures with designed cavity shapes and volumes. One of the earliest supramolecular metal macrocycles **4** was reported by Maverick in 1986.[89] It was the first report of selective complexation of a bifunctional Lewis base (DABCO) to a rigid transition-metal host, see Figure 1.12.

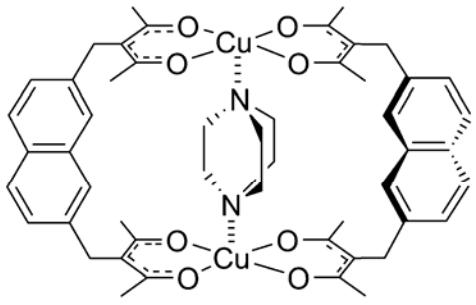

4

Figure 1.12 Maverick's transition-metal 'host-guest' complex.[89]

A little over a decade ago the term 'metallosupramolecular chemistry'[90] was coined by Constable. Since those early endeavors numerous finite architectures have been supramolecular synthesized and reviewed, such as polygons,[29, 91] polyhedrals & cylinders,[30, 91] catenanes,[92] rotaxanes[93] and helicates.[94]

These metalla-suprastructures are synthesized using rigid units having defined angles, Figure 1.13 shows several angular defining precursors.[29, 30, 91, 95]

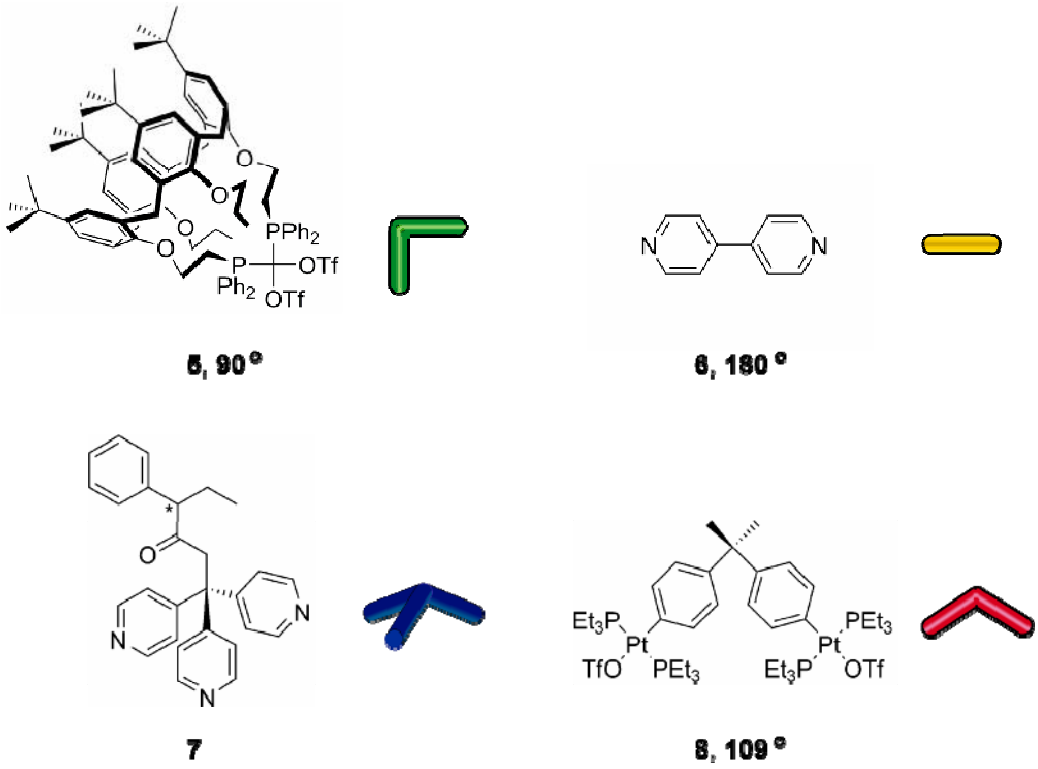

Figure 1.13 Rigid angular ligands for constructing metalla-suprastructures.[29, 30, 91, 95]

These building blocks have been used to construct 2-D and 3-D nanoscopic structures some approaching the size of small proteins.[30] Many different polygons and polyhedrons have been synthesized with tunable internal cavities[96, 97] that may have uses in catalysis,[98] sensing applications or the inclusion of interesting species such as

biomolecules or other functional particles.[30, 99] Shown in Figure 1.14 is molecular square **9** built up from the coordination of **5** and **6**.[96] Optically active adamantoid **10** is self-assembled from chiral ligand **7** and ditopic metal complex **8**.[100, 101] Very recently, Würthner made a metallo-square reminiscent of the light harvesting complex in photosynthetic organisms.[102] His Pd-square used localized tethered pyrene antenna arrays to efficiently transfer energy to the square edge perylene bisimides, making a functional light harvesting device.

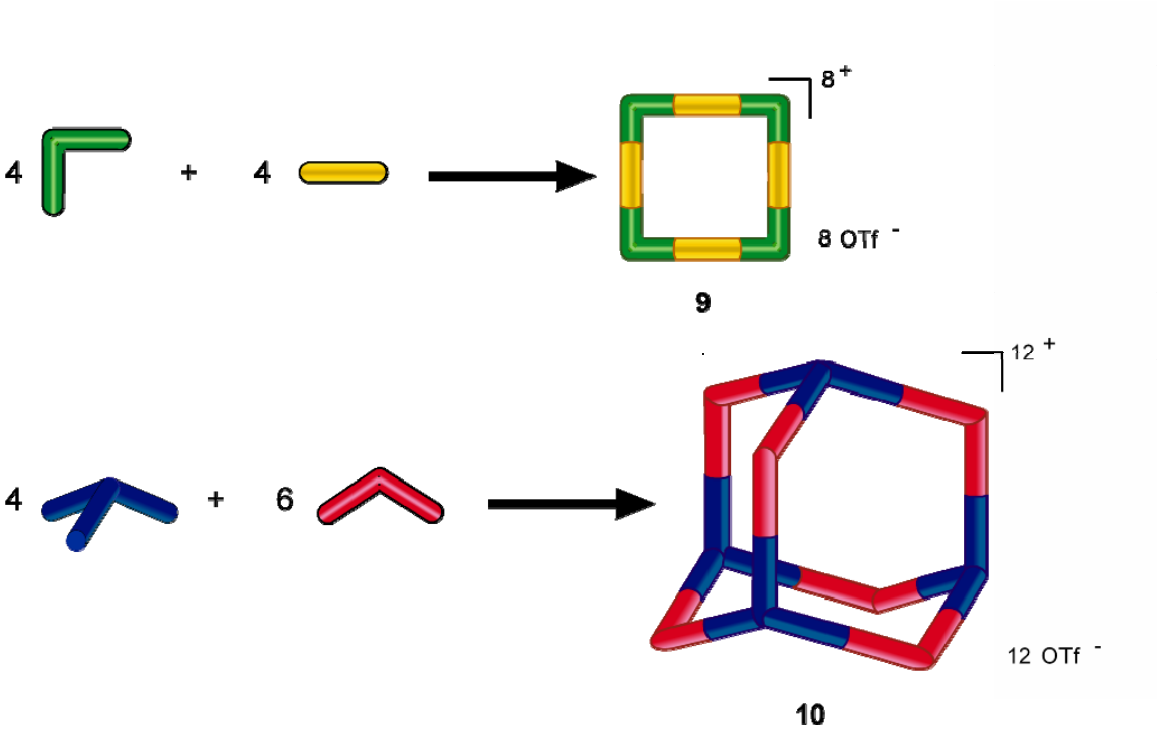

Figure 1.14 A metalla-polygon and -polyhedron made from angular transition-metal centers and ligands.[96, 100, 101]

Dynamic systems will be required to increase the complexity of supramolecules. Some novel efforts towards organometallic supramolecular catalysis have been demonstrated. Fujita used a caged structure for catalytic phase transfer Wacker

oxidations.[103] Mirkin has a clever strategy dubbed the 'weak link approach' (WLA).[39] The distinction of WLA from other transition-metal suprastructures is the use of flexible bidentate ligands that have hemilabile coordinations, *i.e.* one coordinated bond is stronger than the other. This permits additional reactions at the multifunctional metal centers, possibly for catalysis or sensing, while maintaining the supramolecular architecture. The ultimate goal of this research is to synthesize dynamic adaptive architectures, which can mimic the complex and cooperative reactions of biological structures. Mirkin has developed several novel systems using this strategy such as an allosteric catalyst.[98] Mirkin has used the reversible binding of a second ligand to cause a conformational change in the supramolecular architecture of 'molecular tweezers' putting two metal centers in close proximity exploiting its bimetallic catalytic mechanism in the active state of **12**,[104] see Figure 1.15.

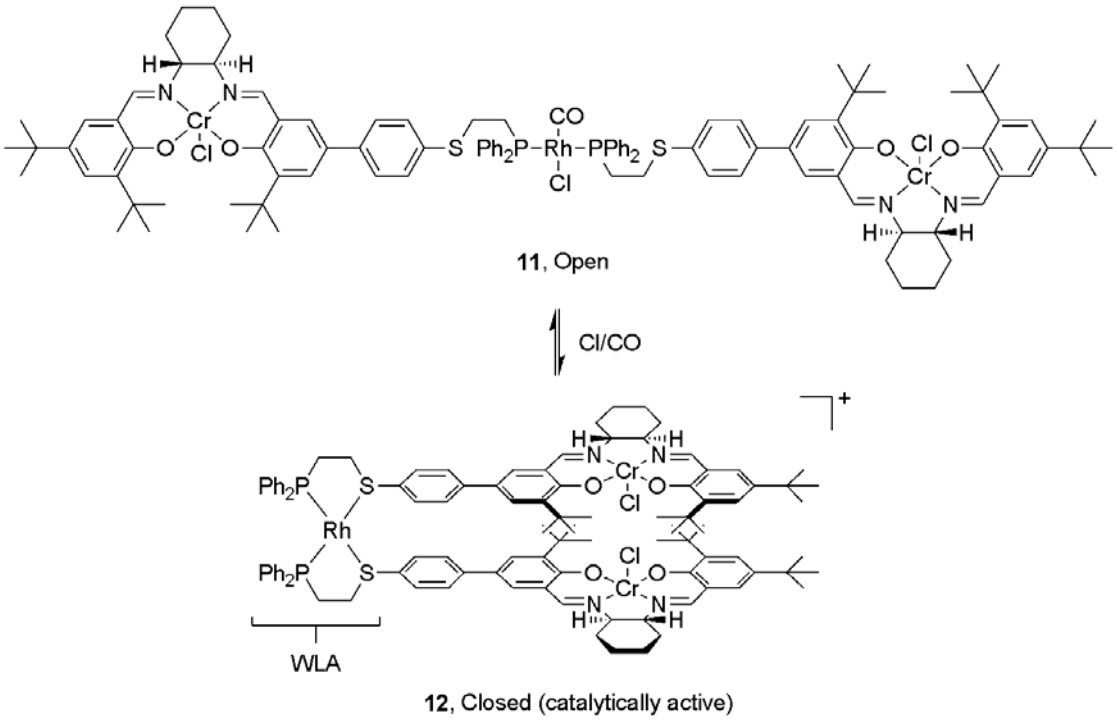

Figure 1.15 WLA allosteric catalyst, Mirkin's 'molecular tweezers' bimetallic catalyst **12**.[104]

Lehn has synthesized numerous organometallic architectures such as helicates,[105] ladders[106] and grids with precise placement of transition metal centers in a nanoscopic rigid framework, a [2x2] iron grid is shown in Figure 1.16. Some of these architectures have interesting electro-optical properties and can be organized into self-assembled monolayers on surfaces,[14, 107] vital features for a "bottom-up" construction of molecular electronics. In **14**, the spin state of the iron atoms can be controlled by external stimuli, such as light, temperature or pressure making this a potential supramolecular switch,[108] which may have applications in nanoelectronics or data storage.[32]

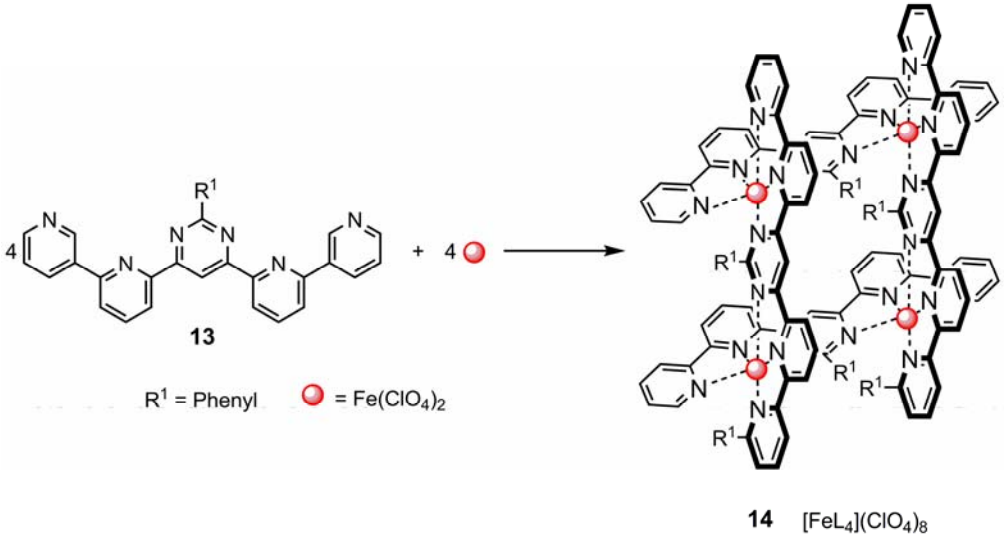

Figure 1.16 [2x2] metal-grid, the spin states of each metal center are switchable via a stimulus.[108]

By controlling the steric demands of flexible H-bonding synthons enthalpically favored finite architectures may be preferentially self-assembled over infinite polymers. These designs create robust, stable suprastructures in apolar solvent environments using organized H-bonding arrays.[62]

Whitesides and later Reinhoudt have done extensive work on the assembly of barbiturates with their melamine compliments creating circular 'rosette' assemblies.[109, 110] Whitesides' first architecture was a single tiered disc structure held together by 18 H-bonds. The first Whiteside rosette shown in Figure 1.17 had pendant bulky aliphatic groups to favor a finite molecular self-assembly over an infinite polymeric assembly.[62]

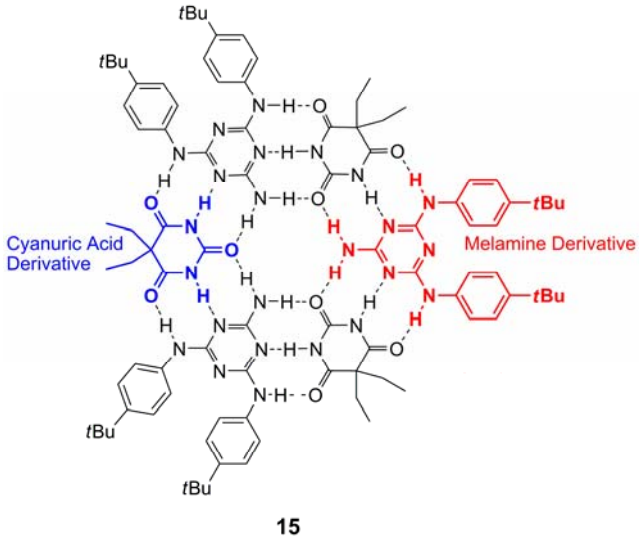

15

Figure 1.17 Single tiered rosette structure held together by 18 H-bonds, self-assembled from cyanuric acid and melamine derivatives.[62]

Reinhoudt's rosette structures were thermodynamically favored to form finite molecular cages by having pendant calixarenes constraining their complexation geometries,[110] as shown in Figure 1.18. These structures can reversible alter their cage volume to accommodate different guests.[111]

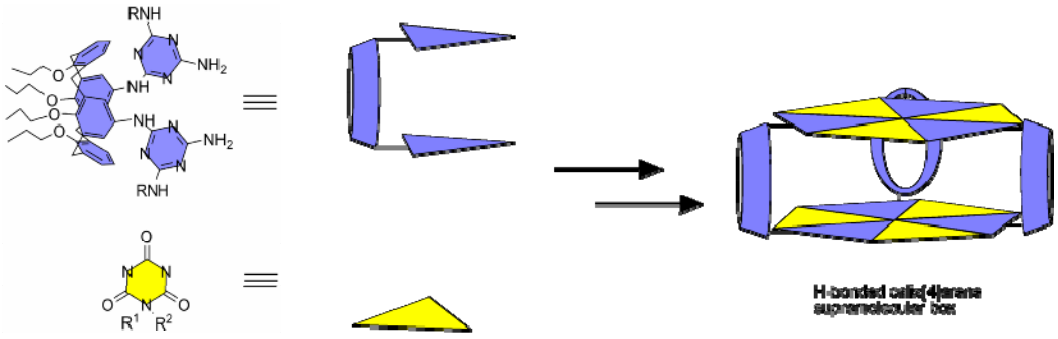

Figure 1.18 Reinhoudt's H-bonded calixarene supramolecular cage.[111]

Later, mega-structure held together by >50 H-bonds were independently self-assembled by Whitesides and Reinhoudt,[109, 112] these architectures had association constant (K_a) $>10^6$ M^{-1} in hydrocarbon solvents. Figure 1.19 shows **18**, a 54 H-bonded mega-structure self-assembled by Whitesides, the rigid tethers of **17** makes this supramolecular architecture thermodynamically the most favorable outcome. Reinhoudt's most massive calixarenes assembly was held together by 144 H-bonds bringing together 27 components to give a nano-cage with eight levels (~ 3 × 6nm, 20 kDa) rivaling the size of a small protein.[113]

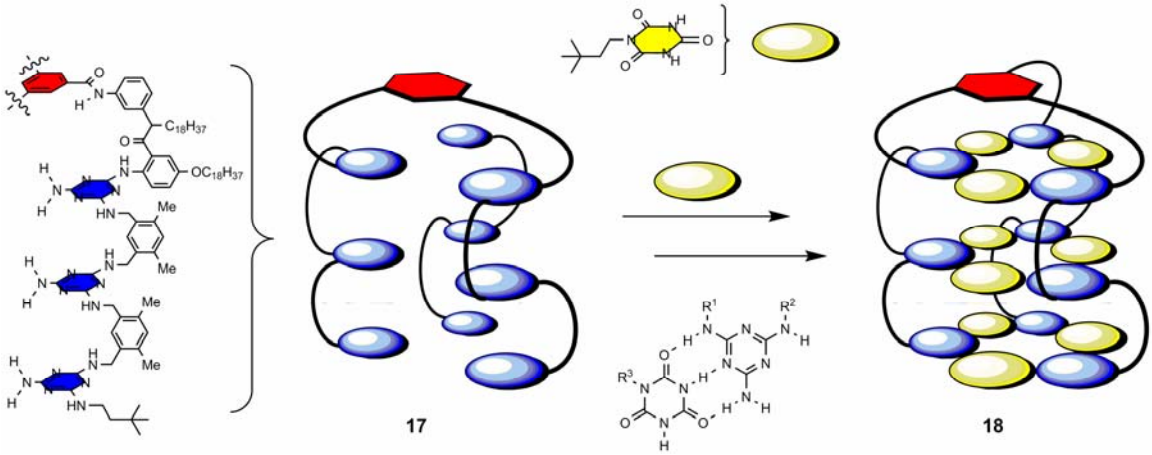

Figure 1.19 Whiteside's 54 H-bonded cyanuric acid-melamine mega-structure.[109]

However, the stability of these structures is highly dependent on the solvent; a polar solvent competes for H-bonding sites and disrupts the assembly. Reinhoudt tried to use these structures as antibody mimics functionalized with biological recognition units, the polar functional groups and the polar solvent led to degradation of the supramolecular architecture into its monomeric components.[114]

Zimmerman has also made supramolecular dendritic hexamer architectures exploiting carboxylic acid H-bonding dimerization, shown in Figure 1.20.[35] The disc shaped 10 nm supramolecular architecture **20** had a 14 Å internal cavity, and a stability beyond the 6 radial –COOH internal dimers in apolar solvents ($CHCl_3$, CH_2Cl_2, toluene). The extra stability was attributed to secondary stabilization of the discs through van der Waals interactions of the peripheral dendrites. However, these systems also disassemble into monomers in more polar environments (THF, DMSO). Unlike these supramolecular systems, which rely on sterics to push the thermodynamic structure to a finite assembly, Mascal devised an H-bonding system that exclusively forms a supermacrocyclic hexamer based solely through its hydrogen bonding codes.[115]

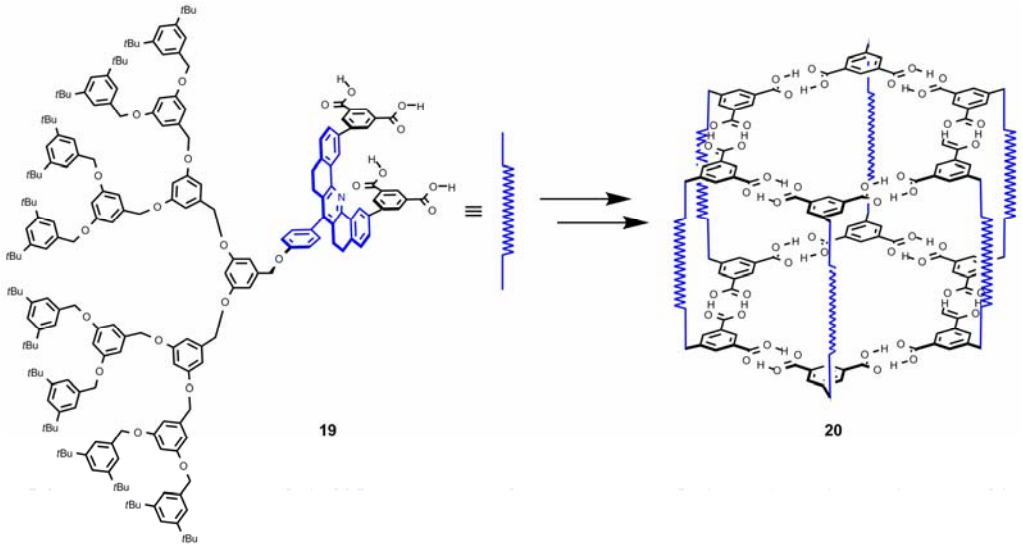

Figure 1.20 Zimmerman's Dendrimer rosette.[35]

These H-bonded studies provide insight into important principles of self-assembly, *i.e.* chiral amplification,[116] "bottom-up" growth to nanoscopic sizes,[113] thermodynamic self-healing,[117] multi-interaction hierarchical growth[117] and different morphologies.[118] However, these attractive architectures use repetitive patterns to give complex structures without a complex function.[37] Additionally, the degradation of these current systems in more polar and physiologically relevant media may limit their potential uses, however in the solid-state their ability to control and direct lattice structures will advance crystal engineering.[119]

1.5.2 Infinite Polymeric Architectures

Unlike biological polymers which rely on main-chain and side-chain inter- and intramolecular weak interactions to induce folding and structuration events supramolecular polymers (SP) rely on intermolecular weak interactions of monomer synthons to assemble their primary structure,[16] a SP is based on the reversible

association of many monomers through weak labile interactions self-assembling into an infinite network.[10] Unlike finite supramolecular systems, whose synthons form thermodynamically stable finite architectures, monomer synthons having multiple recognition sites complex *ad infinitum* until all available synthons have been consumed. These assemblies can be linear, 2-D or 3-D depending on the number of recognition sites per synthons, as shown in Figure 1.21.

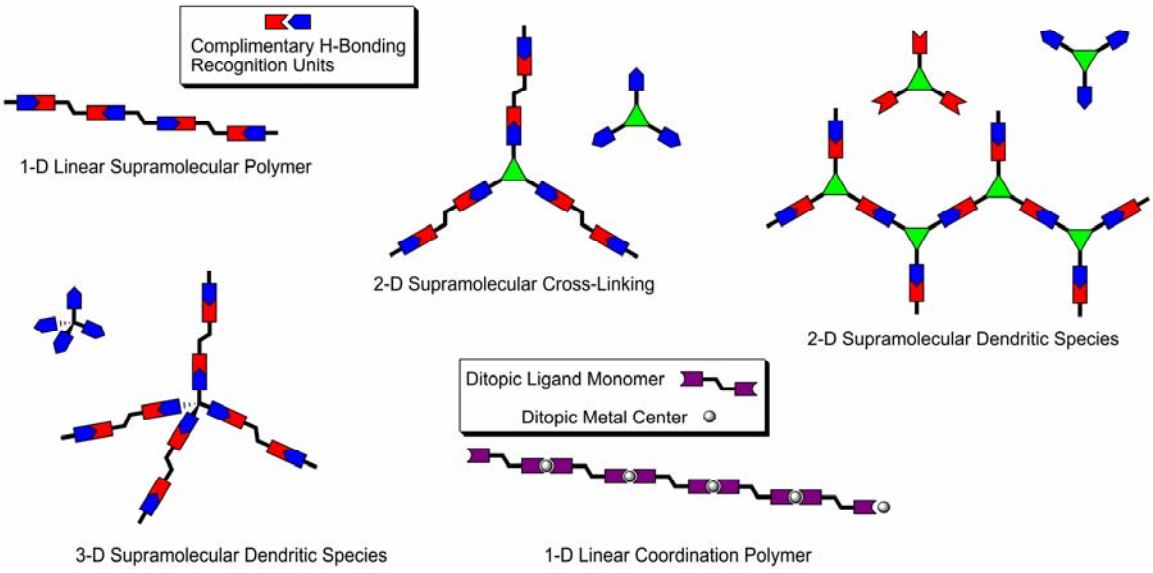

s

Figure 1.21 Potential supramolecular polymeric complexes that can be self-assembled.

Herein, the stricter definition of a spontaneous self-assembly via a recognition event giving a reversible thermodynamically stable system exhibiting chainlike behavior in solution (enhanced viscosity) and bulk will be used for supramolecular polymers (SP).[17] When the supramolecular recognition is due to the coordination between a functionalized ditopic ligand and a ditopic metal complex the metalla-supramolecular polymers are called coordination polymers (CP), lower right of Figure 1.21. CPs are assemblies held

together by bridging ligands, many of these systems are considered purely inorganic, and the 'coordination event' may require thermal or chemically extreme reaction conditions generating more covalent organometallic polymers.[120] Herein, CPs will be defined as supramolecular organometallic polymeric materials, with the donor atoms of the ditopic ligand separated by organic moieties. These CPs have a reversible thermodynamically stable polymeric self-assembly via labile metal-ligand interactions, which requires minimal initiation to reach quantitative conversions. These materials should exhibit chain-like polymeric properties in solution and ideally in bulk. For both SPs and CPs the high directionality of the interactions give these materials a distinct 1-D nature akin to linear covalent polymers.[17] However, an advantage over their covalent predecessors is the ability to produce longer chains, which are by definition defect free.[121] Additionally, the reversible nature of the supramolecular linkages makes these materials self-healing, with a rupture repaired by annealing.[17] The length of these 1-D systems is determined by the degree of polymerization (DP) of the monomer synthons. Using the multistage open association (MSOA) model equation the DP of these systems may be approximated.[10, 122, 123]

$$DP \approx (K_a[\text{monomer}])^{1/2} \qquad \text{(MSOA model equation)}$$

Based on the MSAO model equation the DP is dependent on both the K_a (temperature dependent) and the concentration of the monomeric synthons. An additional requisite to achieve a high DP is to have rigorously pure monomers, monotopic impurities act as chain stoppers severely limiting the maximum DP.[124] A large DP means that high

molecular weight SPs will be formed. The high molecular weight ensures adequate chain entanglement necessary for a solution processing, which is an extremely desirable property of polymeric materials.

The first reported main-chain supramolecular polymer was self-assembled by Lehn using a triply H-bonded diaminopyridine (DAP) system,[125] with a K_a of approximately 10^3 M^{-1} in apolar solvents. SP **23**, shown in Figure 1.22 A, had liquid crystalline behavior and a helical pitch owing to the chirality of the tartrate backbone. This study and others relied on a small number of repeated H-bonding interactions to give interesting solution properties such as liquid crystallinity or light-harvesting,[126] but the K_a was not strong enough to generate reasonable DPs at dilute concentrations. However, in 1997 Meijer and Sijbesma used the quadruple H-bonding dimerization of functionalized 2-ureido-4-pyrimidone (UPy), K_a of dimerization $>10^8$ M^{-1} in apolar solvents,[17, 124, 127] to form SPs with polymeric properties in both concentrated and dilute solutions, shown in Figure 1.22 B. The improved polymeric properties, which allowed for processing into self-supporting solid-state materials, were attributed to the quadruple H-bonded array stabilized by favorable secondary H-bonding interactions.[128]

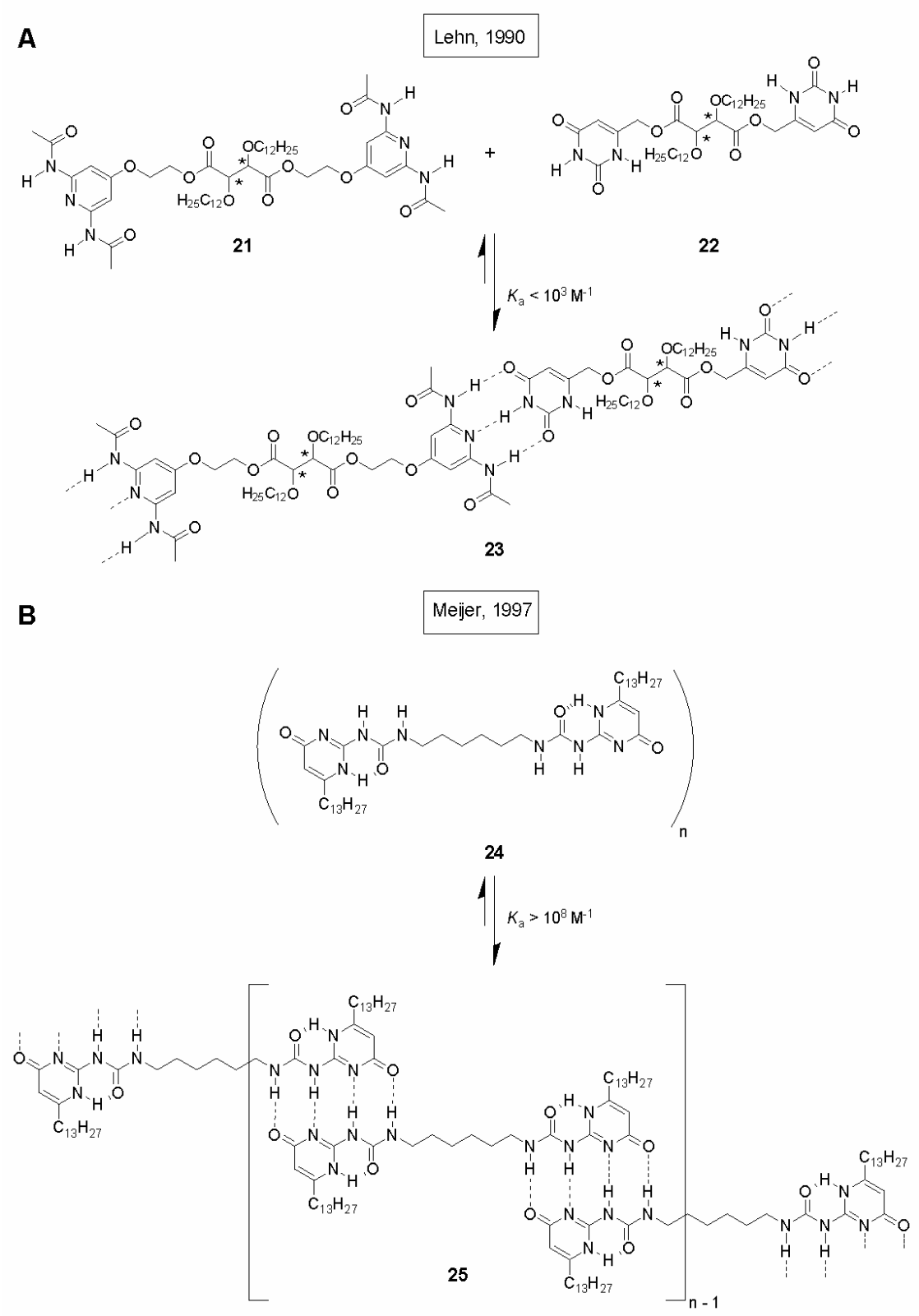

Figure 1.22 A) Lehn's DAP SP; B) Meijer's UPy SP. Stability difference of a triple vs. quadruple H-bonded system.[17, 124, 125, 127]

Meijer's polymer **25** and its analogs, such as telechelic polysiloxanes, -ethers, -esters, -ethylene/butylenes and -carbonates,[127] were shown to have viscoelastic properties similar to those of traditional polymers. However, because of the reversibility of the H-bonding interactions the DP of these materials was responsive to temperature or concentration changes.

This phenomenon allows these materials to have a low melt viscosity behaving like low molecular weight organic compounds. This permits processing at moderate temperatures, below the processing temperatures of their covalent polymeric analogs while still retaining many of their desirable materials properties. Figure 1.23 shows the ease of bulk and solution processing of a patented UPy modified poly(ethylene/butylene) copolymer.

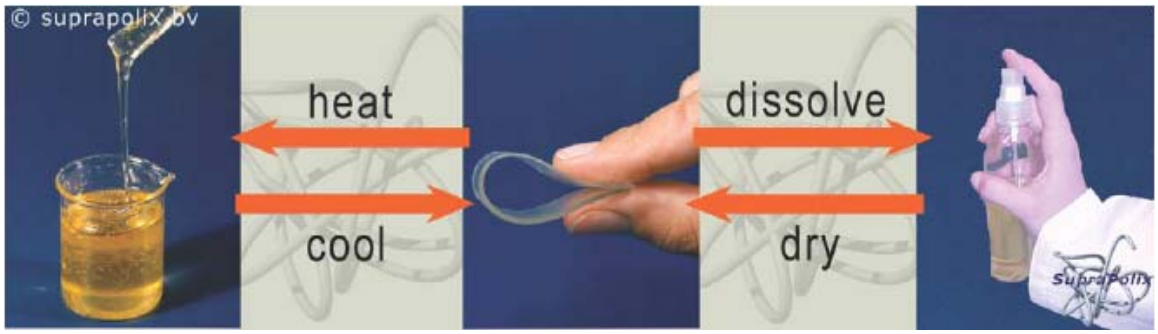

Figure 1.23 Simple processing of Meijer's UPy SPs.[127]

Shortly after Meijer's seminal work, Zimmerman designed comparable systems with similar association strengths.[129, 130] These novel materials have found a range of everyday applications such as adhesives, inks, printing, cosmetics, personal care to

coatings,[127] to more advanced applications such as tissue engineering[131] and plastic electronics.[132]

Bailar began working on inorganic CPs almost 40 years ago.[133, 134] Since this time much of the work on CPs has been on crystal engineering and solid-state structures and applications. These early CPs were not very soluble owing to multiple metal ions and often rigid frameworks, which easily degrade in solution making them difficult to characterize and process in solution.[63, 135]

The metal-ligand interactions of CPs have a wider range of properties compared to the H-bonding interactions of SPs. The coordination is highly directional and can have unique coordination angles, the interaction is generally stronger than H-bonds, and the thermodynamic and kinetic stability can be readily tuned by adjusting either the metal center or the ligands.[136] The variety of possible metal ions and ligands makes functional CPs attractive targets with potential catalytic, conductive, luminescent, magnetic, spin-transition, non-linear optical or porous materials applications.[63, 120]

Common ligand donor atoms are N, O or S, and pyridine is the simplest ligand for CP formation in the solid-state, but its K_a is usually too weak for a reasonable DP in solution.[136] Other common coordination motifs chelate the metal ion increasing the K_a of the metal-ligand interaction through cooperative and entropic effects.[136] Many different CP systems using different ligands and/or metal centers have been reported and have been thoroughly reviewed.[31, 63, 135, 136] Therefore, only several important reports in this area will be highlighted.

Many early CPs were thermodynamically and kinetically stable, making them inert and essentially irreversible polymeric species, thus deviating from the relevant definition

of an SP.[137] The goal of many of these studies was to integrate the attractive electro-optical properties of transition metal complexes into polymeric networks, such as Rehahn's first report of **27**, a soluble CP assembled from phenanthroline ligand **26**, shown in Figure 1.24. Rehahn chelated **26** with Cu^{+} or Ag^{+} salts into robust CP architectures in non-competitive solvents giving kinetically labile species with chain-like polymeric solution properties.[138, 139]

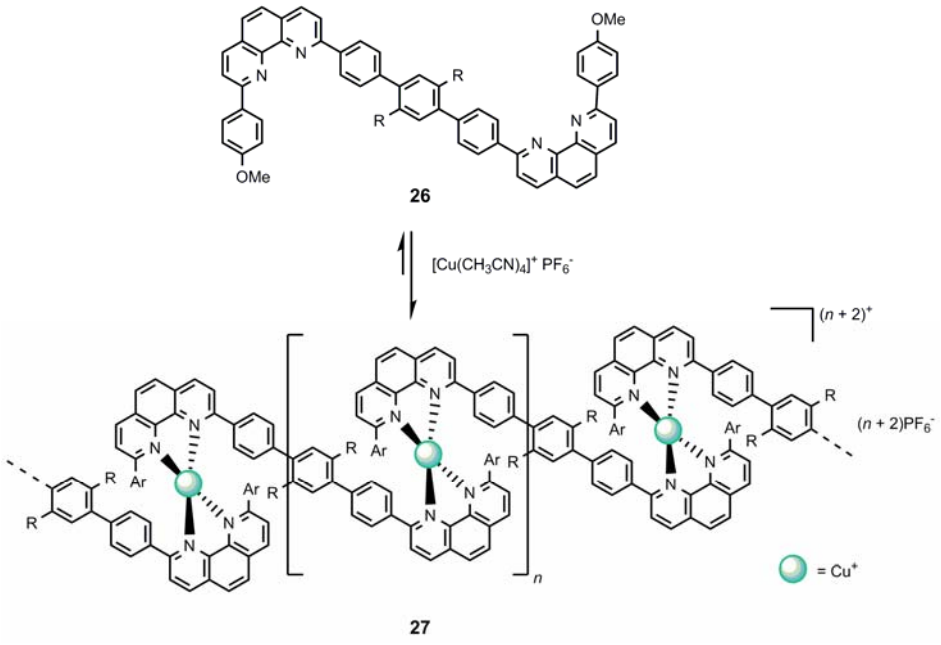

Figure 1.24 Rehahn's soluble copper phenanthroline CP.[138]

Hunter in 2000 used the well-studied coordination of the dye molecule porphyrin,[140] to synthesize labile self-associating pyridyl functionalized Co-porphyrin monomeric synthons **28**, with a $K_a \approx 10^6 - 10^8$ M^{-1}, shown in Figure 1.25. Hunter's CP **29** showed the characteristic traits of a SP in solution, such as a DP approaching 100 (136 kDA) as determined by size-exclusion chromatography (SEC). The length of these robust and

massive polymers could be modulated by concentration changes and chain stopper impurities.[141]

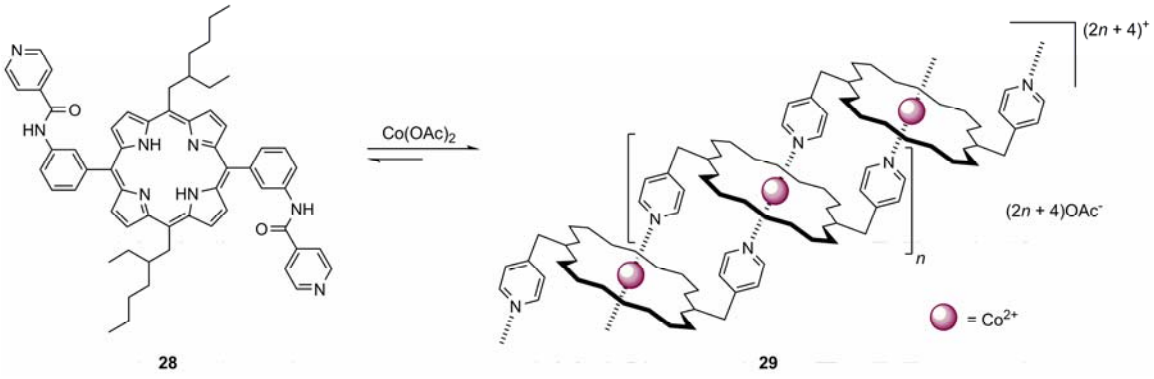

Figure 1.25 Hunter's pyridyl-porphyrin Co CP.[141]

Terpyridine (tpy), another common ligand, has a tridentate chelation making its K_a exceptionally strong.[31] Early work in this area was carried out by Kimura self-assembling tpy binaphthol units into helical CPs with the handedness controlled by the chiral binapthol. These high molecular weight optically active CPs (DP~ 50 by SEC) were investigated as polymeric asymmetric catalysts.[142] Schubert has done extensive work with tpy ligands generating water soluble telechelic tpy poly(ethylene oxide) (tpyPEO) CPs, such as **31** shown in Figure 1.26, with potential applications in water purification, food processing, mining and cosmetics.[143] By employing and substituting a variety of different metal centers (K_a of $Zn^{2+} \approx Cd^{2+} < Fe^{2+} < Ru^{2+}$) Schubert could tune the photophysical and physical properties of the system, *i.e.* from a reversible dynamic polymer (Zn^{2+}) to an irreversible inert polymer (Ru^{2+}).[144]

Figure 1.26 Schubert's Fe-tpy(PEO) water soluble CP.[144]

Electro-optical tpy CPs were independently synthesized by both Würthner[145] and Meijer[146] in 2002 using either Zn^{2+} and Fe^{2+} or Fe^{2+}, respectively. Würthner coordinated the highly fluorescent perylene bisimide dye through the tpy units,[145] and Meijer made CPs from tpy end functionalized oligo(*p*-phenylene vinylene) (OPV) giving π-conjugated systems.[146] Würthner reported that the perylene bisimide retained 95% of its fluorescence after self-assembly showing that the Zn^{2+} metal center acts only as a cohesive unit within the CP due to its closed-shell (d^{10}) electronic configuration. However, upon the addition of an iron(II) salt to the monomer synthons the resultant solution retained the physical polymeric properties but the fluorescence was rapidly and irreversibly quenched, due to metal to ligand charge transfer (MLCT) of the structural and functional Fe^{2+} to the perylene chromophore, shown in Figure 1.27. Meijer's system self-assembled tpy-OPV **34** into high molecular weight polymer **35**, as shown in Figure 1.28. These systems are difficult to obtain using standard covalent protocols. As in the case of Würthner's polymers, the Fe^{2+} centers again acted as both structural and functional components giving a red-shifted absorbance from the OPV.

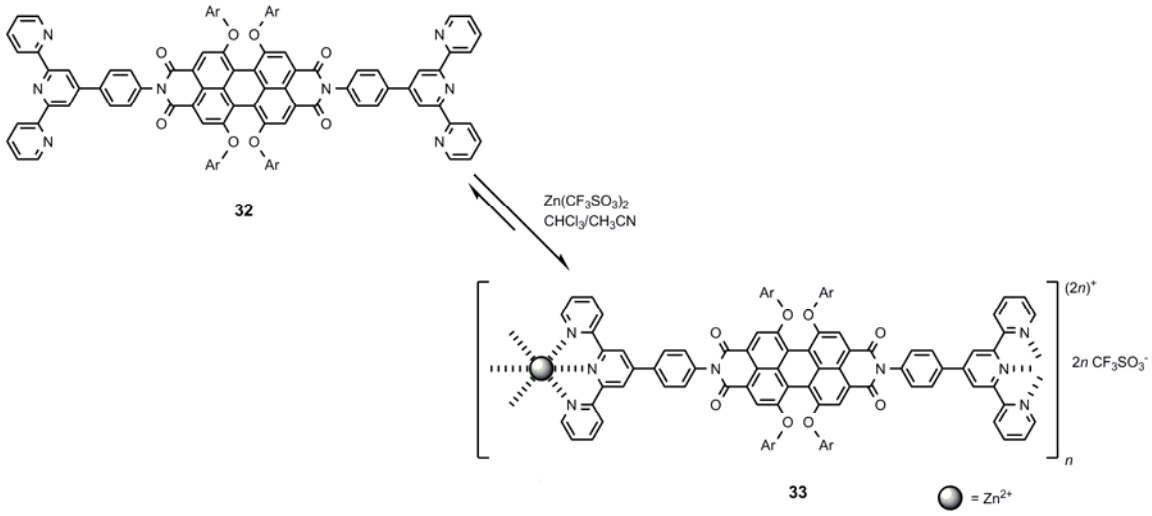

Figure 1.27 Würthner's fluorescent perylene bis-imide CP.[145]

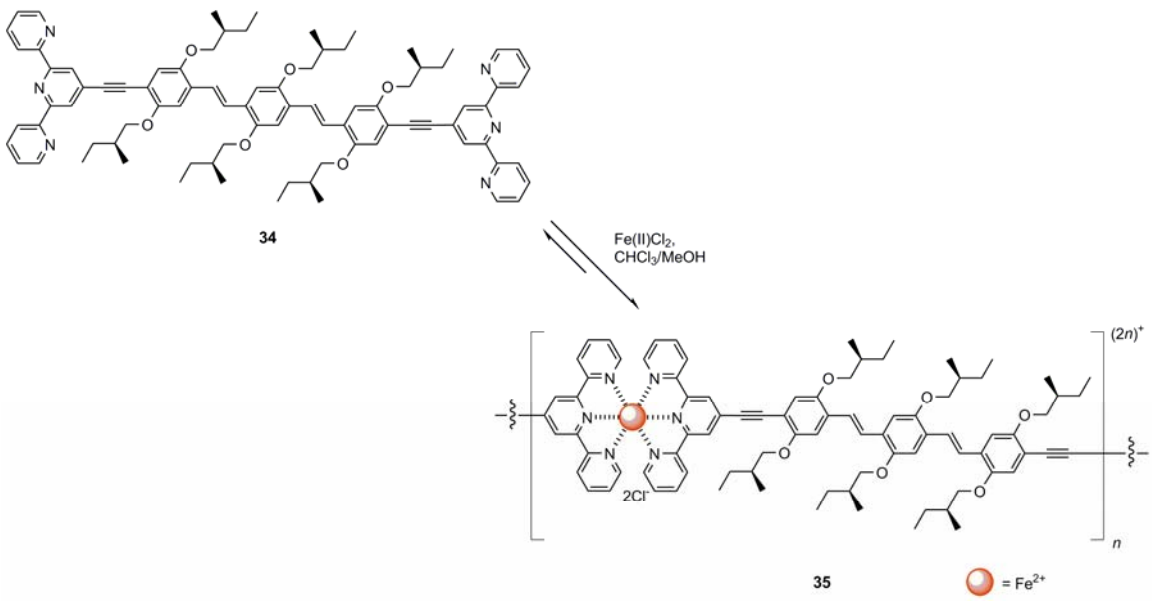

Figure 1.28 Meijer's high molecular weight PPV CP self-assembled from OPV.[146]

Recently, Rowan has carried out elegant studies with tpy-like CPs taking these systems to a new functional level.[122] He fabricated stimuli responsive 3-D gel

networks[147] and also processed 1-D CPs into self-supporting films and fibers with interesting properties much like Meijer's UPy H-bonded SP systems. Rowan end-functionalized low molecular weight poly(*p*-phenylene ethynylene)s (PPE)s or poly(tetrahydrofuran) with the tpy ligand analog 2,6-bis(1'-methylbenzimidazolyl)-pyridine (Mebip) and then self-assembled these monomeric synthons with Zn^{2+}, Fe^{2+} or Cd^{2+} metal ion salts into high molecular weight supramolecular PPVs.[122, 147] Most relevant to this thesis research was the self-assembly of the PPE synthons, these conjugated systems have strong absorbance and photoluminescence characteristics well-suited for a variety of applications. Much like other conjugated systems, difficulties are experienced in synthesizing and purifying defect free materials and solution processing these rigid structures. Therefore, high molecular weight SP PPEs self-assembled from low molecular weight PPEs appears to be a good strategy. After self-assembly of Mebip-PPEs from either Zn^{2+} or Fe^{2+} salts, the CPs displayed good solubility and viscosity traits in apolar organic solvents.[122] Mechanically stable and flexible films and fibers could be further formed from the polymeric solutions, as shown in Figure 1.29. However, the fluorescence emission of both the Zn^{2+} and Fe^{2+} CPs was completely quenched in both the solution and solid-state. The processability of these materials makes them very attractive and optimization of their luminescent properties is the next challenge for Rowan.

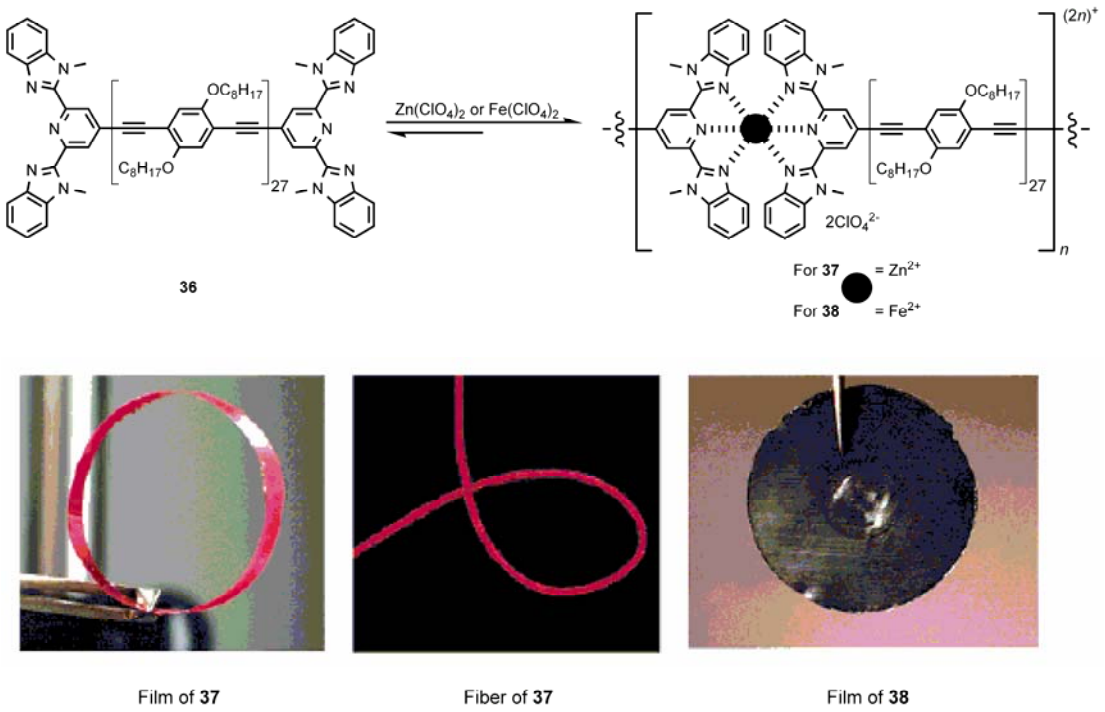

Figure 1.29 Films and fibers formed from Rowan's Mebip-PPE SPs.[122]

Finally merging these two realms of self-assembled polymers are two reports by Schubert that combine both H-bonding and metal-ligand interactions to give hybrid SPs.[148, 149] The SP formed from low molecular weight monomeric synthons had poor solubility due to high charge density of the metal centers in the hybrid polymer. By incorporating a high molecular weight caprolactone poly(ester) spacer between the orthogonal recognition units. The charge density is spread out in this revised system, shown in Figure 1.30, therefore solubility and thus processability was dramatically improved.

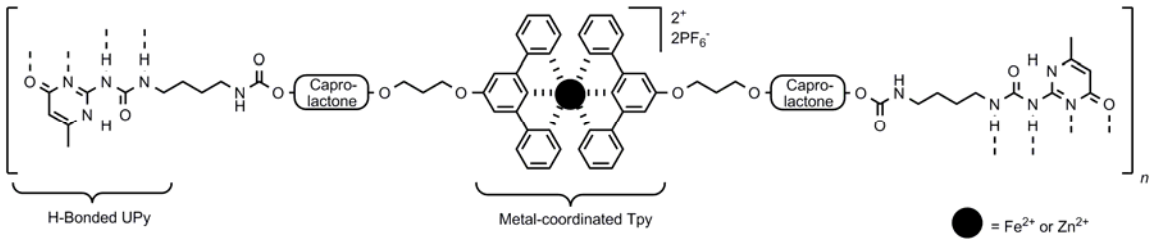

Figure 1.30 Schubert's multifunctional H-bonded/organometallic SP. [148, 149]

1.6 Conclusion

Over the last several decades supramolecular scientist have made great advances from the early ground-breaking 'host-guest' interactions of Pedersen, Lehn and Cram.[20-22] Several strategies for the preparation of finite molecular nanostructures and infinite polymeric systems have been briefly reviewed. The goal of self-assembly is to quickly and spontaneously create novel, robust and functional architectures beyond the scope of traditional covalent synthesis. A variety of novel and robust architectures with primitive functions have been reviewed. Now the current challenge is to increase the functional utility of supramolecular systems.

The intention of all of the projects represented by this thesis is to contribute to both of the synthetic supramolecular arenas elaborated upon, developing new functional nanostructures and polymers that have thus far not been realized. These systems are assembled through the strong and reversible metal-coordination of established recognition units to new complex and functional ligands. The accomplishments of this research will pave the way for larger hierarchical systems. The ultimate success of these proposed systems will further validate this research and the efforts of those who contributed to it.

1.7 References

[1] Danishefsky, S. J., Masters, J. J., Young, W. B., Link, J. T., Snyder, L. B., Magee, T. V., Jung, D. K., Isaacs, R. C. A., Bornmann, W. G., Alaimo, C. A., Coburn, C. A., Di Grandi, M. J. Total Synthesis of Baccatin III and Taxol. *J. Am. Chem. Soc.* **1996**, *118*, 2843-2859.

[2] Holton, R. A., Somoza, C., Kim, H. B., Liang, F., Biediger, R. J., Boatman, D. P., Shindo, M., Smith, C. C., Kim, S., al., e. First total synthesis of taxol. 1. Functionalization of the B ring. *J. Am. Chem. Soc.* **1994**, *116*, 1597-1598.

[3] Holton, R. A., Kim, H. B., Somoza, C., Liang, F., Biediger, R. J., Boatman, D. P., Shindo, M., Smith, C. C., Kim, S., al., e. First total synthesis of taxol. 2. Completion of the C and D rings. *J. Am. Chem. Soc.* **1994**, *116*, 1599-1600.

[4] Woodward, R. B. The total synthesis of vitamin B 12. *Pure Appl. Chem.* **1973**, *33*, 145-177.

[5] Nicolau, K. C., Tiebes, J., Thedorakis, E. A., Rutjes, F. P. J. T., Koide, K., Sato, M., Untersteller, E. Total Synthesis of Truncated Brevetoxin B [AFGHIJK]. *J. Am. Chem. Soc.* **1994**, *116*, 9371-9372.

[6] Whitesides, G. M., Ismagilov, R. F. Complexity in chemistry. *Science* **1999**, *284*, 89-92.

[7] Armstrong, R. W., Beau, J.-M., Cheon, S. H., Christ, W. J., Fujioka, H., Ham, W. H., Hawkins, L. D., Jin, H., Kang, S. H., Kishi, Y., Martinelli, M. J., McWhorter, W. W. J., Mizuno, M., Nakata, M., Stutz, A. E., Talamas, M., Tino, J. A., Ueda, K., Uenishi, J.-i., White, J. B., Yonaga, M. Total synthesis of a fully protected palytoxin carboxylic acid. *J. Am. Chem. Soc.* **1989**, *111*, 7525-7530.

[8] Whitesides, G. M., Mathias, J. P., Seto, C. T. Molecular self-assembly and nanochemistry: a chemical strategy for the synthesis of nanostructures. *Science* **1991**, *254*, 1312-1319.

[9] Ozin, G. A. Nanochemistry: Synthesis in diminishing dimensions. *Adv. Mater.* **1992**, *4*, 612-649.

[10] Ciferri, A., *Supramolecular Polymers, Second Edition*, 2nd ed., CRC Press, Boca Raton, **2005**.

[11] Whitesides, G. M., Grzybowski, B. Self-assembly at all scales. *Science* **2002**, *295*, 2418-2121.

[12] Haddon, R. C., Lamola, A. A. The molecular electronic device and the biochip computer: present status. *Proc. Natl. Acad. Sci. U.S.A.* **1985**, *82*, 1874-1878.

[13] Tullo, A. Pushing Moore's Law. *Chem. Eng. News* **2006**, *84*, 22.

[14] Crespo-Biel, O., Ravoo, B. J., Reinhoudt, D. N., Huskens, J. Noncovalent nanoarchitectures on surfaces: from 2D to 3D nanostructures. *J. Mater. Chem* **2006**, *16*, 3997-4021.

[15] Xia, Y., Whitesides, G. M. Soft lithography. *Angew. Chem. Int. Ed.* **1998**, *37*, 550-575.

[16] Lehn, J. M., *Supramolecular Chemistry: Concepts and Perspectives*, VCH, Weinheim, **1995**.

[17] Brunsveld, L., Folmer, B. J. B., Meijer, E. W., Sijbesma, R. P. Supramolecular Polymers. *Chem. Rev.* **2001**, *101*, 4071-4097.

[18] Lehn, J.-M. Toward complex matter: Supramolecular chemistry and self-organization. *Proc. Natl. Acad. Sci. U.S.A.* **2002**, *99*, 4763-4768.

[19] Steed, J. W., Atwood, J. L., *Supramolecular Chemistry*, John Wiley & Sons, Baffins Lane, **2000**.

[20] Lehn, J.-M. Supramolecular Chemistry - Scope and Perspectives Molecules, Supermolecules, and Molecular Devices (Nobel Lecture). *Angew. Chem. Int. Ed.* **1988**, *27*, 89-112.

[21] Cram, D. J. The Design of Molecular Hosts, Guests, and Their Complexes (Nobel Lecture). *Angew. Chem. Int. Ed.* **1988**, *27*, 1009-1020.

[22] Pedersen, C. J. The Discovery of Crown Ethers (Nobel Lecture). *Angew. Chem. Int. Ed.* **1988**, *27*, 1021-1027.

[23] Dietrich, B., Lehn, J. M., Sauvage, J. P. Diaza-polyoxa-macrocyclic and macrobicyclic compounds. *Tetrahedron Lett.* **1969**, 2885-2888.

[24] Dietrich, B., Lehn, J. M., Sauvage, J. P. Cryptates. *Tetrahedron Lett.* **1969**, 2889-2892.

[25] Sanderson, R. T., *Chemical Bonds and Bond Energy*, 2nd Ed. ed., Academic, New York, **1976**.

[26] Dodziuk, H., *Introduction to Supramolecular Chemistry*, Kluwer Academic Publishers, Dordrecht, **2002**.

[27] Beer, P. D., Gale, P. A., Smith, D. K., *Oxford Chemistry Primers: Supramolecular Chemistry*, Oxford University Press, Oxford, **1999**.

[28] Voet, D., Voet, J. G., Pratt, C. W., *Fundamentals of Biochemistry*, John Wiley & Sons, Inc., New York, **2002**.

[29] Holliday, B. J., Mirkin, C. A. Strategies for the construction of supramolecular compounds through coordination chemistry. *Angew. Chem. Int. Ed.* **2001**, *40*, 2022-2043.

[30] Seidel, R. S., Stang, P. J. High-Symmetry Coordination Cages via Self-Assembly *Acc. Chem. Res.* **2002**, *35*, 972-983.

[31] Schubert, U. S., Eschbaumer, C. Macromolecules containing bipyridine and terpyridine metal complexes: towards metallosupramolecular polymers. *Angew. Chem. Int. Ed.* **2002**, *41*, 2892-2926.

[32] Waldmann, O., Ruben, M., Ziener, U., Müller, P., Lehn, J.-M. Supramolecular Co(II)-[2 x 2] grids: metamagnetic behavior in a single molecule. *Inorg. Chem.* **2006**, *45*, 6535-6540.

[33] Sautter, A., Kaletas, B. K., Schmid, D. G., Dobrawa, R., Zimine, M., Jung, G., van Stokkum, I. H. M., De Cola, L., Williams, R. M., Würthner, F. Ultrafast energy-electron transfer cascade in a multichromophoric light-harvesting molecular square. *J. Am. Chem. Soc.* **2005**, *127*, 6719-6729.

[34] Cassagneau, T., Fendler, J. H., Johnson, S. A., Mallouk, T. E. Self-assembled Diode Junctions Prepared from a Ruthenium Tris (Bipyridyl) Polymer, n-Type TiO2 Nanoparticles and Graphite Oxide Sheets. *Adv. Mater.* **2000**, *12*, 1363-1366.

[35] Zimmerman, S. C., Zeng, F., Reichert, D. E. C., Kolotuchin, S. V. Self-assembling dendrimers. *Science* **1996**, *271*, 1095-1098.

[36] Pollino, J. M., Stubbs, L. P., Weck, M. One-Step Multifunctionalization of Random Copolymers via Self-Assembly. *J. Am. Chem. Soc.* **2004**, *126*, 563-567.

[37] Schalley, C. A., Lützen, A., Albrecht, M. Approaching Supramolecular Functionality. *Chem. Eur. J.* **2004**, *10*, 1072-1080.

[38] Gamez, P., Reedijk, J. 1,3,5-Triazine-based synthons in supramolecular chemistry. *Eur. J. Inorg. Chem.* **2006**, 29-42.

[39] Gianneschi, N. C., Masar, M. S., III, Mirkin, C. A. Development of a Coordination Chemistry-Based Approach for Functional Supramolecular Structures. *Acc. Chem. Res.* **2005**, *38*, 825-837.

[40] Gerhardt, W., Črne, M., Weck, M. Multifunctionalization of synthetic polymer systems through self-assembly. *Chem. Eur. J.* **2004**, *10*, 6212-6221.

[41] Ashkenasay, G., Jagasia, R., Yadav, M., Ghadiri, M. R. Design of a directed molecular network. *Proc. Natl. Acad. Sci. U.S.A.* **2004**, *101*, 10872-10877.

[42] Gohy, J.-F., Lohmeijer, B. G. G., Schubert, U. S. From Supramolecular Block Copolymers to Advanced Nano-Objects. *Chem. Eur. J.* **2003**, *9*, 3472-3479.

[43] Lohmeijer, B. G. G., Schubert, U. S. Playing LEGO with Macromolecules: Design, Synthesis, and Self-Organization with Metal Complexes. *J. Polym. Sci., Part A: Polym. Chem.* **2003**, *41*, 1413-1427.

[44] Hu, Z., Verheijen, W., Hofkens, J., Jonas, A. M., Gohy, J.-F. Formation of Vesicles in Block Copolymer-Fluorinated Surfactant Complexes. *Langmuir* **2007**, *23*, 116-122.

[45] Buhler, E., Candau, S. J., Schmidt, J., Talmon, Y., Kolomiets, E., Lehn, J.-M. Fibrillar structure of self-assemblies formed from heterocomplementary monomers linked through sextuple hydrogen-bonding arrays. *J. Poly. Sci. Part A.: Polym. Chem.* **2006**, *45*, 103-115.

[46] Nakade, H., Ilker, M. F., Jordan, B. J., Uzun, O., LaPointe, N. L., Coughlin, E. B., Rotello, V. M. Duplex strand formation using alternating copolymers. *Chem. Commun.* **2005**, 3271-3273.

[47] Scherman, O. A., Ligthart, G. B. W. L., Ohkawa, H., Sijbesma, R. P., Meijer, E. W. Olefin metathesis and quadruple hydrogen bonding: a powerful combination in multistep supramolecular synthesis. *Proc. Natl. Acad. Sci. U.S.A.* **2006**, *103*, 11850-11855.

[48] Park, T., Zimmerman, S. C. A Supramolecular Multi-Block Copolymer with a High Propensity for Alternation. *J. Am. Chem. Soc.* **2006**, *128*, 13986-13987.

[49] Higley, M. N., Pollino, J. M., Hollembeak, E., Weck, M. A modular approach toward block copolymers. *Chem. Eur. J.* **2005**, *11*, 2946-2953.

[50] Pollino, J. M., Nair, K. P., Stubbs, L. P., Adams, J., Weck, M. Crosslinked and functionalized universal polymer backbones via simple, rapid, and orthogonal multi-site self-assembly. *Tetrahedron* **2004**, *60*, 7205-7215.

[51] Valkama, S., Lehtonen, O., Lappalainen, K., Kosonen, H., Castro, P., Repo, T., Torkkeli, M., Serimaa, R., Brinke, G. T., Leskela, M., Ikkala, O. *Macromol. Rapid Commun.* **2003**, *24*, 556-560.

[52] Gomez, L. M., Stoddart, J. F. *Handbook of Nanostructured Materials and Nanotechnology* **2000**, *5*, 225-275.

[53] Fyfe, M. C. T., Stoddart, J. F. (Supra)Molecular systems based on crown ethers and secondary dialkylammonium ions. *Adv. Supramol. Chem.* **1999**, *5*, 1-53.

[54] Heller, M., Schubert, U. S. Polystyrene with pendant mixed functional ruthenium(II)-terpyridine complexes. *Macromol. Rapid Commun.* **2002**, *23*, 411-415.

[55] Chujo, Y., Sada, K., Saegusa, T. Synthesis of bipyridyl-branched polyoxazoline and its gelation by means of metal coordination. *Polym. J.* **1993**, *25*, 599-608.

[56] Pease, A. R., Jeppesen, J. O., Stoddart, J. F., Luo, Y., Collier, C. P., Heath, J. R. Switching devices based on interlocked molecules. *Acc. Chem. Res.* **2001**, *34*, 433-444.

[57] Badjić, J. D., Balzani, V., Credi, A., Silvi, S., Stoddart, J. F. A molecular elevator. *Science* **2004**, *1845-1849*.

[58] Ballardini, R., Balzani, V., Credi, A., Gandolfi, M. T., Langford, S. J., Menzer, S., Prodi, L., Stoddart, J. F., Venturi, M., Williams, D. J. Simple molecular machines: chemically driven unthreading and rethreading of a [2]pseudorotaxane. *Angew. Chem. Int. Ed. Engl.* **1996**, *35*, 978-981.

[59] Cragg, P. J., *A Practical Guide to Supramolecular Chemistry*, John Wiley and Sons, Ltd., Chichester, **2005**.

[60] Hosseini, M. W. Molecular Tectonics: From Simple Tectons to Complex Molecular Networks. *Acc. Chem. Res.* **2005**, *38*, 313-3232.

[61] Lehn, J.-M. Programmed chemical systems: multiple subprograms and multiple processing/expression of molecular information. *Chem. Eur. J.* **2000**, *6*, 2097-2102.

[62] Zerkowski, J. A., Seto, C. T., Whitesides, G. M. Solid-state structures of rosette and crinkled tape motifs derived from the cyanuric acid melamine lattice. *J. Am. Chem. Soc.* **1992**, *114*, 5473-5475.

[63] Janiak, C. Engineering coordination polymers towards applications. *Dalton Trans.* **2003**, 2781-2804.

[64] Lawrence, D. S., Jiang, T., Levett, M. Self-assembling supramolecular complexes. *Chem. Rev.* **1995**, *95*, 2229-2260.

[65] Elemans, J. A. A. W., Rowan, A. E., Nolte, R. J. M. Mastering molecular matter. Supramolecular architectures by hierarchical self-assembly. *J. Mater. Chem.* **2003**, *13*, 2661-2670.

[66] Watson, J. D., Crick, F. H. Molecular structure of nucleic acids; a structure for deoxyribose nucleic acid. *Nature* **1953**, *171*, 737-738.

[67] Watson, J. D., Crick, F. H. Genetical implications of the structure of deoxyribosenucleic acid. *Nature* **1953**, *171*, 964-967.

[68] Guerrier-Takada, C., Gardiner, K., Marsh, T., Pace, N., Altman, S. The RNA moiety of ribonuclease P is the catalytic subunit of the enzyme. *Cell* **1983**, *35*, 849-857.

[69] Zaug, A. J., Cech, T. R. Oligomerization of intervening sequence RNA molecules in the absence of proteins. *Science* **1985**, *229*, 1060-1064.

[70] Branden, C., Tooze, J., *Introduction to Protein Structure*, Kyoikusha Ltd., Higashimurayama, **1992**.

[71] International Human Genome Sequencing Consortium Finishing the euchromatic sequence of the human genome. *Nature* **2004**, *431*, 931-945.

[72] Martinek, T. A., Fülöp, F. Side-chain control of β-peptide secondary structures *Eur. J. Biochem.* **2003**, *270*, 3657-3666.

[73] Hermans, J. Molecular dynamics simulations of helix and turn propensities in model peptides. *Curr. Opin. Struct. Biol.* **1993**, *3*, 270-276.

[74] Gellman, S. H. Minimal model systems for β–sheet secondary structure in proteins. . *Curr. Opin. Struct. Biol.* **1998**, *2*, 717-725.

[75] Hughes, R. M., Waters, M. L. Model systems for β-hairpins and β-sheets. *Curr. Opin. Struct. Biol.* **2006**, *16*, 514-524.

[76] Radzicka, A., Wolfenden, R. A proficient enzyme. *Science* **1995**, *267*, 90-93.

[77] Bairoch, A. The ENZYME database in 2000. *Nucleic Acids Res.* **2000**, *28*, 304-305.

[78] Jeffery, C. J. Moonlighting proteins: old proteins learning new tricks *Trends Gen.* **2003**, *19*, 415-417.

[79] Birktoft, J. J., Blow, D. M. Structure of crystalline α-chymotrypsin. V. The atomic structure of tosyl-α-chymotrypsin at 2Å resolution. *J. Molec. Biol.* **1972**, *68*, 187-240.

[80] Cacialli, F., Samorì, P., Silva, C. Supramolecular Architectures. *Mater. Today* **2004**, *7*, 24-32.

[81] Pedersen, C. J. Cyclic polyethers and their complexes with metal salts. *J. Am. Chem. Soc.* **1967**, *89*, 2495-2006.

[82] Pedersen, C. J. Cyclic polyethers and their complexes with metal salts. *J. Am. Chem. Soc.* **1967**, *89*, 7017-7036.

[83] Kyba, E. P., Siegel, M. G., Sousa, L. R., Sogah, G. D. Y., Cram, D. J. Chiral, hinged, and functionalized multiheteromacrocycles. *J. Am. Chem. Soc.* **1973**, *95*, 2691-2692.

[84] Kyba, E. B., Koga, K., Sousa, L. R., Siegel, M. G., Cram, D. J. Chiral recognition in molecular complexing. *J. Am. Chem. Soc.* **1973**, *95*, 2692-2693.

[85] Cramer, F., *Einschlussverbindungen*, Springer Verlag, Heidelberg, **1954**.

[86] Leonard, J. P., dos Santos, C. M. G., Plush, S. E., McCabe, T., Gunnlausgsson, T. pH driven self-assembly of a ternary lanthanide luminescence complex: the sensing of anions using a β-diketonate-Eu(III) displacement assay. *Chem. Commun.* **2007**, 129-131.

[87] Cram, D. J., Katz, H. E., Dicker, I. B. *J. Am. Chem. Soc.* **1984**, *106*.

[88] Maverick, A. W., Klavetter, F. E. Cofacial binuclear copper complexes of a bis(β-diketone) ligand. *Inorg. Chem.* **1984**, *23*, 4129-4130.

[89] Maverick, A. W., Buckingham, S. C., Yao, Q., Bradbury, J. R., Stanley, G. G. Intramolecular Coordination of bidentate Lewis Bases to Cofacial Binuclear Copper(II) Complexes. *J. Am. Chem. Soc.* **1986**, *108*.

[90] Constable, E. C. Metallosupramolecular chemistry. *Chem. Ind.* **1994**, *2*, 56-59.

[91] Stang, P. J. Molecular architecture: coordination as the motif in the rational design and assembly of discrete supramolecular species- self-assembly of metallacyclic polygons and polyhedra. *Chem. Eur. J.* **1998**, *4*, 19-27.

[92] Fujita, M., Ibukuro, H., Seki, O., Kamo, M., Imanuri, K., Ogura, J. Catenane Formation from Two Molecular Rings through Very Rapid Slippage. A Möbius Strip Mechanism *J. Am. Chem. Soc.* **1996**, *118*, 899-900.

[93] Lyon, A. P., Macartney, D. H. Kinetic and Spectroscopic Studies on a-Cyclodextrin Rotaxanes with Pentacyano(cyanopyridinium)ferrate(II) Stoppers. *Inorg. Chem.* **1997**, *36*, 729-736.

[94] Constable, E. C. Oligopyridines as helicating ligands *Tetrahedron* **19992**, *48*, 10013-10059.

[95] Amjis, C. H. M., van Klink, G. P. M., van Koten, G. Matellasupramolecular architectures, an overview of functional properties and applications. *Dalton Trans.* **2006**, 308-327.

[96] Stang, P. J., Cao, D. H., Chen, K., Gray, G. M., Muddiman, D. C., Smith, R. D. Molec. Arch. via Coord: marriage of crown ethers and molec. squares, unique tetranucl. metallacycles. *J. Am. Chem. Soc.* **1997**, *119*, 5163-5168.

[97] Würthner, F., You, C.-C., Saha-Möller, C. Metallosupramolecular squares: from structure to function. *Chem. Soc. Rev.* **2004**, *33*, 133-146.

[98] Kovbasyuk, L., Krämer, R. Allosteric supramolecular receptors and catalysts. *Chem. Rev.* **2004**, *104*, 3161-3187.

[99] Gianneschi, N. C., Nguyen, S. T., Mirkin, C. A. Signal amplification and detection via a supramolecular allosteric catalyst. *J. Am. Chem. Soc.* **2005**, *127*, 1644-1645.

[100] Saalfrank, R. W., Stark, A., Peters, K., von Schnering, H. G. The first "Adamantoid" alkaline earth metal chelate complex: Synthesis, structure and reactivity. *Angew. Chem. Int. Ed. Engl.* **1988**, *27*, 851-853.

[101] Schweiger, M., Seidel, R. S., Schmitz, M., Stang, P. J. Rational design of chiral nanoscale adamantoids. *Org. Lett.* **2000**, *2*, 1255-1257.

[102] You, C.-C., Hippius, C., Grüne, M., Würthner, F. Light-harvesting metallosupramolecular squares composed of perylene bisimide walls and fluorescent antenna dyes. *Chem. Eur. J.* **2006**, *12*, 7510-7519.

[103] Ito, H., Kusukawa, T., Fujita, M. Wacker oxidation in an aqueous phase through the reverse phase-transfer catalysis of a self-assembled nanocage. *Chem. Lett.* **2000**, 598-599.

[104] Gianneschi, N. C., Cho, S.-H., Nguyen, S. T., Mirkin, C. A. Reversibly addressing an allosteric catalyst in situ: catalytic molecular tweezers. *Angew. Chem. Int. Ed.* **2004**, *43*, 5503-5507.

[105] Krämer, R., Lehn, J.-M., De Cian, A., Fischer, J. Self-assembly, structure, and spontaneous resolution of a trinuclear triple helix from an oligobipyridine ligand and Ni(II) ions. *Angew., Chem. Int. Ed. Engl.* **1993**, *32*, 703-706.

[106] Baxter, P. N. W., Hanan, G. S., Lehn, J.-M. Inorganic arrays via multicomponent self-assembly: the spontaneous generation of ladder architectures. *Chem. Commun.* **1996**, 2019-2020.

[107] Semenov, A., Spatz, J. P., Möller, M., Lehn, J.-M., Sell, B., Schubert, D., Weidl, C. H., Schubert, U. S. Controlled arrangement of supramolecular metal coordination arrays on surfaces. *Angew. Chem. Int. Ed.* **1999**, *38*, 2547-2550.

[108] Breuning, E., Ruben, M., Lehn, J.-M., Renz, F., Garcia, Y., Ksenofontov, V., Gütlich, P., Wegelius, E., Rissanen, K. Spin crossover in a supramolecular Fe4II [2 * 2] grid triggered by temperature, pressure, and light. *Angew. Chem. Int. Ed.* **2000**, *39*, 2504-2507.

[109] Mathias, J. P., Simanek, E. E., Seto, C. T., Whitesides, G. M. Self-organization via hydrogen-bridge bonds: preparation of a supramolecular aggregate from ten molecules. *Angew. Chem., Int. Ed. Engl.* **1993**, *32*, 1766-1769.

[110] Vreekamp, R. H., van Duynhoven, J. P. M., Hubert, M., Verboom, W., Reinhoudt, D. N. Molecular boxes based on calix[4]arene double rosettes. *Angew. Chem., Int. Ed. Engl.* **1996**, *35*, 1215-1218.

[111] Kerckhoffs, J. M. C. A., van Leeuwen, F. W. B., Spek, A. L., Kooijman, H., Crego-Calama, M., Reinhoudt, D. N. Regulatory strategies in the complexation and release of a noncovalent guest trimer by a self-assembled molecular cage. *Angew. Chem. Int. Ed.* **2003**, *42*, 5717-5722.

[112] Jolliffe, K. A., Timmerman, P., Reinhoudt, D. N. Noncovalent assembly of a fifteen-component hydrogen-bonded nanostructure. *Angew. Chem. Int. Ed.* **1999**, *38*, 933-937.

[113] Paraschiv, V., Crego-Calama, M., Fokkens, R. H., Padberg, C. J., Timmerman, P., Reinhoudt, D. N. Nanostructures via Noncovalent Synthesis: 144 Hydrogen Bonds Bring Together 27 Components. *J. Org. Chem.* **2001**, *66*, 8297-8301.

[114] ten Cate, M. G. J., Omerović, M., Oshovsky, G. V., Crego-Calama, M., Reinhoudt, D. N. Self-assembly and stability of double rosette nanostructures with biological functionalities. *Org. Biomol. Chem.* **2005**, *3*, 3727-3733.

[115] Mascal, M., Hext, N. M., Warmuth, R., Moore, M. H., Turkenburg, J. P. Programming a hydrogen-bonding code for the specific generation of a supermacrocycle. *Angew. Chem., Int. Ed. Engl.* **1996**, *35*, 2203-2206.

[116] Mateos-Timoneda, M. A., Crego-Calama, M., Reinhoudt, D. N. Amplification of chirality in hydrogen-bonded tetrarosette helices. *Chem. Eur. J.* **2006**, *12*, 2630-2638.

[117] Simanek, E. E., Isaacs, L., Li, X., Wang, C. C. C., Whitesides, G. M. Self-Assembly of Zinc Porphyrins around the Periphery of Hydrogen-Bonded Aggregates That Bear Imidazole Groups. *J. Org. Chem.* **1997**, *62*, 8994-9000.

[118] Choi, I. S., Li, X., Simanek, E. E., Akaba, R., Whitesides, G. M. Self-Assembly of Hydrogen-Bonded Polymeric Rods Based on the Cyanuric Acid.Melamine Lattice. *Chem. Mater.* **1999**, *11*, 684-690.

[119] Braga, D., Desiraju, G. R., Miller, J. S., Orpen, A. G., Price, S. L. Innovation in crystal engineering. *Cryst. Eng. Commun.* **2002**, *4*, 500-509.

[120] Chen, C.-T., Suslick, K. S. One-dimensional coordination polymers: applications to material science. *Coord. Chem. Rev.* **1993**, *128*, 293-322.

[121] Bunz, U. H. F. Poly(aryleneethynylene)s: Syntheses, Properties, Strucutres, and Applications. *Chem. Rev.* **2000**, *100*, 1605-1644.

[122] Beck, J. B., Ineman, J. M., Rowan, S. J. Metal/Ligand-Induced Formation of Metallo-Supramolecular Polymers. *Macromolecules* **2005**, *38*, 5060-5068.

[123] Flory, P. J., *Principles of Polymer Chemistry*, Cornell Univ. Press, Ithaca, **1953**.

[124] Sijbesma, R. P., Beijer, F. H., Brunsveld, L., Folmer, B. J. B., Ky Hirschberg, J. H. K., Lange, R. F. M., Lowe, J. K. L., Meijer, E. W. Reversible polymers formed from self-complementary monomers using quadruple hydrogen bonding. *Science* **1997**, *278*, 1601-1604.

[125] Fouquey, C., Lehn, J. M., Levelut, A. M. Molecular recognition directed self-assembly of supramolecular liquid crystalline polymers from complementary chiral components. *Adv. Mater.* **1990**, *2*, 254-257.

[126] Würthner, F., Thalacker, C., Sautter, A., Schärtl, W., Ibach, W., Hollricher, O. Hierarchical self-organization of perylene bisimide-melamine assemblies to fluorescent mesoscopic superstructures. *Chem. Eur. J.* **2000**, *6*, 3871-3886.

[127] Bosman, A. W., Sijbesma, R. P., Meijer, E. W. Supramolecular polymers at work. *Mater. Today* **2004**, *7*, 34-39.

[128] Söntjens, S. H. M., Sijbesma, R. P., van Genderen, M. H. P., Meijer, E. W. Stability and lifetime of quadruply hydrogen bonded 2-ureido-4[1H]-pyrimidinone dimers. *J. Am. Chem. Soc.* **2000**, *122*, 7487-7493.

[129] Corbin, P. S., Zimmerman, S. C. Self-Association without Regard to Prototropy. A Heterocycle That Forms Extremely Stable Quadruply Hydrogen-Bonded Dimers. *J. Am. Chem. Soc.* **1998**, *120*, 9710-9711.

[130] Park, T., Zimmerman, S. C., Nakashima, S. A Highly Stable Quadruply Hydrogen-Bonded Heterocomplex Useful for Supramolecular Polymer Blends. *J. Am. Chem. Soc.* **2005**, *127*, 6520-6521.

[131] Dankers, P. Y. W., Harmsen, M. C., Brouwer, L. A., Van Luyn, M. J. A., Meijer, E. W. A modular and supramolecular approach to bioactive scaffolds for tissue engineering. *Nature Mater.* **2005**, *4*, 568-574.

[132] Schenning, A. P. H. J., Meijer, E. W. Supramolecular electronics; nanowires from self-assembled p-conjugated systems. *Chem. Commun.* **2005**, 3245-3258.

[133] Kauffman, G. B., Girolami, G. S., Busch, D. H. John C. Bailar, Jr. (1904-1991): father of coordination chemistry in the United States. *Coord. Chem. Rev.* **1993**, *128*, 1-48.

[134] Bailar, J. C., Jr. Coordination polymers. *Prep. Inorg. React.* **1964**, *1*, 1-27.

[135] Kitagawa, S., Kitaura, R., Noro, S.-i. Functional porous coordination polymers. *Angew. Chem. Int. Ed.* **2004**, *43*, 2334-2375.

[136] Dobrawa, R., Würthner, F. Metallosupramolecular approach toward functional coordination polymers. *J. Polym. Sci., Part A: Polym. Chem.* **2005**, *43*, 4981-4995.

[137] Ciardelli, F., Tsuchida, E., Woehrle, D., *Macromolecule-Metal Complexes*, Springer, Berlin, **1996**.

[138] Velten, U., Rehahn, M. First synthesis of solbule, well defined coordination polymers from kinetically unstable copper(I) complexes. *Chem. Commun.* **1996**, 2639-2640.

[139] Velten, U., Lahn, B., Rehahn, M. Soluble, well-defined copper(I) and silver(I) coordination polymers from 4,4"-bis((9-aryl)-2-o-phenanthrolinyl)-2',5'-dihexyl-p-terphenyl. *Macromol. Chem. Phys.* **1997**, *198*, 2789-2816.

[140] Hanack, M., Hirsch, A., Lehmann, H. Soluble, oligomeric bridged phthalocyaninatoiron(II) complexes. *Angew. Chem., Int. Ed. Engl.* **1990**, *29*, 1467-1468.

[141] Michelsen, U., Hunter, C. A. Self-Assembled porphyrin polymers. *Angew. Chem. Int. Ed.* **2000**, *39*, 764-767.

[142] Kimura, M., Sano, M., Muto, T., Hanabusa, K., Shirai, H. Self-assembly of twisted bridging ligands to helical coordination polymers. *Macromolecules* **1999**, *32*, 7951-7953.

[143] Schmatloch, S., Schubert, U. S. Engineering with metallo-supramolecular polymers: Linear coordination polymers and networks. *Macromol. Symp.* **2003**, *199*, 483-497.

[144] Holyer, R. H., Hubbard, C. D., Kettle, S. F. A., Wilkins, R. G. The kinetics of replacement reactions of complexes of the transition metals with 2,2',2''-terpyridine. *Inorg. Chem.* **1966**, *5*, 622-625.

[145] Dobrawa, R., Würthner, F. Photoluminescent supramolecular polymers: metal-ion directed polymerization of terpyridine-functionallized perylene bisimide dyes. *Chem. Commun.* **2002**, 1878-1879.

[146] El-Ghayoury, A., Schenning, A. P. H. J., Meijer, E. W. Synthesis of π-conjugated oligomer that can form metallo polymers. *J. Poly. Sci. Part A.: Polym. Chem.* **2002**, *40*, 4020-4023.

[147] Iyer, P. K., Beck, J. B., Weder, C., Rowan, S. J. Synthesis and optical properties of metallo-supramolecular polymers. *Chem. Commun.* **2005**, 319-321.

[148] Hofmeier, H., El-ghayoury, A., Schenning, A. P. H. J., Schubert, U. S. New supramolecular polymers containing both terpyridine metal complexes and quadruple hydrogen bonding units. *Chem. Commun.* **2004**, 318-319.

[149] Hofmeier, H., Hoogenboom, R., Wouters, M. E. L., Schubert, U. S. High Molecular Weight Supramolecular Polymers Containing Both Terpyridine Metal Complexes and Ureidopyrimidinone Quadruple Hydrogen-Bonding Units in the Main Chain. *J. Am. Chem. Soc.* **2005**, *127*, 2913-2921.

Chapter 2

Self-Assembly of Novel Architectures Using Metallated Pincer Complexes

2.1 Abstract

In this chapter the metallated pincer complex is described and introduced as a powerful supramolecular synthon for the synthesis of both finite and infinite architectures. An overview of its current uses by supramolecular scientist, and a description of why and how was used for this thesis research are given.

2.2 Introduction

The major goal of this thesis was to self-assemble new well-defined functional architectures from simpler preprogrammed covalent building blocks. The ultimate architectures will be supramolecular membranes and novel coordination polymers. Several design elements must be addressed to realize these goals. Both projects require two types of supramolecular synthons to elicit the desired properties.

Currently, there are very few reports of peptide-organometallic supramolecular architectures, and in the majority of these reports the metal-coordination stabilizes naturally occurring architectures such as helices, coils or loops.[1-8] We have self-assembled well-defined peptide synthons with angular and rigid metal recognition units to create novel and functional architectures. A supramolecular peptidal membrane having tunable pores, with respect to diameter and function, was chosen as our first target. Requisite for this goal, we designed a cyclic peptide decorated with ligands on the periphery.[9] A cyclic peptide was chosen due to its attractive self-assembling and

transport properties, as well as its synthetically amenable biological scaffold. The ligands on its periphery are able to coordinate to ditopic metal complexes, ideally giving a large porous membrane, Scheme 2.1 depicts a cartoon of the first generation of this supramolecular architecture.

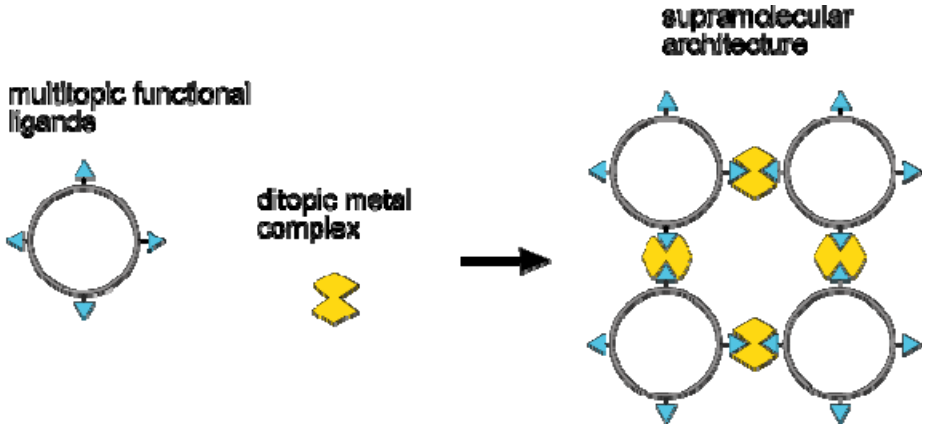

Scheme 2.1 Cartoon depicting the first generation of a supramolecular membrane structure.

For our polymer project, we chose to incorporate cruciform molecules into a supramolecular network. Cruciforms are a class of conjugated "X-shaped" molecules with unique electro-optical properties, which may have potential applications in light emitting devices. However, polymeric cruciform systems will have properties more amenable to solution processing, thus simplifying device fabrication. Before this study, a supramolecular polymeric cruciform system had not been investigated; a supramolecular strategy incorporates the best features of both a small molecule and polymeric system. This design required a cruciform synthon having terminal ligands along one axis that formed an infinite polymeric architecture when coordinated to a ditopic metal complex, as depicted in Scheme 2.2. By switching out one cruciform synthon for another

cruciform, with a different emission and coordination strength, a set of related polymeric materials having a range of physical and photophysical properties were rapidly prepared.

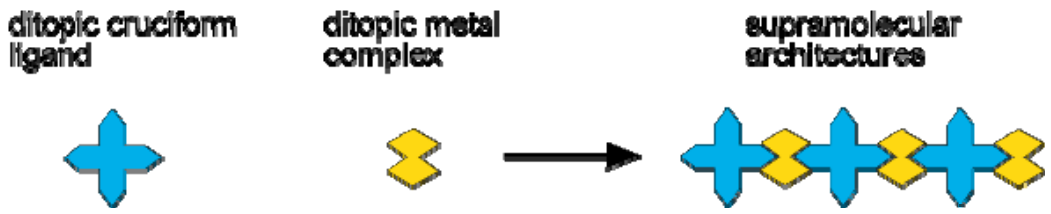

Scheme 2.2 Cartoon of supramolecular polymer.

2.3 Metallated Pincer Complexes

The second synthon for both projects was a metal complex recognition unit, which will acted primarily as a cohesive structural agent holding together the respective supramolecular frameworks. This synthon was required to have a thermodynamically strong and kinetically reversible complexation, which was quick and quantitative in apolar and polar solvents. To create the proposed architectures the recognition needed to also be highly directional and angularly rigid. All of these design elements were satisfied via metal-coordination between a ligand and a transition-metal complex.

Metallated pincer complexes are a popular recognition motif for incorporation into supramolecular synthons owing to their unique properties which met the above design requirements.[10] The metallated pincer complex, named after the pincer military formation where the attack occurs from two flanks and the front, has a central aromatic core with 2,6 substituted donor arms. These arms wraps around the metal center with a tridentate chelation.[11] The ligand then cyclometallates via two dative bonds between the 2,6 neutral 2-electron donors (E), commonly nitrogen, phosphorus or sulfur atoms, and

the metal ion. The metal center (Pd, Pt) then forms a strong organometallic σ-bond to the 1-carbon (C) giving the pincer complexes an ECE nomenclature, substituents at the 4-position can be used to tune the electronics of the system or for tethering of a functional unit.[10, 12-14] Examples of common pincer ligands and the cyclometallation are shown in Figure 2.1.

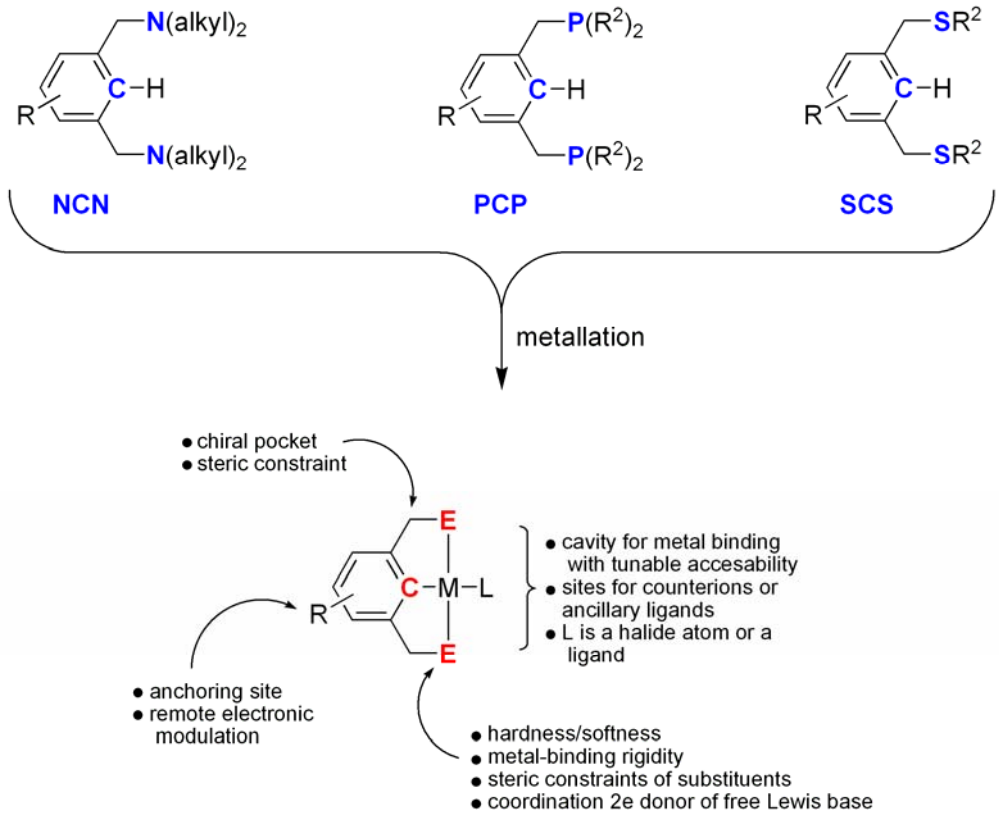

Figure 2.1 Common ECE pincer ligands before and after cyclometallation.[10]

The steric demands of the ligand on the metal center, gives the complex limited reactivity at this position. The most frequently encountered pincer complexes are SCS (Sulfur-Carbon-Sulfur),[12-27] PCP (Phosphorus-Carbon-Phosphorus)[28, 29] and NCN (Nitrogen-Carbon-Nitrogen) complexes,[11, 30-45] the donor atoms have different activation

potentials (S < N < P), thus SCS pincer complexes can only be cyclopalladated, and NCN pincer comlexes may be cyclopalladated or –platinated.[10]

The coordination around the metal ion of this 16e$^-$ neutral complex has a square planar geometry with the fourth coordination site 180° from the C-M bond usually occupied by a halide atom.[10] This halide atom may be abstracted via chemo-activation with a suitable silver salt ($AgBF_4$, AgOTf, $AgNO_3$) precipitating a silver halide and creating a cationic 16e$^-$complex with an open coordination site and a noncoordinating counterion. This open site has been shown by NMR to be occupied by a solvent molecule but has a strong coordination to select ligand classes,[46] specifically: nitriles < pyridines < thioureas < phosphines, which displace the solvent or weaker bound ligand to form a chemo-reversible bond, as shown in Figure 2.2.

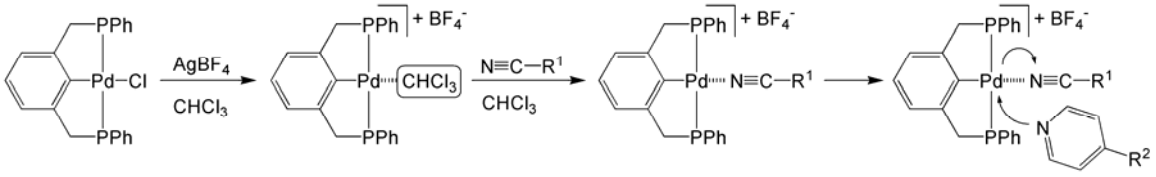

Figure 2.2 Metallated pincer complex activation via halide abstraction and subsequent ligand displacement by a functionalized nitrile and then a functionalized pyridine.

Supramolecular chemist are fond of this particular metal-ligand interaction because of its easily activated, fast and quantitative coordination, which has been exploited to quickly grow an architecture under mild ambient conditions. The single site and directional coordination gives a well-defined architecture, and the ligands can have pendant tethering units providing additional means for functionalization. Finally, because of the established and predicable coordination strength of the above ligand

classes, a weaker ligand may be quantitatively displace by a stronger one easily providing hierarchical architectures.

2.4 Prior Supramolecular Uses of Metallated Pincer Complexes

Reinhoudt has carried out extensive work using both ligand displacement and hierarchical self-assembly strategies to create novel nanostructures such as metallodendrimers using both divergent and convergent synthetic strategies with bifunctional SCS-Pd –cyano and/or -pyridyl dendrons,[12, 17, 18, 22] and multimetallic Ni, Pd and Pt containing dendrimers, metallated from PCP-phosphino pincer complexes.[29] Reinhoudt later used an orthogonal self-assembly methodology to synthesize a unique hierarchical dendrimer with a self-assembled convergent H-bonded rosette core and metallated pincer dendrites grown divergently outward.[21] Shown in Figure 2.3 is the divergent growth of generation three of Reinhoudt's SCS-palladated metallodendrimer.[22]

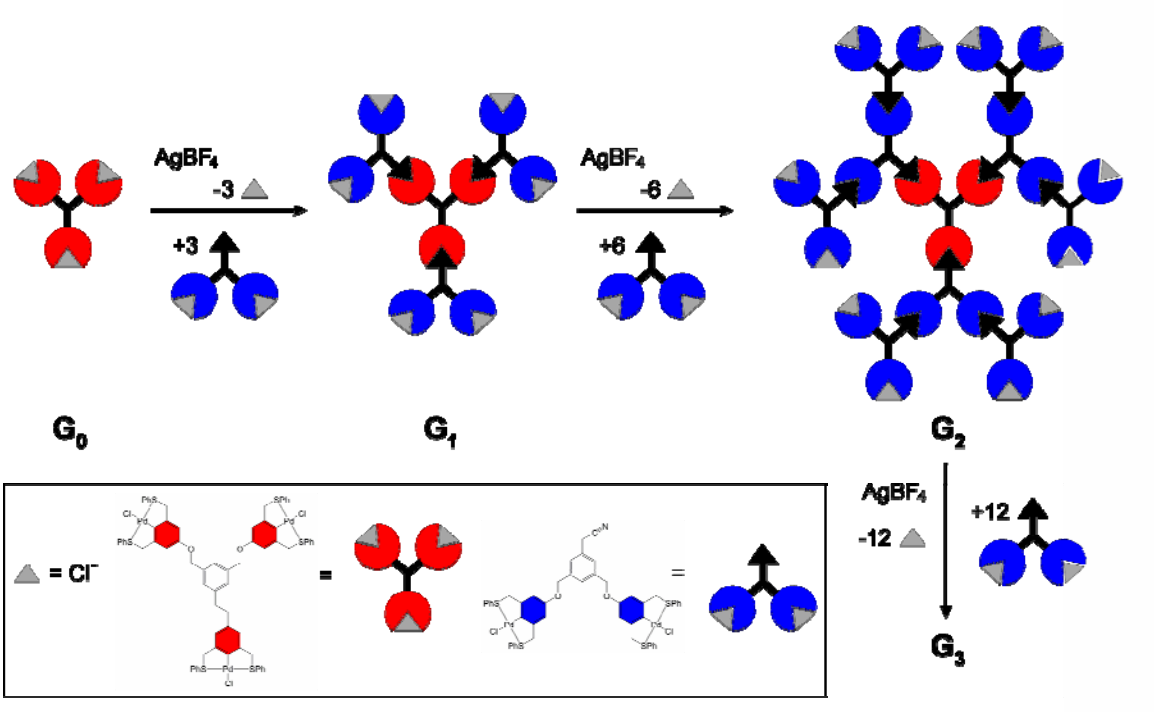

Figure 2.3 Divergent growth of a G3 Pd-metallodendrimer.[22]

Most recently, Reinhoudt has focused on attaching pincer complexes to surfaces in self-assembled monolayers (SAMs), developing "bottom-up" supramolecular strategies, for the controlled placement of metal nanoclusters on the functionalized SAMs, as shown in Figure 2.4.[19] In these reports organometallic dendrimers are grown divergently outward from a single surface bound metallated pincer species giving well-defined nanosized systems.[16, 19, 20]

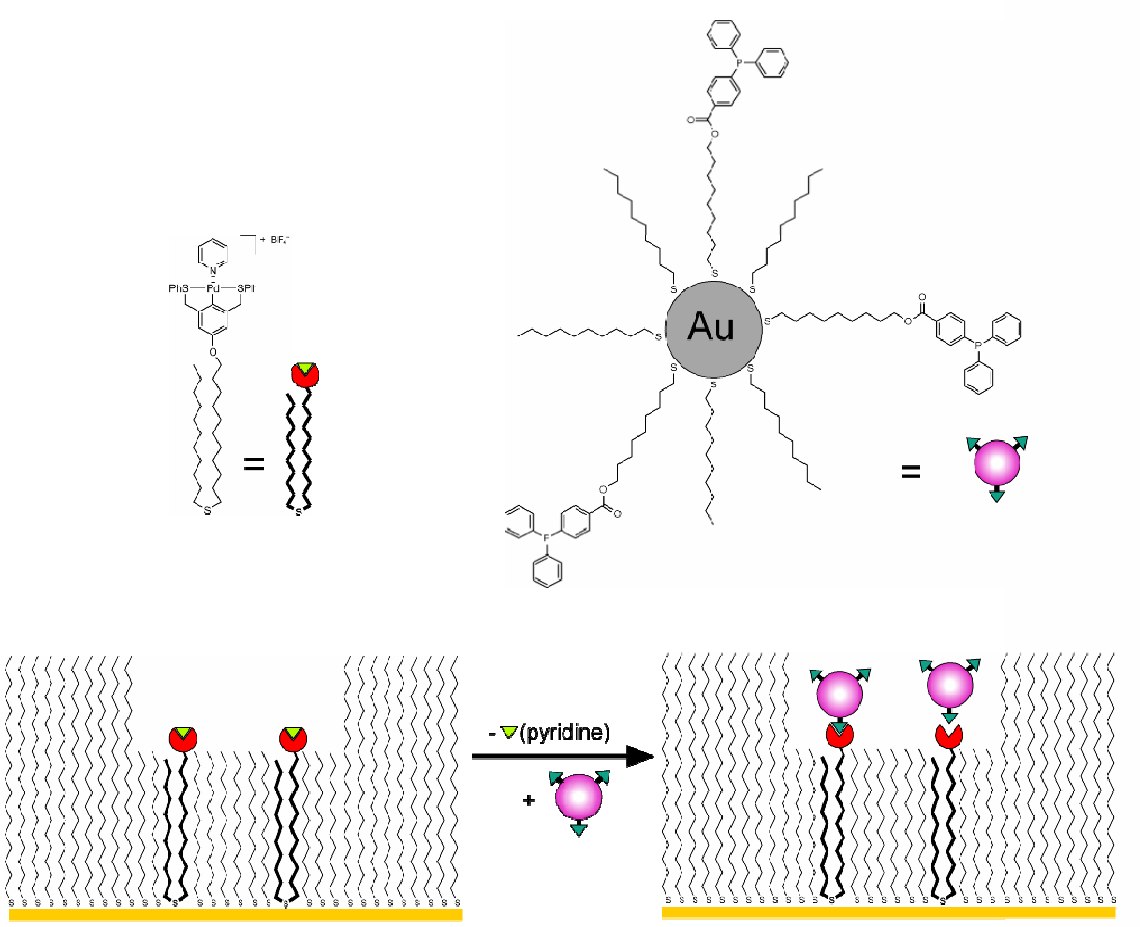

Figure 2.4 Controlled placement of Gold nanoparticles on a pincer complex functionalized SAM.[19]

A second cyclometallation step may be carried out at the 4-position of a 2,3,4,5 donor substituted aromatic core giving bimetallic pincer complexes. These metallated bis-pincer complexes have a planar and rigid 180° ditopic coordination geometry making them ideal synthons for building up supramolecular architectures via their linear coordination geometries. Loeb and van Koten synthesized the first SCS[47] and NCN complexes,[36, 37] respectively, shown in Figure 2.5.

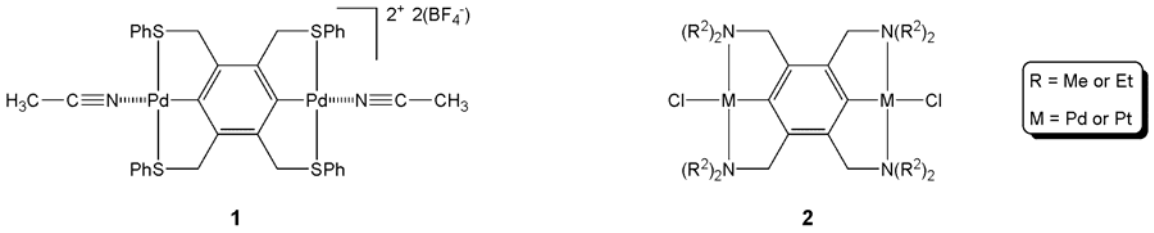

Figure 2.5 Linear ditopic bimetallic pincer complexes **1**[47] and **2**.[36, 37]

Loeb pioneered self-assembly studies with metallated pincer complexes in 1993 using **1** to form infinite CP **3** via coordination with 1:1 stoichiometric ratio of ditopic pyrazine, shown in Figure 2.6.[47] Loeb later coordinated a ditopic phenanthroline unit to **1** forming thermodynamically stable hexameric architecture **4**, shown in Figure 2.6, in quantitative yields.[48] Most recently, Loeb used a monometallic SCS-Pd pincer complex to make a calixarene metalloreceptor, which had a high selectivity for phenylpyridines.[49]

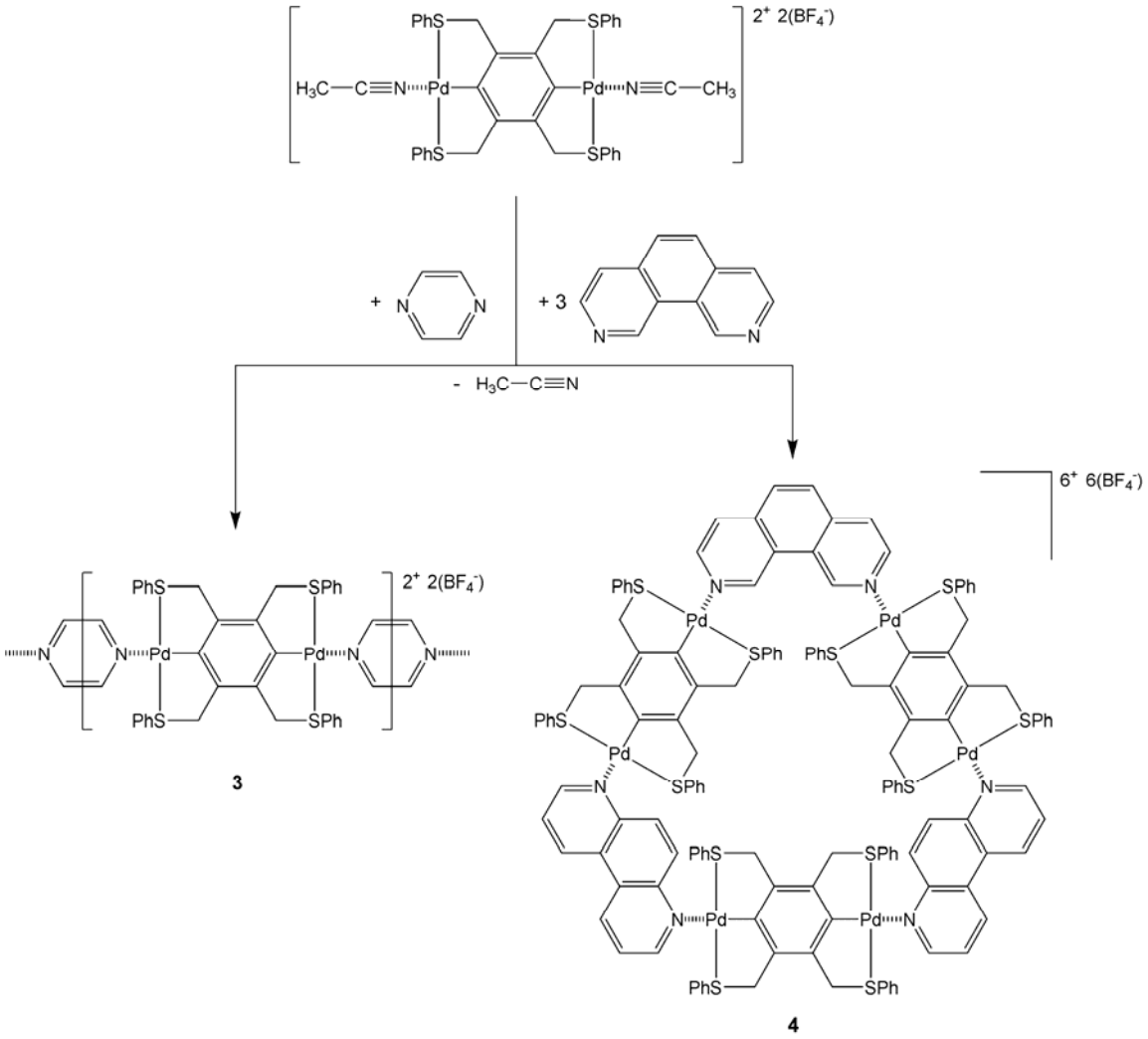

Figure 2.6 Loeb's infinite, **3**[47] and finite, **4**[48] supramolecular architectures.

Van Koten used the fast and reversible Lewis acid-base complexation of NCN-Pt complexes with SO_2(g) in the crystalline solid-state, which lead to a reversible and quantitative transformation of the crystal lattice structure. This system, shown in Figure 2.7, was proposed as a potential SO_2 activated sensor or switch.[39, 40]

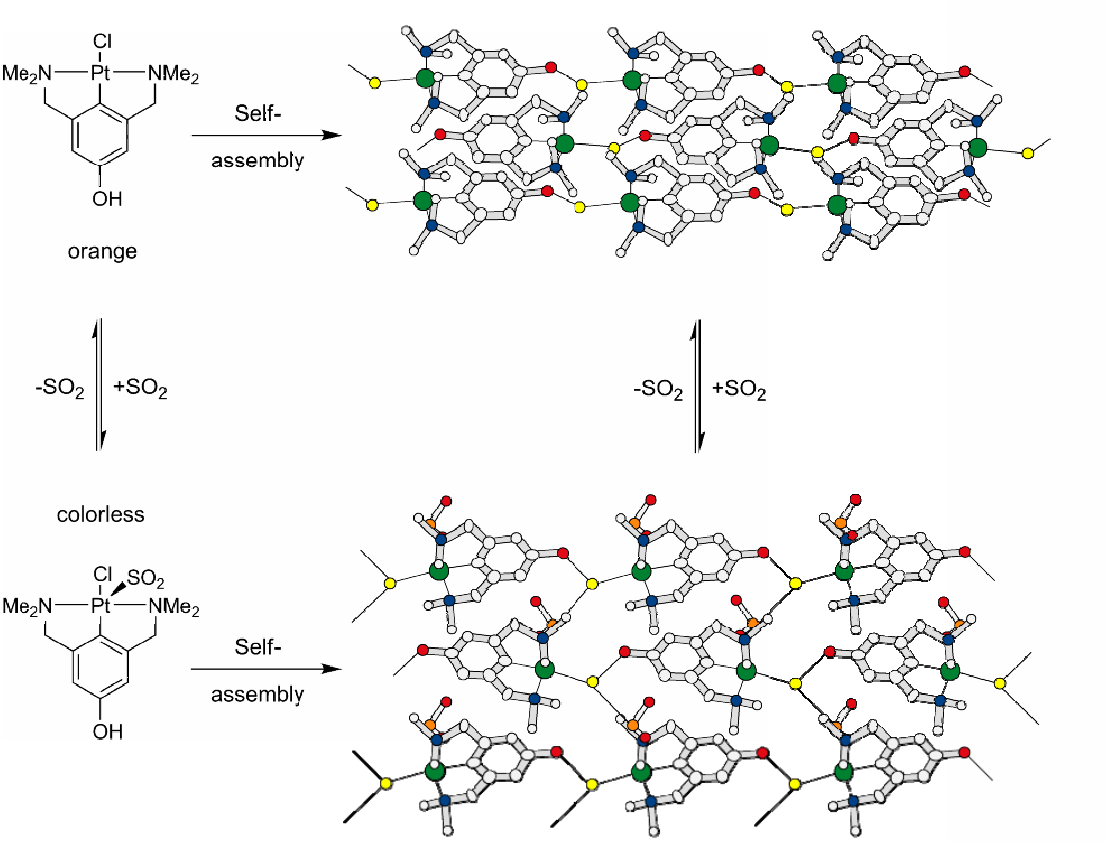

Figure 2.7 van Koten's reversible solid-state SO_2(g) sensor.[40]

More recently, Craig and Weck used metallated pincer complexes for the synthesis of main-chain,[14, 41] side-chain[13, 24, 25] and cross-linked[27, 42, 43, 45] supramolecular polymeric systems. Craig used the self-assembly of functional metallated pincer complexes to examine the dynamics of supramolecular assemblies in order to engineer their final properties. Craig primarily studied the dynamic behavior of NCN-Pd and -Pt main-chain[41] and cross-linked polymers[42, 43, 45] examining different substituents on the E-donor arms of pincer ligand and their effects on the dissociation constant (K_{diss}) and thus physical polymeric properties and cross-linking behavior. Dynamic cross-linking of poly(vinylpyridine) (PVP) via a Pd or Pt complex is shown in Figure 2.8.[45] The cross-

linking is more pronounced when R is an ethyl group due to a slower K_{diss} even though the methyl system has a similar K_a.

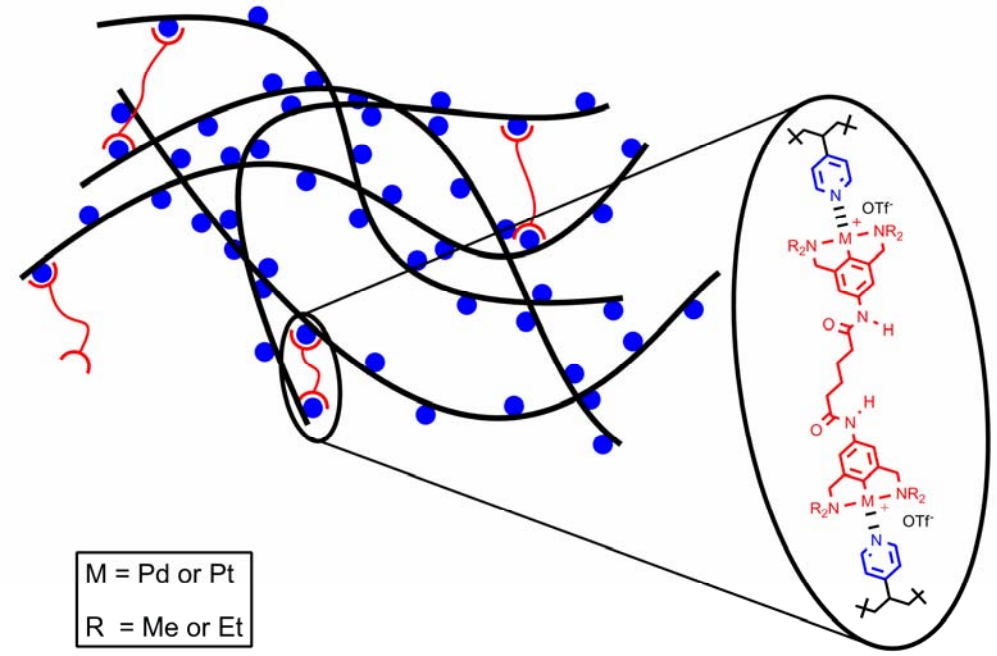

Figure 2.8 Craig's dynamic metal-coordinated cross-linking of PVP.[45]

Weck used an SCS-Pd pincer complex or one of its ligands as side-chain metal-coordinating synthons along a poly(norbornene) backbone in an orthogonal functionalization strategy along with DAP H-bonding side-chain synthons, creating the 'universal polymer backbone' shown in Figure 2.9.[13] Weck used this strategy for rapid optimization of supramolecular polymeric materials through multifunctionalization and for strong vs. weak supramolecularly cross-linking methodologies.[24, 27]

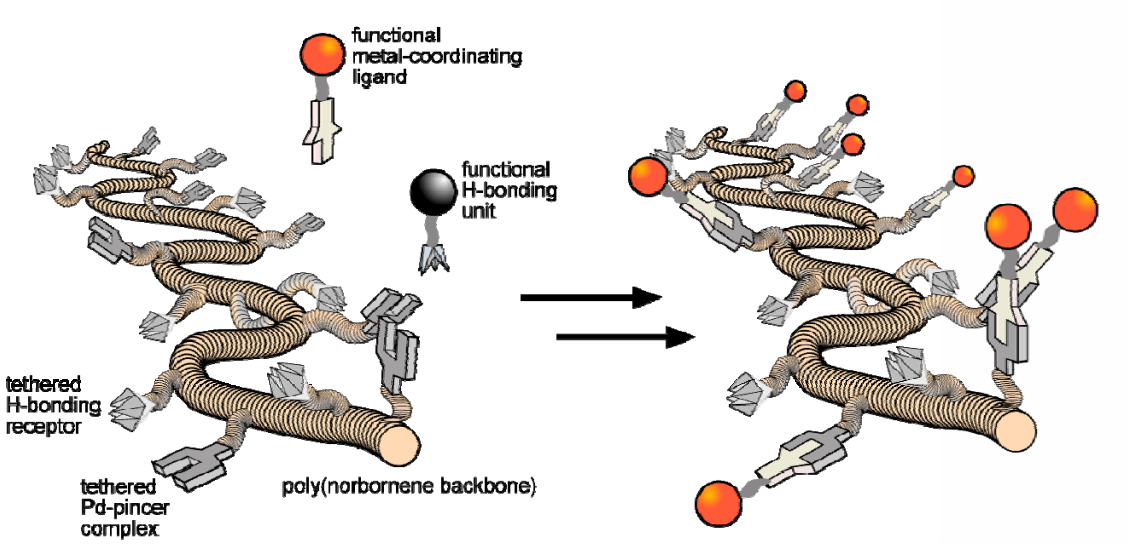

Figure 2.9 Weck's 'universal polymer backbone', orthogonal functionalization of metallated pincer complexes shown.[13]

Reliable supramolecular synthons should have fast, strong and selective recognitions, thus ensuring the formation of kinetically and thermodynamically favored supramolecular architectures. Metallated pincer complexes have been shown by Weck and others to be excellent candidates, satisfying all of these requirements.

All of the provided reports are synthetic accomplishments displaying the ingenuity and creativity of the respective researcher. However, self-assembly studies using metallated pincer complexes have not been carried out on any biological systems. Based on their strong coordination in polar solvents they may be well suited for this role. Furthmore, the majority of the pincer complex polymeric studies were dedicated to side-chain functionalization strategies, or the elucidation of the fundamental behavior of main-chain coordinated polymers as opposed to the development of new functional supramolecular materials. This thesis research has built upon these early investigations making new supramolecular biologically relevant peptide architectures and functional coordination polymeric materials.

2.5 References

[1] Di Costanzo, L., Geremia, S., Randaccio, L., Ichino, T., Yanagihara, R., Yamada, T., Marasco, D., Lombardi, A., Pavone, V. Conformational and coordination properties of a peptide containing the novel a,a-bis(2-pyridyl)glycine amino acid. *Dalton Trans.* **2003**, 787-792.

[2] Di Costanzo, L., Wade, H., Geremia, S., Randaccio, L., Pavone, V., DeGrado, W. F., Lombardi, A. Toward the de novo design of a catalytically active helix bundle: A substrate-accessible carboxylate-bridged dinuclear metal center. *J. Am. Chem. Soc.* **2001**, *123*, 12749-12757.

[3] Doerr, A. J., McLendon, G. L. Design, Folding, and Activities of Metal-Assembled Coiled Coil Proteins. *Inorg. Chem.* **2004**, *43*, 7916-7925.

[4] Gilmartin, B. P., Ohr, K., McLaughlin, R. L., Koerner, R., Williams, M. E. Artificial oligopeptide scaffolds for stoichiometric metal binding. *J. Am. Chem. Soc.* **2005**, *127*, 9546-9555.

[5] Iyer, P. K., Beck, J. B., Weder, C., Rowan, S. J. Synthesis and optical properties of metallo-supramolecular polymers. *Chem. Commun.* **2005**, 319-321.

[6] Ohr, K., Gilmartin, B. P., Williams, M. E. Pyridine-Substituted Oligopeptides as Scaffolds for the Assembly of Multimetallic Complexes: Variation of Chain Length. *Inorg. Chem.* **2005**, *44*, 7876-7885.

[7] Schmuck, C., Wennemers, H., *Highlights in Bioorganic Chemistry: Methods and Applications*, VCH, Weinheim, **2004**.

[8] Tsurkan, M. V., Ogawa, M. Y. Metal-peptide nanoassemblies. *Chem. Commun.* **2004**, 2092-2093.

[9] Clark, T. D., Buriak, J. M., Kobayashi, K., Isler, M. P., McRee, D. E., Ghadiri, M. R. Cyclindrical β-sheet peptide assemblies. *J. Am. Chem. Soc.* **1998**, *120*, 8949-8962.

[10] Albrecht, M., van Koten, G. Platinum group organometallics based on "pincer" complexes: sensors, switches, and catalysts. *Angew. Chem. Int. Ed.* **2001**, *40*, 3750-3781

[11] van Koten, G. Tuning the reactivity of metals held in a rigid ligand environment. *Pure Appl. Chem* **1989**, *61*, 1681-1694.

[12] Huck, W. T. S., van Veggel, F. C. J. M., Kropman, B. L., Blank, D. H. A., Keim, E. G., Smithers, M. M. A., Reinhoudt, D. N. Large self-assembled organopalladium spheres. *J. Am. Chem. Soc.* **1995**, *117*, 8293-8294.

[13] Pollino, J. M., Stubbs, L. P., Weck, M. One-Step Multifunctionalization of Random Copolymers via Self-Assembly. *J. Am. Chem. Soc.* **2004**, *126*, 563-567.

[14] Higley, M. N., Pollino, J. M., Hollembeak, E., Weck, M. A modular approach toward block copolymers. *Chem. Eur. J.* **2005**, *11*, 2946-2953.

[15] van Manen, H.-J., Nakashima, K., Shinkai, S., Kooijman, H., Spek, A. L., van Veggel, F. C. J. M., Reinhoudt, D. N. Coordination chemistry of SCS PdII pincer systems. *Eur. J. Inorg. Chem.* **2000**, 2533-2540.

[16] Friggeri, A., van Manen, H.-J., Auletta, T., Li, X.-M., Zapotoczny, S., Schönherr, H., Vancso, G. J., Huskens, J., van Veggel, F. C. J. M., Reinhoudt, D. N. Chemistry on surface-confined molecules: an approach to anchor isolated functional units to surfaces. *J. Am. Chem. Soc.* **2001**, *123*, 6388-6395.

[17] Huck, W. T. S., Prins, L. J., Fokkens, R. H., Nibbering, N. M. M., van Veggel, F. C. J. M., Reinhoudt, D. N. Convergent and Divergent Noncovalent Synthesis of Metallodendrimers. *J. Am. Chem. Soc.* **1998**, *120*, 6240-6246.

[18] Huck, W. T. S., Van Veggel, F. C. J. M., Reinhoudt, D. N. Self-assembly of hyperbranched spheres. *J. Mater. Chem.* **1997**, *7*, 1213-1219.

[19] Li, X.-M., Auletta, T., van Veggel, F. C. J. M., Huskens, J., Reinhoudt, D. N. Directed, selective insertion of single molecules into patterned self-assembled monolayers of alkanethiols with different chain lengths. *Org. Biomol. Chem* **2004**, *2*, 296-300.

[20] van Manen, H.-J., Auletta, T., Dordi, B., Schönherr, H., Vancso, G. J., van Veggel, F. C. J. M., Reinhoudt, D. N. Non-covalent chemistry on surface-confined isolated dendrimers. *Adv. Funct. Mater.* **2002**, *12*, 811-818.

[21] Huck, W. T. S., Hulst, R., Timmerman, P., van Veggel, F. C. J. M., Reinhoudt, D. N. Noncovalent synthesis of nanostructures: combining coordination chemistry and hydrogen bonding. *Angew. Chem., Int. Ed. Engl.* **1997**, *36*, 1006-1008.

[22] Huck, W. T. S., van Veggel, F. C. J. M., Reinhoudt, D. N. Controlled assembly of nanosized metallodendrimers. *Angew. Chem., Int. Ed. Engl.* **1996**, *35*, 1213-1215.

[23] Gerhardt, W. W., Zucchero, A. J., Wilson, J. N., South, C. R., Bunz, U. H. F., Weck, M. Supramolecular cruciforms. *Chem. Commun.* **2006**, 2141-2143.

[24] Pollino, J. M., Weck, M. Supramolecular side-chain functionalized polymers: synthesis and self-assembly behavior of polynorbornenes bearing PdII SCS pincer complexes. *Synthesis* **2002**, 1277-1285.

[25] Pollino, J. M., Weck, M. Tandem Catalysis and Self-Assembly: A One-Pot Approach to Functionalized Polymers. *Org. Lett.* **2002**, *4*, 753-756.

[26] Gerhardt, W. W., Weck, M. Investigations of Metal-Coordinated Peptides as Supramolecular Synthons. *J. Org. Chem.* **2006**, *71*, 6333-6341.

[27] Pollino, J. M., Nair, K. P., Stubbs, L. P., Adams, J., Weck, M. Crosslinked and functionalized universal polymer backbones via simple, rapid, and orthogonal multi-site self-assembly. *Tetrahedron* **2004**, *60*, 7205-7215.

[28] Moulton, C. J., Shaw, B. L. Transition Metal-Carbon Bonds. Part XLII. Complexes of Nickel, Palladium, Platinum, Rhodium and Iridium with the Tridentate Ligand 2,6-Bis[(di-t-butylphospino)methyl]phenyl. *J. Chem. Soc. Dalton Trans.* **1976**, 1020-1024.

[29] Huck, W. T. S., Snellink-Ruël, B., van Veggel, F. C. J. M., Reinhoudt, D. N. New building blocks for the noncovalent assembly of homo- and hetero-multinuclear metallodendrimers. *Organometallics* **1997**, *16*, 4287-4291.

[30] Stiriba, S.-E., Slagt, M. Q., Kautz, H., Gebbink, R. J. M. K., Thomann, R., Frey, H., van Koten, G. Synthesis and supramolecular association of immobilized NCN-pincer platinum(II) complexes on hyperbranched polyglycerol supports. *Chem. Eur. J.* **2004**, *10*, 1267-1273.

[31] Guillena, G., Rodríguez, G., Albrecht, M., van Koten, G. Covalently bonded platinum(II) complexes of a-amino acids and peptides as a potential tool for protein labeling. *Chem. Eur. J.* **2002**, *8*, 5368-5376.

[32] Guillena, G., Rodríguez, G., van Koten, G. Palladium(II) pincer complexes of a-amino acids: towards the synthesis of catalytically active artificial peptides. *Tetrahedron Lett.* **2002**, *43*, 3895-3898.

[33] Dijkstra, H. P., Kruithof, C. A., Ronde, N., van de Coevering, R., Ramón, D. J., Vogt, D., van Klink, G. P. M., van Koten, G. Shape-Persistent Nanosize Organometallic Complexes: Synthesis and Application in a Nanofiltration Membrane Reactor. *J. Org. Chem.* **2003**, *68*, 675-685.

[34] Amijs, C. H. M., Berger, A., Soulimani, F., Visser, T., van Klink, G. P. M., Lutz, M., Spek, A. L., van Koten, G. Neutral Puridyl-Functionalized C, N-ortho-Chelated Aminoaryl Platinum(II) Corner Building Blocks for Application in Coordination Reactions. *Inorg. Chem.* **2005**, *44*, 6567-6578.

[35] Slagt, M. Q., Rodríguez, G., Grutters, M. M. P., Gebbink, R. J. M. K., Klopper, W., Jenneskens, L. W., Lutz, M., Spek, A. L., van Koten, G. Synthesis and properties of para-substituted NCN-pincer palladium and platinum complexes. *Chem. Eur. J.* **2004**, *10*, 1331-1344.

[36] Steenwinkel, P., James, S. L., Grove, D. M., Kooijman, H., Spek, A. L., van Koten, G. Double Cyclometalation via Carbon-Silicon Bond Cleavage by Palladium(II) Acetate. X-ray Structure of a Cationic 1,4-Dipalladated Benzene Ring and Selective Synthesis of Heterobimetallic 1,4-Phenylene-Bridged Platinum(II)-Palladium(II) Complexes. *Organometallics* **1997**, *16*, 513-515.

[37] Steenwinkel, P., Kooijman, H., Smeets, W. J. J., Spek, A. L., Grove, D. M., van Koten, G. Intramolecularly Stabilized 1,4-Phenylene-Bridged Homo- and Heterodinuclear Palladium and Platinum Organometallic Complexes Containing N,C,N-Coordination Motifs; h1-SO2 Coordination and Formation of an Organometallic Arenium Ion Complex with Two Pt-C s-Bonds. *Organometallics* **1998**, *17*, 5411-5426.

[38] Davies, P. J., Grove, D. M., van Koten, G. Advances in the Synthesis of Multimetallic Systems: Hydroxyl Group Protection in (Aryldiamine)platinum Species. *Organometallics* **1997**, *16*, 800-802.

[39] Albrecht, M., Lutz, M., Spek, A. L., van Koten, G. Organoplatinum crystals for gas-triggered switches. *Nature* **2000**, *406*, 970-974.

[40] Albrecht, M., Lutz, M., Schreurs, A. M. M., Lutz, E. T. H., Spek, A. L., van Koten, G. Self-assembled organoplatinum(II) supermolecules as crystalline, SO^2 gas-triggered switches. *J. Chem. Soc. Dalton Trans.* **2000**, 3797-3804.

[41] Yount, W. C., Juwarker, H., Craig, S. L. Orthogonal Control of Dissociation Dynamics Relative to Thermodynamics in a Main-Chain Reversible Polymer. *J. Am. Chem. Soc.* **2003**, *125*, 15302-15303.

[42] Yount, W. C., Loveless, D. M., Craig, S. L. Small-Molecule Dynamics and Mechanisms Underlying the Macroscopic Mechanical Properties of Coordinatively Cross-Linked Polymer Networks. *J. Am. Chem. Soc.* **2005**, *127*, 14488-14496.

[43] Loveless, D. M., Jeon, S. L., Craig, S. L. Rational Control of Viscoelastic Properties in Multicomponent Associative Polymer Networks. *Macromolecules* **2005**, *38*, 10171-10177.

[44] Kersey, F. R., Yount, W. C., Craig, S. L. Single-Molecule Force Spectroscopy of Bimolecular Reactions: System Homology in the Mechanical Activation of Ligand Substitution Reactions. *J. Am. Chem. Soc.* **2006**, *128*, 3886-3887.

[45] Yount, W. C., Loveless, D. M., Craig, S. L. Strong means slow: dynamic contributions to the bulk mechanical properties of supramolecular networks. *Angew. Chem. Int. Ed.* **2005**, *44*, 2746-2748.

[46] Kraatz, H.-B., Milstein, D. The reactions of tridentate cationic palladium(II) complexes with olefins and nucleophiles. *J. Organomet. Chem.* **1995**, *488*, 223-232.

[47] Loeb, S. J., Shimizu, G. K. H. Dimetalated thioether complexes as building blocks for organometallic coordination polymers and aggregates. *J. Chem. Soc., Chem. Commun.* **1993**, 1395-1397.

[48] Hall, J. R., Loeb, S. J., Shimizu, G. K. H., Yap, G. P. A. Supramolecular arrays of 4,7-phenanthroline complexes: self-assembly of molecular Pd6 hexagons. *Angew. Chem. Int. Ed.* **1998**, *37*, 121-123.

[49] Cameron, B. R., Loeb, S. J., Yap, G. P. A. Calixarene metalloreceptors. Synthesis and molecular recognition properties of upper-rim functionalized calix[4]arenes containing an organopalladium binding site. *Inorg. Chem.* **1997**, *36*, 5498-5504.

Chapter 3

Investigations of Metal-Coordinated Peptides as Biological Supramolecular Synthons

3.1 Abstract

This chapter describes the synthesis and controlled assembly of four model organometallic-peptide assemblies via coordination of a monometallic SCS-Pd pincer complex to four new unnatural pyridyl-tripeptides. This investigational study was carried out to determine if a metallated pincer complex is an adequate recognition unit for the self-assembly of peptidal supramolecular synthons in polar solvents. The assembly events were fully characterized and investigated by ^{1}H NMR, ES-MS, and isothermal titration calorimetry (ITC) to elucidate the coordination behavior of these new supramolecular synthons. Using these characterization techniques, we have shown that the metal-coordination events in all cases is quick and that in each case the peptide backbone does not interfere with the coordination. The ITC analyses showed that the 4–pyridyl tripeptides have a stronger coordination than their 3-pyridyl analogs to the metal center. The measured K_a's are comparable to other pincer-pyridine systems in DMSO suggesting that the controlled coordination of the metallated pincer/pyridine interaction is an interesting biological supramolecular synthon and will allow for the future development of supramolecular cyclic peptide-based nanoporous membranes.

3.2 Introduction

Organic supramolecular structures and assemblies hold great promise as building blocks for precision nano-materials and structures that are otherwise conceptually inaccessible.[1-5] Through the use of controlled metal-coordination at targeted positions in natural or synthetic peptides one might be able to design well-defined persistent architectures,[6-8] thereby creating self-assembled biologically relevant and unique materials. Herein, we present as a step towards this thesis goal the coordination of peptides with metallated pincer complexes, by embedding complementary recognition units in the peptide side-chain.

In biomacromolecules metal-coordination plays an essential role in many of life's processes.[9-11] In the burgeoning field of supramolecular chemistry, metal-coordination already has a vital role in the assembly of purely synthetic systems;[12-14] creating geometric and highly controlled architectures,[12-20] or functional polymeric materials.[21-32] However, its use in the assembly of biological supramolecular archtectures, specifically with peptides is not nearly as developed.

The early use of metal-coordination to control the design and folding of natural peptides was reported in 1990 by Ghadiri[33, 34] and Degrado.[35] Ghadiri coaxed short linear peptides to form helices by crosslinking the peptides with transition metal ions via side-chain coordination of two natural residues at the *i* and *i+4* positions, as shown in Figure 3.1. Degrado used the coordination of histidine residues to Zn^{2+} to fold a peptide into a structural approximation of the enzyme carbonic anhydrase.[36] Sasaki was the first to use unnatural ligands to self-assemble triple helix bundles by chelating Fe^{2+} with bipyridines covalently attatched to the peptides' N-termini.[37, 38]

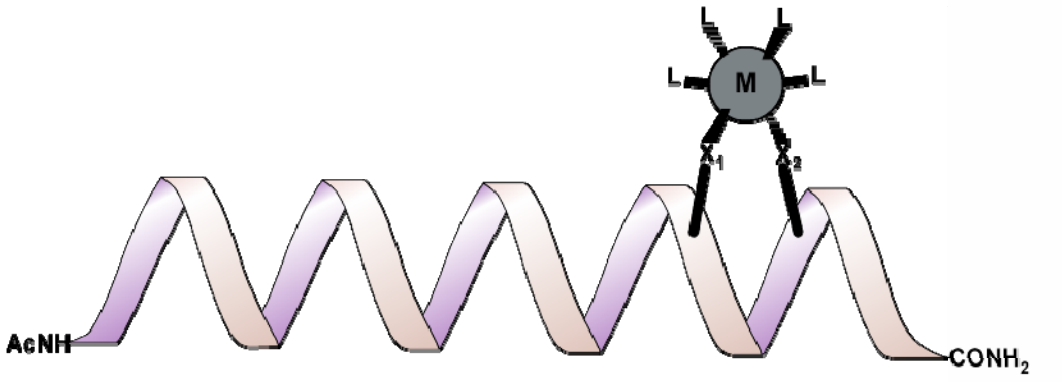

Figure 3.1 Ghadiri's metal-coordinated Helix, X_1= cysteine X_2= histidine, M= Zn^{2+}, Cd^{2+}, Ni^{2+} or Cu^{2+}.[33, 34]

The synthesis of peptides with unnatural residue side-chains was the next step towards greater complexity and control in metal-coordinating peptides. Novel synthetic residues preserve the peptide backbone and can be redefined *ad infinitum* creating diversity within supramolecular systems.[39] Towards this goal, Hopkins synthesized a peptide with two identical unnatural residues containing a diiminoacetic acid side-chain. Similar to Ghadiri's natural peptides this system only formed a helix in the presence of a chelating metal ion.[40]

After Hopkin's seminal work there were many reports using peptides with unnatural amino acids with metal-coordination to stabilize or create nanostructures such as helices,[41, 42] loops,[43] cycles,[39] and other scaffolds.[44-46]

Our report was the first study of peptides containing side-chain recognition units coordinated to a metallated pincer complex. We envision these peptides as models. Once fully understood, they may be situated into a cyclic peptide framework and coordinated with multi-functional/faceted metallated receptors, such as a ditopic bispincer complex, into larger networks and membrane architectures.

The metallated pincer complex was chosen as the metal-coordinating recognition unit,[47] because its chemo-activated, single site metal-coordination step was shown to be fast, quantitative, and chemo-reversible in a variety of solvents.[16, 41, 47-50] In this study, we specifically investigated the coordination between an SCS-Pd pincer complex and pyridyl ligands incorporated into the side-chains of our unnatural peptides. It was envisaged that this design strategy would open up a simple and direct avenue to new peptide-supramolecular structures, making the metallated pincer complex an ideal candidate for achieving our goals.

Currently, the only reported use of a metallated pincer complex with a peptide or an amino acid was described by van Koten.[51-53] In this case, NCN-Pt pincer and Pd pincer complexes were covalently attached to the N-terminus of an amino acid and then peptide chain, as shown in Figure 3.2. However, in their articles the authors did not describe this system as an assembly unit. Nevertheless, we evaluated their elegant approach as a possible strategy towards the controlled noncovalent synthesis of peptide-based materials. Unfortunately, the functionalization at the N-terminus of the peptide clearly limits the use of this design as a general synthon in metal-coordination based peptidal architectures.

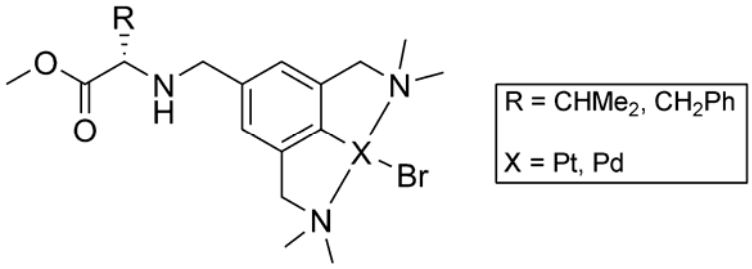

Figure 3.2 Metallated pincer complex terminated amino acids synthesized by van Koten.[51-53]

For our approach, we chose a pyridyl side-chain residue as a selective recognition unit for the metal-coordination to the SCS-Pd pincer complex. A pyridyl moiety was chosen as the functional side-chain since a) there are already a handful of reports using nitrogenous heteroaromatic side-chains as receptors for self-assembly in this area of supramolecular chemistry[41-46] and b) the use of pyridine as a ligand for metallated pincer complexes has been established over the last decade.[15, 25, 26, 32, 47, 48, 54, 55]

In this initial contribution we synthesized and investigated four tripeptides as supramolecular synthons **1**-**4**, shown in Figure 3.3, each with the unnatural pyridyl side-chain residue in the center being flanked by two terminally protected glycine residues.

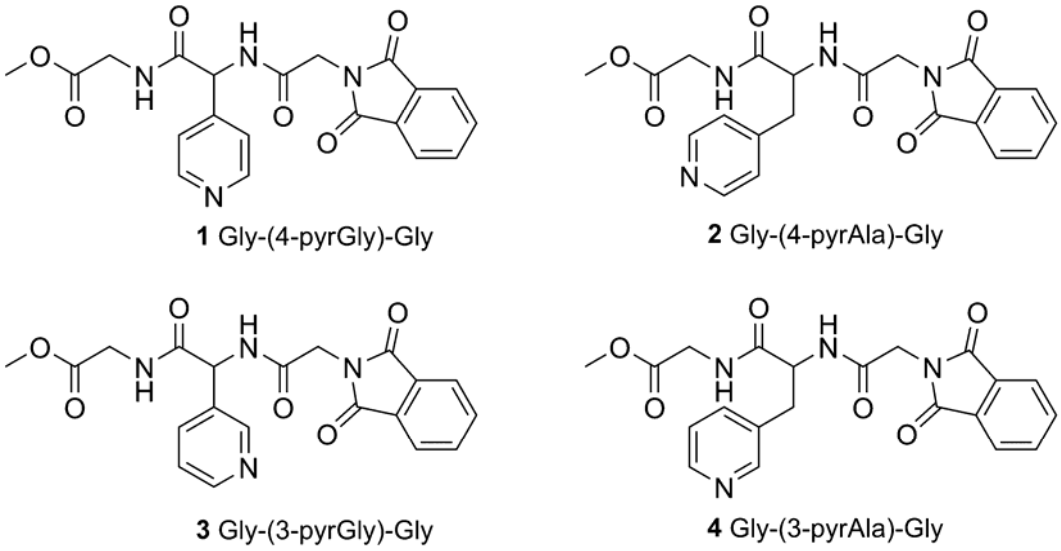

Figure 3.3 Four model tripeptides containing an unnatural pyridyl glycine or pyridyl alanine as the central residue.

Each of these four peptides had a different substitution pattern and spacing of the central pyridine side-chain from the peptide backbone. These variations were expected to lead to different coordination geometries and strengths. We studied the metal coordination capabilities of tripeptides **1**-**4** with *p*-methoxy SCS-Pd pincer complex **5** in

DMSO, shown in Figure 3.4, because a self-assembled biomaterial should have a strong labile interaction that is fast and quantitative in a polar environment. The behavior of each unique coordination event was characterized by ^{1}H NMR spectroscopy, ITC, and ES-mass spectroscopy to determine which substitution pattern and spacing distance is ideal for these model synthons, to establish K_a's, and to ascertain any influences of the peptide backbone on this coordination. Ultimately this detailed analysis allowed us to develop novel cyclic peptide supramolecular synthons, which may be coordinated with metallated pincer complexes giving architecturally complex biomaterials and scaffolds.

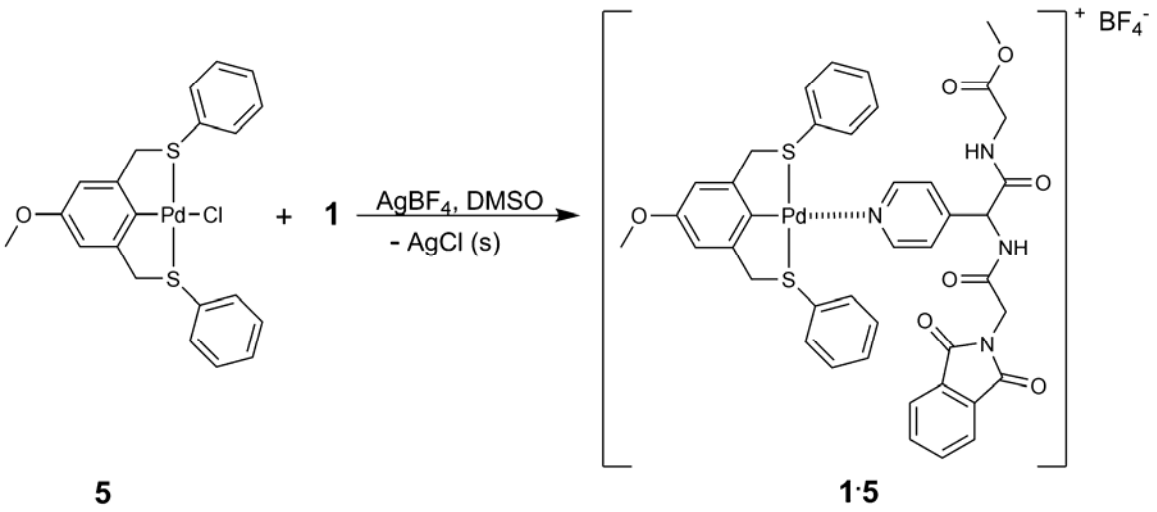

Figure 3.4 Activation and coordination of *p*-Methoxy SCS-Pd pincer complex **5** to tripeptide **1** in DMSO.

3.3 Results and Discussion

Metallated pincer complexes are known to coordinate to nitrogen containing heteroaromatic units other than pyridine, such as pyrazine.[32] Therefore, if histidine with its imidazole side-chain would coordinate quantitatively to metallated pincer complexes, histidyl peptides or related derivatives would be the simplest and most direct route

towards our goal. Therefore, we first examined the coordination of imidazole and methyl imidazole with a SCS-Pd pincer complex as a preliminary study. However, the ^{1}H NMR spectra of the metal-coordination of both imidazole and methyl imidazole to metallated pincer complexes showed no clear or strong coordination pattern indicating that no clean or controlled single metal-coordination event took place.

3.3.1 Peptide Synthesis

Based on the unsatisfactory imidazole/methyl imidazole-Pd pincer study, we used pyridine, which is the most common ligand for metallated pincer complexes,[47] in our design. The four distinct tripeptides (**1-4**) were made with a pyridyl-glycine or -alanine amino acid via solution-phase peptide synthesis using two different strategies, Scheme 3.1 shows the synthesis of the pyridyl-alanines and Scheme 3.2 shows the synthesis of the pyridyl-glycines. The C-termini of all tripeptides were protected as methyl esters and the N-termini were protected with a phthaloyl group. After purification by RP-HPLC, these tripeptides, except **1**, crystallized easily from a CH_3CN/water mixture.

3.3.2 Pyridyl Alanine Tripeptide Synthesis

Protected versions of the 3- and 4-pyridyl alanine amino acids were commercially available and tripeptides **2** and **4** were synthesized using conventional peptide coupling techniques. A nonfunctional isosteric phenylalanine tripeptide **6**, was also synthesized using this route with comparable yields, shown in Scheme 3.2.

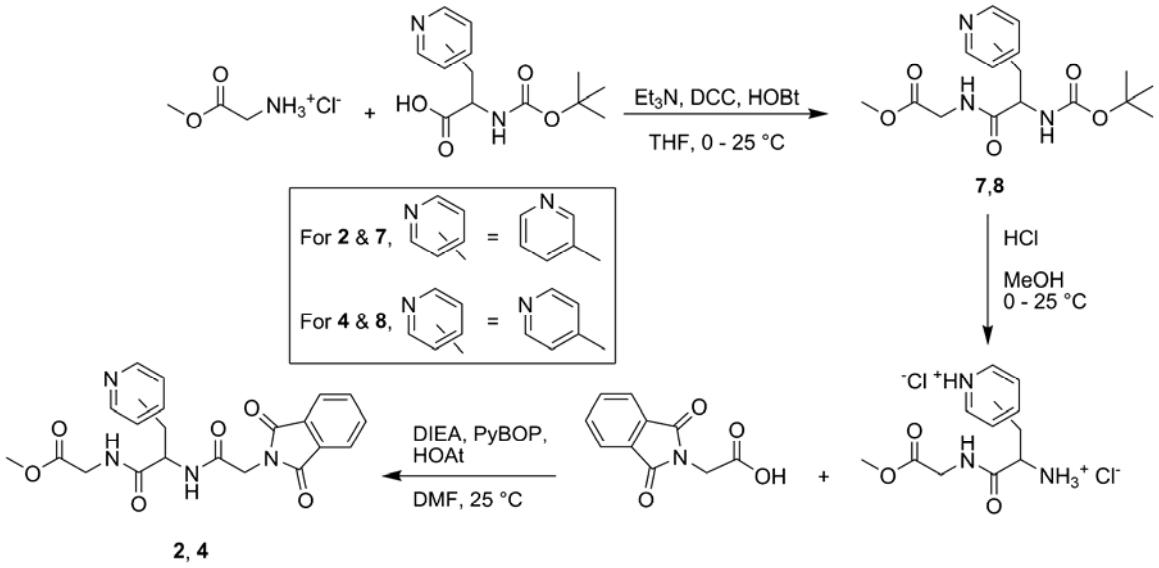

Scheme 3.1 Synthesis of tripeptides **2** and **4**.

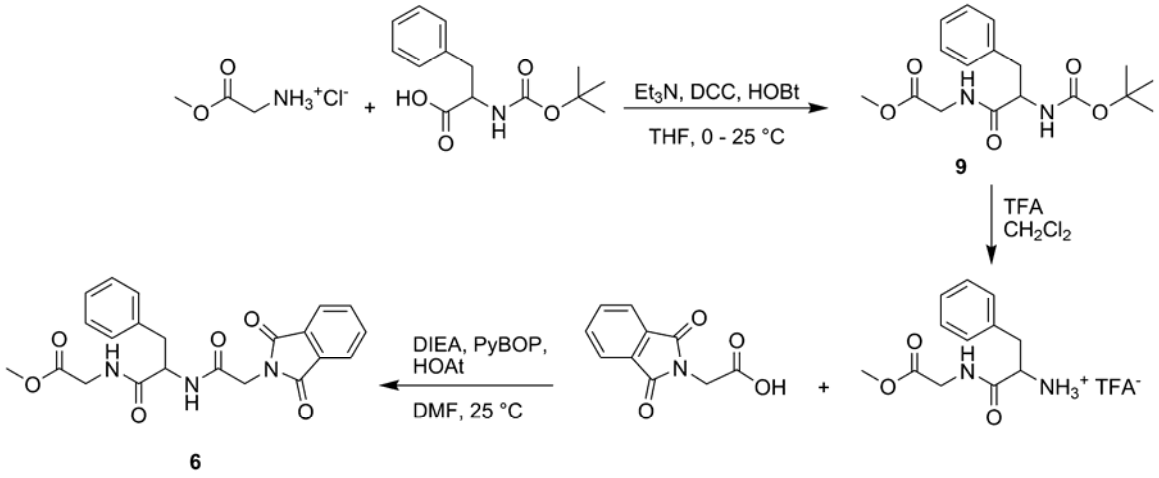

Scheme 3.2 Synthesis of nonfunctional isosteric tripeptide **6**.

The syntheses of the Boc-protected dipeptides **7**-**9** were carried out using dicyclohexyl carbodiimide (DCC) as the condensing agent and the nucleophilic additive 1-hydroxybenzotriazole (HOBt) in THF with yields of 88%, 95%, and 90% for **7**, **8**, and

9 respectively. The Boc-group of dipeptide **9** was removed using a 1:2 TFA:CH_2Cl_2 solution. However Boc-deprotection of dipeptides **7** and **8** with TFA led to trifluoramide terminated dipeptides under a variety of coupling conditions. Therefore, these Boc-groups were removed with a saturated methanolic solution of HCl. The best results for the tripeptidation coupling step were realized with benzotriazole-1-yl-oxy-tris-pyrrolidino-phosphonium hexafluorophosphate (PyBOP) as the condensing agent and the nucleophilic additive 1-hydroxy-7-azabenzotriazole (HOAt), giving overall yields of 78 %, 64 %, and 87 % for **2**, **4**, and **6** respectively. X-Ray structural analysis shows the different orientations of the pyridine nitrogen in peptides **2** and **4**, shown in Figure 3.5 and Figure 3.6, respectively.

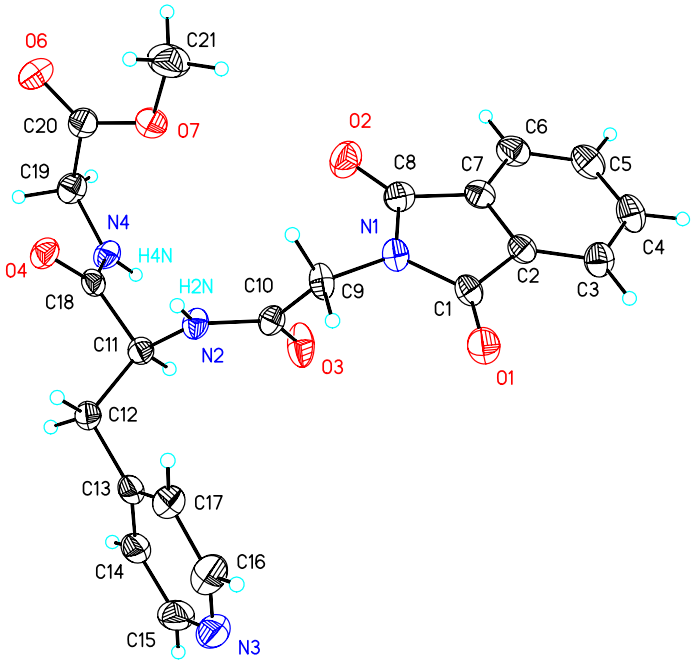

Figure 3.5 Crystal structure of tripeptide **2**.

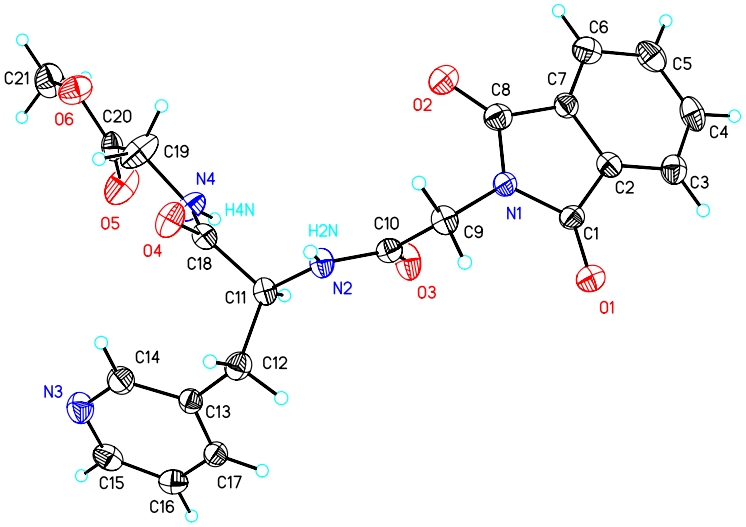

Figure 3.6 Crystal structure of tripeptide **4**.

3.3.3 Pyridyl Glycine Tripeptide Synthesis

The synthetic route towards glycyl derivative **1** was not as straight forward as the alanyl derivatives. Not commercially available, the 4-pyridyl glycine residue was first synthesized but never isolated as the carboxylic acid due to an inherent instability, which led to spontaneously decarboxylation upon acidification of the lithium carboxylate salt to isolate the pyridinium amino acid residue. This exacerbated the synthesis of the pyridyl glycyl amino acid of **1**, therefore a different synthesis in comparison to **2** and **4** was developed that went directly to the dipeptide. This was done using a modified Strecker synthesis developed by Ugi and further expanded by Kunz, shown in Scheme 3.3.[56-62]

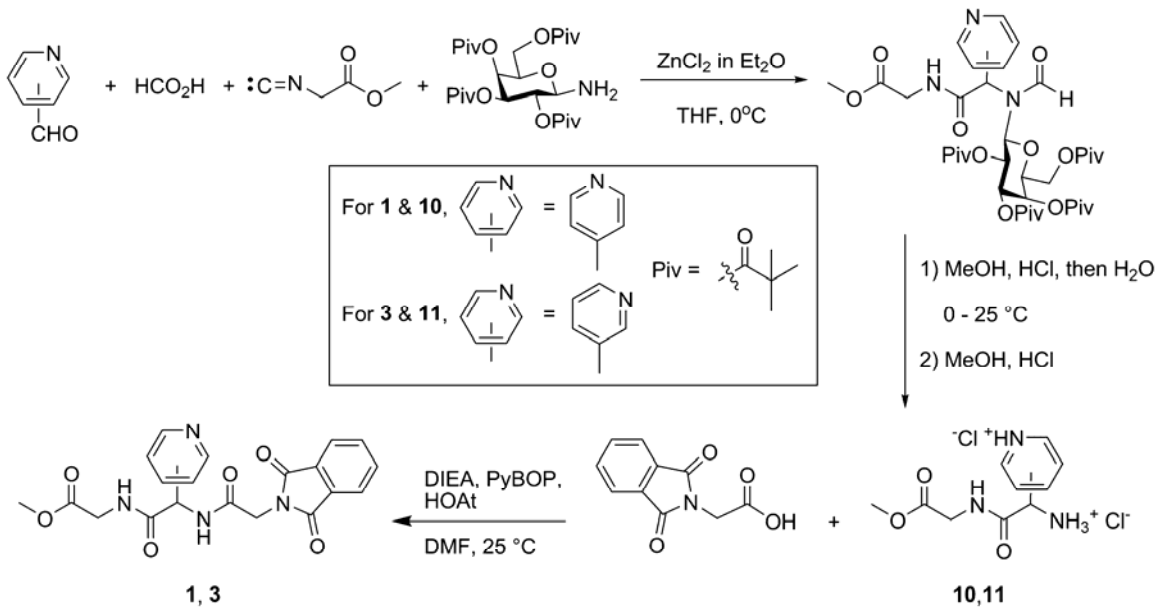

Scheme 3.3 Synthesis of tripeptides **1** and **3** using a modified Strecker synthesis.

The synthetic protocol used a protected amino sugar as an auxiliary, forming an imine with the appropriate pyridine carboxaldehyde precursor, that is attacked by the isonitrile to give the protected dipeptides**10** and **11** with yields greater than 90 %. The N-terminus protections were removed with a two part one-pot methanolic/aqueous HCl deprotection. After reesterification, the HCl salts of **10** and **11** were then converted to tripeptides **1** and **3** using the same tripeptidation step as the alanyl derivatives, with overall yields of 86 % and 70 % for **1** and **3**, respectively. Suitable crystals for peptide **1** could not be obtained, but X-ray structural analysis of peptide **3**, shown in Figure 3.7, shows the rigidity of the pyridine moiety relative to the peptide backbone in comparison to peptides **2** and **4**.

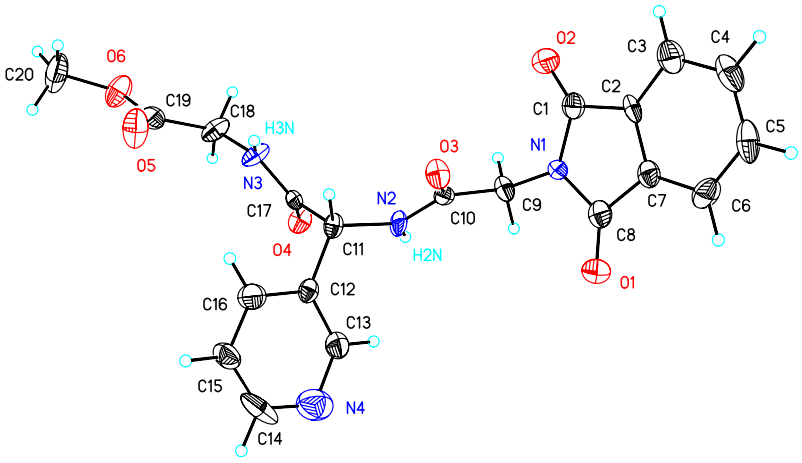

Figure 3.7 Crystal structure of tripeptide 3.

3.3.4 *p*-Methoxy SCS-Pd Pincer Synthesis

The synthesis of the palladated pincer complex **5** started with the methylation of **12** to **13** using iodomethane, which was then palladated to yield **5** following standard literature procedures with an overall yield of 92%, shown in Scheme 3.4.[54, 63, 64]

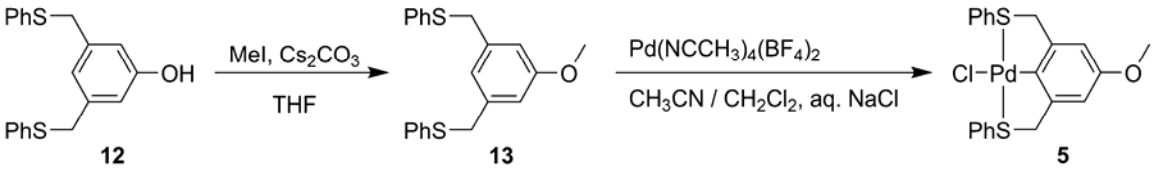

Scheme 3.4 Synthesis of *p*-methoxy SCS-Pd pincer **5**.

Pd-pincer complex **5** could be further recrystallized from $CHCl_3$ as large yellow crystals. X-ray structural analysis shows the thiophenol rings in an anti conformation minimizing steric congestion, as shown in Figure 3.8.

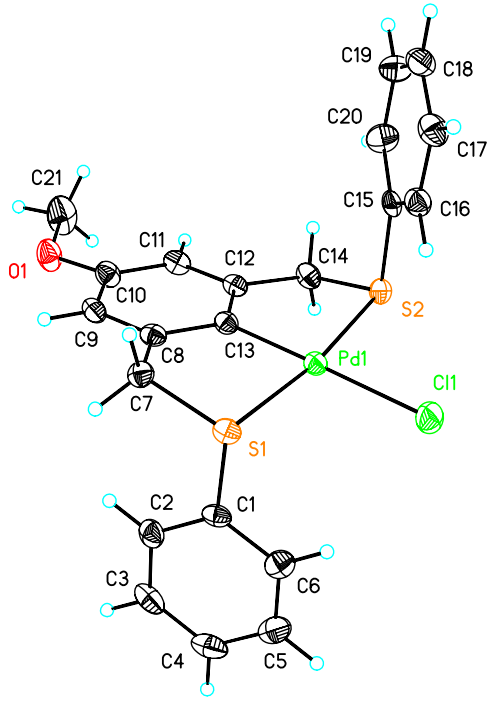

Figure 3.8 Crystal structure of palladated pincer complex **5**.

3.3.5 Coordination

Peptides **1-4** were synthesized to fully characterize and understand the coordination pattern and association strength of each new peptide ligand. The limited solubility of all four peptides and their coordinated complexes in less polar organic solvents ($CHCl_3$ and CH_2Cl_2) that are traditionally used to assemble metallated pincer-ligand complexes was a challenge. Since the overall goal of this project is to develop peptidal metal-coordinated self-assembly in polar solvents, all of our coordination studies were carried out in DMSO. Several contributions of metallated pincer complexations in polar solvents such

as MeOH, H_2O, and DMSO have been reported in the literature.[18, 48-50, 65] A significantly weaker binding in DMSO was expected versus assemblies in $CHCl_3$ and CH_2Cl_2 due to polarity differences as well as its competitive coordination which leads to solvent assisted dissociations and faster exchange rates.

3.3iii NMR characterization of the coordination

For all NMR spectral experiments, peptides **1-4** were dissolved in d_6-DMSO, in an NMR tube, and **5** was titrated into the DMSO solution until a 1:1 molar ratio was established. Then, one equivalent of $AgBF_4$ in d_6-DMSO was added that led to an instant precipitation of AgCl. This was the first evidence of coordination. The salt was then filtered off and each coordinated species analyzed.

Pincer ligand-metal complexes are traditionally characterized by ^{1}H NMR spectroscopy.[48, 66] The protons in resonance with or near the site of coordination generally show characteristic shifts in the ^{1}H NMR spectrum of the coordinated species versus its un-coordinated counterparts.[48] A 1:1 molar solution of the tripeptides and Pd pincer complex **5** in d_6-DMSO showed quantitative shifts in the signals of interest. As an example, Figure 3.9 shows the ^{1}H NMR spectra of the coordination of 4-pyridyl alanyl tripeptide **2** with Pd pincer complex **5**.

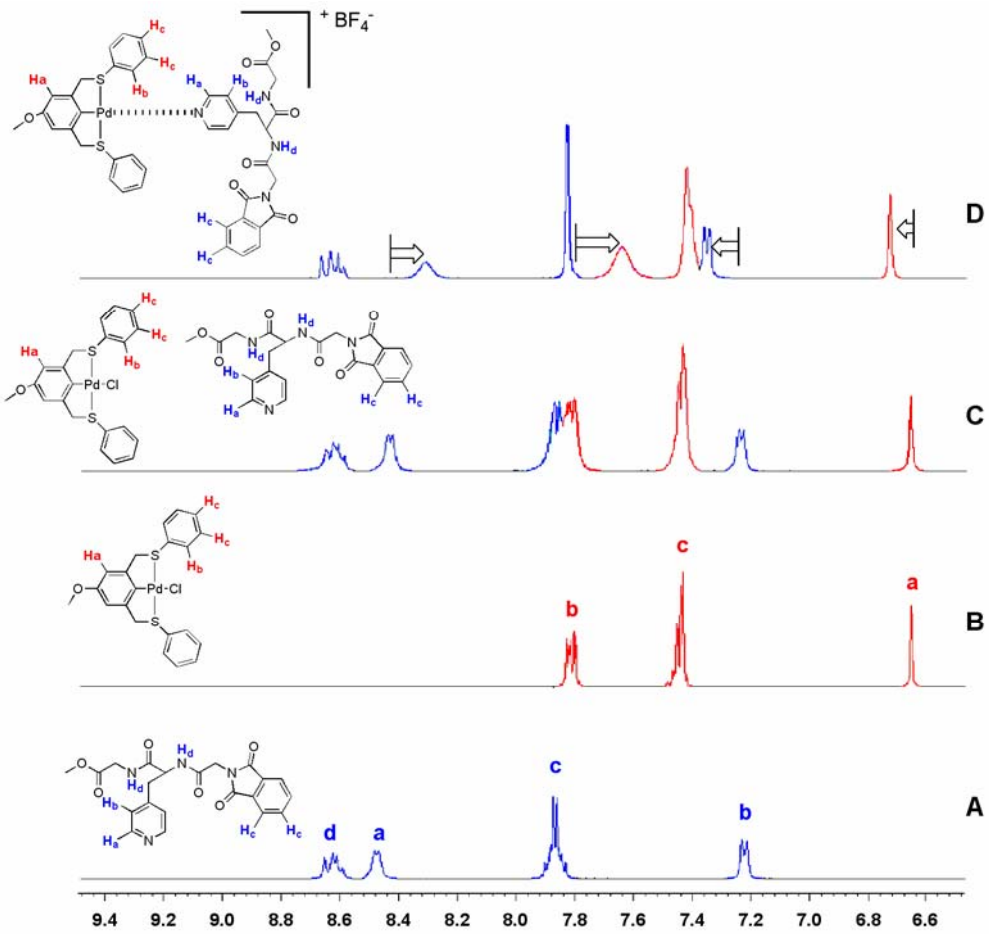

Figure 3.9 Stacked ^{1}H NMR spectra in d_6-DMSO depicting metal-coordination of **5** to **2**, with the arrows in D pointing towards the diagnostic shifts: A) peptide **2**, 0.01 M; B) pincer complex **5**, 0.01 M; C) 1:1 mixture of **2** and **5**, 0.006 M; D) 1:1 mixture of **2** and **5** after the addition of one equivalent of $AgBF_{4(s)}$, 0.006 M.

The observed shifts for the metal-coordination of all four peptides with **5** are tabulated in Tables 3.1 and 3.2 and assigned in Figures 3.10 and 3.11. These characteristic shifts are not as dramatic as shifts seen in less coordinating organic solvents.[19, 26, 66] This is due to the d_6-DMSO, which can facilitate the displacement and exchange of coordinated-uncoordinated pyridines via a solvolysis pathway leading to a signal broadening associated this fast equilibrium.[48] All observed shifts are caused by both changes in the electronics of each unit of the supramolecular system after

coordination and an overlap of protons in new ring-currents as the two coordinated molecules come into close proximity.[48] These effects can counteract and interfere with each other leading to the erratic shifts in each system and complicating the determination of these weaker binding constants using ^{1}H NMR spectroscopy.

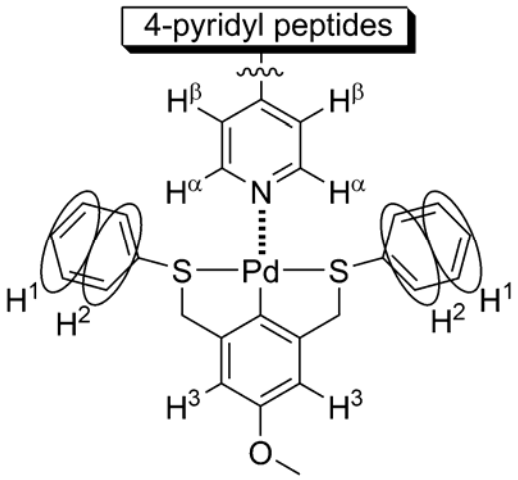

Figure 3.10 Proton assignment for 4-pyridyl peptides (**1** & **2**) coordinated to **5**.

Table 3.1 ^{1}H NMR shifts in ppm of relevant protons on 4-pyridyl peptides (**1** & **2**) and **5** before and after metal-coordination, with a final concentration of 0.006 M of each component in d_6-DMSO.

Peptide **1** Proton #	ppm before self-assembly	ppm after self-assembly	Peptide **2** Proton #	ppm before self-assembly	ppm after self-assembly
H^{α}	8.56	8.48	H^{α}	8.45	8.38
H^{β}	7.45	7.52	H^{β}	7.31	7.35
H^{1}	7.43	7.44	H^{1}	7.43	7.39
H^{2}	7.82	7.65	H^{2}	7.82	7.65
H^{3}	6.65	6.72	H^{3}	6.65	6.72

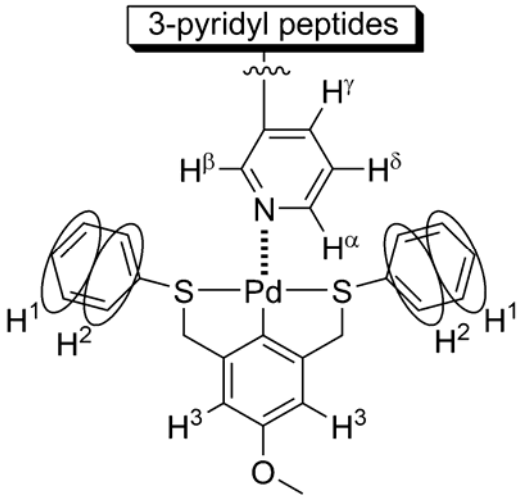

Figure 3.11 Proton assignment for 3-pyridyl peptides (**3** & **4**) coordinated to **5.**

Table 3.2 ^{1}H NMR shifts in ppm of relevant protons on 3-pyridyl peptides (**3** & **4**) and **5** before and after metal-coordination, with a final concentration of 0.006 M of each component in d_6-DMSO.

Peptide **3** Proton #	ppm before self-assembly	ppm after self-assembly	Peptide **4** Proton #	ppm before self-assembly	ppm after self-assembly
H^{α}	8.50	8.36	H^{α}	8.43	8.34
H^{β}	8.62	8.63	H^{β}	8.43	8.34
H^{γ}	7.79	7.90	H^{γ}	7.64	7.73
H^{δ}	7.40	7.47	H^{δ}	7.30	7.41
H^{1}	7.43	7.44	H^{1}	7.43	7.41
H^{2}	7.82	7.72	H^{2}	7.82	7.73
H^{3}	6.65	6.71	H^{3}	6.65	6.65

Since this is the first peptide-pincer complex coordination study, we wanted to clearly establish that all the observed shifts are due to a 1:1 well-defined coordination. In all coordination experiments, subtle shifts of the amide protons between 8.5-9.0 ppm

occurred. These shifts could be innocuously caused by the overall change in the electronics of the molecule through the coordination of the pincer solely at the pyridine, or through a perturbation of the hydrogen-bonding network of these protons via coordination of the amide nitrogens with a small percentage of residual silver salts still in solution. Alternatively, an undesirable complexation of the amide protons to the activated metallated pincer complex may be responsible for these shifts resulting in an ill-defined system.

To determine the nature of the amide proton shifts, we characterized a 1:1 mixture of $AgBF_4$ and peptide **2** using ^1H NMR spectroscopy. The ^1H NMR spectrum showed very slight shifts (less than 0.1 ppm) of the β-pyridine protons and the amide protons, implying that some interaction of backbone nitrogens with excess residual silver ions does occur.

To probe if a noncovalent interaction of the pincer complex with the amide backbone was also taking place, we prepared a 1:1 mixture of nonfunctional isosteric peptide **6** and complex **5** in d_6-DMSO and acquired the ^1H NMR spectrum of the solution before and after the addition of one equivalent of $AgBF_4$. There was no change in any of the peptide signals after addition of the silver salt. Therefore, the shifts observed in the backbone amide protons are due to a change in the overall electronics after coordination and to a lesser extent from secondary interactions of the amide nitrogens with residual silver ions. These two results clearly prove that no coordination took place between the amide backbone and complex **5** and that complexation occurs only at the nitrogen pyridine in a highly controlled fashion.

3.3iv Characterization of the peptide-Pd pincer complex by Mass Spectrometry

In the literature, it has been reported that complexed pincer systems can be analyzed by mass spectrometry (MS) using several different ionization techniques (FAB, MALDI-TOF, ES).[19, 20, 50, 67] We found that electrospray (ES) ionization in a neutral medium of a 1:1 mixture of water and MeOH was mild enough to permit detection of the complexed species. The spectra for the complexes **1**·**5** and **3**·**5** showed a signal at 867.1 corresponding to the molecular ion peak of [(**1**·**5** or **3**·**5**) – BF_4]$^+$. Other significant signals present in the spectrum are at 411.1 (**1**·H$^+$, or **3**·H$^+$) and 457.0 for [**5** – Cl]$^+$ corresponding to the peptide and pincer building blocks, respectively. These signals are most likely due to disassembly events during the ionization in the mass spectrometer. Related signals in the ES-MS spectra of **2**·**5** and **4**·**5** again displayed the characteristic signal at 881.4 corresponding to the molecular ion signal of the complexed species [(**2**·**5** or **4**·**5**) – BF_4]$^+$ and the disassembled signals at 425.2 (**2**·H$^+$, or **4**·H$^+$) and 457.2 for [**5** – Cl]$^+$.

3.3v Characterization of the bond strength using Isothermal Titration Calorimetry (ITC)

After confirmation by ^{1}H NMR and ES MS that complexation had occurred, we next investigated the bond strength of each coordination event using ITC. This was done to identify the optimal synthon, *i.e.* the strongest building block for our envisaged biological cyclic networks. ITC, a technique widely used by biochemists is quickly becoming routine in supramolecular chemistry,[68] because of its ability to directly measure the enthalpy of binding to provide a complete thermodynamic characterization.[69, 70] In our ITC experimental set up, we titrated each peptide into a DMSO solution of the CH_3CN

coordinated Pd pincer complex, shown in Scheme 3.5, all experiments were run in triplicate.

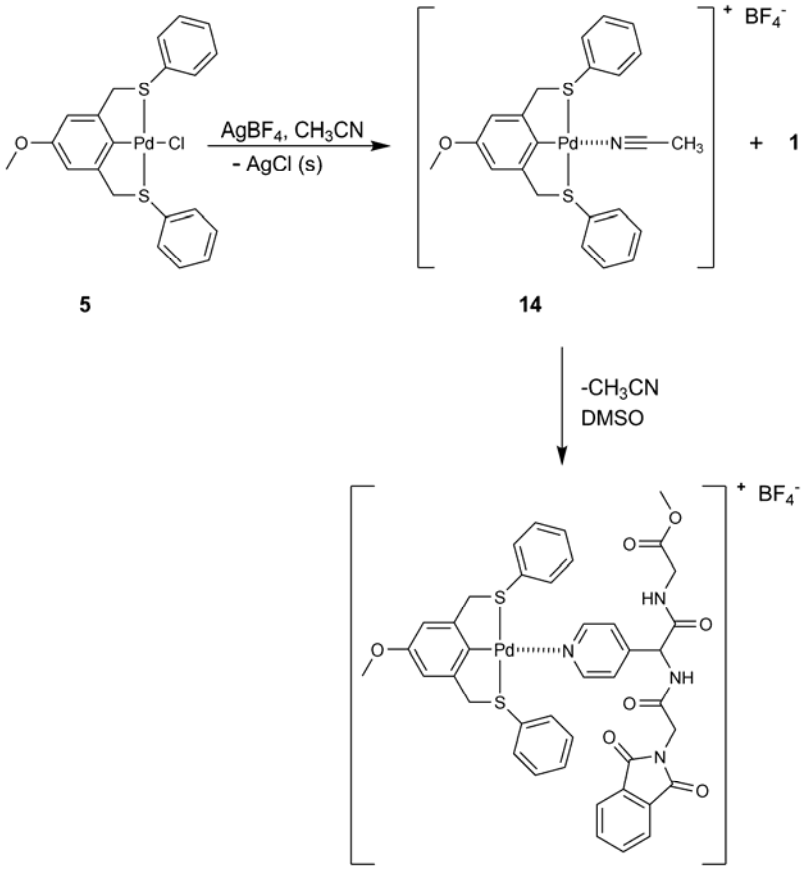

Scheme 3.5 Activation of **5** and coordination with CH_3CN, giving **14**, followed by displacement of CH_3CN by **1**.

Activation of **5** and subsequent coordination with CH_3CN to **14** was carried out prior to the ITC experiments in order to fully remove any AgCl precipitates, which could foul the ITC sample sell. CH_3CN was complexed to the palladium center to occupy this open coordination site. Our naked Pd-pincer complex appears to not be adequately coordinated by the DMSO solvent as a reasonable titration curve could not be generated from it,[65] possibly due to a rapid decomposition. However, it is well documented in the

literature that nitriles are instantaneously replaced as ligands on Pd pincer complexes by pyridines or phosphines.[47, 71] Therefore, the CH_3CN complexed to the Pd center can be viewed as a labile ligand (or protecting group) that is replaced by the pyridyl-tripeptides quantitatively upon addition.

The pincer metal-coordination is regarded as one of the stronger weak labile interactions and is essentially kinetically irreversible in low polarity solvents (ITC measurements of pyridines coordinating to pincer complexes in $CHCl_3$ were above the upper limits of our instrument, K_a values $>10^9$ M^{-1}) but due to the highly polar and coordinating nature of DMSO, the K_a values are known to be significantly lower.[48, 49] We detected the same trend for the coordination of all four tripeptides with **5**. In all cases, highly reproducible hyperbolic titration curves characteristic of a weaker binding event, were observed, with a representative example shown in Figure 3.12.[72]

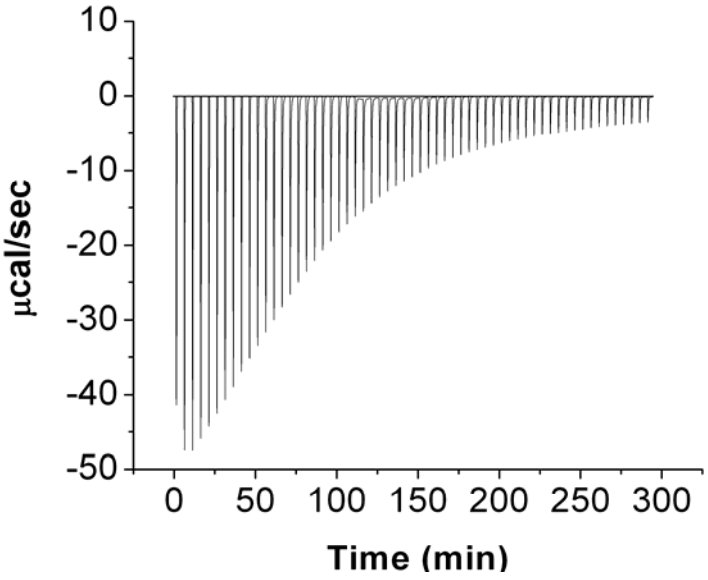

Figure 3.12 ITC curve of tripeptide **2** displacing a CH_3CN ligand from activated pincer complex **14**.

The 4-pyridyl systems have K_a values > 1200 M^{-1} while the 3-pyridyl systems have K_a values < 800 M^{-1}, all values are shown in Table 3.3. These K_a values fall in between those of 4-picoline and pyridine, respectively, showing that the peptide backbone does not interfere with the coordination of the pyridyl moiety to the Pd pincer complex.

Table 3.3 ITC K_a values of tripeptide **1-4**, pyridine, and 4-picoline displacing CH_3CN from activated pincer complex **14**.

Complex	K_a (M^{-1})
1·5	1190 ± 108
2·5	1580 ± 194
3·5	521 ± 54
4·5	757 ± 87
pyridine·5	382 ± 91
4-picoline·5	1730 ± 365

While crystal structures of the coordinated complexes could reveal the nature of the coordination geometries and possibly shed light on each K_a value, none of the tripeptide complexes formed crystals suitable for characterization via single crystal crystallography. Attempts can be made to explain the different K_a values through a combination of sterics and electronics. The ITC data show the superiority of the 4-pyridyl peptides, based on the available X-ray structures of uncoordinated tripeptides **2**-**4**. It can be inferred that the nitrogen of the pyridyl moiety is presumably more sterically accessible in the *para*-substituted 4-pyridyl peptides (**1** and **2**) versus the *meta*-substituted 3-pyridyl peptides (**3** and **4**), accounting for part of the difference in K_a values.The tighter binding of all four tripeptides vs. pyridine can be rationalized entropically with all tripeptides having fewer degrees of freedom compared to pyridine and through the activation via electron donation of the methylene or methine groups adjacent to each of the pyridines in the peptide, which should activate them and ultimately increase their association constants. The stronger association of the alanyl derivatives versus their glycyl homologues can most likely be attributed to this same electronic activation, which is greater in the alanyl derivatives because of the greater electronic decoupling of the pyridine ring from the peptide backbone via the methylene spacer. Similar observations have been reported previously by Reinhoudt[48] and van Koten[73] establishing a Hammett like relationship of binding strength to electron donation ability of the *para*-substitutuent on multiple pyridine ligands. The K_a values of the 4-pyridyl peptides, **1** and **2**, are comparable to the coordination events in other supramolecular systems[74-76] and will make excellent additions to the peptidal-supramolecular repertoire.

3.4 Conclusion

We have synthesized four new unnatural tripeptides (**1**-**4**) containing a central residue with a pyridyl side-chain. The complexation of each tripeptide with a *p*-methoxy terminated SCS-Pd pincer complex (**5**) was investigated in detail. The metal-coordination was characterized and evaluated by ^{1}H NMR spectroscopy, ES-mass spectroscopy, and ITC. Each spectroscopic method confirmed that coordination of each tripeptide to the Pd pincer complex has occurred quantitatively without any competitive coordination of the peptide backbone heteroatoms. The ITC analyses also showed that the 4–pyridyl tripeptides, **1** and **2**, are the tightest binding ligands towards **5**. Alanyl derivative **2** was the strongest overall demonstrating the superiority of the 4-pyridyl peptides over their 3-pyridyl analogs. Finally, the measured K_a values are comparable to other pincer-pyridine systems in DMSO[49, 65] suggesting that the controlled coordination of the metallated pincer-pyridine interaction is an interesting biological synthon and, with the use of multifaceted 3-D receptors, these peptide ligands can be used to assemble new and interesting biological scaffolds.

This is the first study that describes the controlled coordination of a palladated pincer complex with unnatural peptide sequences as its complementary ligand. Our next step in this area will be to incorporate the unnatural residue ligands into cyclic peptides and self-assemble them with ditopic bis-metallated pincer complexes creating well-defined architectures, such as those seen in purely synthetic supramolecular systems.[12-14, 16, 17, 19, 20]

3.5 Experimental

Materials and Methods:

Boc-L-4-pyridyl alanine and boc-L-3-pyridyl alanine were purchased from Peptech Corp. CH_2Cl_2 and THF were dried via passage through Cu_2O and alumina columns. N,N-Diisopropyl-ethyl amine (DIEA) and triethylamine (Et_3N) were distilled from sodium/benzophenone keytl, and TFA was distilled from P_2O_5. DMSO was degassed by stirring under vacuum at 50 mmHg for 30 minutes. All glassware was flame dried or placed in an oven overnight at 130 °C. Compounds were analyzed by use of UV light (254 nm), I_2, or a 0.3% solution of ninhydrin in 3% AcOH/*n*-butanol. RP-HPLC eluant was a mixture of H_2O with an increasing gradient of CH_3CN, on a C18 reverse phase column. NMR spectra were recorded at 298 K (^{1}H NMR: 300 MHz; ^{13}C NMR; 75 MHz). Chemical shifts are reported in parts per million (ppm), using residual solvent as an internal standard. Data reported as follows: chemical shift, multiplicity (s = singlet, d = doublet, t = triplet, q = quartet, dd = doublet of doublets, m = multiplet, b = broad), coupling constants, integration, proton assignment. Mass spectroscopy ionization was either ES or electron impact (EI). Compound **12** was prepared according to previous literature procedures.[25]

(5-methoxy-1,3-phenylene)bis(methylene)bis(phenylsulfane) (13):

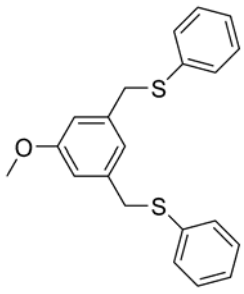

A solution of **12** (1.12 g, 3.3 mmol) and MeI (0.70 g, 5.0 mmol) in anhydrous THF (50 mL) and added Cs_2CO_3 (1.29 g, 4.0 mmol) in one portion and let stir for 12 h at 25 °C, the solids were then filtered off and the solvent under reduced pressure. The crude oil was redissolved in EtOAc and purified by flash column chromatography (silica gel, eluant: 80:20 hexanes:EtOAc) and the product dried *in vacuo* to give a clear oil (1.10 g, 94%). ^{1}H NMR (300 MHz, $CDCl_3$) δ: 7.34-7.13 (m, 10H, Ar H), 6.86 (s, 1H, Ar H), 6.70 (s, 2H, Ar H), 4.04 (s, 4H, Ar-CH_2-S), 3.71 (s, 3H, CH_3-O); ^{13}C NMR (75 MHz, $CDCl_3$) δ:159.7, 139.1, 136.4, 129.9, 128.9, 126.4, 121.7, 113.2, 55.2, 38.94; MS (EI, 70 eV) m/z: M^+ 352 (90), 243 (100), 210 (32), 134 (26), 91 (25); HRMS (EI, 70 eV) calcd for $C_{21}H_{20}OS_2$: 352.09459, found: 352.09556.

Pd-Cl (5-methoxy-1,3-phenylene)bis(methylene)bis(phenylsulfane) (5):

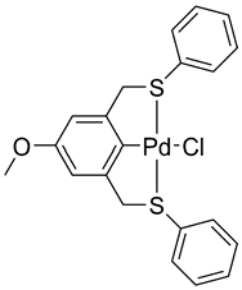

A solution of $PdCl_2(NCPh)_2$ (0.85 g, 2.2 mmol) and **13** (0.82 g, 2.2 mmol) in CH_2Cl_2:CH_3CN 1:1 (20 mL) was allowed to stir at 25 °C for 15 min becoming an opaque orange solution, at which time $AgBF_4$ (1.08 g, 5.55 mmol) was added, a precipitate immediately formed and the mixture was allowed to stir for an additional 30 min at 25 °C, during this time the reaction mixture changed from an orange to a yellow color. The reaction mixture was then diluted with CH_2Cl_2 (200 mL) and poured directly into a saturated aq. NaCl solution (200 mL) and stirred overnight. The organic layer was

separated, dried over $MgSO_4$, filtered through celite and the solvent removed under reduced pressure giving a crude yellow oil which was further purified by flash column chromatography (silica gel, eluant: CH_2Cl_2) to flush out all non-palladated organics and then a 99:1 CH_2Cl_2:MeOH eluant mixture to flush out the final product as a yellow foamy solid (1.07 g, 98%), this could be crystallized from $CHCl_3$ forming large yellow crystals for X-ray structural analysis. ^{1}H NMR (300 MHz,d_6-DMSO) δ: 7.77-7.86 (m, 4H, Ar H), 7.40-7.49 (m, 6H, Ar H), 6.65 (s, 2H, Ar H), 4.73 (bs, 4H, Ar-CH_2-S), 3.65 (s, 3H, CH_3-O); ^{13}C NMR (75 MHz, $CDCl_3$) δ: 157.3, 151.4, 150.0, 132.3, 131.3, 129.6, 129.5, 108.2, 55.2, 51.6; MS (ESI^+) 457.0; HRMS (ESI^+) calcd for $C_{21}H_{19}OPdS_2$: 457.9869, found: 457.9984 [the chlorine atom was labile under these ionization conditions]. Elemental analysis: calcd for $C_{21}H_{19}ClOPdS_2$: C, 51.12; H, 3.88; S, 13.00; Cl, 7.19, O, 3.24; Pd, 21.57. found: C, 50.76; H, 3.89; S, 12.77. M.P. 182-184°C.

[5-methoxy-1,3-phenylene)bis(methylene)bis(phenylsulfane)]MeCN$^{+\cdot}$(BF4)$^-$ (14):

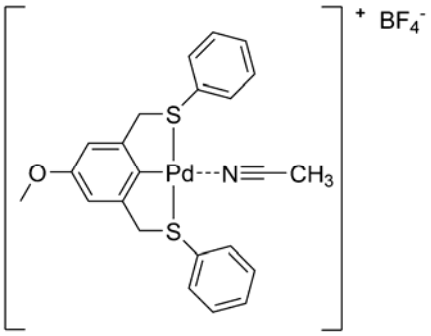

Compound **5** (0.30 g, 0.6 mmol) was dissolved in CH_2Cl_2:CH_3CN 1:1 (20 mL) at 25 °C and $AgBF_4$ (0.13 g, 0.7 mmol) was added in one portion, a precipitate immediately formed and the yellow mixture was allowed to stir for 3 h, it was then filtered through celite, and the solvent removed under reduced pressure and dried in vacou at 40 °C to

give a yellow oily solid (0.34 g, 95%). ^{1}H NMR (300 MHz, d_6-DMSO) δ: 7.81-7.90 (m, 4H, Ar H), 7.47-7.55 (m, 6H, Ar H), 6.66 (s, 2H, Ar H), 4.74 (bs, 4H, Ar-CH_2-S), 3.66 (s, 3H, CH_3-O), 2.06 (s, 3H, CH_3-CN); ^{13}C NMR (75 MHz, d_6-DMSO) δ: 157.2, 151.1, 131.4, 131.1, 130.4, 130.1, 126.1, 118.1, 109.0, 55.0, 48.2, 1.2; MS (FAB^+) m/z (relative intensity) 457.0 (100), 498.0 (5) CH_3CN coordinated; HRMS (FAB^+) calcd for $C_{21}H_{19}OPdS_2$: 457.9869, found: 457.9985 [CH_3CN was labile under these ionization conditions].

Methyl 2-(2-(tert-butoxycarbonylamino)-3-(pyridin-4-yl)propanamido) (7):

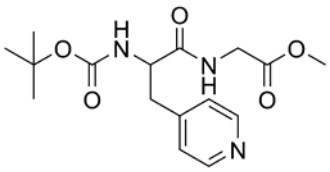

Et_3N (1.9 mL, 13.6 mmol) was added to a suspension of glycine methyl ester·HCl (1.71 g, 13.6 mmol) in THF (75 mL) and allowed to stir for 15 min. Boc-4-pyridyl alanine (1.80 g, 6.8 mmol) and HOBt (0.91 g, 6.8 mmol) were added to the THF mixture and it was cooled to 0 °C and a solution of DCC (1.40 g, 6.8 mmol) in THF (10 mL) was added in one portion, after 5 min the reaction mixture was allowed to warm up to 25 °C and stirred overnight. The dicyclohexyl urea (DCU) precipitate was filtered off, and the THF removed under reduced pressure. The crude oil was redissolved in EtOAc and cooled in a freezer to precipitate out unreacted DCC, which was filtered off. The EtOAc solution was then wash with a saturated aqueous $NaHCO_3$ solution to remove HOBt, and the basic aqueous layer was back extracted with CH_2Cl_2, the organic layers were combined and the solvent removed under reduced pressure. This crude oil was further purified by flash column chromatography (silica gel, eluant: 95:5 EtOAc:MeOH) and the

product dried *in vacuo* to give a white foam (2.00 g, 88%). ^{1}H NMR (300 MHz, $CDCl_3$) δ: 8.42 (dd, *J* = 5.8, 2H, α-pyr H), 7.11 (d, *J* = 5.8, 2H, β-pyr H), 7.11 (d, *J* = 3.2, 1H, CH_2-N**H**-CO), 5.45 (d, *J* = 8.2, 1H, C-NH-CO-*t*Bu), 4.49 (q, *J* = 6.8, 1H, C-CH-N), 3.96 (t, *J* = 4.0, 2H, C-CH_2-N), 3.68 (s, 3H, CH_3-O), 3.14 (dd, *J* = 6.0, 13.9, 1H, Ar-C**H**(H)-C), 2.93 (dd, *J* = 7.7, 13.9, 1H, Ar-CH(**H)**-C), 1.32 (s, 9H, *t*-Bu); ^{13}C NMR (75 MHz, $CDCl_3$) δ: 171.1, 169.8, 155.3, 149.5, 145.9, 124.6, 80.4, 54.5, 52.4, 41.1, 37.6, 28.2; MS (ESI^+) [M + H^+] 338.2; HRMS (ESI^+) [M + H^+] calcd for $C_{16}H_{24}N_3O_5$: 338.1736, found: 338.1710.

Methyl 2-(2-(tert-butoxycarbonylamino)-3-(pyridin-3-yl)propanamido) (8):

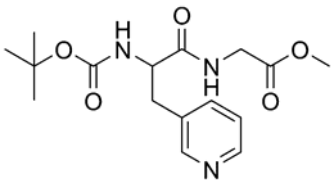

Et_3N (1.9 mL, 13.6 mmol) was added to a suspension of glycine methyl ester·HCl (1.71 g, 13.6 mmol) in THF (75 mL) and allowed to stir for 15 min. Boc-3-pyridyl alanine (1.80 g, 6.8 mmol) and HOBt (0.91 g, 6.8 mmol) were added to the THF and it was cooled to 0 °C and a solution of DCC (1.40 g, 6.8 mmol) in THF (10 mL) was added in one portion, after 5 min the reaction mixture was allowed to warm up to 25 °C and stirred overnight. The DCU precipitate was filtered off, and the THF removed under reduced pressure. The crude oil was redissolved in EtOAc and cooled in a freezer to precipitate out unreacted DCC, which was filtered off. The EtOAc solution was then wash with a saturated aqueous $NaHCO_3$ solution to remove HOBt, and the basic aqueous layer was back extracted with CH_2Cl_2, the organic layers were combined and the solvent

removed under reduced pressure. This crude oil was further purified by flash column chromatography (silica gel, eluant: 95:5 EtOAc:MeOH) and the product dried *in vacuo* to give a white foam (2.10 g, 95%). ^{1}H NMR (300 MHz, $CDCl_3$) δ: 8.44 (dd, *J* = 1.7, 4.7, 1H, pyr H), 8.40 (d, *J* = 1.7, 1H, pyr H), 7.54 (dt, *J* = 1.9, 7.7, 1H, pyr H), 7.19 (dd, *J* = 4.9, 7.1, 1H, pyr H), 6.85 (t, *J* = 5.2, 1H, CH_2-N**H**-CO), 5.23 (d, *J* = 8.8, 1H, C-NH-CO-*t*Bu), 4.44 (q, *J* = 6.6, 1H, C-CH-N), 3.98 (dd, *J* = 3.9, 5.5, 2H, C-CH_2-N), 3.71 (s, 3H, CH_3-O), 3.15 (dd, *J* = 6.0, 14.3, 1H, Ar-C**H**(H)-C), 2.97 (dd, *J* = 7.1, 14.3, 1H, Ar-CH(**H**)-C), 1.35 (s, 9H, *t*-Bu); ^{13}C NMR (75 MHz, $CDCl_3$) δ: 171.7, 170.3, 155.7, 150.4, 147.9, 137.7, 133.0, 123.8, 80.4, 55.2, 52.5, 41.3, 35.9, 28.4; MS (ESI^+) [M + H^+] 338.2; HRMS (ESI^+) [M + H^+] calcd for $C_{16}H_{24}N_3O_5$: 338.1726, found: 338.1705.

Methyl 2-(2-(tert-butoxycarbonylamino)-3-phenylpropanamido)acetate (9):

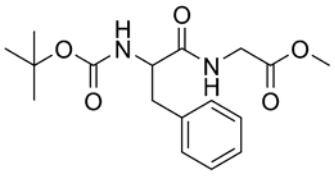

Et_3N (1.1 mL, 7.6 mmol) was added to a suspension of glycine methyl ester·HCl (0.95 g, 7.6 mmol) in THF (75 mL) and allowed to stir for 15 min. Phenylalanine (1.00 g, 3.8 mmol) and HOBt (0.51 g, 3.8 mmol) were added to the THF and it was cooled to 0 °C and a solution of DCC (0.78 g, 3.8 mmol) in THF (10 mL) was added in one portion, after 5 min the reaction mixture was allowed to warm up to 25 °C and stirred overnight. The dicyclohexyl urea (DCU) precipitate was filtered off, and the THF under reduced pressure. The crude oil was redissolved in EtOAc and cooled in a freezer to precipitate out unreacted DCC, which was filtered off. The EtOAc solution was then wash with a saturated aqueous $NaHCO_3$ solution to remove HOBt, and the basic aqueous layer was

back extracted with CH_2Cl_2, the organic layers were combined and the solvent removed under reduced pressure giving a white solid (1.15 g, 90%). ^{1}H NMR (300 MHz, $CDCl_3$) δ: 7.18-7.35 (m, 5H, ArH), 6.38 (m, 1H, CH_2-N**H**-CO), 4.96 (d, m, 1H, C-NH-CO-*t*Bu), 4.40 (q, *J* = 7.0, 1H, C-CH-N), 4.01 (m, 2H, C-CH_2-N), 3.73 (s, 3H, CH_3-O), 3.11 (m, 2H, Ar-CH_2-C), 1.40 (s, 9H, *t*-Bu); ^{13}C NMR (75 MHz, $CDCl_3$) δ:171.7, 170.4, 155.7, 136.9, 129.2, 128.4, 126.7, 80.3, 55.4, 52.1, 41.0, 38.3, 28.1; MS (FAB^+) [M + H^+] 337.1; HRMS (FAB^+) [M + H^+] calcd for $C_{17}H_{25}N_2O_5$: 337.17577, found: 337.17627.

4-(1-ammonio-2-(2-methoxy-2-oxoethylamino)-2-oxoethyl)pyridinium chloride (10):

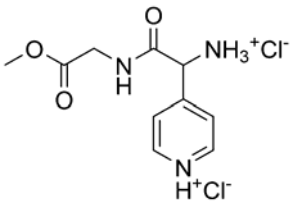

$ZnCl_2$ in Et_2O (11.7 mL, 11.7 mmol) was added to a 0 °C solution of 2,3,4,6-tetra-O-pivaloyl-β-D-galactopyranosylamine (3.00 g, 5.8 mmol), 4-pyridinecarboxaldehyde (0.56 mL, 5.8 mmol), formic acid (0.24 mL, 6.4 mmol), and methyl isocyanoacetate (0.56 mL, 6.1 mmol) in anhydrous THF (25 mL), after 30 min the reaction mixture was allowed to warm up to 25 °C and monitored by TLC which showed complete consumption of the aldehyde after 12 h. The solvent was removed under reduced pressure and the crude mixture redissolved in EtOAc forming an orange solution, which was washed with a 1N aqueous $KHSO_4$ solution (2 x) removing the orange color, leaving a pale yellow solution. The organic layer was then washed (3 x) with a saturated aqueous $NaHCO_3$ solution precipitating out a white solid (presumably a Zn salt). Residual precipitate was filtered from the organic layer and the solvent was removed under reduced pressure giving a

yellow solid which was further purified by flash column chromatography (silica gel, eluant: EtOAc) and the product dried *in vacuo* to give a yellow foam (4 g, 92%). This sugar-formyl protected dipeptide intermediate was dissolved in MeOH (20 mL) cooled to 0 °C and saturated with dry HCl gas for 15 min and stirred at 0 °C for 1 h, the reaction mixture was allowed to warm up to 25 °C and stirred for an additional 4 h to remove the formyl group. Water (20 mL) was then added to the methanolic reaction mixture and stirred for an additional 10 h to remove the the sugar. The MeOH was then removed under reduced pressure and the aqueous reaction mixture was washed with CH_2Cl_2 until the organic washes were colorless. The water was then removed under reduced pressure to give the hydrolyzed dipeptide which was redissolved in MeOH (30 mL) and saturated with dry HCl gas for 15 min and allowed to stir for 3 h to reesterified the carboxylate terminus. Et_2O was added to the methanolic solution to precipate out the crude dipeptide·HCl salt which was further purified by repeated triturations from a boiling Et_2O:MeOH solution and isolated as an off-white solid (1.46 g, 85%). ^{1}H NMR (300 MHz, d_6-DMSO) δ: 9.62 (t, 1H,C-NH-CO), 9.35 (bs, 3H, NH_3^+), 8.98 (m, 2H, α-pyr H) 8.15 (d, 2H, J = 6.7, β-pyr H), 5.51 (bs, 1H, C-CH-N), 3.91 (t, 2H, J = 6.7, C-CH_2-N), 3.55 (s, 3H, CH_3-O); ^{13}C NMR (75 MHz, d_6-DMSO) δ: 169.2, 165.7, 150.8, 143.4, 125.6, 54.2, 51.9, 40.9; MS (FAB^+) [M + H^+] 224.1; HRMS (FAB^+) [M + H^+] calcd for $C_{10}H_{14}N_3O_3$: 224.10183, found: 224.10352.

3-(1-ammonio-2-(2-methoxy-2-oxoethylamino)-2-oxoethyl)pyridinium chloride (11):

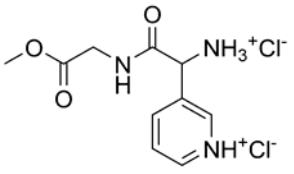

$ZnCl_2$ in Et_2O (28.1 mL, 28.1 mmol) was added to a 0 °C solution of 2,3,4,6-tetra-O-pivaloyl-β-D-galactopyranosylamine (7.24 g, 14.1 mmol), 3-pyridinecarboxaldehyde (1.3 mL, 14.1 mmol), formic acid (0.58 mL, 15.5 mmol), and methyl isocyanoacetate (1.4 mL, 14.8 mmol) in anhydrous THF (50 mL), after 30 min the reaction mixture was allowed to warm up to 25 °C and monitored by TLC which showed complete consumption of the aldehyde after 12 h. The solvent was removed under reduced pressure and the crude mixture redissolved in EtOAc forming an orange solution, which was washed with a 1N aqueous $KHSO_4$ solution (2 x) removing the orange color, leaving a yellow solution. The solvent was removed under reduced pressure giving a light brown solid which was further purified by flash column chromatography (silica gel, eluant: EtOAc) and the product dried *in vacuo* to give an orange foam (9.3 g, 88%). This sugar-formyl protected dipeptide intermediate was dissolved in MeOH (50 mL) cooled to 0 °C and saturated with dry HCl gas for 15 min and stirred at 0 °C for 1 h, the reaction mixture was allowed to warm up to 25 °C and stirred for an additional 4 h to remove the formyl group. Water (40 mL) was then added to the methanolic reaction mixture and stirred for an additional 10 h to remove the the sugar. The MeOH was then removed under reduced pressure and the aqueous reaction mixture was washed with CH_2Cl_2 until the organic washes were colorless. The water was then removed under reduced pressure to give the hydrolyzed dipeptide which was redissolved in MeOH (30 mL) and saturated with dry HCl gas for 15 min and allowed to stir for 3 h to reesterified the carboxylate terminus. Et_2O was added to the methanolic solution to precipate out the crude dipeptide·HCl salt which was further purified by repeated triturations from a boiling Et_2O:MeOH solution and isolated as a light brown solid (3.58 g, 86 %). ^{1}H NMR (300 MHz, d_6-DMSO) δ:

9.62 (t, 1H,C-NH-CO), 9.35 (bs, 3H, NH_3^+), 8.98 (m, 2H, α-pyr H) 8.15 (d, 2H, *J* = 6.7, β-pyr H), 5.51 (bs, 1H, C-CH-N), 3.91 (t, 2H, *J* = 6.7, C-CH_2-N), 3.55 (s, 3H, CH_3-O); ^{13}C NMR (75 MHz, d_6-DMSO) δ:; MS (FAB^+) [M + H^+] 224.1; HRMS (FAB^+) [M + H^+] calcd for $C_{10}H_{14}N_3O_3$: 224.10183, found: 224.10352.

Methyl 2-(2-(2-(1,3-dioxoisoindolin-2-yl)acetamido)-3-(pyridin-4-yl)propanamido)acetate (2):

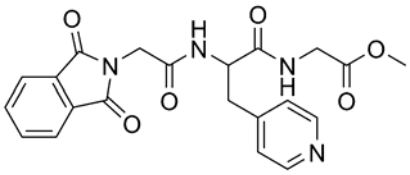

Boc protected dipeptide **6** (2.10 g, 6.2 mmol) was dissolved in MeOH (50 mL) and saturated with HCl gas for 15 min with agitation while keeping the temperature constant at 25 °C, after HCl addition the reaction was stirred for an additional 30 min, the solvent was then removed under reduced pressure and dried in vacuo (complete deprotection was confirmed by ^{1}H NMR of a small aliquot). The HCl salt of deprotected dipeptide **6** was dissolved in a solution of DIEA (2.0 mL, 12.3 mmol) in anhydrous DMF (20 mL), and the mixture incubated for 10 min. In a separate flask a solution of PyBOP (3.85 g, 7.4 mmol), phthaloyl glycine (1.51 g, 7.4 mmol), HOAt (1.01 g, 7.4 mmol), and DIEA (3.7 mL, 22.2 mmol) in anhydrous DMF (10 mL) was allowed to incubate for 5 min and then added in one portion to the deprotected dipeptide **6** solution. The reaction became a red color after 30 min and a precipitate formed after one h, stirring was continued for 12 h, the DMF was removed under reduced pressure and the mixture taken up in CH_2Cl_2, the insoluble material was filtered off and washed with CH_2Cl_2 and dried to give a white

powder which was further purified by RP-HPLC (water:CH_3CN gradient; C18 column) giving a white solid (2.30 g, 89 %), which could be crystallized from a 95:5 CH_3CN:water mixture as thin white needles for X-ray structural analysis. ^{1}H NMR (300 MHz, d_6-DMSO) δ: 8.60-8.69 (m, 1H, CH_2-N**H**-CO), 8.60-8.69 (m, 1H, CH-N**H**-CO), 8.49 (d, *J* = 5.2, 2H, α-pyr H), 7.83-7.92 (m, 4H, Ar H), 7.3 (d, *J* = 5.3, 2H, β-pyr H), 4.58-4.68 (m, 1H, C-CH-N), 4.17 (dd, *J* = 10, 16.8, 2H, pyr-CH_2-C), 3.88 (dd, *J* = 2.2, 3.5, 2H, N-CH_2-CO-N), 3.63 (s, 3H, CH_3-O), 3.06 (dd, *J* = 4.7, 13.8, 2H, N-C**H**(H)-CO-O), 2.81 (dd, *J* = 9.6, 13.8, 2H, N-CH(**H**)-CO-O); ^{13}C NMR (75 MHz, d_6-DMSO) δ: 170.8, 170.1, 167.4, 166.0, 148.5, 147.8, 134.6, 131.6, 125.2, 123.2, 52.7, 51.8, 40.6. 39.9, 37.1; MS (ESI$^+$) [M + H$^+$] 425.1473; HRMS (ESI$^+$) [M + H$^+$] calcd for $C_{21}H_{21}N_4O_6$: 425.1472, found: 425.1456; Elemental analysis: calcd for $C_{21}H_{20}N_4O_6$: C, 59.43; H, 4.75; N, 13.20; O, 22.62. found: C, 59.27; H, 4.71; N, 13.21; O, 22.81; The onset of decomposition between 239-243 °C occurred before a melting point.

Methyl 2-(2-(2-(1,3-dioxoisoindolin-2-yl)acetamido)-3-(pyridin-3-yl)propanamido)acetate (4):

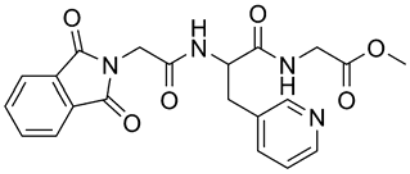

Boc protected dipeptide **7** (2.02 g, 6.0 mmol) was dissolved in MeOH (50 mL) and saturated with HCl gas for 15 min with agitation while keeping the temperature constant at 25 °C, after HCl addition the reaction was stirred for an additional 30 min, the solvent was then removed under reduced pressure and dried *in vacuo* (complete deprotection was

confirmed by ^{1}H NMR of a small aliquot). The HCl salt of deprotected dipeptide **7** was dissolved in a solution of DIEA (2.0 mL, 12.3 mmol) in anhydrous DMF (20 mL), and the mixture incubated for 10 min. In a separate flask a solution of PyBOP (3.76 g, 7.2 mmol), phthaloyl glycine (1.48 g, 7.2 mmol), HOAt (0.98 g, 7.2 mmol), and DIEA (3.6 mL, 21.7 mmol) in anhydrous DMF (10 mL) was allowed to incubate for 5 min and then added in one portion to the deprotected dipeptide **7** solution. The reaction became a red color after 30 min and a precipitate formed after one h, stirring was continued for 12 h, at which time the DMF was removed under reduced pressure, yielding a crude brown viscous oil. The oil was dissolved in a minimum amount of CH_2Cl_2 with a few drops of TFA and semi-purified by flash column chromatography (silica gel, eluant; 94:5:1 EtOAc:MeOH:Et_3N) and the product dried *in vacuo* to give a yellow powder, which was further purified by RP-HPLC (water:CH_3CN gradient; C18 column) giving a white solid (1.65 g, 65%), which could be crystallized from a 95:5 CH_3CN:water mixture as thin white needles for X-ray structural analysis. ^{1}H NMR (300 MHz, d_6-DMSO) δ: 8.58-8.65 (m, 1H, CH_2-N**H**-CO), 8.58-8.65 (m, 1H, CH-N**H**-CO), 8.41-8.43 (m, 2H, pyr H), 7.83-7.91 (m, 4H, Ar H), 7.61-7.66 (m, 1H, pyr H), 7.25-7.33 (m, 1H, pyr H), 4.53-4.63 (m, 1H, C-CH-N), 4.18 (dd, J = 10.8, 16.8, 2H, pyr-CH_2-C), 3.9 (dd, J = 2.2, 3.5, 2H, N-CH_2-CO-N), 3.61 (s, 3H, CH_3-O), 2.91 (dd, J = 4.7, 13.9, 1H, N-C**H**(H)-CO-O), 2.79 (dd, J = 9.2, 13.9, 1H, N-CH(**H**)-CO-O); ^{13}C NMR (75 MHz, d_6-DMSO) δ: 171.0, 170.1, 167.4, 165.9, 149.9, 147.4, 137.0, 131.7, 131.6, 123.4, 123.2, 53.3, 51.8, 40.6. 39.8, 34.9; MS (ESI^+) [M + H^+] 425.1469; HRMS (ESI^+) [M + H^+] calcd for $C_{21}H_{21}N_4O_6$: 425.1459, found: 425.1456; Elemental analysis: calcd for $C_{21}H_{20}N_4O_6$: C, 59.43; H, 4.75; N, 13.20;

O, 22.62. found: C, 59.02; H, 4.83; N, 13.25; O, 22.90; The onset of decomposition between 222-227 °C occurred before a melting point.

Methyl 2-(2-(2-(1,3-dioxoisoindolin-2-yl)acetamido)-3-phenylpropanamido)acetate (6):

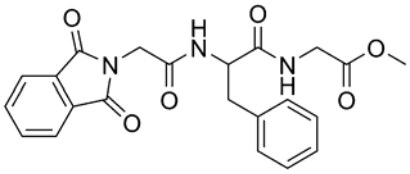

Boc protected dipeptide **9** (0.47 g, 1.4 mmol) was dissolved in a 1:1 CH_2Cl_2:TFA solution (10 mL) at 25 °C and allowed to react for 1.5 h, the solvent was then removed under reduced pressure and dried *in vacuo*. The TFA salt of deprotected dipeptide **9** was dissolved in a solution of DIEA (0.2 mL, 1.4 mmol) in anhydrous DMF (12 mL), and the mixture incubated for 10 min. In a separate flask a solution of PyBOP (0.88 g, 1.7 mmol), phthaloyl glycine (0.35 g, 1.7 mmol), HOAt (0.23 g, 1.7 mmol), and DIEA (0.8 mL, 5.1 mmol) in anhydrous DMF (8 mL) was allowed to incubate for 5 min and then added in one portion to the deprotected dipeptide **9** solution. The reaction became a red color after 30 min, stirring was continued for 12 h, at which time the DMF was removed under reduced pressure, yielding a brown viscous oil. The oil was partially dissolved in EtOAc and washed with a saturated aqueous $NaHCO_3$ solution, Et_2O was then added to the organic layer precipitating out the semi-pure tripeptide which was collected by filtration and further purified by RP-HPLC (water:CH_3CN gradient; C18 column) giving a white solid (0.59 g, 96%). ^{1}H NMR (300 MHz, d_6-DMSO) δ: 8.53-8.62 (m, 1H, CH_2-N**H**-CO), 8.53-8.62 (m, 1H, CH-N**H**-CO), 7.79-7.95 (m, 4H, Ar), 7.13-7.33 (m, 5H, Ar H), 4.54 (sextet, 1H, C-CH-N), 4.18 (dd, J = 17.0, 28.6, 2H, Ar-CH_2-C), 3.86 (dd, J =

2.0, 5.8, 2H, N-CH_2-CO-N), 3.63 (s, 3H, CH_3-O), 3.01 (dd, *J* = 4.6, 14.0, 1H, N-C**H**(H)-CO-O), 2.76 (dd, *J* = 9.8, 14.0, 1H, N-CH(**H**)-CO-O); ^{13}C NMR (75 MHz, d_6-DMSO) δ: 171.5, 170.2, 167.4, 165.9, 137.6, 134.5, 131.6, 129.2, 128.0, 123.1, 53.7, 51. 6, 40.6; MS (ESI^+) [M + H^+] 424.2; HRMS (ESI^+) [M + H^+] calcd for $C_{22}H_{22}N_3O_6$: 424.1512, found: 424.1503; Elemental analysis: calcd for $C_{22}H_{21}N_3O_6$: C,62.41; H, 5.00; N, 9.92; O, 22.67. found: C, 62.67; H, 5.17; N, 9.85; O, 22.31. M.P. 232-234 °C.

Methyl 2-(2-(2-(1,3-dioxoisoindolin-2-yl)acetamido)-2-(pyridin-4-yl)acetamido)acetate (1):

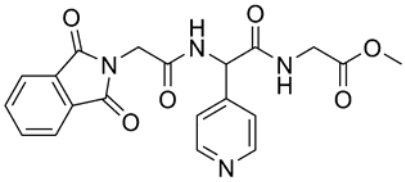

The HCl salt of deprotected dipeptide **10** (1.50g, 5.10 mmol) was dissolved in a solution of DIEA (1.7 mL, 10.2 mmol) in anhydrous DMF (20 mL), the reaction mixture instantly became a yellow color, and the mixture incubated for 10 min. In a separate flask a solution of PyBOP (3.18 g, 6.1 mmol), phthaloyl glycine (1.26 g, 6.1 mmol), HOAt (0.83 g, 6..1 mmol), and DIEA (3.0 mL, 18.4 mmol) in anhydrous DMF (10 mL) was allowed to incubate for 5 min and then added in one portion to the deprotected dipeptide **10** solution. The reaction became a red color after 30 min and a precipitate formed after one h, stirring was continued for 12 h, the DMF was removed under reduced pressure and the mixture taken up in CH_2Cl_2, the insoluble material was filtered off and washed with CH_2Cl_2 and dried to give a white powder which was further purified by RP-HPLC (water:CH_3CN gradient; C18 column) giving a white solid (1.93 g, 93 %). ^{1}H

NMR (300 MHz, d_6-DMSO) δ: 9.62 (d, J = 8.2, 1H, CH-N**H**-CO), 9.35 (t, J = 5.9, 1H, CH_2-N**H**-CO), 8.98 (d, J = 5.4, 2H, α-pyr H), 7.82-7.93 (m, 4H, Ar H), 7.41 (d, J = 6.0, 2H, β-pyr H), 5.51 (d, J = 8.2, 1H, C-CH-N), 4.38 (s, 2H, N-CH_2-CO-N), 3.91 (dd, J = 3.0, 5.7, 2H, N-CH_2-CO-O), 3.55 (s, 3H, CH_3-O); ^{13}C NMR (75 MHz, d_6-DMSO) δ: 169.9, 168.9, 167.5, 166.1, 149.7, 147.0, 134.7, 131.6, 123.3, 122.0, 55.1, 51.8, 40.7, 39.9; MS (ESI^+) [M + H^+] 411.1311; HRMS (ESI^+) [M + H^+] calcd for $C_{20}H_{19}N_4O_6$: 411.1307, found: 411.1299; Elemental analysis: calcd for $C_{20}H_{18}N_4O_6$: C, 58.53; H, 4.42; N, 13.65; O, 23.39. found: C, 58.49; H, 4.58; N, 13.59; O, 23.34; The onset of decomposition between 252-255 °C occurred before a melting point.

Methyl 2-(2-(2-(1,3-dioxoisoindolin-2-yl)acetamido)-2-(pyridin-3-yl)acetamido)acetate (3):

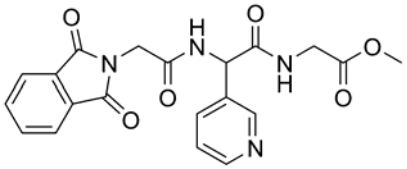

The HCl salt of deprotected dipeptide **11** (1.50 g, 5.1 mmol) was dissolved in a solution of DIEA (1.7 mL, 10.2 mmol) in anhydrous DMF (20 mL), the reaction mixture instantly became a yellow color, and the mixture incubated for 10 min. In a separate flask a solution of PyBOP (3.18 g, 6.1 mmol), phthaloyl glycine (1.26 g, 6.1 mmol), HOAt (0.83 g, 6..1 mmol), and DIEA (3.0 mL, 18.4 mmol) in anhydrous DMF (10 mL) was allowed to incubate for 5 min and then added in one portion to the deprotected dipeptide **11** solution. The reaction became a red color after 30 min and a precipitate formed after one h, stirring was continued for 12 h, at which time the DMF was removed

under reduced pressure, yielding a crude brown viscous oil. The oil was dissolved in a minimum amount of MeOH:H_2O:TFA and semi-purified by flash column chromatography (silica gel, eluant; 94:5:1 EtOAc:MeOH:Et_3N) and the product dried *in vacuo* to give a yellow powder, which was further purified by RP-HPLC (water:CH_3CN gradient; C18 column) giving a white solid (1.67 g, 80%), which could be crystallized from a 95:5 CH_3CN:water mixture as thin white needles for X-ray structural analysis. ^1H NMR (300 MHz, d_6-DMSO) δ: 9.16 (d, J = 7.9, 1H, CH-N**H**-CO), 8.93 (t, J = 5.6, 1H, CH_2-N**H**-CO), 8.63 (s, 1H, pyr H), 8.51 (d, J = 4.5, 2H, pyr H), 7.82-7.92 (m, 4H, Ar H), 7.79 (dt, J = 1.7, 7.7, 1H, pyr H), 7.40 (dd, J = 4.7, 7.9, 1H, pyr H), 5.61 (d, J = 8.0, 1H, C-CH-N), 4.34 (dd, J = 3.4, 20.5, 2H, N-CH_2-CO-N), 3.90 (dd, J = 1.3, 6.0, 2H, N-CH_2-CO-O), 3.61 (s, 3H, CH_3-O); ^{13}C NMR (75 MHz, d_6-DMSO) δ: 169.9, 169.4, 167.5, 165.9, 148.9, 148.6, 134.7, 134.6, 131.6, 123.6, 123.5, 123.2, 54.0, 51.8, 40.7, 39.9; MS (ESI^+) [M + H^+] 411.13; HRMS (ESI^+) [M + H^+] calcd for $C_{20}H_{19}N_4O_6$: 411.1302, found: 411.1299; Elemental analysis: calcd for $C_{20}H_{18}N_4O_6$: C, 58.53; H, 4.42; N, 13.65; O, 23.39. found: C, 58.22; H, 4.59; N, 13.64; O, 23.55; The onset of decomposition between 244-247 °C occurred before a melting point.

General procedure for the coordination of tripeptides 1-4 with pincer complex 5:

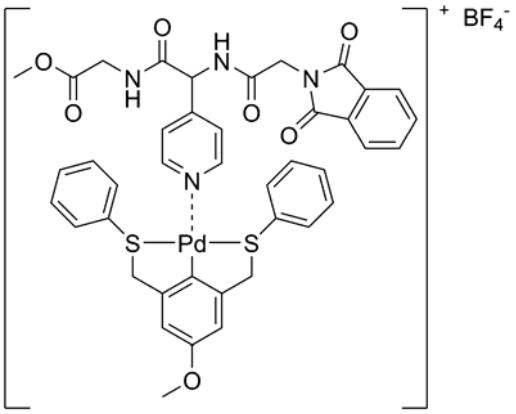

Each tripeptide (5.0 or 5.2 mg, 0.012 mmol) was dissolved in d_6-DMSO (1 mL) in an NMR tube and one equivalent of pincer complex **5** (6.0 mg, 0.012 mmol) was titrated in from a 0.6 M d_6-DMSO stock solution (1:1 molar ratio based on ^{1}H NMR integration of an aromatic signal from each molecule), $AgBF_4$ was then added to the solution in one portion and a precipitate instantly crashed out. The NMR tube mixture was oscillated for 2 h and then filtered through celite and a 0.2 μm PTFE syringe filter and the clear yellow solution was reanalyzed.

General procedure for the ITC measurements of the coordination of tripeptides 1-4 with pincer complex 14:

The ITC syringe was filled with a degassed DMSO tripeptide solution (50 mM) and titrated into the sample cell, which was filled with a degassed DMSO solution of pincer complex **14** (5 mM).

3.6 References

[1] Lehn, J.-M., *Supramolecular Chemistry*, VCH, Weinheim, **1995**.

[2] Steed, J. W., Atwood, J. L., *Supramolecular Chemistry: a concise introduction*, John Wiley & Sons, Chichester, **2000**.

[3] Whitesides, G. M., Mathias, J. P., Seto, C. T. Molecular self-assembly and nanochemistry: a chemical strategy for the synthesis of nanostructures. *Science* **1991**, *254*, 1312-1319.

[4] Lindsey, J. S. Self-assembly in synthetic routes to molecular devices. Biological principles and chemical perspectives: a review. *New J. Chem.* **1991**, *15*, 153-180.

[5] Lehn, J.-M. Toward complex matter: Supramolecular chemistry and self-organization. *Proc. Natl. Acad. Sci. USA* **2002**, *99*, 4763-4768.

[6] Zhang, S. Fabrication of novel biomaterials through molecular self-assembly. *Nature Biotechnology* **2003**, *21*, 1171-1178.

[7] Seeman, N. C., Belcher, A. M. Emulating biology: building nanostructures from the bottom up. *Proc. Natl. Acad. Sci. USA* **2002**, *99*, 6451-6455.

[8] Jones, D. D., Barker, P. D. Controlling self-assembly by linking protein folding, DNA binding, and the redox chemistry of heme. *Angew. Chem. Int. Ed.* **2005**, *44*, 6337-6341.

[9] Voet, D., Pratt, C. W., Voet, J. G., *Fundamentals of Biochemistry*, John Wiley & Sons, Chichester, **2004**.

[10] Parraga, G., Horvath, S. J., Eisen, A., Taylor, W. E., Hood, L., Young, E. T., Klevit, R. E. Zinc-dependent structure of a single-finger domain of yeast ADR1. *Science* **1988**, *241*, 1489-1492.

[11] Warner, M., Gustafsson, J. A. Cytochrome P450 in the brain: neuroendocrine functions. *Frontiers Neuroendocrinology* **1995**, *16*, 224-236.

[12] Seidel, S. R., Stang, P. J. High-Symmetry Coordination cages via Self-Assembly *Acc. Chem. Res.* **1998**, *35*, 972-983.

[13] Stang, P. J. Molecular architecture: coordination as the motif in the rational design and assembly of discrete supramolecular species - self-assembly of metallacyclic polygons and polyhedra. *Chem. Eur. J.* **1998**, *4*, 19-27.

[14] Holliday, B. J., Mirkin, C. A. Strategies for the construction of supramolecular compounds through coordination chemistry. *Angew. Chem. Int. Ed.* **2001**, *40*, 2022-2043.

[15] Huck, W. T. S., Hulst, R., Timmerman, P., van Veggel, F. C. J. M., Reinhoudt, D. N. Noncovalent synthesis of nanostructures: combining coordination chemistry and hydrogen bonding. *Angew. Chem., Int. Ed. Engl.* **1997**, *36*, 1006-1008.

[16] Huck, W. T. S., van Veggel, F. C. J. M., Kropman, B. L., Blank, D. H. A., Keim, E. G., Smithers, M. M. A., Reinhoudt, D. N. Large Self-Assembled Organopalladium Spheres. *J. Am. Chem. Soc.* **1995**, *117*, 8293-8294.

[17] Fujita, M., Umemoto, K., Yoshizawa, M., Fujita, N., Kusukawa, T., Biradha, K. Molecular Paneling *via* Coordination. *Chem. Commun.* **2001**, 509-518.

[18] Amijs, C. H. M., Berger, A., Soulimani, F., Visser, T., van Klink, G. P. M., Lutz, M., Spek, A. L., van Koten, G. Neutral Pyridyl-Functionalized C, N-ortho-Chelated Aminoaryl Platinum(II) Corner Building Blocks for Application in Coordination Reactions. *Inorg. Chem.* **2005**, *44*, 6567-6578.

[19] Hall, J. R., Loeb, S. J., Shimizu, G. K. H., Yap, G. P. A. Supramolecular arrays of 4,7-phenanthroline complexes: self-assembly of molecular Pd6 hexagons. *Angew. Chem. Int. Ed.* **1998**, *37*, 121-123.

[20] Dijkstra, H. P., Kruithof, C. A., Ronde, N., van de Coevering, R., Ramón, D. J., Vogt, D., van Klink, G. P. M., van Koten, G. Shape-Persistent Nanosize Organometallic Complexes: Synthesis and Application in a Nanofiltration Membrane Reactor. *J. Org. Chem.* **2003**, *68*, 675-685.

[21] Brunsveld, L., Folmer, B. J. B., Meijer, E. W., Sijbesma, R. P. Supramolecular Polymers. *Chem. Rev.* **2001**, *101*, 4071-4097.

[22] Hofmeier, H., El-ghayoury, A., Schenning, A. P. H. J., Schubert, U. S. New supramolecular polymers containing both terpyridine metal complexes and quadruple hydrogen bonding units. *Chem. Commun.* **2004**, 318-319.

[23] Hofmeier, H., Schubert, U. S. Combination of orthogonal supramolecular interactions in polymeric architectures. *Chem. Commun.* **2005**, 2423-2432.

[24] Gerhardt, W., Črne, M., Weck, M. Multifunctionalization of synthetic polymer systems through self-assembly. *Chem. Eur. J.* **2004**, *10*, 6212-6221.

[25] Higley, M. N., Pollino, J. M., Hollembeak, E., Weck, M. A modular approach toward block copolymers. *Chem. Eur. J.* **2005**, *11*, 2946-2953.

[26] Pollino, J. M., Stubbs, L. P., Weck, M. One-Step Multifunctionalization of Random Copolymers via Self-Assembly. *J. Am. Chem. Soc.* **2004**, *126*, 563-567.

[27] Pollino, J. M., Weck, M. Non-covalent side-chain polymers: design principles, functionalization strategies, and perspectives. *Chem. Soc. Rev.* **2005**, *34*, 193-207.

[28] Valkama, S., Lehtonen, O., Lappalainen, K., Kosonen, H., Castro, P., Repo, T., Torkkeli, M., Serimaa, R., ten Brinke, G., Leskelä, M., Ikkala, O. Multicomb polymeric supramolecules and their self-organization: Combination of coordination and ionic interactions. *Macromol. Rapid Commun.* **2003**, *24*, 556-560.

[29] Calzia, K. J., Tew, G. N. Methacrylate Polymers Containing Metal Binding Ligands for Use in Supramolecular Materials: Random Copolymers Containing Terpyridines. *Macromolecules* **2002**, *35*, 6090-6093.

[30] Iyer, P. K., Beck, J. B., Weder, C., Rowan, S. J. Synthesis and optical properties of metallo-supramolecular polymers. *Chem. Commun.* **2005**, 319-321.

[31] Dobrawa, R., Würthner, F. Metallosupramolecular approach toward functional coordination polymers. *J. Polym. Sci., Part A: Polym. Chem.* **2005**, *43*, 4981-4995.

[32] Loeb, S. J., Shimizu, G. K. H. Dimetalated thioether complexes as building blocks for organometallic coordination polymers and aggregates. *J. Chem. Soc., Chem. Commun.* **1993**, 1395-1397.

[33] Ghadiri, M. R., Choi, C. Secondary structure nucleation in peptides. Transition metal ion stabilized a-helices. *J. Am. Chem. Soc.* **1990**, *112*, 1630-1632.

[34] Ghadiri, M. R., Fernholz, A. K. Peptide architecture. Design of stable a-helical metallopeptides via a novel exchange-inert ruthenium(III) complex. *J. Am. Chem. Soc.* **1990**, *112*, 9633-9635.

[35] Handel, T., DeGrado, W. F. De novo design of a Zn2+-binding protein. *J. Am. Chem. Soc.* **1990**, *112*, 6710-6711.

[36] Hamachi, I., Kasagi, N., Kiyonaka, S., Nagase, T., Mito-oka, Y., Shinkai, S. Pd(en) as a sequence-selective molecular pinch for a-helical peptides. *Chem. Lett.* **2001**, 16-17.

[37] Lieberman, M., Sasaki, T. Iron(II) organizes a synthetic peptide into three-helix bundles. *J. Am. Chem. Soc.* **1991**, *113*, 1470-1471.

[38] Lieberman, M., Tabet, M., Sasaki, T. Dynamic Structure and Potential Energy Surface of a Three-Helix Bundle Protein. *J. Am. Chem. Soc.* **1994**, *116*, 5035-5044.

[39] Schmuck, C., Wennemers, H., *Highlights in Bioorganic Chemistry: Methods and Applications*, VCH, Weinheim, **2004**.

[40] Ruan, F., Chen, Y., Hopkins, P. B. Metal ion-enhanced helicity in synthetic peptides containing unnatural, metal-ligating residues. *J. Am. Chem. Soc.* **1990**, *112*, 9403-9404.

[41] Doerr, A. J., McLendon, G. L. Design, Folding, and Activities of Metal-Assembled Coiled Coil Proteins. *Inorg. Chem.* **2004**, *43*, 7916-7925.

[42] Di Costanzo, L., Geremia, S., Randaccio, L., Ichino, T., Yanagihara, R., Yamada, T., Marasco, D., Lombardi, A., Pavone, V. Conformational and coordination properties of a peptide containing the novel a,a-bis(2-pyridyl)glycine amino acid. *Dalton Trans.* **2003**, 787-792.

[43] Ishida, H., Kyakuno, M., Oishi, S. Molecular design of functional peptides by utilizing unnatural amino acids: toward artificial and photofunctional protein. *Biopolymers* **2004**, *76*, 69-82.

[44] Ohr, K., Gilmartin, B. P., Williams, M. E. Pyridine-Substituted Oligopeptides as Scaffolds for the Assembly of Multimetallic Complexes: Variation of Chain Length. *Inorg. Chem.* **2005**, *44*, 7876-7885.

[45] Tsurkan, M. V., Ogawa, M. Y. Metal-peptide nanoassemblies. *Chem. Commun.* **2004**, 2092-2093.

[46] Gilmartin, B. P., Ohr, K., McLaughlin, R. L., Koerner, R., Williams, M. E. Artificial oligopeptide scaffolds for stoichiometric metal binding. *J. Am. Chem. Soc.* **2005**, *127*, 9546-9555.

[47] Albrecht, M., van Koten, G. Platinum group organometallics based on "pincer" complexes: sensors, switches, and catalysts. *Angew. Chem. Int. Ed.* **2001**, *40*, 3750-3781

[48] van Manen, H.-J., Nakashima, K., Shinkai, S., Kooijman, H., Spek, A. L., van Veggel, F. C. J. M., Reinhoudt, D. N. Coordination chemistry of SCS PdII pincer systems. *Eur. J. Inorg. Chem.* **2000**, 2533-2540.

[49] Yount, W. C., Loveless, D. M., Craig, S. L. Strong means slow: Dynamic contributions to the bulk mechanical properties of supramolecular networks. *Angew. Chem. Int. Ed.* **2005**, *44*, 2746-2748

[50] van Manen, H.-J., Fokkens, R. H., van Veggel, F. C. J. M., Reinhoudt, D. N. Noncovalent synthesis of water-soluble SCS PdII pincer assemblies. *Eur. J. Org. Chem.* **2002**, 3189-3197.

[51] Albrecht, M., Rodríguez, G., Schoenmaker, J., van Koten, G. New Peptide Labels Containing Covalently Bonded Platinum(II) Centers as Diagnostic Biomarkers and Biosensors. *Org. Lett.* **2000**, *2*, 3461-3464.

[52] Guillena, G., Rodríguez, G., van Koten, G. Palladium(II) pincer complexes of a-amino acids: towards the synthesis of catalytically active artificial peptides. *Tetrahedron Lett.* **2002**, *43*, 3895-3898.

[53] Guillena, G., Rodríguez, G., Albrecht, M., van Koten, G. Covalently bonded platinum(II) complexes of a-amino acids and peptides as a potential tool for protein labeling. *Chem. Eur. J.* **2002**, *8*, 5368-5376.

[54] Huck, W. T. S., Van Veggel, F. C. J. M., Reinhoudt, D. N. Self-assembly of hyperbranched spheres. *J. Mater. Chem.* **1997**, *7*, 1213-1219.

[55] Pollino, J. M., Nair, K. P., Stubbs, L. P., Adams, J., Weck, M. Crosslinked and functionalized universal polymer backbones via simple, rapid, and orthogonal multi-site self-assembly. *Tetrahedron* **2004**, *60*, 7205-7215.

[56] Ugi, I. Potential of four component condensations for peptide syntheses. Study in isonitrile and ferrocene chemistry as well as stereochemistry and logics of syntheses. *Intra-Science Chem. Rep.* **1971**, *5*, 229-261.

[57] Kunz, H., Sager, W. Diastereoselective Strecker synthesis of a-amino nitriles in carbohydrate matrixes. *Angew. Chem., Int. Ed. Engl.* **1987**, *26*, 557-559.

[58] Kunz, H., Pfrengle, W. Asymmetric synthesis on carbohydrate templates: stereoselective Ugi-synthesis of α-amino acid derivatives. *J. Am. Chem. Soc.* **1988**, *110*, 651-652.

[59] Kunz, H., Pfrengle, W. Carbohydrates as chiral templates: asymmetric Ugi-synthesis of a-amino acids using galactosylamines as the chiral matrices. *Tetrahedron* **1988**, *44*, 5487-5494.

[60] Kunz, H., Pfrengle, W., Sager, W. Carbohydrates as chiral templates: diastereoselective Ugi synthesis of (S)-amino acids using O-acylated D-arabinopyranosylamine as the auxiliary. *Tetrahedron Lett.* **1989**, *30*, 4109-4110.

[61] Kunz, H., Pfrengle, W., Rück, K., Sager, W. Stereoselective synthesis of L-amino acids via Strecker and Ugi reactions on carbohydrate templates. *Synthesis* **1991**, 1039-1042.

[62] Tamura, S. Y., Levy, O. E., Uong, T. H., Reiner, J. E., Goldman, E. A., Ho, J. Z., Cohen, C. R., Bergum, P. W., Nutt, R. F., Brunck, T. K., Semple, J. E. Guanylpiperidine peptidomimetics: potent and selective bis-cation inhibitors of factor Xa. *Bioorg. Med. Chem. Lett.* **2000**, *10*, 745-749.

[63] Sen, A., Lai, T.-W. Catalysis by solvated transition-metal cations. Novel catalytic transformations of alkenes by tetrakis(acetonitrile)palladium ditetrafluoroborate. Evidence for the formation of incipient carbonium ions as intermediates. *J. Am. Chem. Soc* **1981**, *103*, 4627-4629.

[64] Pollino, J. M., Weck, M. Supramolecular side-chain functionalized polymers: synthesis and self-assembly behavior of polynorbornenes bearing PdII SCS pincer complexes. *Synthesis* **2002**, 1277-1285.

[65] Yount, W. C., Juwarker, H., Craig, S. L. Orthogonal Control of Dissociation Dynamics Relative to Thermodynamics in a Main-Chain Reversible Polymer. *J. Am. Chem. Soc.* **2003**, *125*, 15302-15303.

[66] Pollino, J. M., Weck, M. Tandem Catalysis and Self-Assembly: A One-Pot Approach to Functionalized Polymers. *Org. Lett.* **2002**, *4*, 753-756.

[67] Huck, W. T. S., van Veggel, F. C. J. M., Reinhoudt, D. N. Controlled assembly of nanosized metallodendrimers. *Angew. Chem., Int. Ed. Engl.* **1996**, *35*, 1213-1215.

[68] Arnaud, A., Bouteiller, L. Isothermal Titration Calorimetry of Supramolecular Polymers. *Langmuir* **2004**, *20*, 6858-6863.

[69] Holdgate, G. A., Ward, W. H. J. Measurements of binding thermodynamics in drug discovery. *Drug Discovery Today* **2005**, *10*, 1543-1550.

[70] Holdgate, G. A. Making cool drugs hot: isothermal titration calorimetry as a tool to study binding energetics. *Biotechniques* **2001**, *31*, 164-185.

[71] Huck, W. T. S., Prins, L. J., Fokkens, R. H., Nibbering, N. M. M., van Veggel, F. C. J. M., Reinhoudt, D. N. Convergent and Divergent Noncovalent Synthesis of Metallodendrimers. *J. Am. Chem. Soc.* **1998**, *120*, 6240-6246.

[72] Zhang, Y.-L., Zhang, Z.-Y. Low-affinity binding determined by titration calorimetry using a high-affinity coupling ligand: a thermodynamic study of ligand binding to protein tyrosine phosphatase 1B. *Anal. Biochem.* **1998**, *261*, 139-148.

[73] Slagt, M. Q., Rodríguez, G., Grutters, M. M. P., Gebbink, R. J. M. K., Klopper, W., Jenneskens, L. W., Lutz, M., Spek, A. L., van Koten, G. Synthesis and properties of para-substituted NCN-pincer palladium and platinum complexes. *Chem. Eur. J.* **2004**, *10*, 1331-1344.

[74] Cooke, G., Rotello, V. M. Methods of modulating hydrogen bonded interactions in synthetic host-guest systems. *Chem. Soc. Rev.* **2002**, *31*, 275-286.

[75] Burd, C., Weck, M. Self-Sorting in Polymers. *Macromolecules* **2005**, *38*, 7225-7230.

[76] Murray, T. J., Zimmerman, S. C. New triply hydrogen bonded complexes with highly variable stabilities. *J. Am. Chem. Soc.* **1992**, *114*, 4010-4011.

Chapter 4

The Synthesis of a Pyridyl Cyclic Peptide: A Preprogrammed Building Block For Supramolecular Architectures

4.1 Abstract

This chapter introduces D,L cyclic peptides. They are supramolecular synthons, which readily self-assemble into well-defined organic nanotubes. By incorporating a pyridyl functionality into one of the side-chains, the cyclic peptide was converted into a multifunctional supramolecular synthon, becoming a ligand for a metallated pincer complex. The synthesis of this new pyridyl side-chain functionalized cyclic octapeptide has been described, multiple solid-phase strategies were initially attempted following similar literature protocols. However, this route was abandoned for a solution-phase approach. Several different solution-phase routes starting from different points in the cycle were attempted until the intricacies of the synthesis were determined and the most efficient route was chosen. Purification was an additional hurdle; the final product could not be purified using RP-HPLC, the literature protocol for cyclic peptides. Therefore, preparatory TLC was used to purify the cyclic peptide > 90%. The final product was characterized by 1-D and 2-D NMR and ES-MS. The next phase for this research is to carry out self-assembly studies and fully characterize the coordination complex formed from these new supramolecular synthons.

4.2 Introduction

Bases on a theoretical analysis in 1974 on the β-sheet conformations of alternating D,L, linear peptides, the possibility that their cyclic peptide analogs could self-assemble

into ring-stacked structures was put forth.[1] Inspired by this study, Ghadiri, in 1993, synthesized a cyclic octapeptide with the residue sequence *cyclo*[(D-alanine-L-glutamic acid-D-alanine-L-glutamine)$_2$].[2] The near planar ring of the peptide had the backbone amide protons and carbonyl oxygens pointing both above and below the plane of the backbone, while the stereogenic arrangement of the side-chains placed them in the plane pointing out towards the periphery, as shown in Figure 4.1.

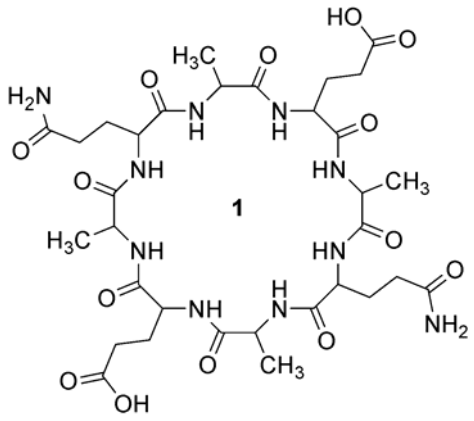

Figure 4.1 Ghadiri's first octa-cyclic peptide with D-alanine, L-glutamine and L-glutamic acid acting as a self-assembling proton-trigger.[2]

Upon acidification of an alkaline solution of cyclic peptide **1** the repulsive ionic side-chain interactions are nullified and attractive backbone H-bonding interactions lead to the self-assembly of infinite linear organic nanotubes through antiparallel β-sheet H-bonding, shown in Figure 4.2.[2]

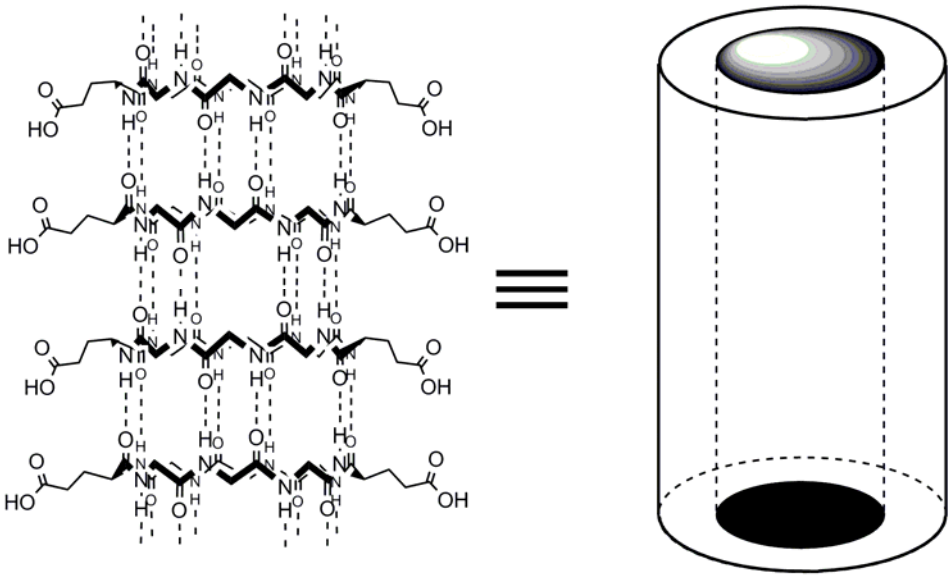

Figure 4.2 Self-assembly of D,L-cyclic octapeptide **1** into a well-defined organic nanotube.

Since this time, many alterations to the cyclic structure have been made by a number of different researchers.[2-27] The hydrophilicity of the exterior and interior can be modulated by the amino acids chosen.[13, 22] The inner diameter can be tuned by altering the even number of residues in the cycle's backbone.[4] Overall, the organic framework in conjunction with the mild self-assembly protocol allows for direct modification of these systems using traditional synthetic protocols makes cyclic peptides as a class of molecules a good candidate for a variety of potential applications.

Of particular interest to this research and its ultimate goal, is the use of cyclic peptides for membrane engineering. The first example ever of an artificial transmembrane channel was shown using side-chain modified α-cyclic peptide **2**, shown in Figure 4.3. The ten residue cycle had tryptophan and leucine modified exteriors (for membrane insertion), which self-assemble into membranes and have shown transport of glucose molecules.[4]

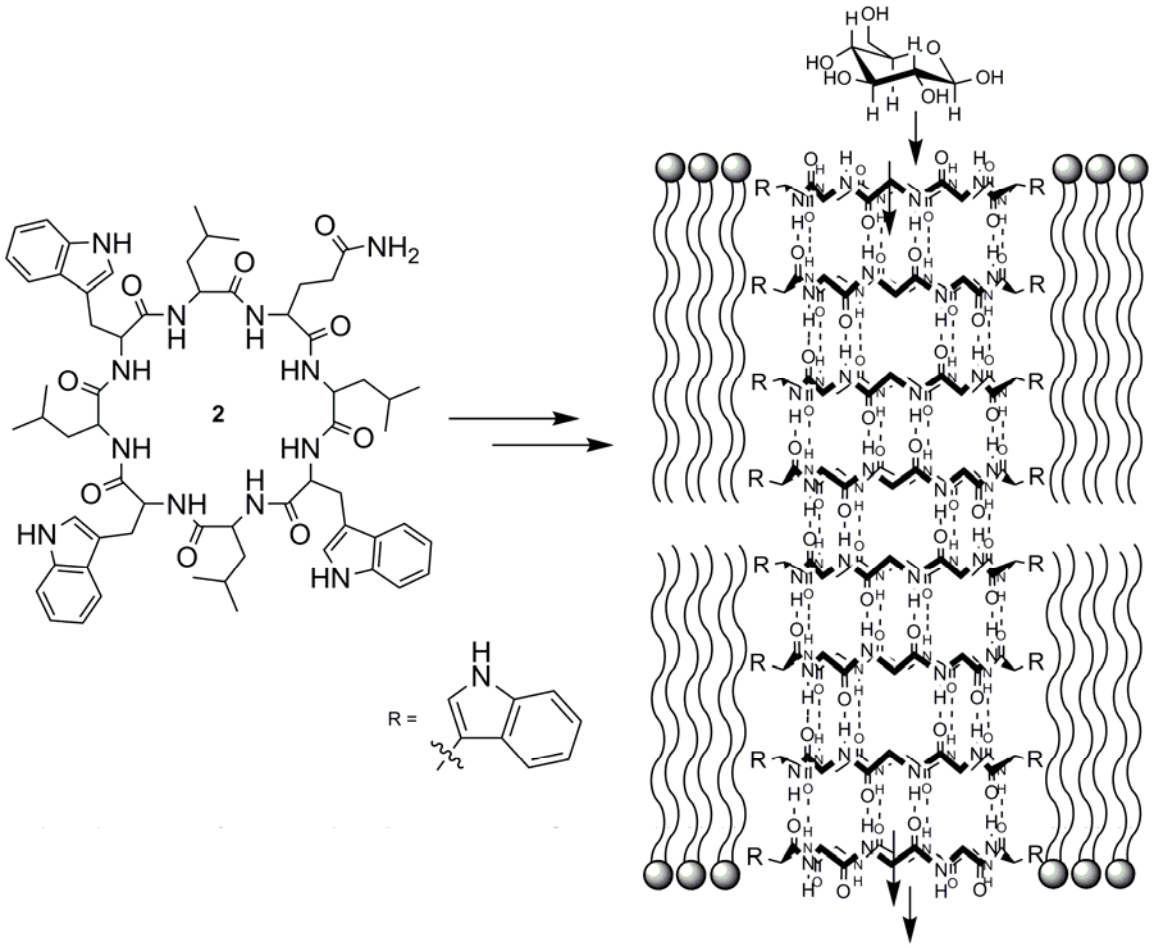

Figure 4.3 Tryptophan decorated **2** inserts into a lipid bilayer membrane and efficiently transporting glucose.[4]

By incorporating β- and γ-amino acids into the cyclic backbone, the functional range of these systems has also been expanded.[22-24, 26] Unlike α-amino acid cycles, β-amino acid cycles self-assemble through a parallel β-sheet H-bonding motif, this unidirectional arrangement of polar moieties gives the tubular architectures a net dipole moment improving the conductance properties and ion selectivity.[13] Hetero-nanotubes with tryptophan side-chain cycles 'capped' with hydrophilic side-chain cycles led to controlled rectifications and ion selectivity across lipid bilayer membranes.[15] These capping cycles

were used again as pore adapters in conjuction with a transmembrane pore protein, altering the selectivity of the original protein.[19] Recently, heterocyclic peptide structures made up of α,-amino acids/triazoles,[11, 18] α-amino acids/benzoic acids[25, 28] and α/γ-amino acids have provided new interior sites amenable to synthetic modifications,[22-24, 26] as shown in Figure 4.4.

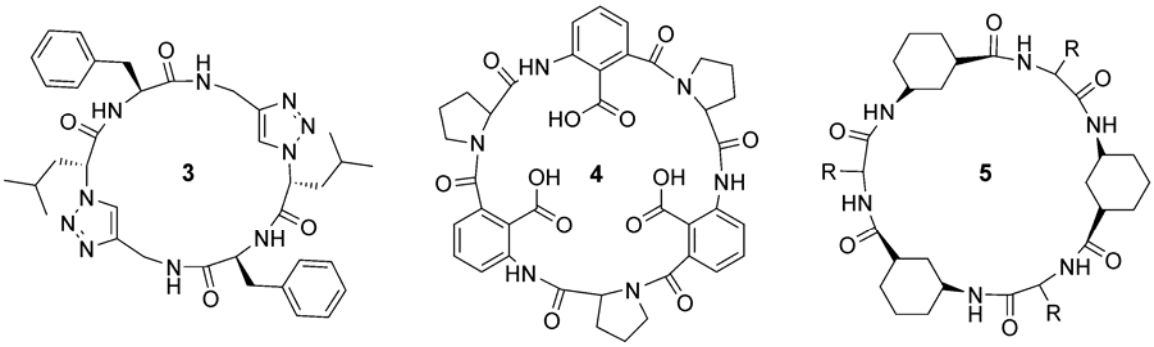

Figure 4.4 Recently synthesized cyclic peptides **3**,[11, 18] **4**[25, 28] and **5**[22-24, 26] have internal positions available for synthetic modifications.

Despite these many uses of cyclic peptides as attractive and functional supramolecular synthons, there are still a variety of potential modifications that can be made to the exterior and interior expanding the repertoire of this interesting class of molecules.[21, 27] By incorporating ligands into the side-chains, the cyclic peptide can be converted into a multifunctional supramolecular synthon with a unique 2-D self-assembly of orthogonal recognition units. While this research was commencing, Ghadiri published a report of a heterocyclic peptide formed through a 1,3 dipolar cycloaddition to give heterocyclic triazole cyclic peptide **6** with pendant tpy units for metal-coordination, as shown in Figure 4.5.[18] Ghadiri did not report on any metal-coordination studies with **6**,

and the harsher conditions required for coordination may limit the self-assembling potential of these systems.

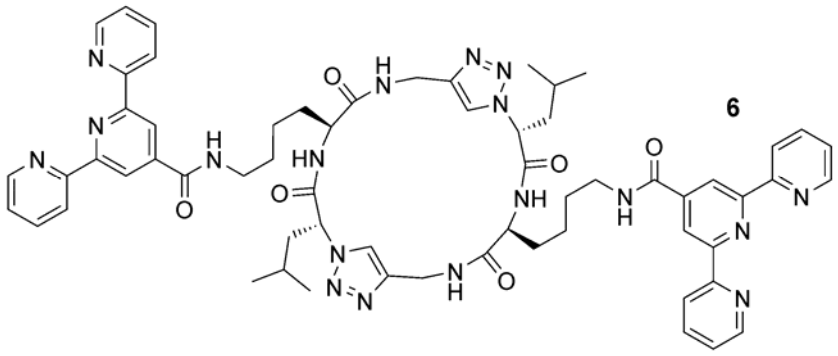

Figure 4.5 Tpy pendant triazole cyclic peptide.[18]

As an alternative to this system, we chose to incorporate a pyridyl unit into the side-chain owing to its well-established and straightforward coordination to a variety of transition-metal complexes.[29] The metallated pincer complex was chosen as the metal-coordinating unit, owing to its fast and quantitative coordination in a variety of solvents to a select class of ligands.[30] Investigational research into this new coordination between a ligand functionalized peptide and the metallated pincer complex was elaborated in Chapter 3.[32] Several different pyridyl substitution and spatial separation patterns from a linear peptide backbone were investigated to determine their affect and the affect of backbone functionalities on the metal-ligand interaction.

These preliminary studies revealed that all the peptides were quantitatively coordinated to the metallated pincer complex by ^{1}H NMR, but based on ITC experiments the 4-pyridyl systems were shown to be superior owing to their favorable steric and electronic effects versus their 3-pyridyl analogs. Based on these results we anticipated

that a multitopic cyclic peptide such as **7**, shown in Figure 4.6, could be used as a new supramolecular synthon for the generation of attractive biological architectures, such as that shown in Figure 4.7.

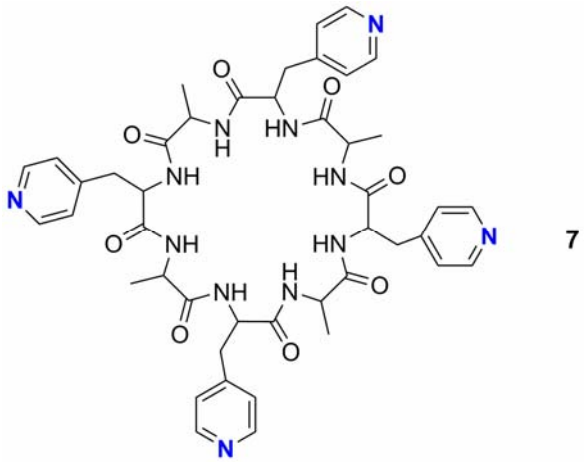

Figure 4.6 Envisaged cyclic peptide supramolecular synthon.

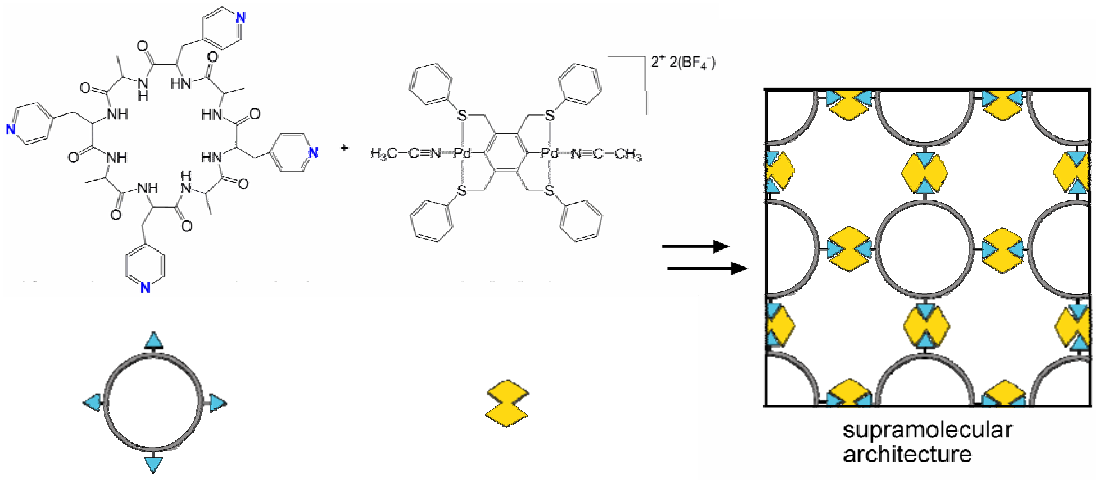

Figure 4.7 Proposed supramolecular architecture from cyclic peptide synthons and metallated pincer complexes.

4.3 Cyclic Peptide Design and Synthesis

Our first cyclic peptide was purposely modeled after an early cycle from Ghadiri, *cyclo*[(D-alanine-L-phenylalanine)-4],[8] with only one of the L-phenylalanines replaced with an L-pyridylalanine making monotopic cyclic peptide ligand **8**, shown in Figure 4.8. In both of these cycles all of the alanyl amido nitrogens are N-methylated. N-methylation of every other residue eliminates H-bonding interactions from one face of the cycle leading to self-assembly of dimeric structures,[17] as shown in Figure 4.8, instead of infinite tubular assemblies dramatically improving the solubility and simplifying the characterization of these systems. Later on, preliminary coordination studies will also be simplified using these N-methylated cyclic peptides.

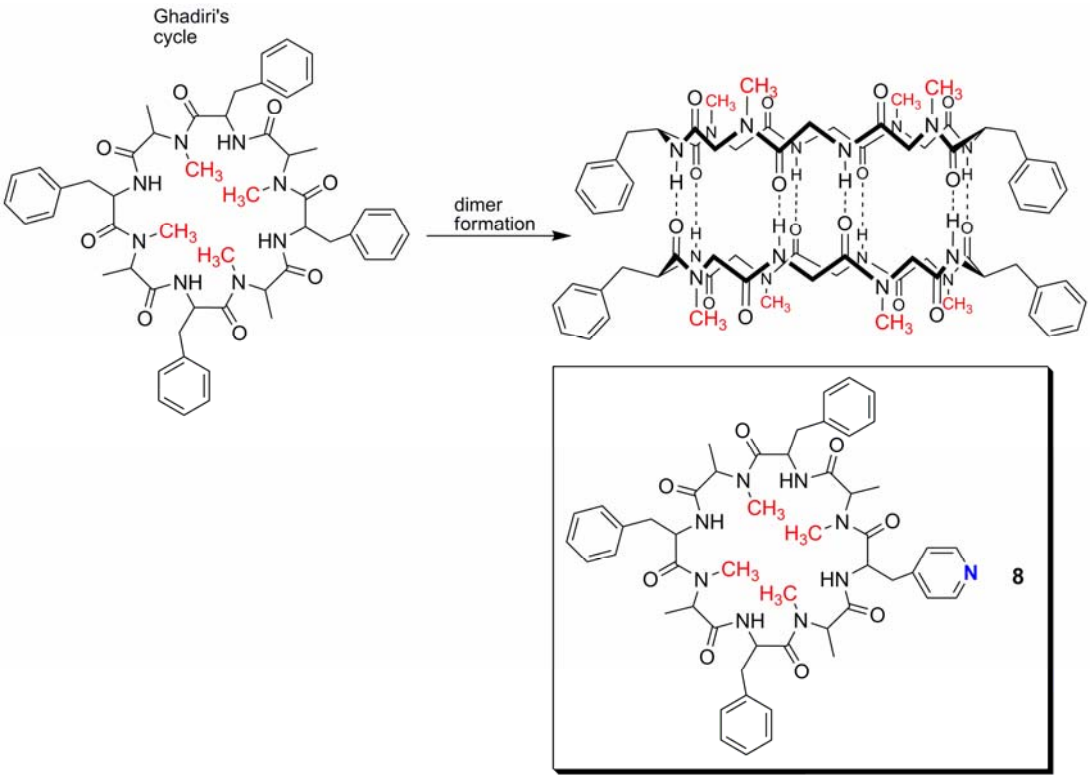

Figure 4.8 Dimer formation due to amido N-methylation of one face of the cyclic peptide; 1st cyclic peptide target **8**.[17]

4.3.1 Resin Supported Solid-Phase Syntheses

Initially the Fmoc solid-phase synthetic strategy of Ghadiri was closely followed,[21] with several significant differences: 1) the substitution of one of the Fmoc-L-phenylalanines for an Fmoc-L-pyridylalanine; 2) the Wang residue was loaded with an Fmoc-L-phenylalanine instead of an N-methylated D-alanine, which was not commercially available. It is known that peptide cyclizations from a terminal N-methylated residue attacking from a 2° nitrogen are sterically more difficult than a 1° amine.[33] Coupling N-methylated amino acids to a resin also has diminished yields, which were hopefully minimized by repeating all coupling steps along the way. Following Ghadiri, the first solid-phase synthesis was carried out in DMF using 2-(1H-benzotriazol-1-yl)-1,1,3,3-tetramethyluronium hexafluorophosphate (HBTU) as the carboxylic acid activator with 2-(1H-7-azabenzotriazol-1-yl)-1,1,3,3-tetramethyluronium hexafluorophosphate (HATU) used during coupling of only the third residue to minimize diketopiperazine formation.[21] After acidic cleavage and RP-HPLC purification the off-white powder recovered was shown by ES-MS to be linear pyridyl octapeptide **9**, with a 35% yield, shown in Figure 4.9.

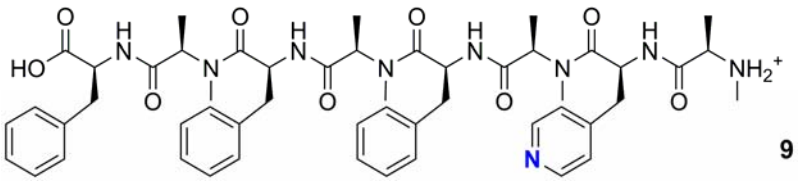

Figure 4.9 First monopyridyl linear octapeptide form solid-phase synthetic strategy.

After subsequent cyclization attempts using HATU activation along with HOAt as a nucleophilic additive in DMF, **8** was observed in the ES-MS of the crude sample, but multiple RP-HPLC attempts to isolate it were unsuccessful. The same results were obtained using other common activators such as HBTU, and 7-benzotriazole-1-yl-oxy-tris-pyrrolidino-phosphonium hexafluorophosphate (PyAOP). Based on these results we initially suspected that cyclization yields were critically low due to the ineffective cyclization from the 2° amine terminus. Additionally, the N-methylated residues were most likely limiting solid-phase yields of the linear peptide (overall linear yields were ~30%). Therefore, a new solid-phase route beginning from a Wang resin loaded with an Fmoc-D-alanine and ending with an unmethylated D-phenylalanine was carried out that would give cyclic peptide **10** shown in Figure 4.10. The third D-alanyl residue, fifth overall residue, was also left unmethylated in attempts to improve the overall yield, based on Ghadiri's report that N-methylation of only two of the four amido nitrogens on one face of the cycle was sufficient to suppress H-bonding and induce dimerization.[8]

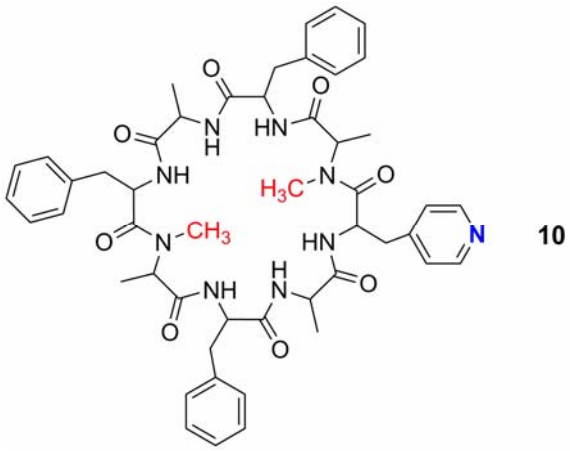

Figure 4.10 Half methylated face of 2nd cyclic peptide target **10**, expected to have a higher yielding solid-phase synthesis and cyclization.

After repeated RP-HPLC runs this new solid-phase synthesis still had a low overall yield of 25-35%, using several different activators. And cyclization attempts of the linear peptide also using a range of conditions showed the cyclic product by ES-MS, yet attempts to isolate the pure product by RP-HPLC were unsuccessful.

4.3.2 Solution-Phase Syntheses

Based on the inability to isolate pure cyclic peptide via a solid-phase approach, and the successful syntheses of linear pyridyl peptides from Chapter 3, it was decided that a solution-phase approach would yield larger quantities of cyclic peptide to work with during optimization of the final cyclization step. A solution-phase approach also permits characterization along the way, which may reveal a synthetically problematic point along the linear peptide synthesis that was surreptitiously handicapping the solid-phase yields.

Owing to the repetition of alternating units, the solution-phase approach was expedited by splitting each product and coupling at either end to incrementally double the linear peptide length. This approach also gave us the freedom to easily choose, the N-methylation pattern for the amino acids, and because the reaction were not done at an interface (like on a resin) the yields during the coupling of N-methylated amino acids were also improved. It was decided at this time that dimerization of the final cyclic product would still make characterization of a self-assembled system difficult owing to the two pyridyl units expected from the dimeric assembly, which may or may not be in register with one another. Based on Ghadiri's report, N-methylation of the L-phenylalanine residues led to complete suppression of all self-associations.[8] Therefore, the first solution-phase synthesis, cyclic peptide **11**, was designed with methyl groups at

the three L-phenylalanine and the L-pyridylalanine amido nitrogens, as shown in Figure 4.11.

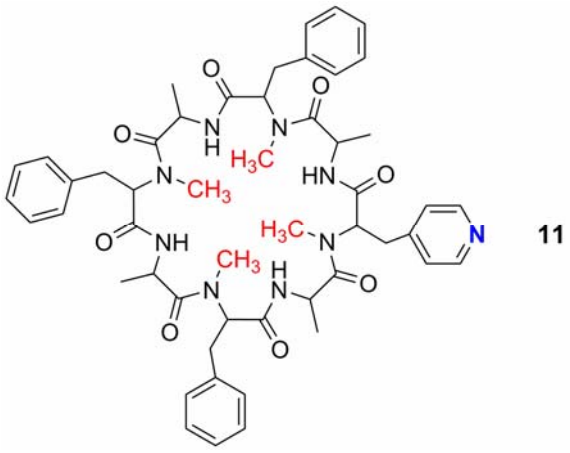

Figure 4.11 3rd cyclic target **11**, with 4-pyrAla and all three Phe's amido nitrogens N-methylated.

N-methylated derivatives of common amino acids are commercially available, but synthetic strategies were used to N-methylate L-pyridylalanine. The most direct synthetic route appeared to be N-methylation of a dipeptide with the L-pyridyl alanine unit at the N-terminus. The N-methylation protocol converts a terminal 1° amine into a methyl iminium ion and then formed an azanorbornene through a hetero Diels-Alder reaction, with the N-methylated product of the retro Diels-Alder captured by an ionic hydrogenation giving **13**, shown in Scheme 4.1.[34]

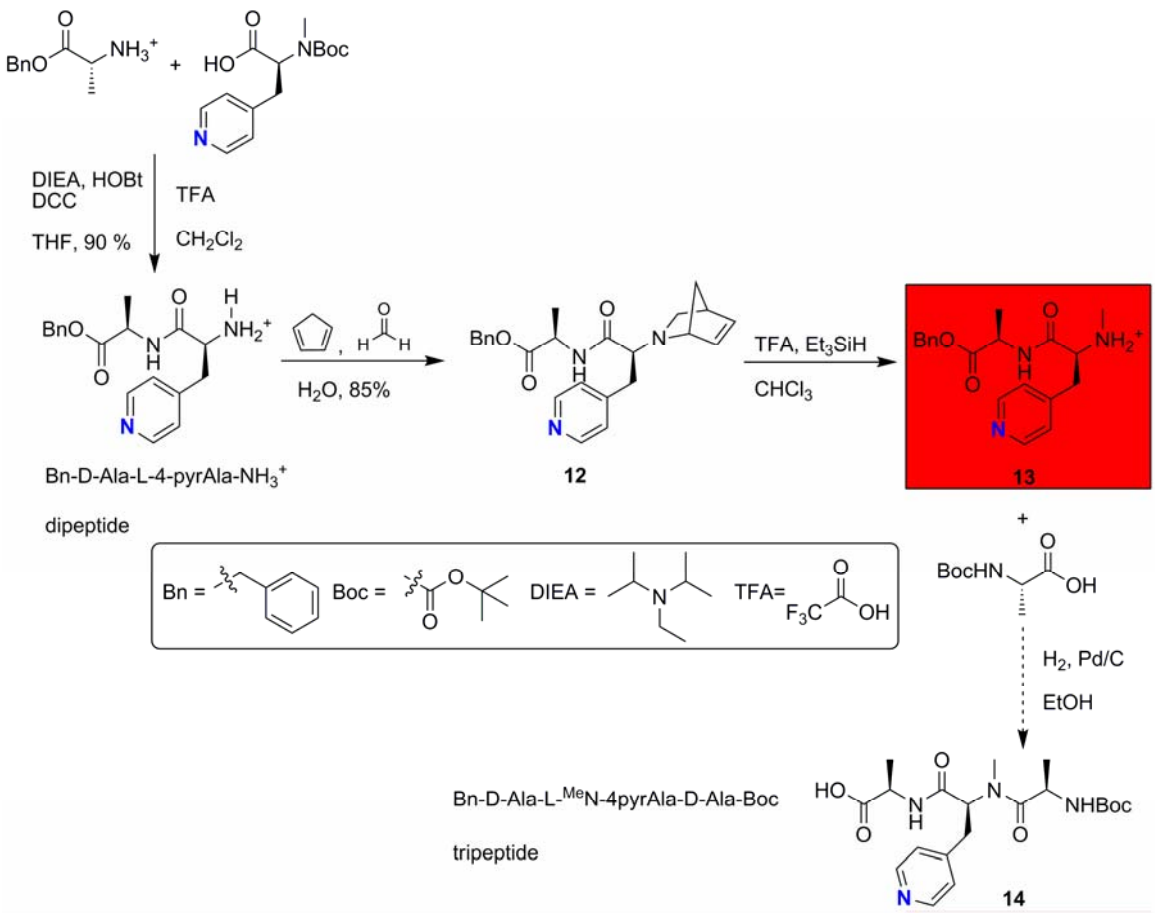

Scheme 4.1 Proposed synthesis of N-methylated pyridyltripeptide **14**.

Following this N-methylation route the most efficient overall synthesis is shown in Scheme 4.2. After coupling a D-alanine residue to **13**, tripeptide **14** could be coupled to pentapeptide **19** to give the final linear octapeptide **20**.

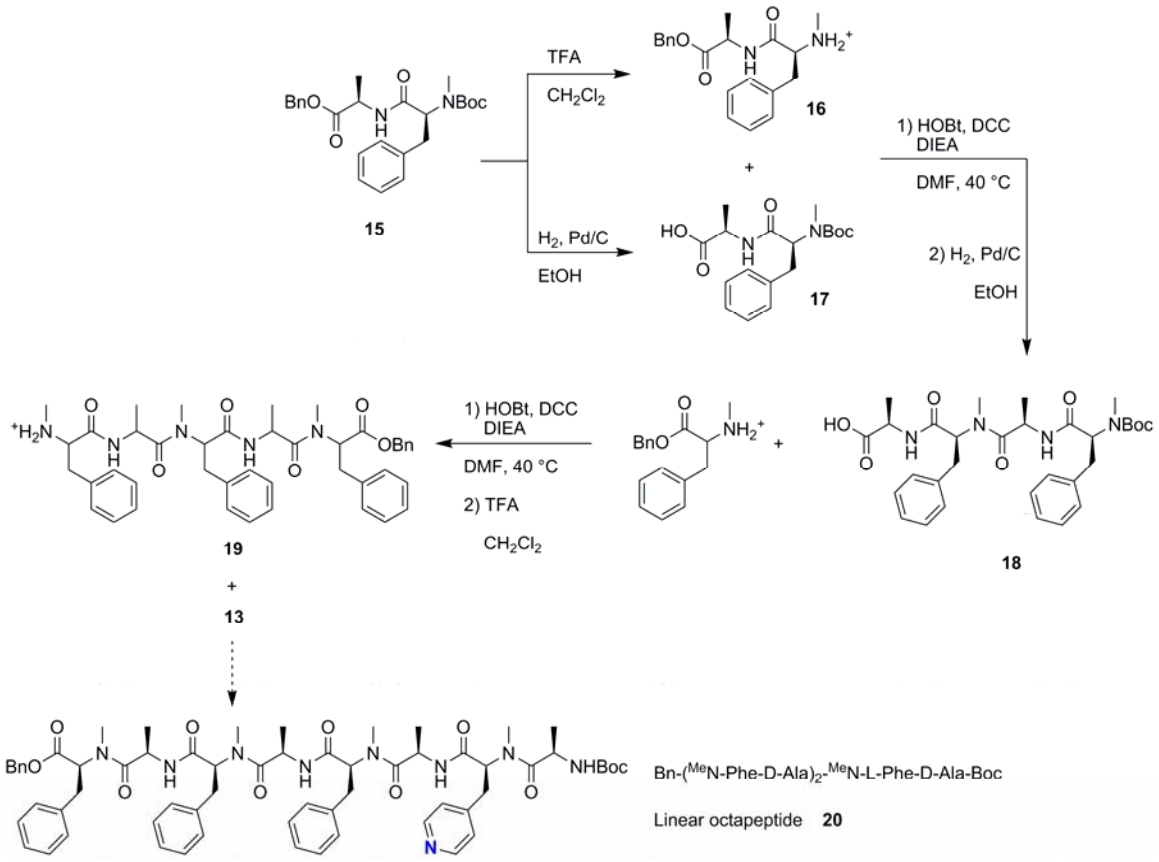

Scheme 4.2 Proposed synthesis of N-methylated pyridyl octapeptide **20**.

The syntheses of **14** and **19** were simultaneously carried out, each presenting a major problem. First, the retro Diels-Alder synthesis of **13** failed. And the coupling yields for **18** and **19**, using conditions taken from a relevant procedure of N-methylated residues,[35] were significantly lower than anticipated (~20%) presumed to be due to the poor coupling of terminal N-methylated L-phenylalanines.

Based on these unsatisfactory results a new solution-phase synthetic route was devised, to the 4th cyclic peptide target, **28**. This new route makes the assumption that N-methylating only half of the L-phenylalanies amido nitrogens will be sufficient to completely suppress self-association just as N-methylation of only half of the D-alanines

was sufficient to force dimerization.[8] Also, by only using a half N-methylation approach, the difficult amidation of the N-methyl amine terminus could be carried out on the very first step using a large excess of activators and the readily available Boc-D-alanine to maximize yields. After this step all subsequent amidations are with a 1° amino nucleophile, as shown in Scheme 4.3.

Each step along Scheme 4.3 was optimized for maximum yields. Yields of **22** were maximized by carrying out the amidation with 2.5 equivalents of Boc-D-alanine to counteract the lower nucleophilicity of the hindered amine of N-methylated **21**. Diketopiperazine formation was problematic during the amidations of deblocked **22** to pyridyl tripeptide **23** and tripeptide **24**, respectively.

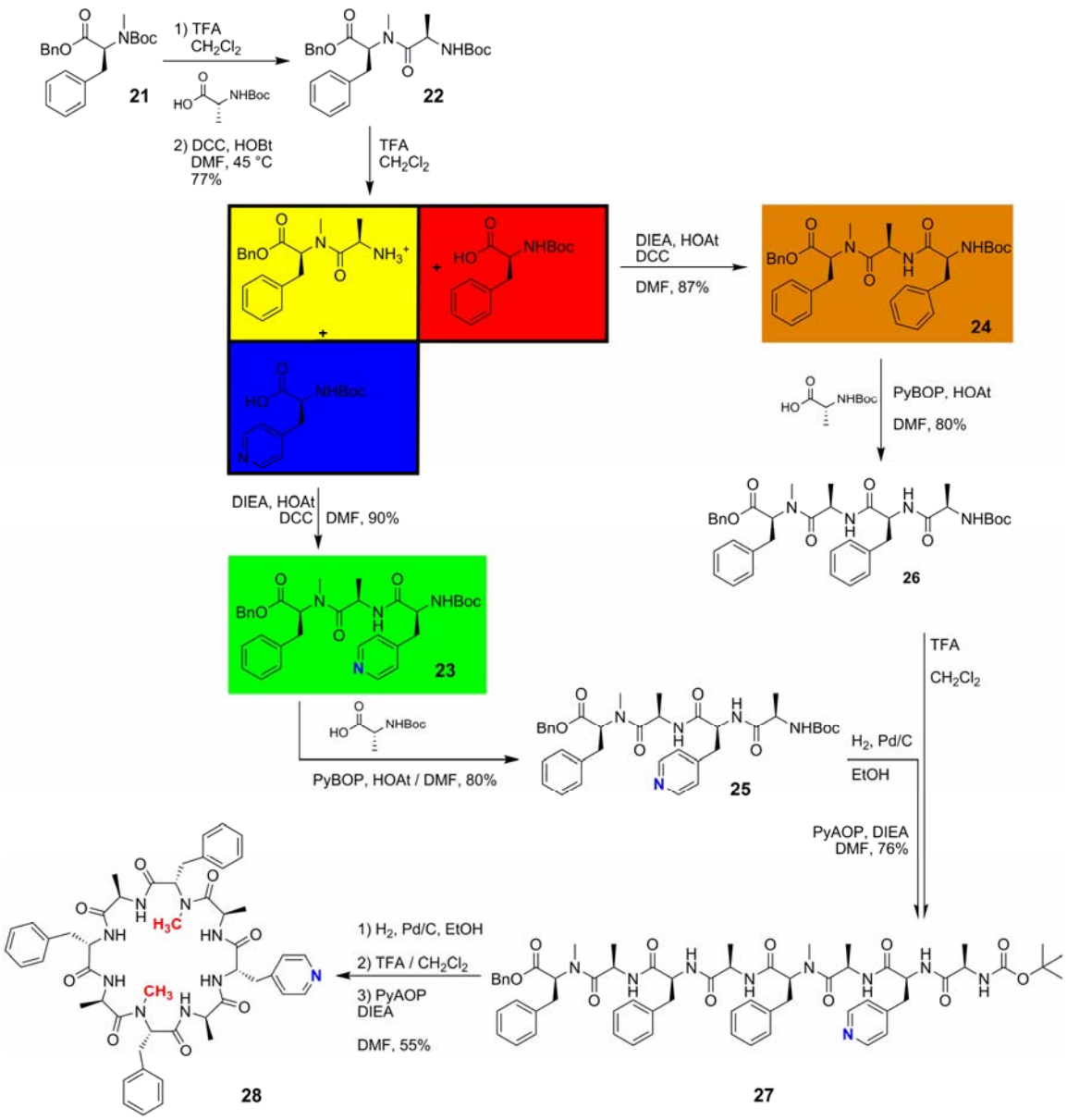

Scheme 4.3 Final synthetic scheme for synthesis of cyclic peptide **28**, the only N-methyl amidation step is during coupling of **21** to Boc-D-alanine in the first step.

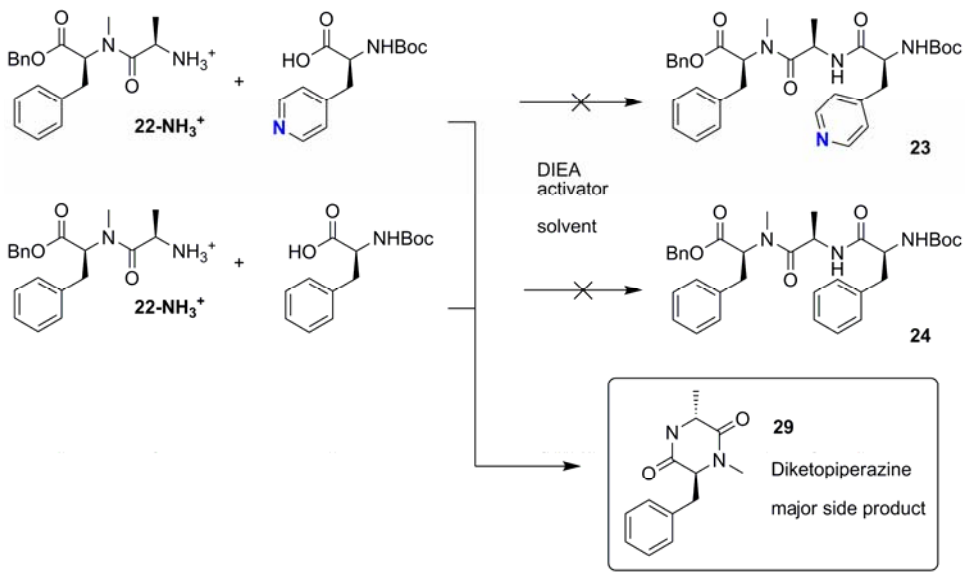

Scheme 4.4 Formation of diketopiperazine **29** during amidation of dipeptides to tripeptides.

Regardless of the activator used, formation of **29**, the entropically and enthalpically favored 6-membered lactam, was the major product with almost quantitative yields. This cyclization was completely suppressed by activating each carboxylic acid, Boc-L-phenylalanine and Boc-L-4-pyralanine, with DCC in DMF, then displacing the reactive O-acyl urea intermediate with HOAt forming a stable but labile active ester species, which was slowly amidated by the drop by drop addition of deprotected dipeptide **22** via a syringe pump giving excellent yields of tripeptide **23** and **24**.

After these couplings all additional amidations were formed in high yields using either phosphonium activators. Linear octapeptide **27** was biterminally deprotected and cyclization using PyAOP activation in DMF afforded the highest yields, 55%.

After cyclization, purification of cyclic peptide **28** was the final challenge. The same difficulties were experienced during RP-HPLC, a signal for **28** was observed on the chromatogram, but significant quantities of the product were inexplicably not recovered

from the eluent. At this point purification was attempted with normal phase flash column chromatography, during method development on silica TLC plates it was noticed that exposure to UV light led to decomposition of the spotted product.

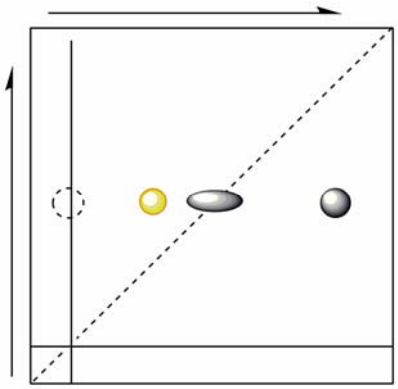

Figure 4.12 2-D Silica TLC plate, EtOAC/MeOH 95:5 mobile phase, solid circles off of dashed diagonal are decomposition products, additional impurities have been omitted for clarity.

Shown in Figure 4.12 is a diagram of the TLC retention of **28** on a 2-D TLC plate, the dashed circle to the far left was the R_f of **28** after the first run. After the first run, the TLC plate was positioned under a UV light (λ max = 254 nm) for two minutes. After this the plate was rotated 90° and developed again. The two spots off the diagonal appear to be decomposition products, one having a visible yellow color. While neither spot has been characterized, this decomposition may be complicating the RP-HPLC purification, which relies on a UV detector. Despite these results, TLC seemed to separate **28** from its impurities. Therefore, preparatory TLC was used to overcome the obstacles encountered with RP-HPLC purification, several iterative preparatory TLC developments were required to get cyclic peptide **28** to > 90% purity by ^{1}H NMR.

4.4 Experimental

Materials and Methods:

Boc-L-4-pyralanine was purchased from Peptech Corp. CH_2Cl_2 and THF were dried via passage through Cu_2O and alumina columns. N,N-Diisopropyl-ethyl amine (DIEA) was distilled from sodium/benzophenone keytl, and TFA was distilled from P_2O_5. All glassware was flame dried or placed in an oven overnight at 130 °C. Compounds were analyzed by use of UV light (254 nm), I_2, or a 0.3% solution of ninhydrin in 3% AcOH/*n*-butanol. HPLC eluant was a mixture of H_2O with an increasing gradient of CH_3CN, on a C18 reverse phase column. NMR spectra were recorded at 298 K (^{1}H NMR: 300 MHz; ^{13}C NMR; 75 MHz). Chemical shifts are reported in parts per million (ppm), using residual solvent as an internal standard. Data reported as follows: chemical shift, multiplicity (s = singlet, d = doublet, t = triplet, q = quartet, dd = doublet of doublets, m = multiplet, b = broad, p = pentet), coupling constants, integration, proton assignment.

General solid-phase synthesis procedure:

Fmoc-L-Phe or Fmoc-D-Ala loaded Wang resin was weighed out (0.72 mmol/g) into a sintered glass peptide synthesis vessel and allowed to swell in CH_2Cl_2 for 45 min and then in DMF for 10 min. The resin was treated with piperidine/DMF (20%, 2x for 8 min) to remove the Fmoc group, and washed with DMF (3x). A solution of the next residue, HBTU (1.01 g, 2.66 mmol), and diisopropylethylamine in DMF was allowed to prereact for 2 min and then added to the resin. The resin suspension was agitated for 30 min, drained, and washed with DMF (3x). During coupling of the third residue and all N-methylated residues HATU (1.12 g, 2.95 mmol) was used as the activator. All coupling

procedures were performed twice to ensure complete reaction. This deprotection coupling cycle was repeated to provide the full-length peptide. After the final coupling step, the resin was thoroughly washed (5x DMF, 3x CH_2Cl_2, 3x MeOH) and dried under high vacuum. The peptide was cleaved from the resin by treatment with TFA/triisopropylsilane/water (95:2.5:2.5) for 3 h. The cleavage mixture was collected by filtration and the resin was washed twice with TFA. The filtrated were combined and concentrated under vacuum to afford an oily residue, which was further purified by RP-HPLC (water 0.1% TFA:CH_3CN gradient; C18 column). Later attempts using 2-(6-Chloro-1H-benzotriazole-1-yl)-1,1,3,3-tetramethyluronium hexafluorophosphate (HCTU) as an activator gave similar results.

Benzyl 2-(tert-butoxycarbonyl(methyl)amino)-3-phenylpropanoate (21):

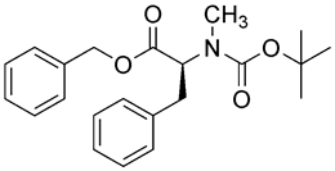

A solution of DCC (4.06 g, 19.7 mmol) in CH_2Cl_2 (15 mL) was slowly added to a solution of Boc-N^{Me}-L-Phe (5.00 g, 17.9 mmol), benzyl alcohol (8 mL, 71.2 mmol), DMAP (1.09 g, 8.9 mmol) in CH_2Cl_2 (20 mL) at 0 °C and allowed to warm to 25 °C at which point a white precipitate formed. The reaction mixture was stirred for 2 h, and then filtered through celite, then washed with a 10% citric acid solution, a saturated aqueous $NaHCO_3$ solution, a saturated brine solution and dried over $MgSO_4$. The solvent was removed under reduced pressure and EtOAc was added to the crude mixture and it was cooled precipitating any unreacted DCC, this was again filtered through celite then the oil was placed in a Kugelrohr and distilled at 65 °C and 50 mmHg to remove excess

benzyl alcohol giving an off white solid [if necessary can be further purified via column chromatography (silica gel, eluant: 50:50 EtOAc:hexanes)] (6.5 g, 99%). ^{1}H NMR (300 MHz, $CDCl_3$) δ: 7.42-7.11 (m, 10H, Ar **H**), 5.24-5.10 (m, 2H, ester benzylic **H**), 4.99-4.90 (m, 0.5H, CO-C**H**$_{(Phe)}$-N^{Me}), 4.66-4.56 (m, 0.5H, CO-C**H**$_{(Phe)}$-N^{Me}), 3.38-3.25 (m, 1H, Phe benzylic **H**), 3.09-2.97 (m, 1H, Phe benzylic **H**), 2.70 (d, *J* = 17.7, 3H, C**H**$_3$-N), 1.33 (d, *J* = 25.5, 9H, *t*-Bu); ^{13}C NMR (75 MHz, $CDCl_3$) δ: 171.0, 170.7, 155.9, 154.6, 153.4, 138.2, 137.2, 135.5, 135.3, 128.8, 128.7, 128.4, 128.3, 128.2, 128.0, 127.9, 126.5, 126.4, 126.3, 80.3, 79.9, 66.9, 66.7, 61.6, 59.8, 35.5, 35.1, 35.0, 32.5, 32.2, 28.3, 28.2.

Benzyl 2-(2-(tert-butoxycarbonylamino)-N-methylpropanamido)-3-phenylpropanoate (22):

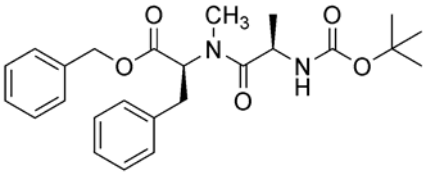

21 (5.90 g, 15.5 mmol) was dissolved in a 20% TFA/CH_2Cl_2 solution at 0 °C, allowed to warm to 25 °C and stirred for 3 h (complete deprotection confirmed by TLC). The solvent was removed under reduced pressure and the crude oil was recrystallized from a hexanes/CH_2Cl_2 solution filtered and dried giving white fluffy needles, which were dissolved in a solution of DIEA (2.6 mL, 15.5 mmol) in anhydrous DMF (35 mL) and allowed to stir at 25 °C for 15 min and then added in one portion to a premixed solution *(prepared at 0 °C and allowed to incubate at 25 °C for 20 min)* of Boc-D-Ala (6.10 g, 32.0 mmol), HOBt (4.30 g, 32 mmol) and DCC (6.60 g, 32 mmol) in anhydrous DMF (50 mL) and stirred at 45 °C for 12 h. The solvent was removed under reduced

pressure. EtOAc (50 mL) was added to the crude mixture, it was cooled and the DCU and unreacted DCC filtered off through celite, then a pipette of NH_4OH in ethanol (3 mL) was added and the solution was stirred for 15 min forming another precipitate which was filtered off through celite. The solution was then washed with water, a 10% citric acid solution, a saturated aqueous $NaHCO_3$ solution, a saturated brine solution and dried over $MgSO_4$. The crude solid was further purified by either column chromatography (silica gel, eluant: 25:75 EtOAc:hexanes) or recrystallized from Et_2O/hexanes filtered and dried giving a white foamy solid (5.20 g, 77%). ^{1}H NMR (300 MHz, $CDCl_3$) δ: 7.30-7.18 (m, 5H, Ar **H**), 7.18-7.12 (m, 2H, Ar **H**), 7.12-7.04 (m, 3H, Ar **H**), 5.41 (d, *J*= 8, 3H, $C_{(Ala)}$-N**H**-CO), 5.18-5.29 (m, 1H, CO-C**H**$_{(Ala)}$-N), 5.07 (m, 2H, ester benzylic **H**), 4.43-4.34 (m, 1H, CO-C**H**$_{(Phe)}$-N^{Me}), 3.38-3.28 (m, 1H, Phe benzylic **H**), 3.02-2.89 (m, 1H, Phe benzylic **H**), 2.70 (s, 3H, C**H**$_3$-N), 1.33 (s, 9H, *t*-Bu), 1.09 (d, J= 6.8, 3H, C**H**$_3$-$C_{(Ala)}$); ^{13}C NMR (75 MHz, $CDCl_3$) δ: 173.3, 160.9, 154.7, 136.3, 135.2, 128.5, 128.3, 128.2, 128.1, 127.9, 126.5, 79.0, 66.7, 58.3, 46.1, 34.4, 32.4, 28.1, 17.9; MS (ESI^+) [M + H^+] 441.2; HRMS (ESI^+) [M + H^+] calcd for $C_{25}H_{33}N_2O_5$: 441.2384, found: 441.2501.

Benzyl 12-benzyl-2,2,9,11-tetramethyl-4,7,10-trioxo-6-(pyridin-4-ylmethyl)-3-oxa-5,8,11-triazatridecan-13-oate (23):

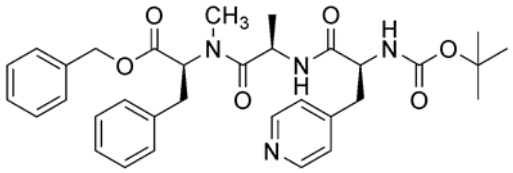

A solution of DCC (0.65 g, 3.2 mmol) in anhydrous THF (20 mL) was added in one portion to a solution of Boc-L-4-pyrAla (0.84 g, 3.2 mmol) and HOAt (0.89 g, 6.5 mmol) in anhydrous THF (30 mL) at 0 °C and the reaction was allowed to warm up to 25 °C. After 20 min DIEA (0.43 mL, 2.6 mmol) was added to the reaction mixture in one portion and then a deblocked solution of **22** (1.14 g, 2.6 mmol) (*Deblocking procedure: **22** was dissolved in a 20% TFA/CH_2Cl_2 solution at 0 °C, allowed to warm to 25 °C and stirred for 3 h (complete deprotection confirmed by TLC). The solvent was removed under reduced pressure and the crude oil dried under high vac (>20 mmHg for 3 h*) in anhydrous THF (20 mL) was added dropwise over 2 h via a syringe pump at 25 °C and stirred for 6 h **(Note: This activation and addition order supresses diketopiperazine formation)**. The solvent was removed under reduced pressure. EtOAc (50 mL) was added to the crude mixture, it was cooled and the DCU and unreacted DCC filtered off through celite, then a pipette of NH_4OH in ethanol (3 mL) was added and the solution was stirred for 15 min forming another precipitate which was filtered off through celite. The solution was then washed with water, a 10% citric acid solution, a saturated aqueous $NaHCO_3$ solution, a saturated brine solution and dried over $MgSO_4$. The crude solid was further purified by column chromatography (silica gel, eluant: EtOAc) giving a white foamy solid (1.37 g, 90%). ^{1}H NMR (300 MHz, $CDCl_3$) δ: 8.47 (d, 2H, *J* = 6.9, α-pyr **H**)

7.38-6.96 (m, 14H, Ar **H**), 7.2 (s, 1H, $C_{(Ala)}$-N**H**-CO), 5.37 (dd, *J* = 4.4, 11.5, 1H, CO-C**H**$_{(Phe)}$-N^{Me}), 5.16 (dd, 2H, *J* = 11.8, 17.5, ester benzylic **H**), 4.66 (p, *J*= 6.8, 1H, CO-C**H**$_{(Ala)}$-N), 4.50-4.36 (m, 1H, CO-C**H**$_{(pyrAla)}$-N), 4.16 (t, 1H, *J*= 4.0, $C_{(pyrAla)}$-N**H**-CO), 3.45-2.85 (m, 4H, (pyrAla)benzylic **H**; (N^{Me}-Phe)benzylic **H**), 2.80 (s, 3H, C**H**$_3$-N), 1.35 (d, *J* = 13.3, 9H, *t*-Bu), 0.70 (d, *J* = 6.9, 3H, C**H**$_3$-$C_{(Ala)}$); ^{13}C NMR (75 MHz, $CDCl_3$) δ: 172.9, 170.0, 169.5, 149.5, 136.2, 135.2, 129.8, 129.7, 128.6, 128.5, 128.4, 128.3, 124.7, 77.4, 67.2, 45.4, 34.6, 32.9, 32.4, 28.1, 17.4; MS (ESI^+) [M + H^+] 589.3; HRMS (ESI^+) [M + H^+] calcd for $C_{33}H_{41}N_4O_6$: 589.3020, found: 589.2990.

Benzyl 6,12-dibenzyl-2,2,9,11-tetramethyl-4,7,10-trioxo-3-oxa-5,8,11-triazatridecan-13-oate (24):

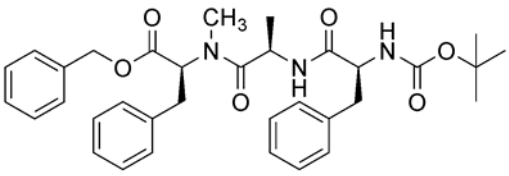

A solution of DCC (0.27 g, 1.3 mmol) in anhydrous THF (10 mL) was added in one portion to a solution of Boc-L-Phe (0.35 g, 1.3 mmol) and HOAt (0.30 g, 2.2 mmol) in anhydrous THF (50 mL) at 0 °C and the reaction was allowed to warm up to 25 °C. After 20 min DIEA (0.2 mL, 1.1 mmol) was added to the reaction mixture in one portion and then a deblocked solution of **22** (0.49 g, 1.1 mmol) [*Deblocking procedure: **22** was dissolved in a 20% TFA/CH_2Cl_2 solution at 0 °C, allowed to warm to 25 °C and stirred for 3 h (complete deprotection confirmed by TLC). The solvent was removed under reduced pressure and the crude oil dried under high vac (>20 mmHg for 3 h*)] in anhydrous THF (10 mL) was added dropwise over 2 h via a syringe pump at 25 °C and stirred for 6 h **(Note: This activation and addition order supresses diketopiperazine**

formation). The solvent was removed under reduced pressure. EtOAc (50 mL) was added to the crude mixture, it was cooled and the DCU and unreacted DCC filtered off through celite, then a pipette of NH_4OH in ethanol (3 mL) was added and the solution was stirred for 15 min forming another precipitate which was filtered off through celite. The solution was then washed with water, a 10% citric acid solution, a saturated aqueous $NaHCO_3$ solution, a saturated brine solution and dried over $MgSO_4$. The crude solid was further purified by column chromatography (silica gel, eluant: 50:50 EtOAc:hexanes) giving a white foamy solid (0.54 g, 84%). ^{1}H NMR (300 MHz, $CDCl_3$) δ: 7.42-7.14 (m, 15H, Ar **H**), 6.65 (d, *J* = 6.9, 1H, $CH_{(Ala)}$-N**H**-CO), 5.36 (dd, *J* = 6.6, 4.9, 1H, CO-C**H**$_{(Phe)}$-N^{Me}), 5.21 (dd, 2H, *J* = 12.2, 39.1, ester benzylic **H**), 5.00-4.82 (m, 1H, CO-C**H**$_{(Ala)}$-N), 4.74-4.66 (m, 1H, CO-C**H**$_{(Phe)}$-N), 4.44-4.33 (m, 1H, $C_{(Phe)}$-N**H**-CO), 3.44 (dd, 1H, *J* = 5.1, 14.8, Phe benzylic **H**), 3.11-3.05 (m, 1H, Phe benzylic **H**), 3.05-2.96 (m, 2H, (N^{Me}-Phe) benzylic **H**), 2.83 (s, 3H, C**H**$_3$-N), 1.43 (d, *J* = 13.3, 9H, *t*-Bu), 0.72 (d, *J* = 6.9, 3H, C**H**$_3$-$C_{(Ala)}$); ^{13}C NMR (75 MHz, $CDCl_3$) δ: 172.8, 170.3, 162.0, 136.6, 136.4, 136.3, 129.4, 129.31, 129.29, 128.75, 128,71, 128.65, 128.60, 128.57, 128.50, 128.4, 126.95, 126.90, 77.2, 67.2, 45.3, 34.7, 32.5, 28.3, 28.2, 17.7; MS (ESI^+) [M + H^+] 588.3; HRMS (ESI^+) [M + H^+] calcd for $C_{34}H_{42}N_3O_6$: 588.3068, found: 588.3111.

Benzyl 15-benzyl-2,2,6,12,14-pentamethyl-4,7,10,13-tetraoxo-9-(pyridin-4-ylmethyl)-3-oxa-5,8,11,14-tetraazahexadecan-16-oate (25):

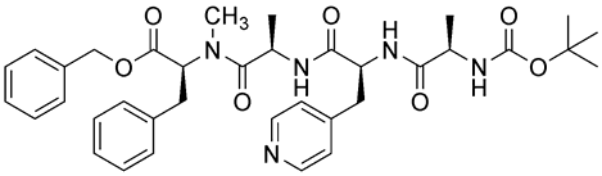

Boc protected tripeptide **23** (0.75 g, 0.9 mmol) was dissolved in a 20% TFA/CH_2Cl_2 solution at 0 °C, allowed to warm to 25 °C and stirred for 3 h (complete deprotection confirmed by TLC). The solvent was removed under reduced pressure and dried in vacuo, the crude oil was dissolved in a solution of DIEA (0.3 mL, 1.8 mmol) in anhydrous DMF (8 mL), and the mixture incubated for 10 min. In a separate flask a solution of PyBOP (1.4 g, 2.7 mmol), Boc-D-Ala (0.51 g, 2.7 mmol), HOAt (0.37 g, 2.7 mmol), and DIEA (1.3 mL, 8.1 mmol) in anhydrous DMF (50 mL) was allowed to incubate for 5 min and then added in one portion to the free based solution of deprotected dipeptide **23**, which instantly became a yellow color. After stirring for 3 h, the DMF was removed under reduced pressure and the mixture taken up in EtOAc (20 mL) and a pipette of NH_4OH in ethanol (3 mL) was added and the solution was stirred for 15 min forming a white precipitate which was filtered off through celite. The solution was then washed with water, a saturated aqueous $NaHCO_3$ solution, a saturated brine solution and dried over $MgSO_4$. The crude solid was further purified by column chromatography (silica gel, eluant: EtOAc) giving a white solid (0.46 g, 80%). MS (ESI^+) [M + H^+] 660.3; HRMS (ESI^+) [M + H^+] calcd for $C_{36}H_{46}N_5O_7$: 660.3392, found: 660.3348.

Benzyl 9,15-dibenzyl-2,2,6,12,14-pentamethyl-4,7,10,13-tetraoxo-3-oxa-5,8,11,14-tetraazahexadecan-16-oate (26):

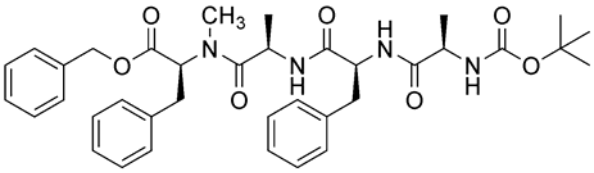

Boc protected tripeptide **24** (0.54 g, 0.92 mmol) was dissolved in a 20% TFA/CH_2Cl_2 solution at 0 °C, allowed to warm to 25 °C and stirred for 3 h (complete deprotection confirmed by TLC). The solvent was removed under reduced pressure and dried *in vacuo*, the crude oil was dissolved in a solution of DIEA (0.15 mL, 0.92 mmol) in anhydrous DMF (8 mL), and the mixture incubated for 10 min. In a separate flask a solution of PyBOP (0.58 g, 1.1 mmol), Boc-D-Ala (0.21 g, 1.1 mmol), HOAt (0.15 g, 1.1 mmol), and DIEA (0.55 mL, 3.3 mmol) in anhydrous DMF (50 mL) was allowed to incubate for 5 min and then added in one portion to the free based solution of deprotected dipeptide **24**, which instantly became a yellow color. After stirring for 3 h, the DMF was removed under reduced pressure and the mixture taken up in EtOAc (20 mL) and a pipette of NH_4OH in ethanol (3 mL) was added and the solution was stirred for 15 min forming a white precipitate which was filtered off through celite. The solution was then washed with water, a 10% citric acid solution, a saturated aqueous $NaHCO_3$ solution, a saturated brine solution and dried over $MgSO_4$. The crude solid was further purified by column chromatography (silica gel, eluant: 25:75 EtOAc:hexanes with an increasing EtOAc gradient) giving a white solid (0.47 g, 77%). MS (ESI^+) [M + H^+] 659.3; HRMS (ESI^+) [M + H^+] calcd for $C_{37}H_{47}N_4O_7$: 659.3439, found: 659.3447.

Benzyl 15,27-dibenzyl-2,2,6,12,14,18,24,26-octamethyl-4,7,10,13,16,19,22,25-octaoxo-9,21-bis(pyridin-4-ylmethyl)-3-oxa-5,8,11,14,17,20,23,26-octaazaoctacosan-28-oate (27):

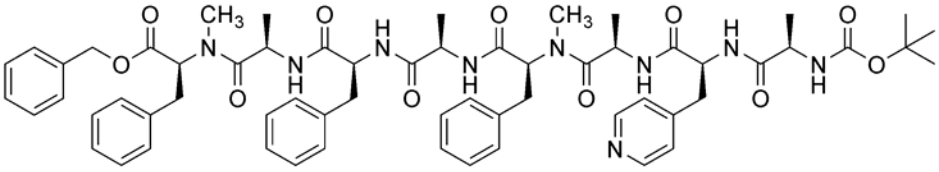

Boc protected tripeptide **26** (0.43 g, 0.65 mmol) was dissolved in a 20% TFA/CH_2Cl_2 solution at 0 °C, allowed to warm to 25 °C and stirred for 3 h (complete deprotection confirmed by TLC). The solvent was removed under reduced pressure and dried in vacuo, the crude oil was added to a solution of PyAOP (0.46 g, 0.89 mmol), HOAt (0.12 g, 0.89 mmol) and Benzyl ester deprotected **25** (0.48 g, 0.85 mmol) (*Hydrogenolysis procedure: **25** (0.56 g, 0.85 mmol) was dissolved in ethanol (15 mL) in a pressure flask, a catalytic amount of Pd/C (10%) was added and the flask was secured in a Parr hydrogenation apparatus, pressurized with an atmosphere of H_2 (50 PSI) and shaken. After 24 h, the solution was filtered through celite, the solvent was removed under reduced pressure and dried in vacuo giving a white solid.*) in anhydrous DMF (25 mL). DIEA (1.4 mL, 8.4 mmol) was added in one portion and the solution instantly became yellow. After stirring for 3 h, the DMF was removed under reduced pressure and the mixture taken up in EtOAc (50 mL) and a pipette of NH_4OH in ethanol (3 mL) was added and the solution was stirred for 15 min forming a white precipitate which was filtered off through celite (Note: linear octapeptide has limited solubility in EtOAc, hold on to all solvent layers and check for product by TLC, R_f = 0.4 on silica TLC with 97:3 EtOAc/MeOH mobile phase). The solution was then washed with water, a saturated aqueous $NaHCO_3$ solution, a saturated brine solution and dried over $MgSO_4$. The crude

solid was further purified by column chromatography (silica gel, eluant: 98:2 EtOAc/EtOH) giving a white solid (0.55 g, 76%). MS (ESI^+) [M + H^+] 1110.6; HRMS (ESI^+) [M + H^+] calcd for $C_{61}H_{76}N_9O_{11}$: 1110.5658, found: 1110.58.

6,12,24-Tribenzyl-1,3,9,13,15,21-hexamethyl-18-(pyridin-4-ylmethyl)-1,4,7,10,13,16,19,22-octaazacyclotetracosan-2,5,8,11,14,17,20,23-octaone (28):

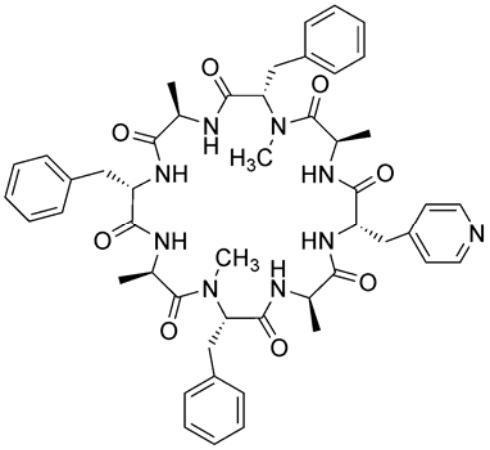

Benzyl protected octapeptide **27** (0.042 g, 0.038 mmol) was dissolved in ethanol (15 mL) in a pressure flask, a catalytic amount of Pd/C (10%) was added and the flask was secured in a Parr hydrogenation apparatus, pressurized with an atmosphere of H_2 (50 PSI) and shaken. After 24 h, the solution was filtered through celite, the solvent was removed under reduced pressure and dried in vacuo giving a white solid. This was dissolved in a 20% TFA/CH_2Cl_2 solution at 0 °C, allowed to warm to 25 °C and stirred for 3 h (complete deprotection was confirmed by TLC). The solvent was removed under reduced pressure and dried in vacuo, the crude solid was added to a solution of PyAOP (0.059 g, 0.113 mmol) in anhydrous DMF (50 mL). DIEA (50 μL, 0.30 mmol) was added in one portion and the solution instantly became yellow. After stirring for 3 h, the DMF was removed under reduced pressure and the mixture taken up in CH_2Cl_2 and

DIEA (62 μL, 0.37 mmol) then glacial acetic acid (17 μL, 0.30 mmol) was added (*this was done to decompose the excess PyAOP*). The crude product was then purified by preparatory TLC (silica plate [20 × 20 cm], eluant: 94:6 CH_2Cl_2/MeOH) giving a white solid (0.019 g, 55%). MS (ESI^+) [M + H^+] 902.47; HRMS (ESI^+) [M + H^+] calcd for $C_{49}H_{60}N_9O_8$: 902.4559, found: 902.4609.

4.5 References

[1] De Santis, P., Morosetti, S., Rizzo, R. Conformational Analysis of Regular Enantiomeric Sequences. *Macromolecules* **1974**, *7*, 52-58.

[2] Ghadiri, M. R., Granja, J. R., Milligan, R. A., McRee, D. E., Khazanovich, N. Self-assembling organic nanotubes based on a cyclic peptide architecture. *Nature* **1993**, *366*, 324-327.

[3] Fernandez-Lopez, S., Kim, H.-S., Choi, E. C., Delgado, M., Granja, J. R., Khasanov, A., Kraehenbuehl, K., Long, G., Weinberger, D. A., Wilcoxen, K. M., Ghadiri, M. R. Antibacterial agents based on the cyclic D,L-α-peptide architecture. *Nature* **2001**, *414*, 452-455.

[4] Granja, J. R., Ghadiri, M. R. Channel-Mediated Transport of Glucose across Lipid Bilayers. *J. Am. Chem. Soc.* **1994**, *116*, 10785-10786.

[5] Engels, M., Bashford, D., Ghadiri, M. R. Structure and Dynamics of Self-Assembling Peptide Nanotubes and the Channel-Mediated Water Organization and Self-Diffusion. A Molecular Dynamics Study. *J. Am. Chem. Soc.* **1995**, *117*, 9151-9158.

[6] Ghadiri, M. R. Self-assembled nanoscale tubular ensembles. *Adv. Mater.* **1995**, *7*, 675-677.

[7] Hartgerink, J. D., Clark, T. D., Ghadiri, M. R. Peptide nanotubes and beyond. *Chem. Eur. J.* **1998**, *4*, 1367-1372.

[8] Clark, T. D., Buriak, J. M., Kobayashi, K., Isler, M. P., McRee, D. E., Ghadiri, M. R. Cyclindrical β-sheet peptide assemblies. *J. Am. Chem. Soc.* **1998**, *120*, 8949-8962.

[9] Steinem, C., Janshoff, A., Vollmer, M. S., Ghadiri, M. R. *Langmuir* **1999**, *15*, 3956-3964.

[10] Motesharei, K., Ghadiri, M. R. Diffucison limited size-selective ion sensing based on SAM supported peptides nanotubes. *J. Am. Chem. Soc.* **1997**, *119*, 11306-11312.

[11] Horne, W. S., Stout, C. D., Ghadiri, M. R. A Heterocyclic Peptide Nanotube. *J. Am. Chem. Soc.* **2003**, *125*, 9372-9376.

[12] Bong, D. T., Clark, T. D., Granja, J. R., Ghadiri, M. R. Self assembling Organic Nanotubes. *Angew. Chem. Int. Ed* **2001**, *40*, 988-1011.

[13] Clark, T. D., Buehler, L. K., Ghadiri, M. R. Self-Assembling Cyclic β^3-peptides Nanotubes as artificial transmembrabe Ion channels. *J. Am. Chem. Soc.* **1998**, *120*, 651-656.

[14] Hartgerink, J. D., Granja, J. R., Milligan, R. A., Ghadiri, M. R. Self-assembling peptides nanotubes. *J. Am. Chem. Soc.* **1996**, *118*, 43-50.

[15] Sanchez-Quesada, J., Isler, M. P., Ghadiri, M. R. Modulating Ion Channel Properties of Transmembrane Peptide Nanotubes through Heteromeric Supramolecular Assemblies. *J. Am. Chem. Soc.* **2002**, *124*, 10004-10005.

[16] Kobayashi, K., Granja, J. R., Ghadiri, M. R. β-Sheet Peptide Architecture: Measuring the Relative Stability of Parallel vs. Antiparallel β-Sheets. *Angew. Chem., Int. Ed. Engl.* **1995**, *34*, 95-98.

[17] Ghadiri, M. R., Kobayashi, K., Granja, J. R., Chadha, R. K., McRee, D. E. The Strucutral and Thermodynamic Basis for the Formation of Self-Assembled Peptide Nanotubes. *Angew. Chem., Int. Ed. Engl.* **1995**, *34*, 93-95.

[18] van Maarseveen, J. H., Horne, W. S., Ghadiri, M. R. Efficient Route to C_2 Symmetric Heterocyclic Backbone Modified Cyclic Peptides. *Org. Lett.* **2005**, *7*, 4503-4506.

[19] Sanchez-Quesada, J., Ghadiri, M. R., Bayley, H., Braha, O. Cyclic Peptides as Molecular Adapters for a Pore-Forming Protein. *J. Am. Chem. Soc.* **2000**, *122*, 11757-11766.

[20] Clark, T. D., Ghadiri, M. R. Supramolecular Design by Covalent Capture. Design of a Peptide Cylinder via Hydrogen-Bond-Promoted Intermolecular Olefin Metathesis. *J. Am. Chem. Soc.* **1995**, *117*, 12364-12365.

[21] Horne, W. S., Ashenasy, N., Ghadiri, M. R. Modulating Charge Transfer through Cyclic D,L-α-Peptide Self-Assembly. *Chem. Eur. J.* **2005**, *11*, 1137-1144.

[22] Amorín, M., Castedo, L., Granja, J. R. New Cyclic Peptide Assemblies with Hydrophobic Cavities: The Structural and Thermodynamic Basis of a New Class of Peptide Nanotubes. *J. Am. Chem. Soc.* **2003**, *125*, 2844-2845.

[23] Amorín, M., Castedo, L., Granja, J. R. Self-assembled peptide tubelets with 7 Å pores. *Chem. Eur. J.* **2005**, *11*, 6543-6551.

[24] Brea, R. J., Amorín, M., Castedo, L., Granja, J. R. Methyl-blocked dimeric α,γ-peptide nanotube segments: formation of a peptide heterodimer through backbone-backbone interactions. *Angew. Chem. Int. Ed.* **2005**, *44*, 5710-5713.

[25] Bitta, J., Kubik, S. Cyclic Hexapeptides with Free Caboxylate Groups as New Receptors for Monosaccharides. *Org. Lett.* **2001**, *3*, 2637-2640.

[26] Amorín, M., Brea, R. J., Castedo, L., Granja, J. R. The Smallest α,γ-Peptide Nanotubulet Segments: Cyclic α,γ-Tetrapeptide Dimers. *Org. Lett.* **2005**, *7*, 4681-4684.

[27] Couet, J., Jeyaprakash, J. D., Samuel, S., Kopyshev, A., Santer, S., Biesalski, M. Peptide-Polymer Hybrid Nanotubes. *Angew. Chem. Int. Ed* **2005**, *44*, 3297-3301.

[28] Rodriguez-Docampo, Pascu, S. I., Kubik, S., Otto, S. Noncovalent Interactions within a Synthetic Receptor Can Reinforce Guest Binding. *J. Am. Chem. Soc.* **2006**, *128*, 11206-11210.

[29] Dobrawa, R., Würthner, F. Metallosupramolecular approach toward functional coordination polymers. *J. Polym. Sci., Part A: Polym. Chem.* **2005**, *43*, 4981-4995.

[30] van Manen, H.-J., Nakashima, K., Shinkai, S., Kooijman, H., Spek, A. L., van Veggel, F. C. J. M., Reinhoudt, D. N. Coordination chemistry of SCS PdII pincer systems. *Eur. J. Inorg. Chem.* **2000**, 2533-2540.

[31] Albrecht, M., van Koten, G. Platinum group organometallics based on "pincer" complexes: sensors, switches, and catalysts. *Angew. Chem. Int. Ed.* **2001**, *40*, 3750-3781

[32] Gerhardt, W. W., Weck, M. Investigations of Metal-Coordinated Peptides as Supramolecular Synthons. *J. Org. Chem.* **2006**, *71*, 6333-6341.

[33] Davies, J. S. The Cyclization of eptides and Depsipeptides. *J. Peptide Sci.* **2003**, *9*, 471-501.

[34] Greico, P. A., Bahsas, A. Immonium Ion Based Synthetic Methodology: A Novel Method for the N-Methylation of Dipeptides and Amino Acid Derivatives via Retro Aza Diels-Alder Reactions. *J. Org. Chem* **1987**, 52, 5746–5749.

[35] Gianluca, D., Wang, D., Chapman, R. N., Arora, P. S. Solid-Phase Synthesis of Hydrogen-Bonded Surrogate-Drived α-Helices. *Org. Lett*. **2005**, *7*, 2389-2392.

Chapter 5

Controlling Polymer Properties through Dynamic Metal-ligand Interactions: Supramolecular Cruciforms Made Easy

5.1 Abstract

A straightforward methodology towards the supramolecular synthesis of novel coordination polymers with attractive optical properties is presented. By coordinating bifunctional fluorescent cruciform molecules through ditopic metallated pincer complexes (Pd or Pt), we have synthesized a new class of well-defined coordination polymers having controllable and tunable physical and photophysical properties. The formation of these new materials via metal coordination was monitored using ^{1}H NMR spectroscopy, the K_a of the metal-ligand interaction was measured using isothermal titration calorimetry (ITC), the solution polymeric properties were evaluated using viscometry and the optical properties were measured and observed using fluorescence spectroscopy. The fast and quantitative synthesis of a wide range of pre-fabricated monomeric cruciform and metallated pincer complex components will allow for the rapid generation, growth and optimization of this new class of functional polymers having potential electronic and optical applications.

5.2 Introduction

Conjugated and fluorescent molecules are candidates for integration into electro-optical and light-emitting devices (LEDs) because of their electrical, optical, and redox properties.[1-6] Polymeric-based systems are desirable owing to their good mechanical and film forming properties, which are amenable to solution processing.[7] Supramolecular polymeric systems based on the assembly of monomeric units via noncovalent

interactions add an additional level of control. Such materials have the potential to combine the processability and mechanical properties of a traditional polymeric system without the long-range defects and functional group intolerance of covalent polymerization methodologies.[8] Self-assembled materials are dynamic systems with reversible interactions that are responsive to environmental stimuli allowing for the adjustment of polymeric properties for specific applications. Intense research in this area has yielded new supramolecular polymeric materials based on conjugated building blocks with novel applications ranging from tissue engineering[9] to electronic applications.[10] Rowan and Weder have used metal-ligand interactions to form supramolecular fluorescent phenylene-ethynylene coordination polymers that can be processed easily into films and fibers.[11-14] The Bunz group has investigated cross-conjugated fluorescent cruciform-shaped molecules as new electro-optical materials, owing to their unique properties[15-21] as well as distyrylbenzene-substituted poly(*para*phenylene-ethynylene)s as covalent PPE-PPV hybrids.[20]

The ultimate goal is to prepare functional and solution processable materials with tailorable physical and optical properties. Towards this, a discrete toolbox of supramolecular monomers was polymerized using weak labile interactions. By readily exchanging monomer components we were able to augment the final properties of the materials to fit a specific need via a simple assembly step, which minimized or obviated more costly and time consuming synthetic steps. This chapter reports the employment of two metal centers, palladium and platinum, for the coordination event as well as two cruciforms, which coordinate along different conjugated axes. The resulting functional polymeric material displayed the fluorescence of the small molecule cruciform species

within a well-defined supramolecular polymeric framework capable of solution processing. The toolbox employed included building blocks **1-4**, shown in Figure 5.1.

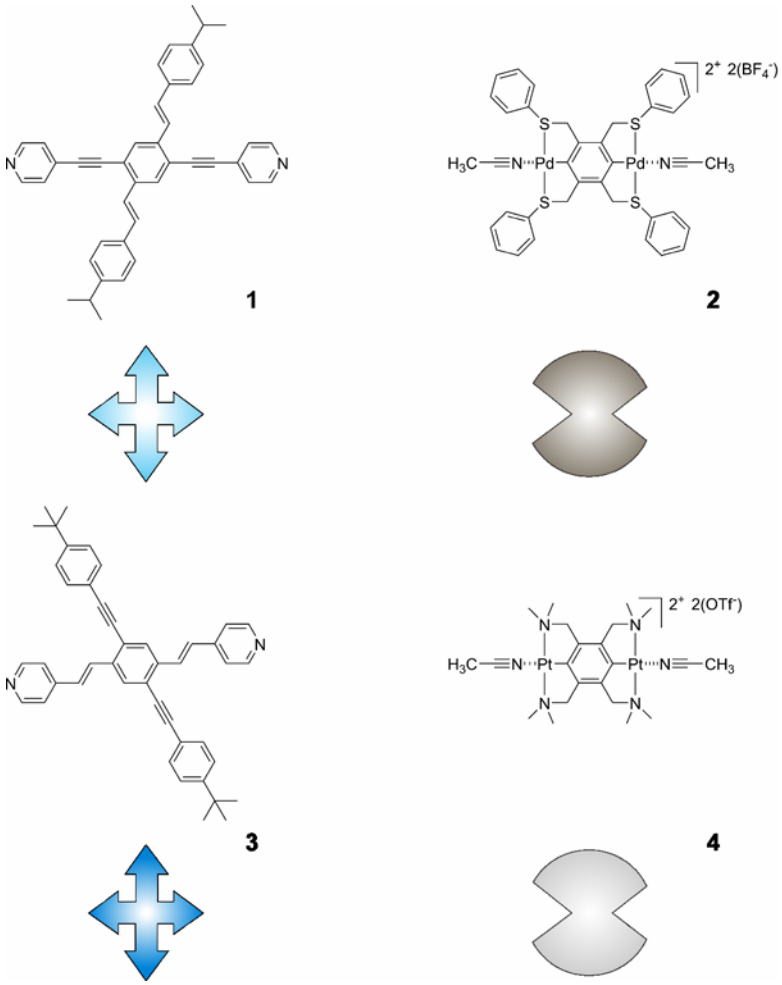

Figure 5.1 Four monomers in the supramolecular toolbox.

Coordinating cruciforms through a pyridyl unit on either the styryl or arylethynylene axis, to either a bis-Pd or bis-Pt pincer complex provided a library of related polymers having a range of physical and optical properties, as shown at the top of Scheme 5.1. The

coordination polymers formed are depicted in Scheme 5.1 with their respective luminescence.

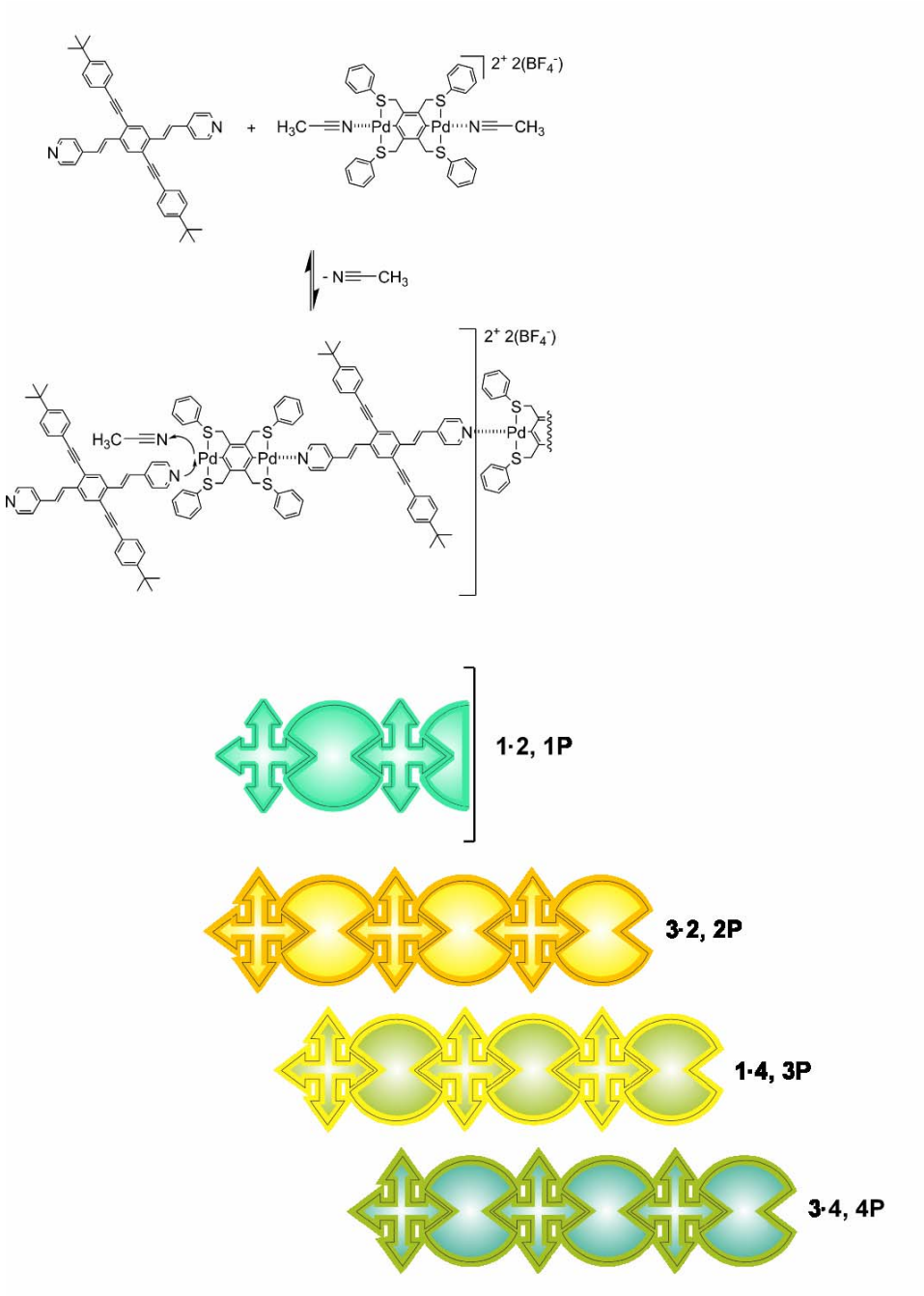

Scheme 5.1 Coordination of **1** to **2** giving fluorescent polymer **1P**; **2P**, **3P** and **4P** are the fluorescent polymers formed from their respective monomers.

The cruciform building blocks investigated (1,4 distyryl-2,5-bisarylethynylbenzenes) are part of a larger class of "X-shaped" molecules with attractive electro-optical properties.[15-19, 21-30] Haley and coworkers examined tetra arylethynyl substituted cruciforms providing in-depth luminescence characterizations and self-association studies.[22, 23] Both Bunz and Haley have independently demonstrated that donor and acceptor groups placed on separate axial paths led to molecules in which the frontier molecular orbitals (FMOs) were confined to their respective donor (HOMO) and acceptor (LUMO) substituted arms.[16, 17, 22, 23]

The second class of building blocks, bis-metallated pincer complexes, are capable of forming strong, single-site, directional coordinations, which are both fast and quantitative to a variety of ligands[31-44] and able to provide supramolecular architectures.

Using building blocks **1**–**4** we were able to fine-tune the K_a of the coordination events and ultimately the polymer properties. The K_a value of the metal-pyridyl ligand interaction of each cruciform was expected to vary depending on the *para* substituent, which was an alkenyl group in **1** and an alkynyl group in **3**. This electronic effect has been shown to fit the Hammett equation using the σ^+ constant[45] of the *para* substituent.[31] Furthermore, Pt pincer complexes are known to have a significantly stronger association in comparison to Pd pincer complexes, allowing us to also control the association via the metal center.[46] Therefore, the uniqueness of each metal-ligand interaction within these structurally related supramolecular materials led to polymers with a set of properties that were easily controlled.

5.3 Results and Discussion

Cruciform monomers **1**[15] and **3**[16] were synthesized in the Bunz group, and pincer complex monomers **2**[47] and **4**[48, 49] were synthesized in the Weck group following literature procedures. In **2** and **4**, acetonitrile molecules were coordinated to the metal centers of each respective pincer complex. The weaker coordination of nitriles led to a spontaneous and quantitative exchange of the acetonitriles for the pyridyl functionalized cruciform ligands giving **1P-4P** in excellent yields. Self-assembly was accomplished by combining the bis-metallated pincer complexes with the cruciform of choice. For solubility purposes all of the physical characterization studies were carried out in DMF except for fluorescence studies, which were performed in a $CHCl_3$/DMSO mixture.

Using ^{1}H NMR spectroscopy, the self-assembly was monitored by shifts of diagnostic signals pre- and post-coordination in d_7-DMF. Both **2** and **4** showed shifts characteristic of quantitative metal-coordination events. The doublet at 8.65 ppm, representative of the α-pyridyl protons of cruciform **1**, showed a quantitative upfield shift to 8.50 ppm after coordination to **2** and a quantitative downfield shift to 9.21 ppm after coordination to **4**. In cruciform **3** the α-pyridyl signal has an upfield shift from 8.80 to 8.63 ppm after coordination to **2**, and a downfield shift to 9.35 ppm after coordination to **4**.[50] We observed a broadening of all the signals for **1P-4P**, typical of polymers. Shown in Figure 5.2 is a representative ^{1}H NMR spectrum for the formation of **1P-4P**, displaying the aromatic region of **1** before and after coordination to **4** in d_7-DMF. The quantitative shifts of every proton along the distyryl axis are shown; protons farther from the coordinated pyridyl nitrogen have smaller shifts as they experience less of an electronic perturbation. Also, the unaffected doublet of doublets labeled **ε** and **ζ** in the spectra

clearly shows the electronically decoupled nature of the cross-conjugated arylethynylene axis.

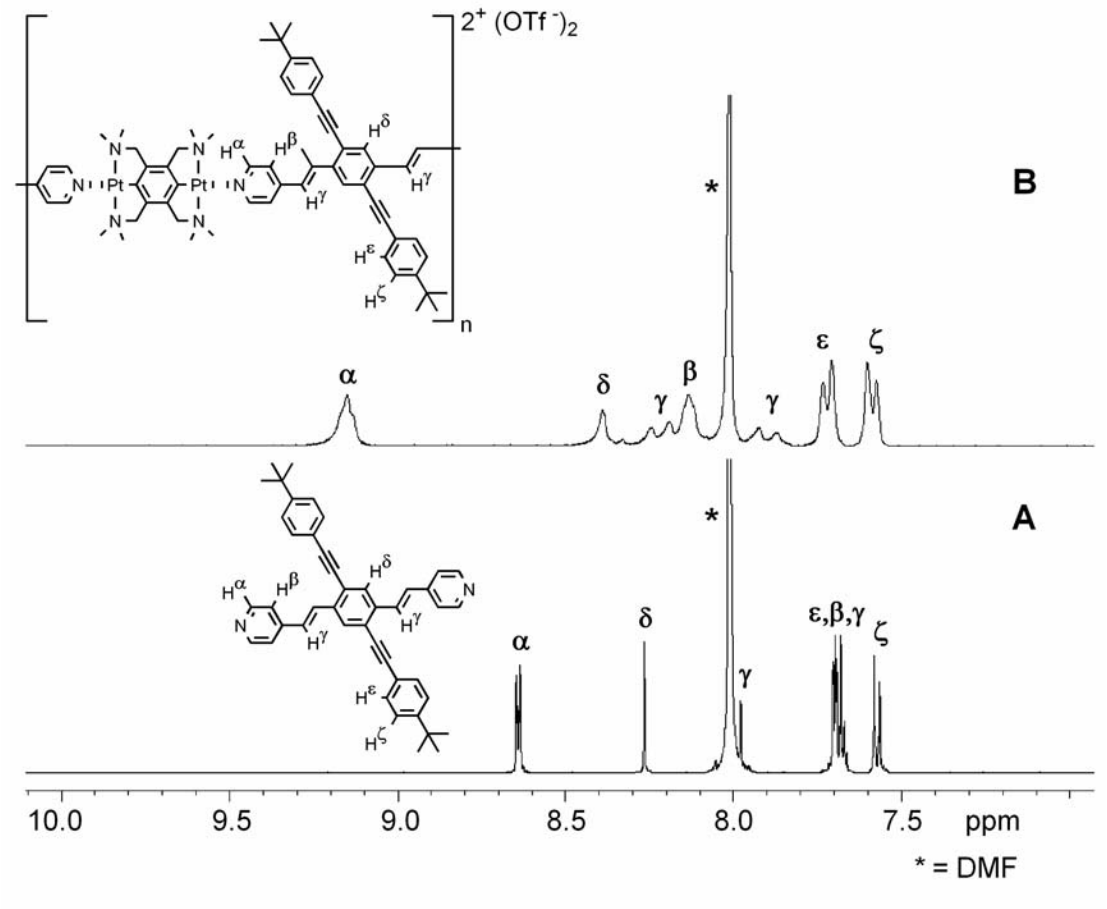

Figure 5.2 Stacked ^{1}H NMR spectra of aromatic region in d_7-DMF depicting metal coordination of **1** to **4**: A) cruciform **1,** 0.006 M; B) 1:1 mixture of **1** and **4** giving polymer **3P**, 0.006 M.

The strength of the metal-ligand interactions was quantified using ITC, providing a complete thermodynamic characterization. In these experiments it was assumed that the K_a value of the interaction was independent of the polymer length, *i.e.* $K_{average} \approx K_1 \approx K_n$. By titrating a DMF solution of each bis-metallated pincer complex (10 mM) into a DMF solution of each cruciform (1 mM) at 22 °C an isotherm was generated, from which a K_a

($K_{average}$) value was calculated. All titrations were carried out in triplicate to validate the reported K_a values, as shown in Table 5.1. Furthermore, all isotherms showed a hyperbolic shape characteristic of a weaker dynamic on/off binding event with the isotherm of **3P** as a representative shown in Figure 5.3.

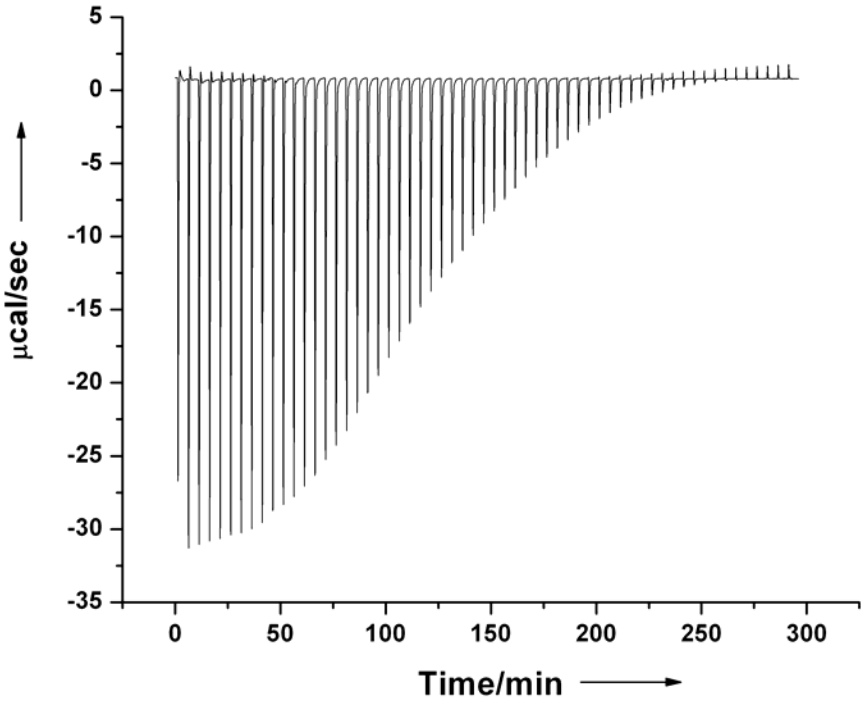

Figure 5.3 Isotherm generated from the titration of **4** into **1** in DMF to give **3P**.

The polymer K_a values were higher when using **4** than when using **2** by approximately an order of magnitude. Literature reports indicate that the Pt-based coordination using pincer complexes was significantly stronger than their palladium analogues,[46] which tracks well with our results. The range of association strengths available for coordination events involving cruciforms was used to control the properties

of the supramolecular material. However, the assumption that $K_a = K_{average}$ was first validated. To this end, small molecule binding studies were carried out with pincer complexes **2** and **4** and cruciform **1**, measuring the K_a values and comparing them to the measured coordination polymer K_a ($K_{average}$) values. The K_a values for pincer complexes **2** and **4** coordinated to pyridine and cruciform **1** coordinated to monotopic Pd and Pt pincer complexes, **5** and **6**, respectively, were measured in DMF. Complexes **5** and **6** are shown in Figure 5.4.

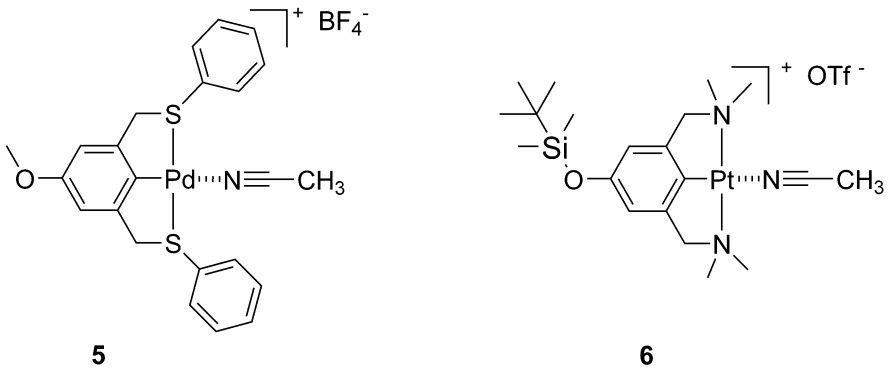

Figure 5.4 Monotopic Pd pincer complex **5** and monotopic Pt pincer complex **6** coordinated to cruciform molecules.

The close agreement of the small model K_a values to the polymeric K_a values strengthens the notion that $K_a = K_{average}$. Plugging these K_a values into the MSOA model equation we obtain a range of DPs listed in Table 5.1.

Table 5.1 ITC K_a values and degree of polymerization of each supramolecular complex.

Complex	K_a (M^{-1})	Maximum DP[a]
1P	5.7 (± 1.6) 10^3	14
2P	2.1 (± 0.5) 10^3	10
3P	44.3 (± 5.4) 10^3	53
4P	15.2 (± 2.9) 10^3	31
2·Pyr	6.0 (± 0.5) 10^3	-
4·Pyr	60.0 (± 7.8) 10^3	-
1·5	9.8 (± 3.2) 10^3	-
1·6	53.0 (± 4.8) 10^3	-

[a] Maximum DP ≈ $(K_a[\text{monomer}])^{1/2}$; based on a 1:1 A-B supramolecular monomer concentration of 0.033 M in DMF.

Confirming and quantifying the self-assembly of each polymeric system with ^{1}H NMR and ITC, the solution properties of these polymer were then analyzed. Owing to the weaker K_a values of the metal-ligand interactions in DMF, size-exclusion chromatography proved to be unreliable in determining their molecular weights and polydispersities. Therefore, viscometry was used to analyze the materials using a Cannon-Ubbelohde semi-micro type viscometer. It was demonstrated that there was a molecular weight dependence of **1P** based on the monomer feed ratios in DMF, with a maximum relative viscosity (η_r) at a stoichiometric equivalence of **1** and **2**. This was interpreted as the longest possible length of the polymers in solution, assuming maximum coordination. Deviation from a 1:1 monomer feed ratio led to chain termination and a

less viscous solution, as the length of the supramolecular polymer decreased, as shown in Figure 5.5.

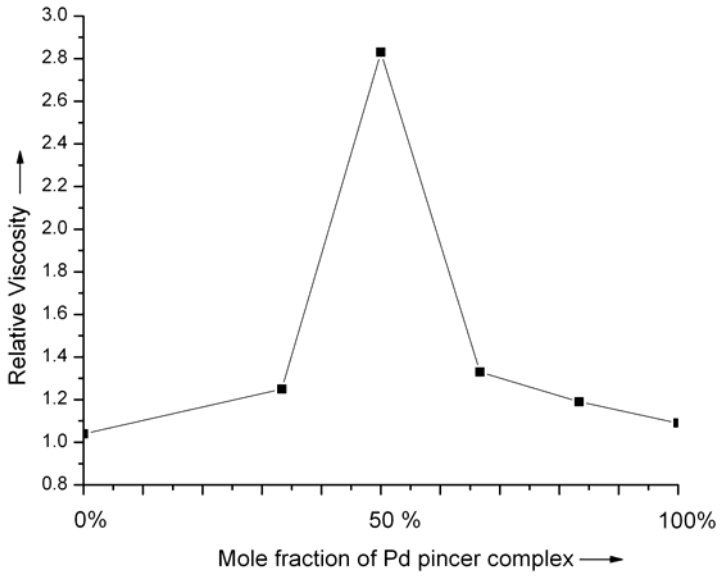

Figure 5.5 Degree of polymerization dependence on the stoichiometry of **1** to **2** in DMF, a maximum DP is seen at a 1:1 stoichiomtric equivalence.

Next the η_r at different concentrations in DMF was investigated. A linear increase in η_r. is generally expected as one increases the concentration of a covalent polymer solution. However, because the metal-ligand interactions are more favored at higher concentrations, a non-linear increase was observed.

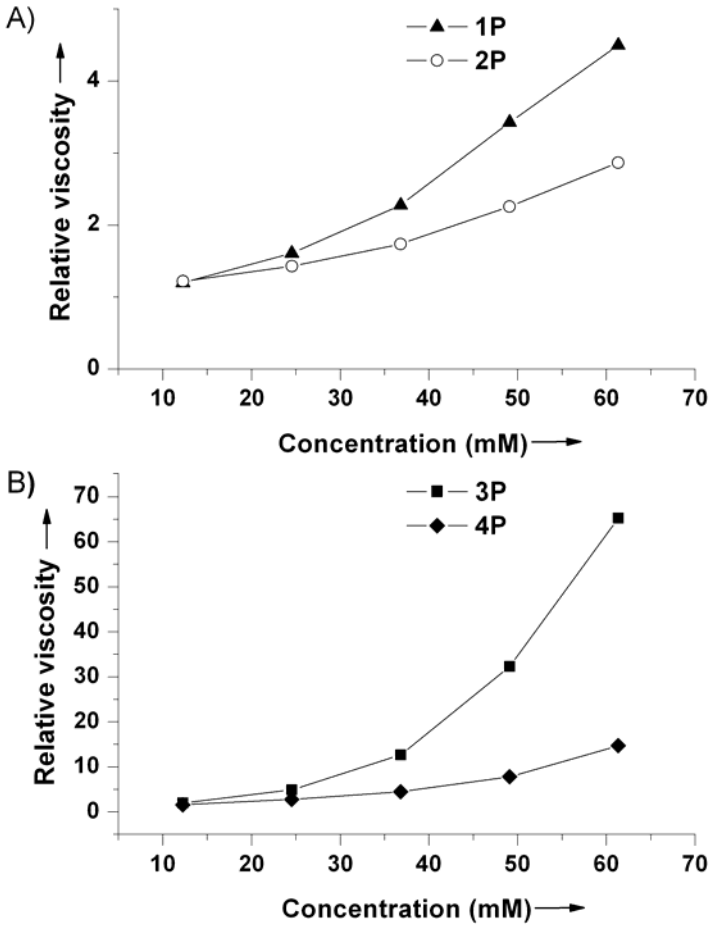

Figure 5.6 A) Plot of relative viscosity of bis-Pd pincer complexed materials **1P** and **2P**. B) Plot of relative viscosity of bis-Pt pincer complexed materials **3P** and **4P** all in DMF.

Figure 5.6 shows the viscometry results. The expected non-linear increase is seen for all of the polymeric materials. The viscosity measurements are also in accord with the ITC determined K_a values, with the polymer **3P** solution being 70 times more viscous than pure DMF, and both bis-Pt pincer complexed polymeric solutions **3P** and **4P** significantly more viscous than the bis-Pd pincer complexed polymeric solutions **1P** and **2P**. Polymers **1P** and **3P**, coordinating to the metal through the more electron-rich pyridyl groups on the distyryl axis, had a higher relative viscosity as compared to the

polymers formed from cruciform **3**, which coordinated along the less electron releasing arylethynylene axis.

The viscosity results illustrated the inherent control over the polymer properties in each supramolecular system. By simply switching one monomeric component with an alternate one from the toolbox we were able to quickly tune the DP and thus viscosity.

Finally, the luminescent properties of these supramolecular materials were examined by the Bunz group. Fluorescence spectroscopy was used, comparing the emissions of **1P-4P** to their small molecule analogues. Unlike the characterizations of the polymer physical properties, spectroscopic studies in DMF were not possible as the self-assembly was not readily observed at the dilute concentrations necessary for fluorescent measurements. As a result, all spectroscopic studies were conducted in a mixture of $CHCl_3$-DMSO (95:5).[51] For each supramolecular material red-shifted emissions were observed compared to the uncoordinated cruciforms. A decrease in fluorescence intensity for each material proportional to the measured K_a values of each metal-ligand interaction was also observed. The results of this study are summarized in Figure 5.7 and Tables 5.2 and 5.3, with additional spectra included in the Experimental section.

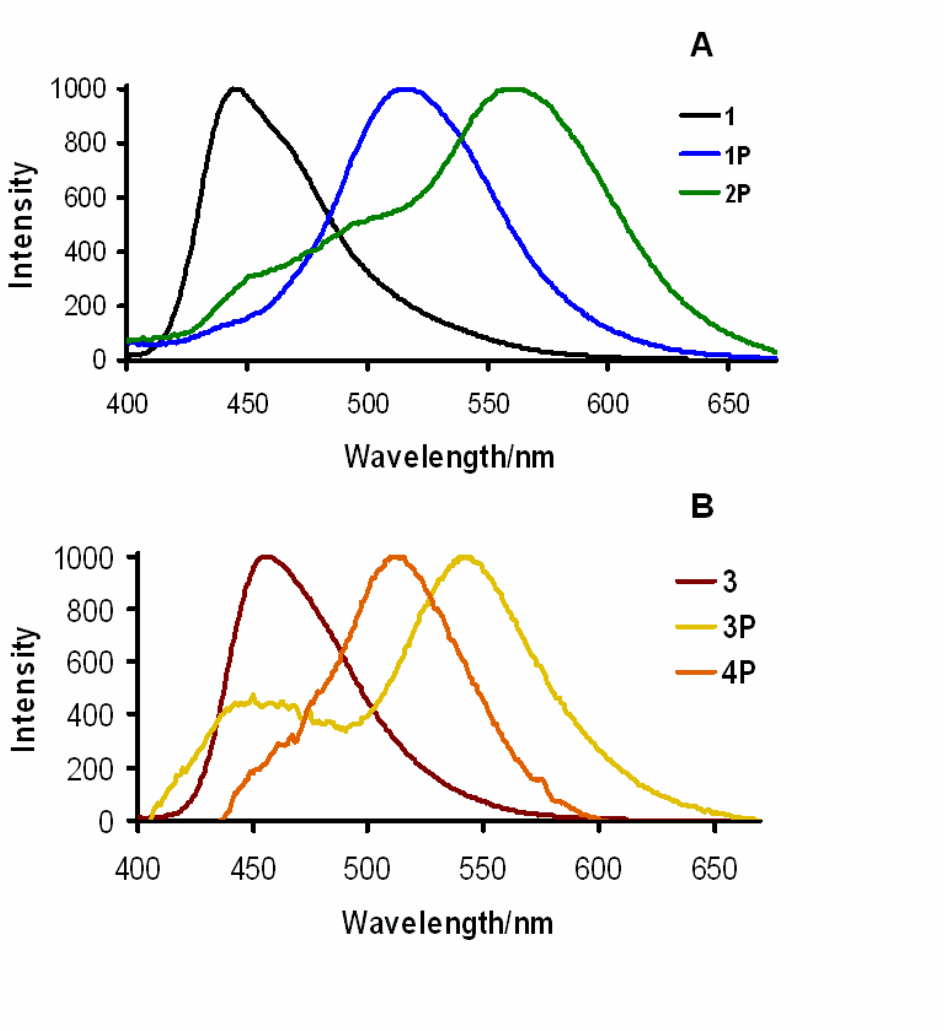

Figure 5.7 Normalized emission of cruciforms **1** and **3** and λ_{max} of the farthest red-shifted emissions of polymers **1P-4P** (precipitation seen at these maximum DPs) all at 0.0445 mM. A) Emission of cruciform **1** (black) and Pd coordination polymers **1P** (blue) and **3P** (green). B) Emission of cruciform **3** (maroon) and Pt coordination polymers **2P** (yellow) and **4P** (orange).

Table 5.2 Summary of the changes in emission observed upon the addition of increasing equivalents of 2 or 4 to 1 or 3. The concentration of the cruciform in all samples was 0.0445 mM in a mixture of $CHCl_3$-DMSO (95:5).

Supramolecular complex	Cruciform Emission (nm)	Supramolecular Complex Emission (nm)[a]	Excess Pincer Emission (nm)[a]	Solid State Emission (nm)
1P	445	515 (2.0 eq.)	485 (15.0 eq.)	520
2P	455	560 (3.6 eq.)	512 (20.0 eq.)	544
3P	445	542 (1.4 eq.)	N.A.	N.A.
4P	455	510 (3.0 eq.)	504 (15.0 eq.)	504

[a] Parentheses refer to the number of equivalents of ditopic pincer complex added to achieve shift

Table 5.3 Summary of the changes in emission observed upon the addition of 5 or 6 to 1 or 3. The concentration of the cruciform in all samples was 0.0445 mM in a mixture of $CHCl_3$-DMSO (95:5).

Supramolecular complex	Cruciform Emission (nm)	Supramolecular Complex Emission (nm)
1·5	445	491
3·5	455	507
1·6	445	540
3·6	455	515

Uncoordinated **1** possessed a vibrant blue emission at 445 nm. Upon titration of 2.0 equivalents of **2** into a solution of 1, a bathochromic shift (445→515 nm) was observed. If a large excess (15.0 equivalents) of **2** was added, a subsequent hypsochromic shift (515→485 nm) resulted. In order to rationalize these changes in emission, a similar emission study coordinating monotopic Pd pincer complex **5** to **1** was performed. In the case of this model system, a similar bathochromic shift (445→491 nm) during the titration of **5** was observed.

These emission shifts were explained by the perpendicular arrangement of the frontier molecular orbitals in the cruciforms. Coordination in the cruciforms occurs along the

LUMO axis. As corroborated in the ^{1}H NMR spectroscopy studies, the HOMO axis was largely unaffected post-coordination. Therefore, the LUMO is stabilized and the energy band-gap in every system decreases, resulting in the observed bathochromic shifts.

This effect partially explained the change in emission observed upon the titration of **2** into **1**. During the early stages of the titration, coordination resulted in the assembly of polymer **1P** with an increasing DP. This putative high molecular weight material had limited solubility in the $CHCl_3$-DMSO mixture used for fluorescent measurements, which led to aggregation. This was visually observed in the samples by clouding and the formation of a precipitate. Previous investigations of cruciform aggregates and polymorphs in the solid-state displaying differences in their emissive behavior have been observed,[18] therefore the red-shifted emission to 515 nm at 2 equivalents of **2** into **1** was attributed to both the LUMO stabilization and aggregation effects. This conclusion was further supported by the solid-state emission of **1P** at 520 nm (dropcast film from a 1:2 mixture of **1** and **2**). However, upon the addition of 15 equivalents of **2**, this large excess of pincer complex led to the formation of smaller end-capped oligomers, *e.g.* **2-1-2** complexes. Unlike the high charge density of polymer **1P**, these smaller charged species were soluble in $CHCl_3$, and therefore the emission appeared at a slightly lower wavelength (485 nm) from the initial uncoordinated cruciform. This was similar to the emission observed from the soluble model complex formed upon the addition of monotopic **5** to **1** (491 nm) solely representing the emission change from the stabilization of the LUMO after self-assembly.

A similar trend was observed for the self-assembly of **2P**, with a bathochromic shift (455→560 nm) detected during the beginning stages of the titration of pincer complex **2**

(3.6 equivalents) into **3**; further addition of **2** (20.0 equivalents) resulted in a blue-shift (560→512 nm). Once again, a substantial bathochromic shift was observed, which resulted from the complexation to **2** as well as the aggregation effect associated with the growing polymers. This resulted in a red-shifted emission similar to that observed for **2P** in the solid state (544 nm). Upon the addition of 20 equivalents of **2** the aggregates were broken up forming soluble oligomers, which emitted at 512 nm. Again this was comparable to the emission observed upon the addition of monotopic **5** (507 nm) to **3**.

Changes in the optical properties of **1** and **3** were also observed upon assembly with bis-Pt pincer complex **4**. In the case of **3**, a bathochromic shift (455→510 nm) was observed upon the addition of 3.0 equivalents of **4**. This emission was consistent with the observed solid state emission of 504 nm. Further addition of **4** (15.0 equivalents) resulted in a small blue-shift (510→504 nm) corresponding to short-chain soluble oligomers. This emission was consistent with the emission observed for the model complex formed from cruciform **3** and monotopic Pt pincer **6** (515 nm). Assembly of **1** with **4** also resulted in a bathochromic shift (445–542 nm) upon the addition of 1.4 equivalents of **4**. However, further fluorescence measurements at higher equivalents of pincer complex were not detected due to near baseline fluorescence intensity. Limited intensity also prevented the measurement of the solid state emission of **3P**.

The decrease in fluorescence intensity observed upon the self-assembly of each material also occurred in other cruciform coordination studies. We previously demonstrated that upon exposure to protons or metal cations, cruciforms **1** and **3** experience a sharp decrease in fluorescence quantum yield.[21] This effect was greater for protonation than for binding to metal cations, which suggested that a greater positive

charge at the pyridine nitrogen resulted in a greater decrease in fluorescence intensity. It is suggested that binding of a proton or metal at the pyridyl nitrogen results in a stronger vibronic coupling between the ground and excited states, in addition the heavy atom effect exerted by the Pt-pincer complex. Therefore, as the binding increased, non-radiative relaxation pathways from the excited state to the ground state become more accessible, which resulted in a decreased fluorescence intensity.

5.4 Conclusion

In summary, four new supramolecular polymers were assembled by coordinating pyridyl functionalized cruciforms **1** and **3** to either ditopic bis-Pd complex **2** or bis-Pt pincer complex **4**. The fast and quantitative self-assembly was characterized by ^{1}H NMR and the association strength of each metal-ligand interaction was evaluated by ITC. From these values approximate degrees of polymerization were calculated. This data pegs the pyridyl distyryl-Pt coordination as the strongest and the pyridyl arylethynylene-Pd interaction as the weakest. The solution polymeric properties were characterized using viscometry, complementing the calculated ITC association strengths with the **3P** solution the most viscous and **2P** the least viscous. Finally, the luminescent properties were measured using fluorescence spectroscopy. The emissions of the supramolecular materials were significantly red-shifted from their uncoordinated cruciforms. The fluorescence intensity decreased in the order **3P** < **1P** < **2P** < **4P**, *proportional to their association strength*.

By developing, expanding and studying the building blocks available for self-assembly, the presented strategy allows for the design and synthesis of a class of novel functional organometallic polymers with predictable and tunable properties from a

discrete set of monomers, circumventing problems associated with traditional covalent polymer synthesis. Each component in this system is amenable to further functionalizations and modification giving us a virtually unlimited pool of monomers to investigate and exploit in future studies.

5.5 Experimental

Materials and Methods:

All chemicals were purchased from Aldrich Chemical, Acros, or Fisher Scientific and used as received unless otherwise specified. NMR spectra were recorded at 298 K on a Varian Mercury spectrometer (^{1}H = 300 MHz), residual solvent was used as an internal standard.

General procedures for ITC characterization of coordination complexes:

All measurements were carried out on a Microcal VP-ITC Microcalorimeter at 22 °C in anhydrous DMF degassed under reduced pressure.

Bis-metallated pincer complex:cruciform:

The bis-metallated pincer complex in DMF (10 mM) was titrated (5 μL injections over 10 sec followed by an equilibration period) into a DMF solution of the cruciform (1 mM). A reference run of each bis-metallated pincer complex solution titrated into pure DMF was subtracted from each measurement to account for the heat of dilution. Each experiment was done in triplicate to validate all K_a values.

Monotopic pincer complex:cruciform:

The monotopic metallated pincer complex in DMF (20 mM) was titrated (5 μL injections over 10 sec followed by an equilibration period) into a DMF solution of the cruciform (1 mM). A reference run of each monotopic metallated pincer complex solution titrated into pure DMF was subtracted from each measurement to account for the heat of dilution. Each experiment was done in triplicate to validate all K_a values. The reverse addition was also carried out to corroborate the data by titrating a DMF cruciform solution (10 mM) into a DMF monotopic metallated pincer complex solution (1 mM) under identical conditions.

Bis-metallated pincer complex:pyridine:

The bis-metallated pincer complex solution in DMF (10 mM) was titrated (5 μL injections over 10 sec followed by an equilibration period) into a DMF solution of anhydrous pyridine (1 mM). A reference run of each bis-metallated pincer complex solution titrated into pure DMF was subtracted from each measurement to account for the heat of dilution. Each experiment was done in triplicate to validate all K_a values. The reverse addition was also carried out to corroborate the data by titrating a DMF anhydrous pyridine solution (20 mM) into a DMF bis-metallated pincer complex solution (1 mM) under identical conditions.

Viscometry:

All studies were carried out in HPLC grade DMF, in a Cannon-Ubbelohde semi-micro type viscometer No. 100 L182, timed with a stopwatch at 25 °C. Initial solutions

of 0.033 mM of each supramolecular material at a 1:1 stoichiometric ratio were prepared by dissolving 0.033 mmol of each component in DMF (1 mL) in the viscometer, sonicating it for 10 min, incubating it for 10 min and then acquiring three efflux times. Then the solution within the viscometer was diluted to 0.025 mM, 0.018 mM, 0.012 mM and 0.006 mM; between each of these concentrations the solutions were equilibrated and the efflux times measured in triplicate.

Optical Spectra:

All samples and data were prepared and collected by A. J. Zucchero in the Bunz Laboratory. All samples were prepared using spectroscopic grade solvents purchased from OmniSolv. All fluorescence spectra were recorded on a Shimadzu RF-5301PC spectrofluorophotometer and acquired in a triangular quartz cuvette to minimize spectral artifacts (specifically self absorption). Solutions were mixed (as enumerated in the tables below) such that the final concentration of cruciform in all samples measured was 0.0445 mM in a mixture of $CHCl_3$-DMSO (95:5). All solution volumes were measured using Eppendorf *Reference* variable volume pipettors. Significant noise was present due to near baseline fluorescence intensity in some cases. In addition, scattering peaks were present. A spectra of the triangular cuvette filled with solvent was obtained and subtracted to minimize scattering artifacts.

Procedure for the preparation of cruciform 1:bis-Pd pincer 2 solutions for fluorescence spectroscopy:

A stock solution of cruciform **1** (1.78 mM) was prepared by dissolving **1** (106.2 mg, 0.178 mmol) in $CHCl_3$ (100.0 mL). A stock solution of bis-Pd pincer **2** (0.0177 M) was prepared by dissolving **2** (92.0 mg, 0.086 mmol) in DMSO (5.0 mL). Individual solutions were then prepared as outlined in Table 5.4 below:

Table 5.4

Equivalents of 2	Stock Solution 1 (μL)	Stock Solution 2 (μL)	DMSO (μL)	$CHCl_3$ (μL)
0.0	100	0	200	3700
1.0	100	10	190	3700
1.4	100	14	186	3700
1.6	100	16	184	3700
1.8	100	18	182	3700
2.0	100	20	180	3700
3.0	100	30	170	3700
4.0	100	40	160	3700
5.0	100	50	150	3700
10.0	100	100	100	3700
15.0	100	150	50	3700
20.0	100	200	0	3700

Fluorescence spectra were then obtained and are presented in Figure 5.8. Additionally, the traces were normalized and plotted to highlight the observed shifts in emission, shown in Figure 5.9.

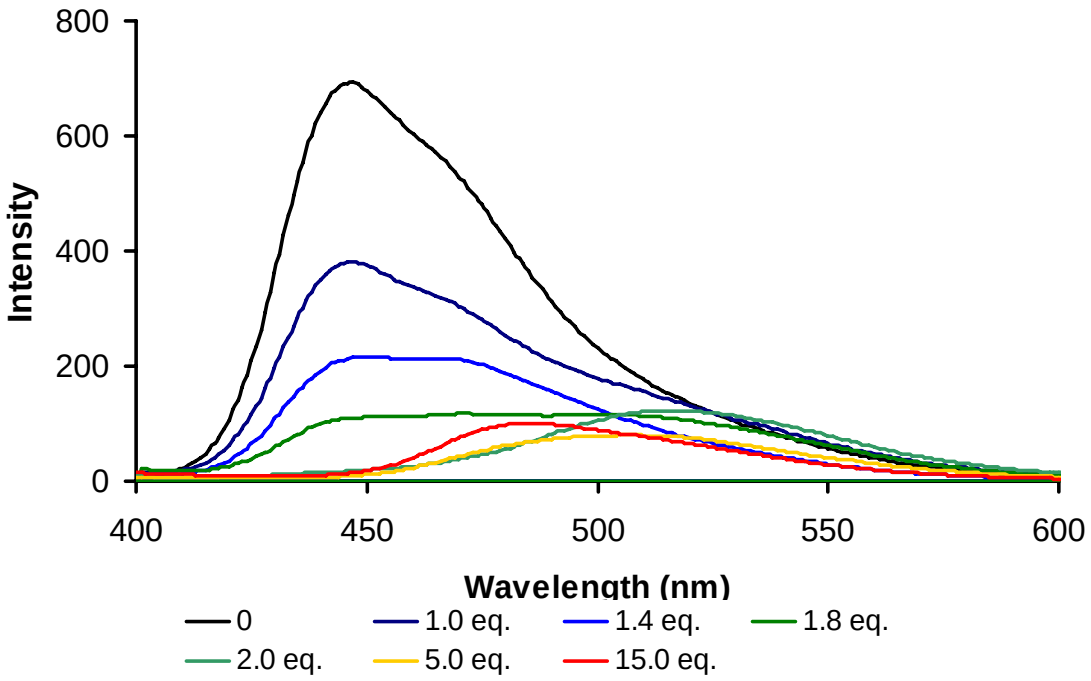

Figure 5.8 Emission Spectra of **1** upon the addition of increasing equivalents of **2**.

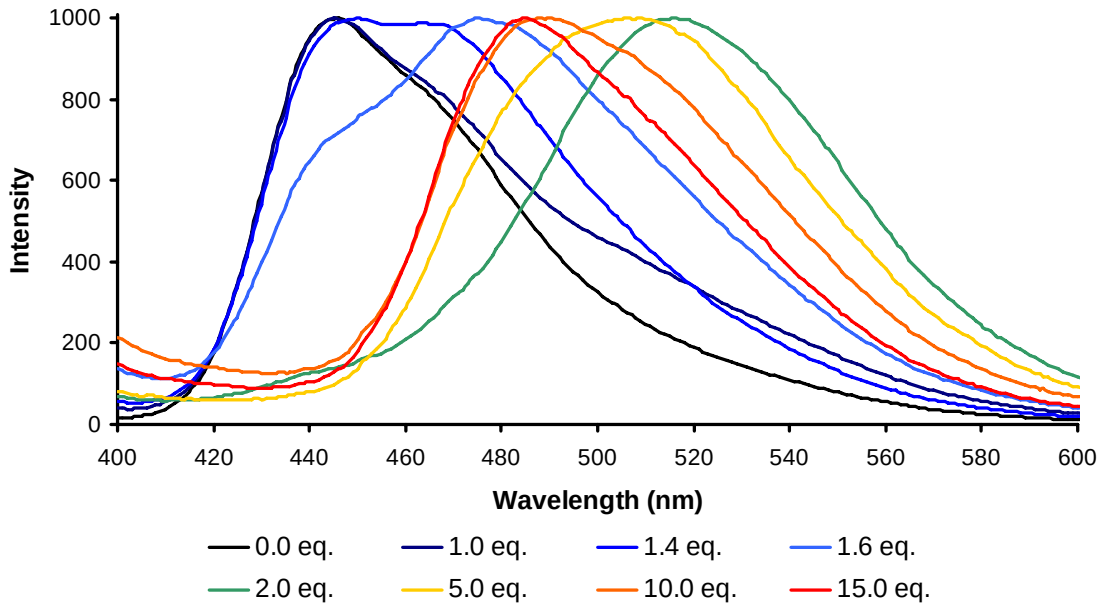

Figure 5.9 Normalized spectra showing the emission of **1** upon the addition of increasing equivalents of **2**.

Procedure for the preparation of cruciform 3:bis-Pd pincer 2 solutions for fluorescence spectroscopy:

A stock solution of cruciform **3**(1.78 mM) was prepared by dissolving **3**(101.0 mg, 0.178 mmol) in $CHCl_3$ (100.0 mL). A stock solution of bis-Pd pincer **2** (0.0177 M) was prepared by dissolving **2** (92.0 mg, 0.086 mmol) in DMSO (5.0 mL). Individual solutions were then prepared as outlined in Table 5.5 below:

Table 5.5

Equivalents of **2**	Stock Solution **3** (μL)	Stock Solution **2** (μL)	DMSO (μL)	$CHCl_3$ (μL)
0.0	100	0	200	3700
1.0	100	10	190	3700
1.2	100	12	188	3700
1.6	100	16	184	3700
2.0	100	20	180	3700
2.2	100	22	178	3700
2.6	100	26	174	3700
3.0	100	30	170	3700
3.2	100	32	168	3700
3.6	100	36	164	3700
4.0	100	40	160	3700
5.0	100	50	150	3700
10.0	100	100	100	3700
15.0	100	150	50	3700
20.0	100	200	0	3700

Fluorescence spectra were then obtained and are presented in Figure 5.10. Additionally, the traces were normalized. Upon normalization, noise was observed in the fluorescence spectra, due to near baseline fluorescence intensity, the use of a triangular fluorescence cuvette, and the presence of aggregates in solution. To remove some of this noise, a spectrum of a triangular cuvette filled with a control solution of **2** was obtained. A baseline subtraction was performed to remove some artifacts present in the raw emission spectra. The corrected spectra are presented as Figure 5.11.

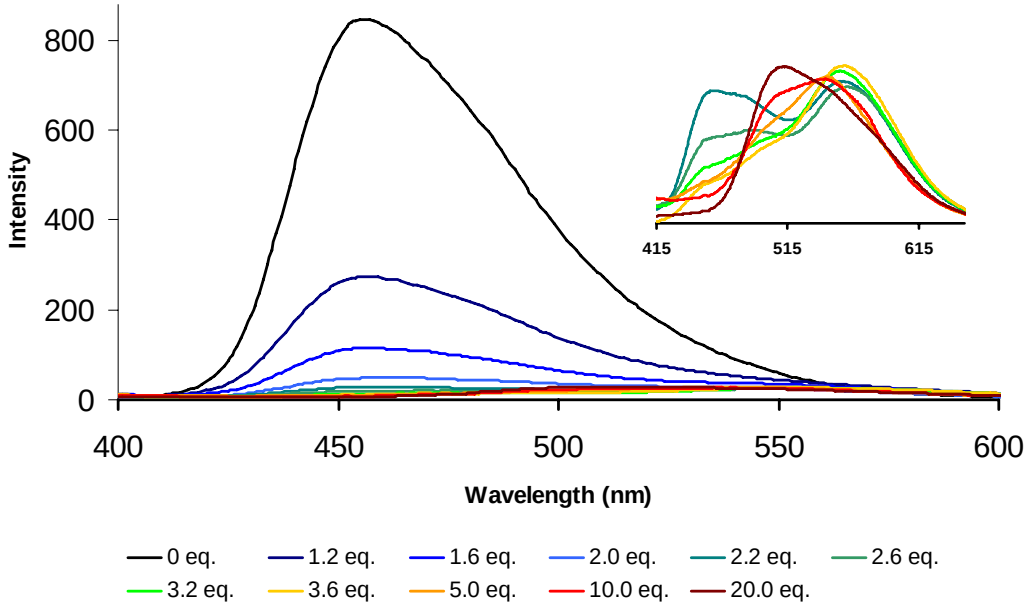

Figure 5.10 Emission Spectra of **3** upon the addition of increasing equivalents of **2**.

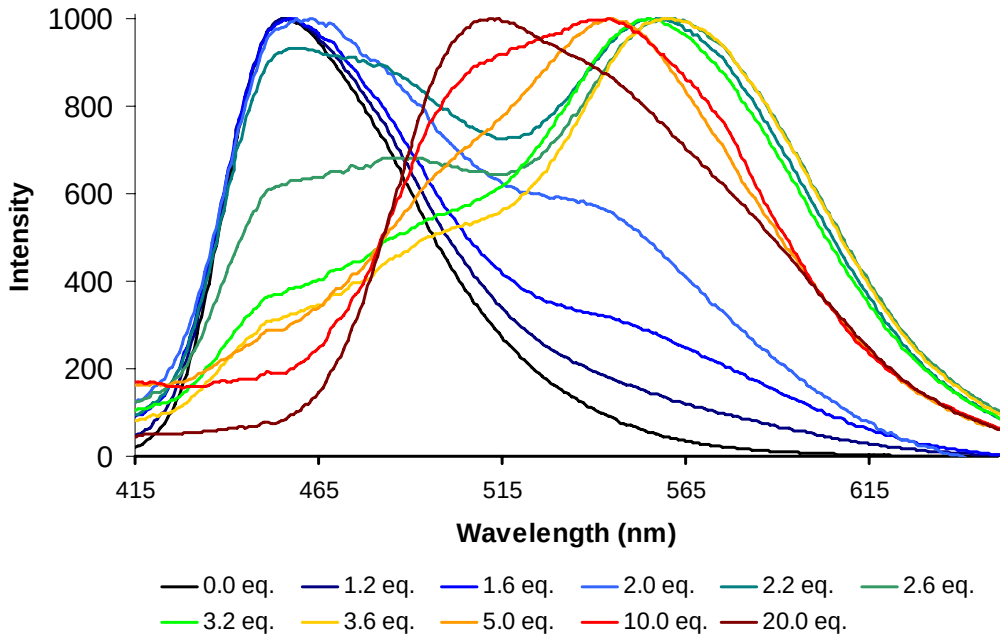

Figure 5.11 Corrected and normalized spectra showing the emission of **3** upon the addition of increasing equivalents of **2**.

Procedure for the preparation of cruciform 1:bis-Pt pincer 4 solutions for fluorescence spectroscopy:

A stock solution of cruciform **1** (1.78 mM) was prepared by dissolving **1** (106.2 mg, 0.178 mmol) in $CHCl_3$ (100.0 mL). A stock solution of bis-Pt pincer **4** (0.0177 M) was prepared by dissolving **4** (95.7 mg, 0.086 mmol) in DMSO (5.0 mL). Individual solutions were then prepared as outlined in Table 5.6 below:

Table 5.6

Equivalents of **4**	Stock Solution **1** (μL)	Stock Solution **4** (μL)	DMSO (μL)	$CHCl_3$ (μL)
0.0	100	0	200	3700
0.4	100	4	196	3700
0.8	100	8	192	3700
1.0	100	10	190	3700
1.2	100	12	188	3700
1.4	100	14	186	3700
2.0	100	20	180	3700
3.0	100	30	170	3700
4.0	100	40	160	3700
5.0	100	50	150	3700
10.0	100	100	100	3700
15.0	100	150	50	3700
20.0	100	200	0	3700

Fluorescence spectra were then obtained and are presented in Figure 5.12. Additionally, the traces were normalized. Upon normalization, noise was observed in the fluorescence spectra, due to near baseline fluorescence intensity, the use of a triangular fluorescence cuvette, and the presence of aggregates in solution. To remove some of this noise, a spectrum of a triangular cuvette filled with a control solution of **4** was obtained. A baseline subtraction was performed to remove some artifacts present in the raw emission spectra. The corrected spectra are presented in Figure 5.13.

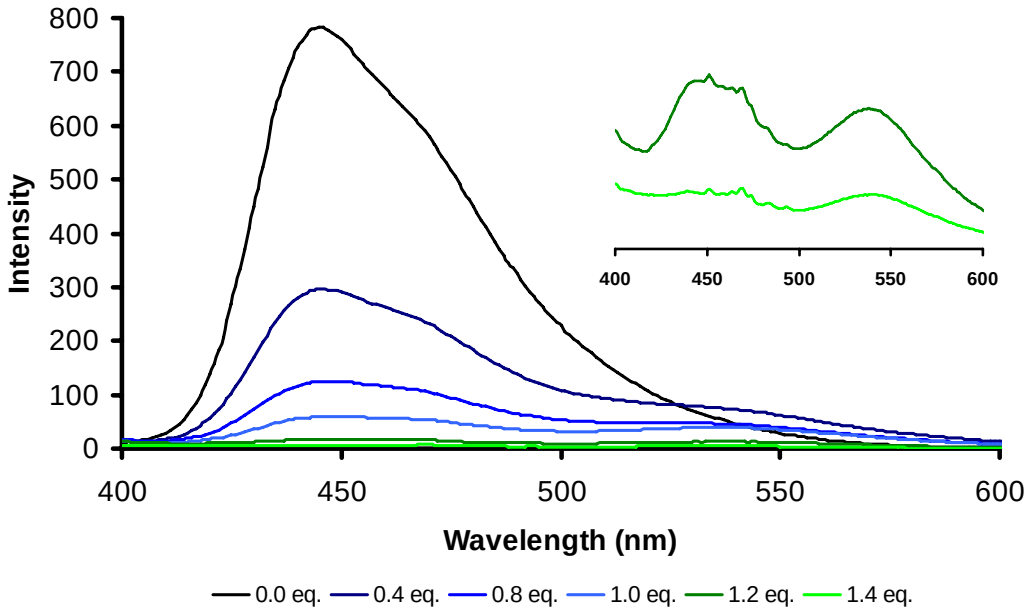

Figure 5.12 Emission Spectra of **1** upon the addition of increasing equivalents of **4**. Residual fluorescence was observed at 542 nm upon further addition of **4**; however, it could not be measured due to near baseline fluorescence intensity.

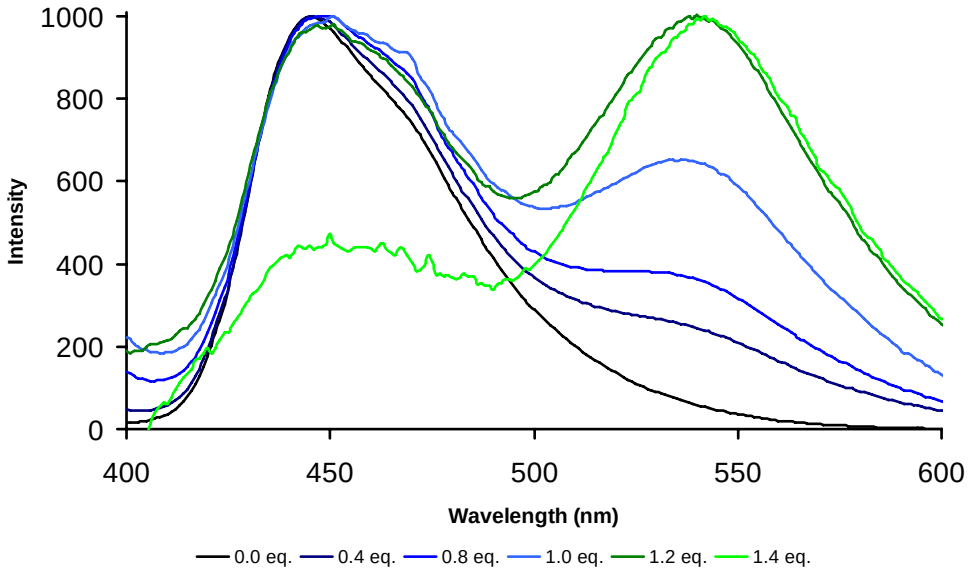

Figure 5.13 Corrected and normalized spectra showing the emission of **1** upon the addition of increasing equivalents of **4**.

Procedure for the preparation of cruciform 3:bis-Pt pincer 4 solutions for fluorescence spectroscopy:

A stock solution of cruciform **3** (1.78 mM) was prepared by dissolving **3** (101.0 mg, 0.178 mmol) in $CHCl_3$ (100.0 mL). A stock solution of bis-Pt pincer **4** (0.0177 M) was prepared by dissolving **4** (95.7 mg, 0.086 mmol) in DMSO (5.0 mL). Individual solutions were then prepared as outlined in Table 5.7 below:

Table 5.7

Equivalents of **4**	Stock Solution **3** (μL)	Stock Solution **4** (μL)	DMSO (μL)	$CHCl_3$ (μL)
0.0	100	0	200	3700
0.5	100	5	195	3700
1.0	100	10	190	3700
1.4	100	14	186	3700
1.6	100	16	184	3700
1.8	100	18	182	3700
2.0	100	20	180	3700
3.0	100	30	170	3700
4.0	100	40	160	3700
5.0	100	50	150	3700
10.0	100	100	100	3700
15.0	100	150	50	3700
20.0	100	200	0	3700

Fluorescence spectra were then obtained and are presented in Figure 5.14. Additionally, the traces were normalized. Upon normalization, noise was observed in the fluorescence spectra, due to near baseline fluorescence intensity, the use of a triangular fluorescence cuvette, and the presence of aggregates in solution. To remove some of this noise, a spectrum of a triangular cuvette filled with a control solution of **4** was obtained. A baseline subtraction was performed to remove some artifacts present in the raw emission spectra. The corrected spectra are presented as Figure 5.15.

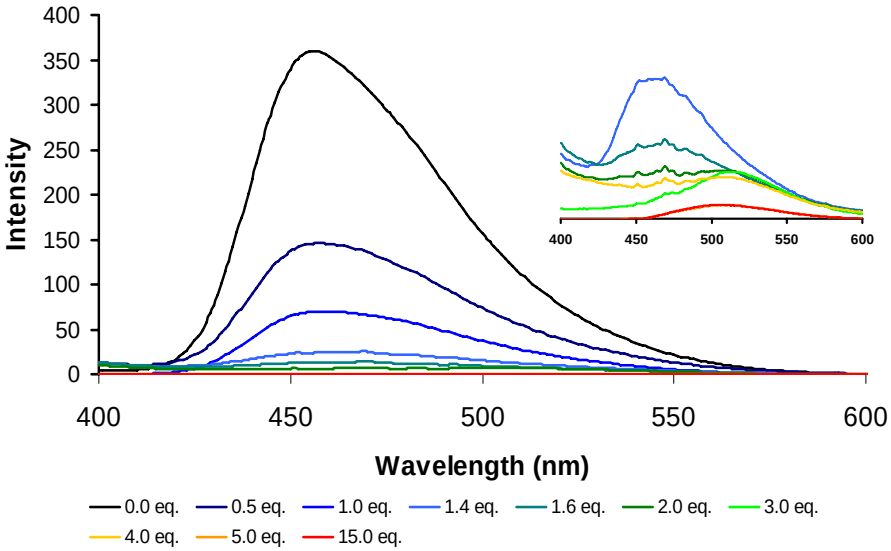

Figure 5.14 Emission Spectra of **3** upon the addition of increasing equivalents of **4**.

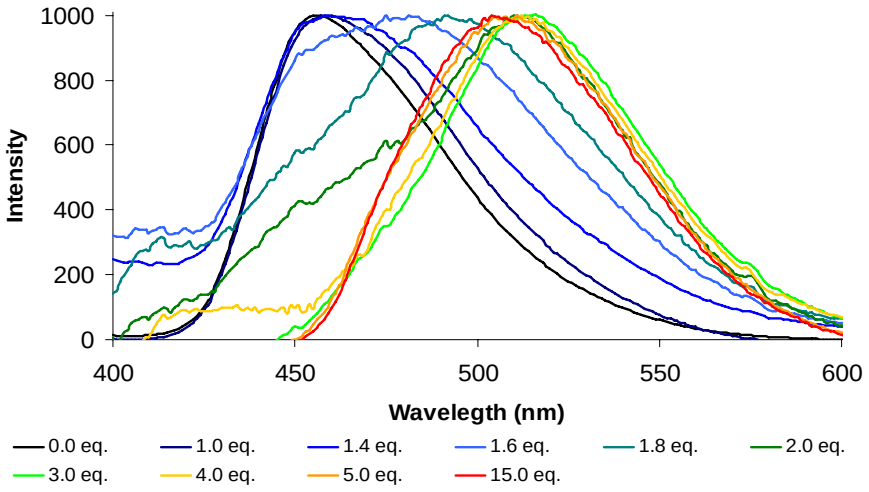

Figure 5.15 Corrected and normalized spectra showing the emission of **3** upon the addition of increasing equivalents of **4**.

Solid-State Emission of 1P, 2P, and 4P:

Thin films were prepared for assemblies **1P**, **2P**, and **4P** by dropcasting solutions of polymers in $CHCl_3$:DMSO (95:5) onto glass slides. Slides were dried under a flow of air. Emission spectra were collected for all three polymers. The spectrum of a glass slide was then subtracted to remove minor scattering effects. The corrected spectra are included as Figure 5.16.

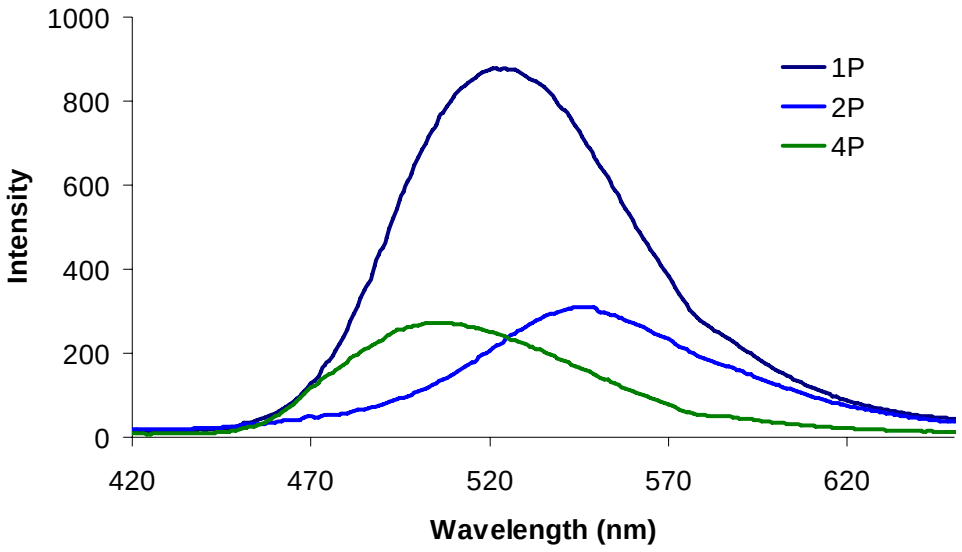

Figure 5.16 Emission of thin films of polymers **1P**, **2P**, and **4P** after baseline-subtraction of the glass slide.

Procedure for the preparation of cruciform 1:mono-Pd pincer 5 solutions for fluorescence spectroscopy:

A stock solution of cruciform **1** (1.78 mM) was prepared by dissolving **1** (106.2 mg, 0.178 mmol) in $CHCl_3$ (100.0 mL). A stock solution of mono-Pd pincer **5** (0.0177 M) was prepared by dissolving **5** (51.9 mg, 0.086 mmol) in DMSO (5.0 mL). Individual solutions were then prepared as outlined in Table 5.8:

Table 5.8

Equivalents of **5**	Stock Solution **1** (μL)	Stock Solution **5** (μL)	DMSO (μL)	$CHCl_3$ (μL)
0.0	100	0	200	3700
1.0	100	10	190	3700
2.0	100	20	180	3700
3.0	100	30	170	3700
4.0	100	40	160	3700
5.0	100	50	150	3700
20.0	100	200	0	3700

Fluorescence spectra were then obtained and are presented as Figure 5.17.

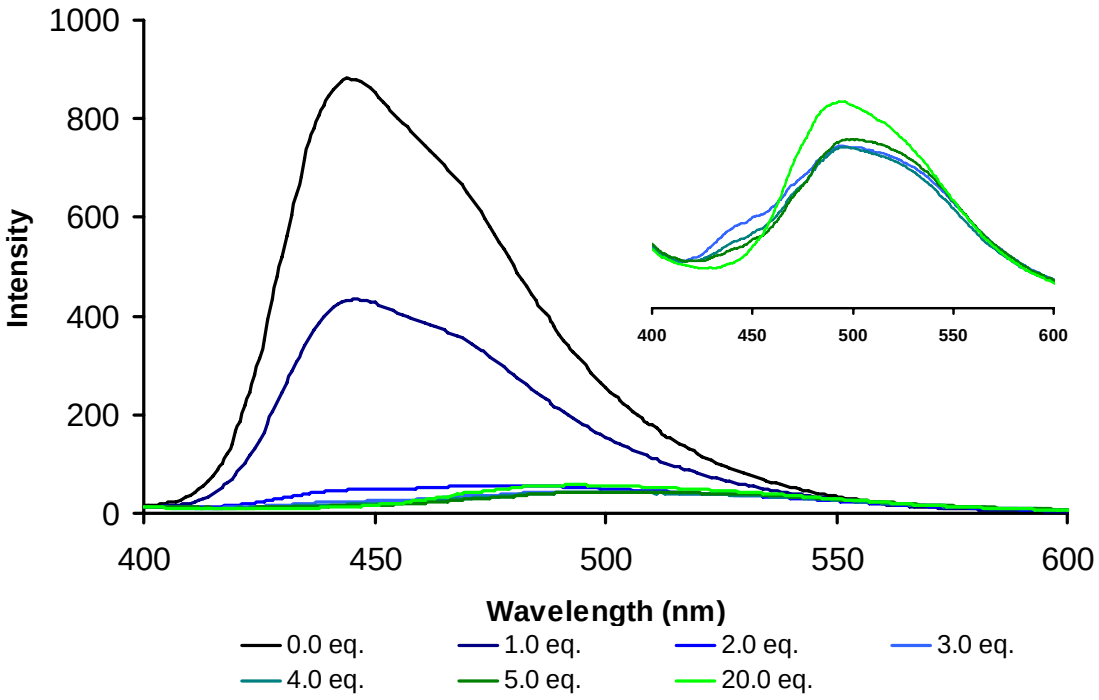

Figure 5.17 Emission Spectra of **1** upon the addition of increasing equivalents of mono-Pd pincer **5**.

Procedure for the preparation of cruciform 1:mono-Pt pincer 6 solutions for fluorescence spectroscopy:

A stock solution of cruciform **1** (1.78 mM) was prepared by dissolving **1** (106.2 mg, 0.178 mmol) in $CHCl_3$ (100.0 mL). A stock solution of mono-Pt pincer **6** (0.0177 M) was prepared by dissolving **6** (62.6 mg, 0.086 mmol) in DMSO (5.0 mL). Individual solutions were then prepared as outlined in Table 5.9:

Table 5.9

Equivalents of **6**	Stock Solution **1** (μL)	Stock Solution **6** (μL)	DMSO (μL)	$CHCl_3$ (μL)
0.0	100	0	200	3700
1.0	100	10	190	3700
2.0	100	20	180	3700
3.0	100	30	170	3700
4.0	100	40	160	3700

Fluorescence spectra were then obtained and are presented as Figure 5.18.

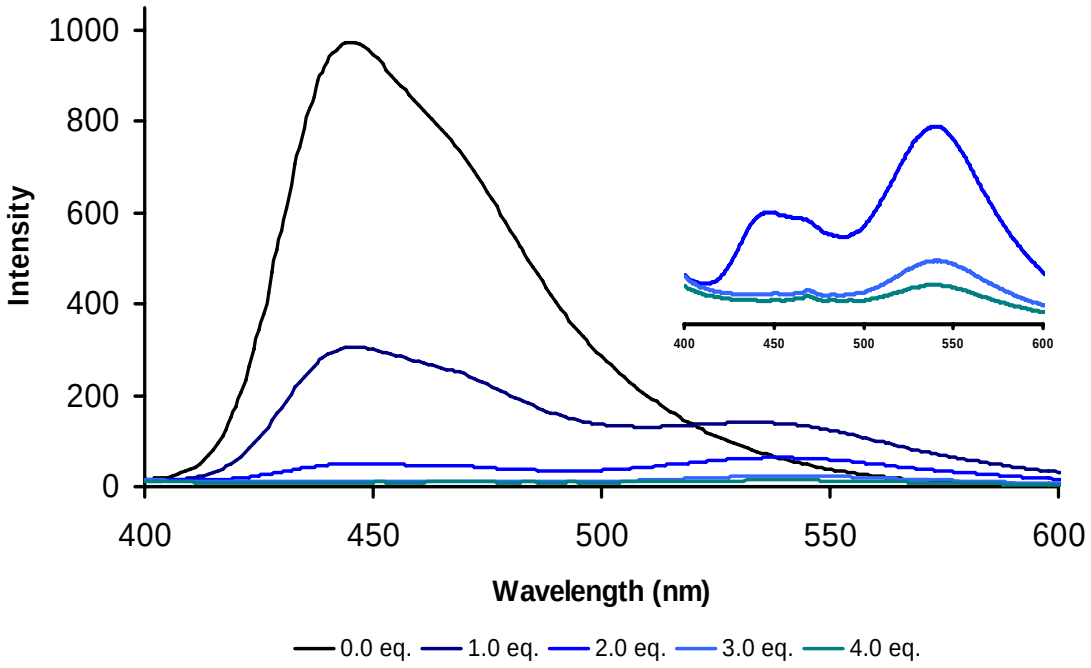

Figure 5.18 Emission Spectra of **1** upon the addition of increasing equivalents of mono-Pt pincer **6**.

Procedure for the preparation of cruciform 3:mono-Pd pincer 5 solutions for fluorescence spectroscopy:

A stock solution of cruciform **3** (1.78 mM) was prepared by dissolving **3** (101.0 mg, 0.178 mmol) in $CHCl_3$ (100.0 mL). A stock solution of mono-Pd pincer **5** (0.0177 M) was prepared by dissolving **5** (51.9 mg, 0.086 mmol) in DMSO (5.0 mL). Individual solutions were then prepared as outlined in Table 5.10 below:

Table 5.10

Equivalents of **5**	Stock Solution **3** (μL)	Stock Solution **5** (μL)	DMSO (μL)	$CHCl_3$ (μL)
0.0	100	0	200	3700
2.0	100	20	180	3700
3.0	100	30	170	3700
4.0	100	40	160	3700
5.0	100	50	150	3700
10.0	100	100	100	3700
15.0	100	150	50	3700
20.0	100	200	0	3700

Fluorescence spectra were then obtained and are presented as Figure 5.19.

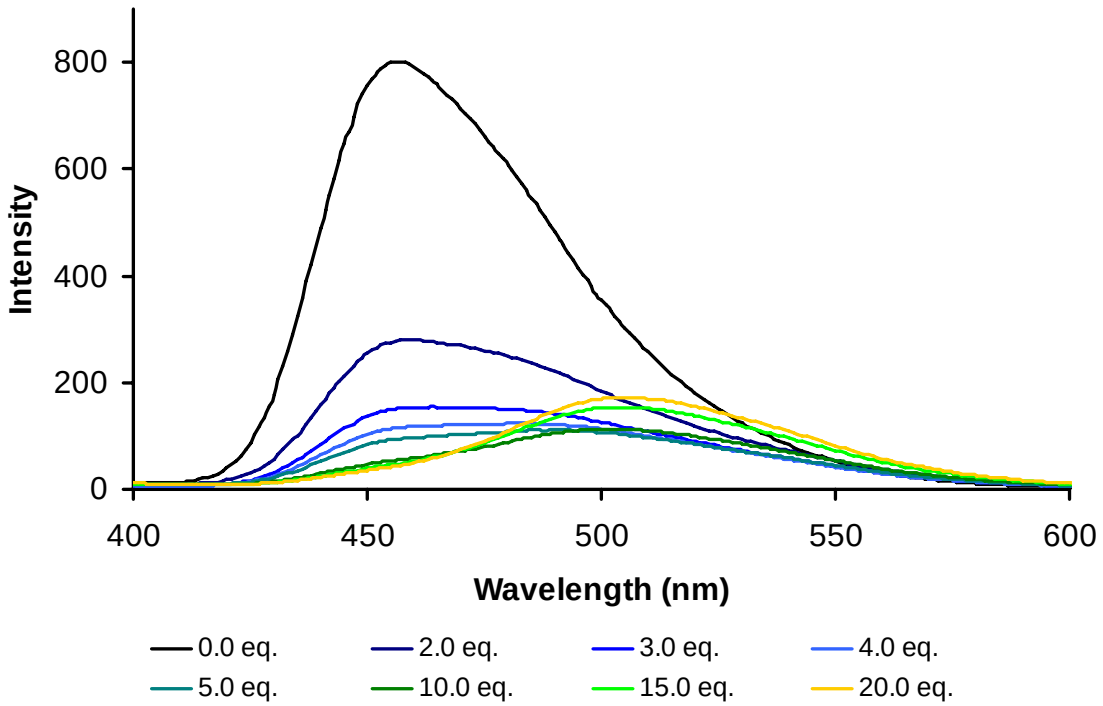

Figure 5.19 Emission Spectra of **3** upon the addition of increasing equivalents of mono-Pd pincer **5**.

Procedure for the preparation of cruciform 3:mono-Pt pincer 6 solutions for fluorescence spectroscopy:

A stock solution of cruciform **3** (1.78 mM) was prepared by dissolving **3** (101.0 mg, 0.178 mmol) in $CHCl_3$ (100.0 mL). A stock solution of mono-Pt pincer **6** (0.0177 M) was prepared by dissolving **6** (62.6 mg, 0.086 mmol) in DMSO (5.0 mL). Individual solutions were then prepared as outlined in Table 5.11:

Table 5.11

Equivalents of **6**	Stock Solution **3** (μL)	Stock Solution **6** (μL)	DMSO (μL)	$CHCl_3$ (μL)
0.0	100	0	200	3700
2.0	100	20	180	3700
3.0	100	30	170	3700
4.0	100	40	160	3700
5.0	100	50	150	3700
10.0	100	100	100	3700

Fluorescence spectra were then obtained and are presented as Figure 5.20.

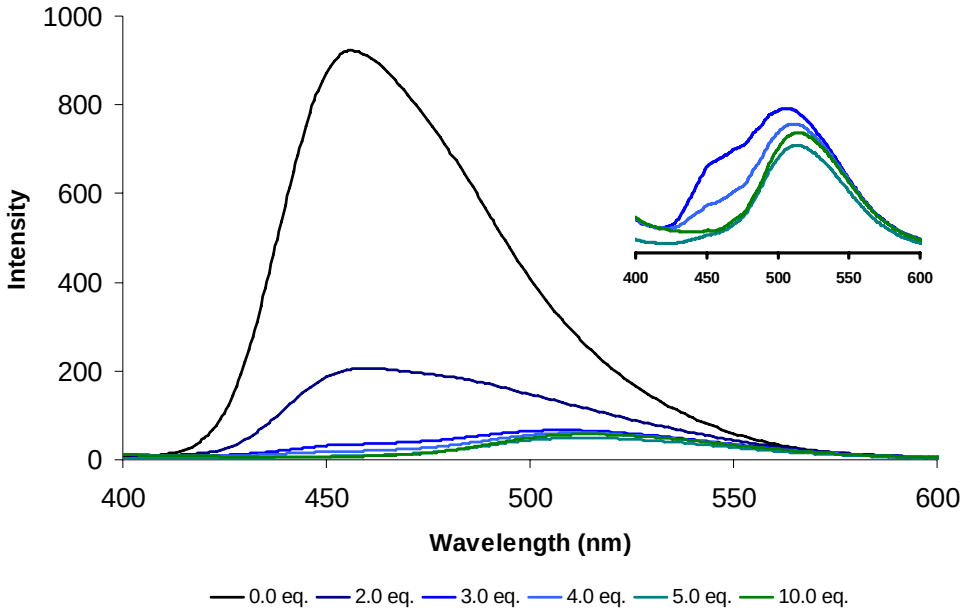

Figure 5.20 Emission Spectra of **3** upon the addition of increasing equivalents of mono-Pt pincer **6**.

5.6 References

[1] Wegner, G., Müllen, K., Editors, *Electronic Materials: The Oligomer Approach*, Wiley-VCH, Weinheim, **1996**.

[2] Kraft, A., Grimsdale, A. C., Holmes, A. B. Electroluminescent conjugated polymers-seeing polymers in a new light. *Angew. Chem. Int. Ed.* **1998**, *37*, 402-428.

[3] Dimitrakopoulos, C. D., Malenfant, P. R. L. Organic thin film transistors for large area electronics. *Adv. Mater.* **2002**, *14*, 99-117.

[4] Mitschke, U., Bäuerle, P. The electroluminescence of organic materials. *J. Mater. Chem.* **2000**, *10*, 1471-1507.

[5] Shirota, Y. Organic materials for electronic and optoelectronic devices. *J. Mater. Chem.* **2000**, *10*, 1-25.

[6] McCullough, R. D. The Chemistry of Conducting polythiophenes. *Adv. Mater.* **1998**, *10*, 93-116.

[7] Friend, R. H., Gymer, R. W., Holmes, A. B., Burroughes, J. H., Marks, R. N., Taliani, C., Bradley, D. D. C., Dos Santos, D. A., Brédas, J. L., Lögdlund, M., Salaneck, W. R. Electroluminescence in conjugated polymers. *Nature* **1999**, *397*, 121-128.

[8] Dobrawa, R., Lysetska, M., Ballester, P., Grüne, M., Würthner, F. Fluorescent Supramolecular Polymers: Metal Directed Self-Assembly of Perylene Bisimide Building Blocks. *Macromolecules* **2005**, *38*, 1315-1325.

[9] Dankers, P. Y. W., Harmsen, M. C., Brouwer, L. A., Van Luyn, M. J. A., Meijer, E. W. A modular and supramolecular approach to bioactive scaffolds for tissue engineering. *Nature Mater.* **2005**, *4*, 568-574.

[10] Chang, M. H., Hoeben, F. J. M., Jonkheijm, P., Schenning, A. P. H. J., Meijer, E. W., Silva, C., Herz, L. M. Influence of mesoscopic ordering on the photoexcitation transfer dynamics in supramolecular assemblies of oligo-p-phenylenevinylene. *Chem. Phys. Lett.* **2006**, *418*, 196-201.

[11] Iyer, P. K., Beck, J. B., Weder, C., Rowan, S. J. Synthesis and optical properties of metallo-supramolecular polymers. *Chem. Commun.* **2005**, 319-321.

[12] Knapton, D., Rowan, S. J., Weder, C. Synthesis and properties of metallo-supramolecular poly(p-phenylene ethynylene)s. *Macromolecules* **2006**, *39*, 651-657.

[13] Beck, J. B., Ineman, J. M., Rowan, S. J. Metal/Ligand-Induced Formation of Metallo-Supramolecular Polymers. *Macromolecules* **2005**, *38*, 5060-5068.

[14] Kokil, A., Yao, P., Weder, C. Organometallic Networks Based on 2,2'-Bipyridine-Containing Poly(p-phenylene ethynylene)s. *Macromolecules* **2005**, *38*, 3800-3807.

[15] Wilson, J. N., Josowicz, M., Wang, Y., Bunz, U. H. F. Cruciform π-systems: hybrid phenylene-ethynylene/phenylene-vinylene oligomers. *Chem. Commun.* **2003**, 2962-2963.

[16] Wilson, J. N., Bunz, U. H. F. Switching of Intramolecular Charge Transfer in Cruciforms: Metal Ion Sensing. *J. Am. Chem. Soc.* **2005**, *127*, 4124-4125.

[17] Wilson, J. N., Hardcastle, K. I., Josowicz, M., Bunz, U. H. F. Synthesis and electronic properties of bis-styryl substituted trimeric aryleneethynylenes. Comparison of cruciforms with iso-cruciforms. *Tetrahedron* **2004**, *60*, 7157-7167.

[18] Wilson, J. N., Smith, M. D., Enkelmann, V., Bunz, U. H. F. Cruciform π-systems: effect of aggregation on emission. *Chem. Commun.* **2004**, 1700-1701.

[19] Ciurtin, D. M., Pschirer, N. G., Smith, M. D., Bunz, U. H. F., zur Loye, H.-C. Two Luminescent Coordination Polymers with a Triple-Helix Structure: HgX2(C31H24N2).CH2Cl2 (X = Cl and Br). *Chem. Mater.* **2001**, *13*, 2743-2745.

[20] Wilson, J. N., Windscheif, P. M., Evans, U., Myrick, M. L., Bunz, U. H. F. Band Gap Engineering of Poly(p-phenyleneethynylene)s: Cross-Conjugated PPE-PPV Hybrids. *Macromolecules* **2002**, *35*, 8681-8683.

[21] Zucchero, A. J., Wilson, J. N., Bunz, U. H. F. Cruciforms as Functional Fluorophores: Response to Protons and Selected Metal Ions. *J. Am. Chem. Soc.* **2006**, *128*, 11872-11881.

[22] Marsden, J. A., Miller, J. J., Shirtcliff, L. D., Haley, M. M. Structure-Property Relationships of Donor/Acceptor-Functionalized Tetrakis(phenylethynyl)benzenes and Bis(dehydrobenzoannuleno)benzenes. *J. Am. Chem. Soc.* **2005**, *127*, 2464-2476.

[23] Spitler, E. L., Shirtcliff, L. D., Haley, M. M. Systematic Structure-Property Investigations and Ion-Sensing Studies of Pyridine-Derivatized Donor/AcceptorTetrakis(phenylethynyl)benzenes. *J. Org. Chem.* **2006**, *72*, 86-96.

[24] Klare, J. E., Tulevski, G. S., Sugo, K., de Picciotto, A., White, K. A., Nuckolls, C. Cruciform pi-systems for molecular electronics applications. *J. Am. Chem. Soc.* **2003**, *125*, 6030-6031.

[25] Klare, J. E., Tulevski, G. S., Nuckolls, C. Chemical Reactions with Upright Monolayers of Cruciform p-Systems. *Langmuir* **2004**, *20*, 10068-10072.

[26] Kang, H., Zhu, P., Yang, Y., Facchetti, A., Marks, T. J. Self-assembled electrooptic thin films with remarkably blue-shifted optical absorption based on an x-shaped chromophore. *J. Am. Chem. Soc.* **2004**, *126*, 15974-15975.

[27] Kang, H., Evmenenko, G., Dutta, P., Clays, K., Song, K., Marks, T. J. X-Shaped Electro-optic Chromophore with Remarkably Blue-Shifted Optical Absorption. Synthesis, Characterization, Linear/Nonlinear Optical Properties, Self-Assembly, and Thin Film Microstructural Characteristics. *J. Am. Chem. Soc.* **2006**, *128*, 6194-6205.

[28] Sørensen, J. K., Vestergaard, M., Kadziola, A., Kilså, K., Nielsen, M. B. Synthesis of Oligo(phenyleneethynylene)-Tetrathiafulvalene Cruciforms for Molecular Electronics. *Org. Lett.* **2006**, *8*, 1173-1176.

[29] Wang, H.-Y., Feng, J.-C., Wen, G.-A., Jiang, H.-J., Wan, J.-H., Zhu, R., Wang, C.-M., Wei, W., Huang, W. Cruciform p-n diblock conjugated oligomers for electroluminescent applications. *New J. Chem.* **2006**, *30*, 667-670.

[30] Li, Z. H., Wong, M. S., Tao, Y. Two-dimensional oligoarylenes: synthesis and structure-properties relationships. *Tetrahedron* **2005**, *61*, 5277-5285.

[31] van Manen, H.-J., Nakashima, K., Shinkai, S., Kooijman, H., Spek, A. L., van Veggel, F. C. J. M., Reinhoudt, D. N. Coordination chemistry of SCS PdII pincer systems. *Eur. J. Inorg. Chem.* **2000**, 2533-2540.

[32] Pollino, J. M., Stubbs, L. P., Weck, M. One-Step Multifunctionalization of Random Copolymers via Self-Assembly. *J. Am. Chem. Soc.* **2004**, *126*, 563-567.

[33] Gerhardt, W. W., Zucchero, A. J., Wilson, J. N., South, C. R., Bunz, U. H. F., Weck, M. Supramolecular cruciforms. *Chem. Commun.* **2006**, 2141-2143.

[34] Pollino, J. M., Weck, M. Supramolecular side-chain functionalized polymers: synthesis and self-assembly behavior of polynorbornenes bearing PdII SCS pincer complexes. *Synthesis* **2002**, 1277-1285.

[35] Pollino, J. M., Weck, M. Tandem Catalysis and Self-Assembly: A One-Pot Approach to Functionalized Polymers. *Org. Lett.* **2002**, *4*, 753-756.

[36] Higley, M. N., Pollino, J. M., Hollembeak, E., Weck, M. A modular approach toward block copolymers. *Chem. Eur. J.* **2005**, *11*, 2946-2953.

[37] Huck, W. T. S., Van Veggel, F. C. J. M., Reinhoudt, D. N. Self-assembly of hyperbranched spheres. *J. Mater. Chem.* **1997**, *7*, 1213-1219.

[38] Huck, W. T. S., Prins, L. J., Fokkens, R. H., Nibbering, N. M. M., van Veggel, F. C. J. M., Reinhoudt, D. N. Convergent and Divergent Noncovalent Synthesis of Metallodendrimers. *J. Am. Chem. Soc.* **1998**, *120*, 6240-6246.

[39] Stiriba, S.-E., Slagt, M. Q., Kautz, H., Gebbink, R. J. M. K., Thomann, R., Frey, H., van Koten, G. Synthesis and supramolecular association of immobilized NCN-pincer platinum(II) complexes on hyperbranched polyglycerol supports. *Chem. Eur. J.* **2004**, *10*, 1267-1273.

[40] Kersey, F. R., Yount, W. C., Craig, S. L. Single-Molecule Force Spectroscopy of Bimolecular Reactions: System Homology in the Mechanical Activation of Ligand Substitution Reactions. *J. Am. Chem. Soc.* **2006**, *128*, 3886-3887.

[41] Friggeri, A., van Manen, H.-J., Auletta, T., Li, X.-M., Zapotoczny, S., Schönherr, H., Vancso, G. J., Huskens, J., van Veggel, F. C. J. M., Reinhoudt, D. N. Chemistry on surface-confined molecules: an approach to anchor isolated functional units to surfaces. *J. Am. Chem. Soc.* **2001**, *123*, 6388-6395.

[42] Gerhardt, W. W., Weck, M. Investigations of Metal-Coordinated Peptides as Supramolecular Synthons. *J. Org. Chem.* **2006**, *71*, 6333-6341.

[43] Guillena, G., Rodríguez, G., Albrecht, M., van Koten, G. Covalently bonded platinum(II) complexes of a-amino acids and peptides as a potential tool for protein labeling. *Chem. Eur. J.* **2002**, *8*, 5368-5376.

[44] Guillena, G., Rodríguez, G., van Koten, G. Palladium(II) pincer complexes of a-amino acids: towards the synthesis of catalytically active artificial peptides. *Tetrahedron Lett.* **2002**, *43*, 3895-3898.

[45] Brown, H. C., Okamoto, Y. Electrophilic substituent constants. *J. Am. Chem. Soc.* **1958**, *80*, 4979-4987.

[46] Yount, W. C., Loveless, D. M., Craig, S. L. Small-Molecule Dynamics and Mechanisms Underlying the Macroscopic Mechanical Properties of Coordinatively Cross-Linked Polymer Networks. *J. Am. Chem. Soc.* **2005**, *127*, 14488-14496.

[47] Loeb, S. J., Shimizu, G. K. H. Dimetalated thioether complexes as building blocks for organometallic coordination polymers and aggregates. *J. Chem. Soc., Chem. Commun.* **1993**, 1395-1397.

[48] Steenwinkel, P., James, S. L., Grove, D. M., Kooijman, H., Spek, A. L., van Koten, G. Double Cyclometalation via Carbon-Silicon Bond Cleavage by Palladium(II) Acetate. X-ray Structure of a Cationic 1,4-Dipalladated Benzene Ring and Selective Synthesis of Heterobimetallic 1,4-Phenylene-Bridged Platinum(II)-Palladium(II) Complexes. *Organometallics* **1997**, *16*, 513-515.

[49] Steenwinkel, P., Kooijman, H., Smeets, W. J. J., Spek, A. L., Grove, D. M., van Koten, G. Intramolecularly Stabilized 1,4-Phenylene-Bridged Homo- and Heterodinuclear Palladium and Platinum Organometallic Complexes Containing N,C,N-Coordination Motifs; h1-SO2 Coordination and Formation of an Organometallic Arenium Ion Complex with Two Pt-C s-Bonds. *Organometallics* **1998**, *17*, 5411-5426.

[50] The directionally opposite shift of the α-pyridyl cruciform signal in the ^{1}H NMR spectrum observed upon coordination to the bis-Pd pincer complex **2** compared to the shift after coordination to the bis-Pt pincer compex **4** is due to an overlap of the pyridyl protons with the thiophenyl ring currents of bis-Pd pincer complex **2**, see ref # 34

[51] Due to the highly dilute $CHCl_3$:DMSO solvent mixture we did not observe the expected polymerization at a 1:1 metal-ligand stoichiometry. Putative high molecular weight polymers, which precipitated out of solution were not seen until an excess of the pincer complex was titrated into the cruciform solution. As the K_a increased precipitation of the respective complex occurred closer to the expected 1:1 stoichiometry.

Chapter 6

Cyclic Peptide Supramolecular Architectures: Today and Tomorrow

6.1 Abstract

This chapter summarizes the objectives of this research and the accomplishments, which have brought us closer to realizing our initial goal, the supramolecular synthesis of a cyclic peptide membrane. This membrane architecture, once achieved will ideally be the beginning of a new research arm of supramolecular synthesis branching off into many other exciting areas. This chapter puts forth multiple different uses, optimization strategies, and developmental evolutions that should be investigated in order for this research to mature and prosper.

6.2 Current Status of Cyclic Peptide Supramolecular Architectures

The overall objective of this project is to create biologically relevant and functional supramolecular architectures, such as a well-defined membrane. We chose to work with peptides, because of the wide range of natural and synthetic amino acids available with functional and amenable side-chains. At the commencement of this thesis research, synthetic self-assembly of peptidal and proteinaceous architectures was very limited. It was only 16 years ago that the first coordination of a metal ion salt to a peptide side-chain was reported.[1-4] And currently, there are no reports of well-defined finite peptide-organometallic supramolecular architectures.

Early objectives to reach this goal were to synthesize a biological supramolecular synthon and to coordinate it via complementary cohesive recognition units.

An alternating D,L cyclic peptide was chosen as the biological synthon owing to its: tunable pore diameter, selectivity and transport of guest molecules and vertical self-assembling behavior.[1, 2, 5-17]

A bis-metallated pincer complex was chosen as the ditopic metal-coordinating unit due to its single site, directional and 180° linear coordination in a variety of solvents.[18-21] This metal-ligand interaction has already found a variety of uses in purely synthetic supramolecular architectures,[18] and has thus far not been assembled with any biological synthons.

Early research for this project was spent synthesizing pyridyl functionalized linear peptide units and then coordinating them to monometallic pincer complexes.[21] This was done to elucidate and understand the coordination behavior of metallated pincer complexes with peptide functionalized ligands, something unknown until now. Our primary concern was that the ancillary functionalities of our peptide system may interfere with this otherwise well-defined metal-ligand interaction. This cautious study was done to validate the complex synthesis of a pyridyl functionalized cyclic peptide.

The results from this study singled out an optimum pyridyl unit from the four peptides investigated. Cyclic peptide **28**, which incorporated this residue, an L-4-pyridyl alanine into the cyclic backbone, was designed and synthesized. The accomplishment of this research includes an optimized synthesis using a solution-phase synthetic route with high coupling yields at every step, and a new purification using preparatory TLC.

Cyclic octapeptide **28** was successfully synthesized and obtained in great enough quantity and purity to carry out preliminary coordination studies. ^{1}H NMR and ES-MS analysis showed quantitative coordination. Detection via MS was shown to be inversely

relative to the cone voltage strength of the spectrometer, which fragments the molecular ion signal of bicylic bis Pd-pincer complex **1** as it is increased.

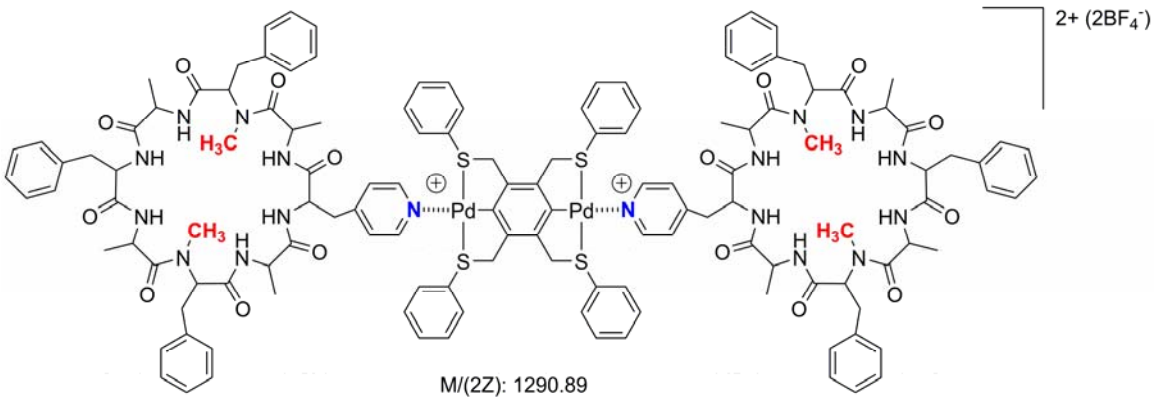

1

Figure 6.1 Bicyclic nanostructure observed in ES-MS.

6.3 Future Work Towards Cyclic Peptide Supramolecular Architectures

Based on the very preliminary but promising coordination results shown in Figure 6.1, an expansion of the coordination behavior is the next phase.

The ultimate goal of this work is to develop engineered membranes, possibly for sensing purposes of small analytes.[22-28] As with our initial coordination studies of linear tripeptides the research building up to this goal is best done incrementally. By synthesizing pyridyl cyclic peptides with an ever increasing number of pyridyl units, different supramolecular architectures may be realized, such as the homo-cyclic supramolecular architectures and hetero-cyclic supramolecular architecture shown in Schemes 6.1 and 6.2, respectively.

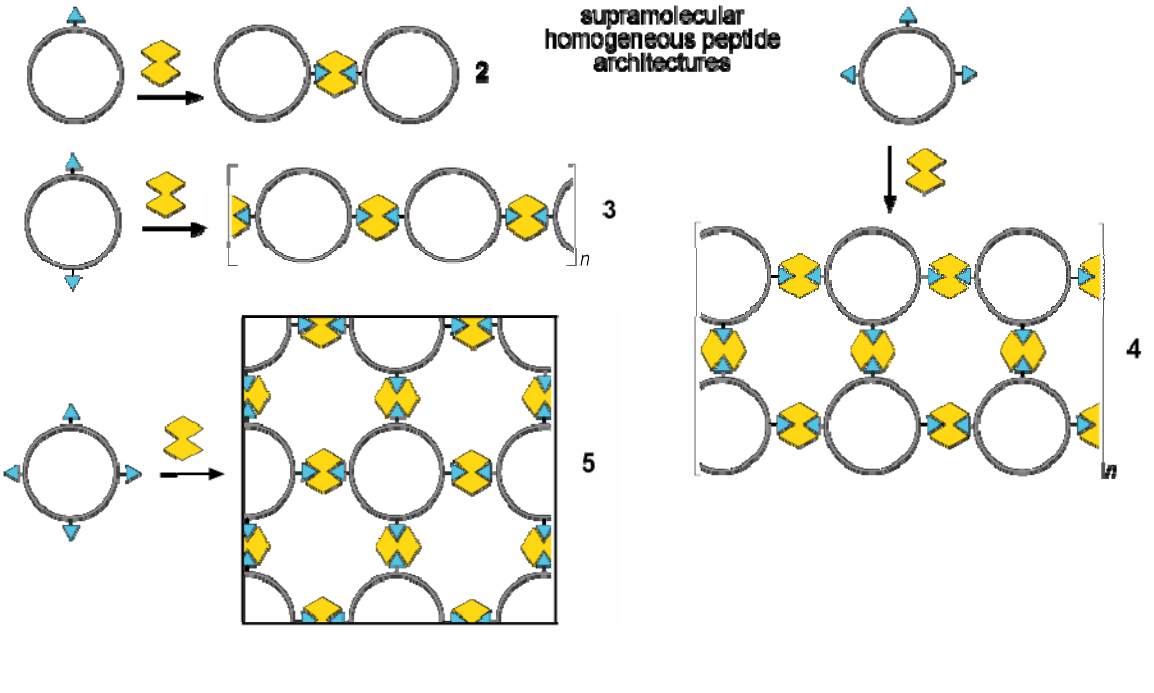

Scheme 6.1 Homo-architectures composed of cyclic peptides with an increasing number of pyridyl units and a ditopic metallated pincer complex, for the tripyridyl cyclic peptide on the right the ladder architecture is only one possible supramolecular isomer.

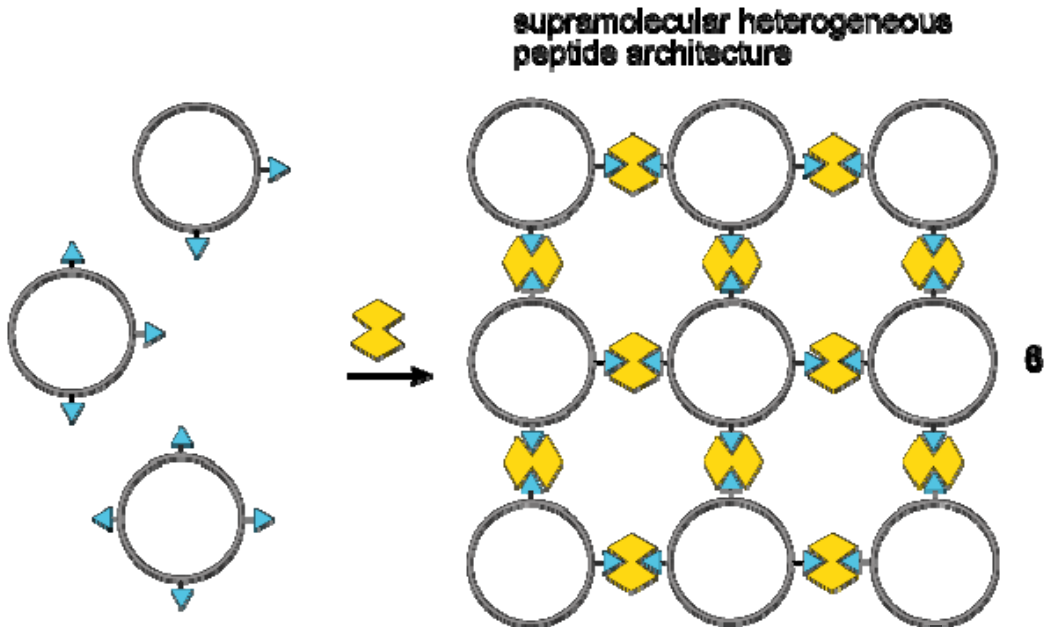

Scheme 6.2 Hetero-architectures composed of different pyridyl cyclic peptides and a ditopic metallated pincer complex, this is only one of several different supramolecular isomers.

If accessible, all of these structures will have unique characterization demands, most likely based on their solubility. As the structures grow larger, both increased charge density of the metal centers and rigidity may limit the solubility of materials such as **5** or **6** shown in Schemes 6.1 and 6.2, respectively. More polar solvents may be required to solvate these poly(organometallic) structures, this will in turn weaken the association strength of the entire assembly and may be a later concern for potential applications. Additionally, supramolecular isomerism for tripyridyl and hetero systems may limit the predictability of these self-assembled systems, although continuous planar structures may be thermodynamically favored once several of the structural pieces are properly aligned and coordinated as in **6** of Scheme 6.2 as compared to the vacant ligand and metal center sites of **7**, shown in Figure 6.2, a possible supramolecular isomer of **6**.

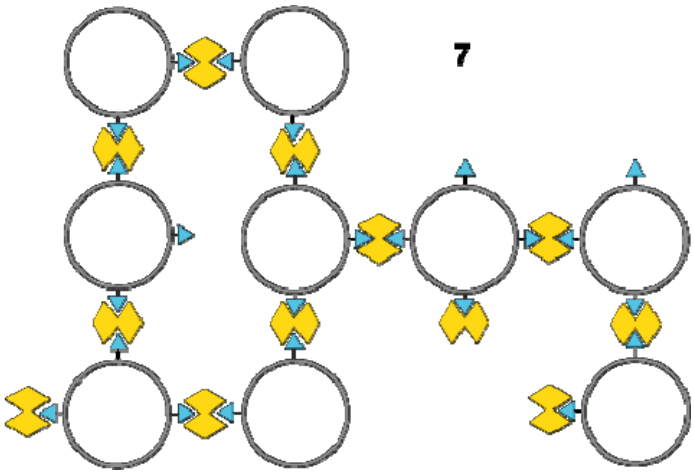

Figure 6.2 Possible supramolecular isomer of architecture **6**.

The ultimate goal of a final freestanding membrane architecture may be logistically difficult, and raises several questions.

1) How do we retrieve the self-assembled architecture without disrupting the metal-coordination?

2) How do we localize or place the architecture?

3) How do we characterize the system?

By self-assembling these architectures off and from a surface, several of these issues may be mitigated. Stochastic membrane sensors are frequently assembled within a diaphragm having an aperture,[16, 25, 27] held together by very weak attractive forces. By functionalizing the surface of the aperture with pyridines a finite and peripherally tethered supramolecular membrane can be assembled and then characterized by conductance measurements as analytes pass through it, as shown in Figure 6.3. This envisaged system would be superior to current engineered membranes in that it would have multiple well-defined pores for analyte transport as compared to a single pore created by a transmembrane pore protein in the current systems.[10, 29, 30] Metallated pincer complexes and other units have previously been functionalized on surfaces as nucleation sites, and the use of earlier cyclic peptides as membrane channels, and Pd-pincer complexes off surfaces establishes precedence for this idea.[31-34]

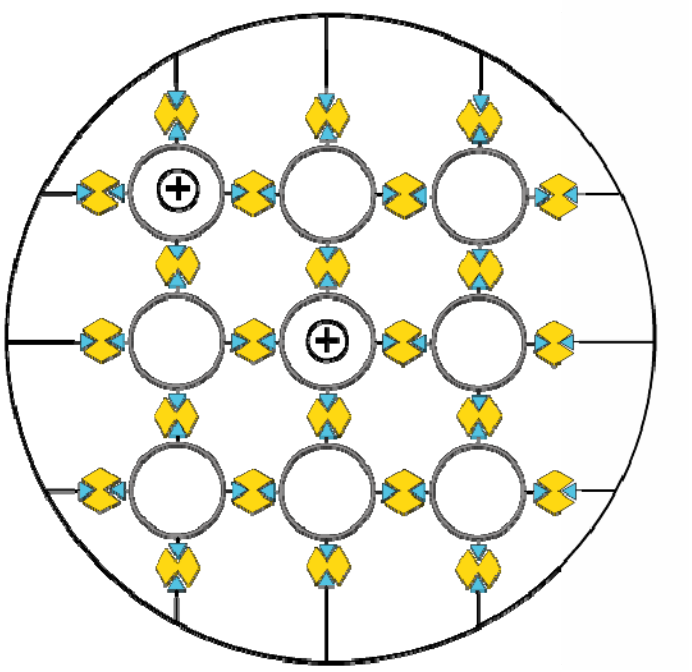

Figure 6.3 Pyridyl functionalized aperture, which tetrapyridyl cyclic peptides have been self-assembled into giving a membrane with well-defined pore sizes. Circled "+" are cations selectively passing through.

These systems are all based on cyclic peptides with partially N-methylated backbone amido nitrogens. By synthesizing unmethylated systems the cycles can have an orthogonal H-bonded self-assembly along a vertical axis to give organic nanotubes.[12] This behavior has been fully characterized in earlier cyclic systems with different peripheral functionalizations,[10, 35, 36] and may allow for more elaborate self-assembled tubular arrays, such as the one shown in Figure 6.4. This system's bottom layer would have bipyridyl cyclic peptides that have a half N-methylated faces at the Ala amido nitrogens, this would allow for self-assembly on one face. By adding unmethylated cyclic peptides, this lowest face could be a nucleation site for the vertical growth of aligned tubular arrays.

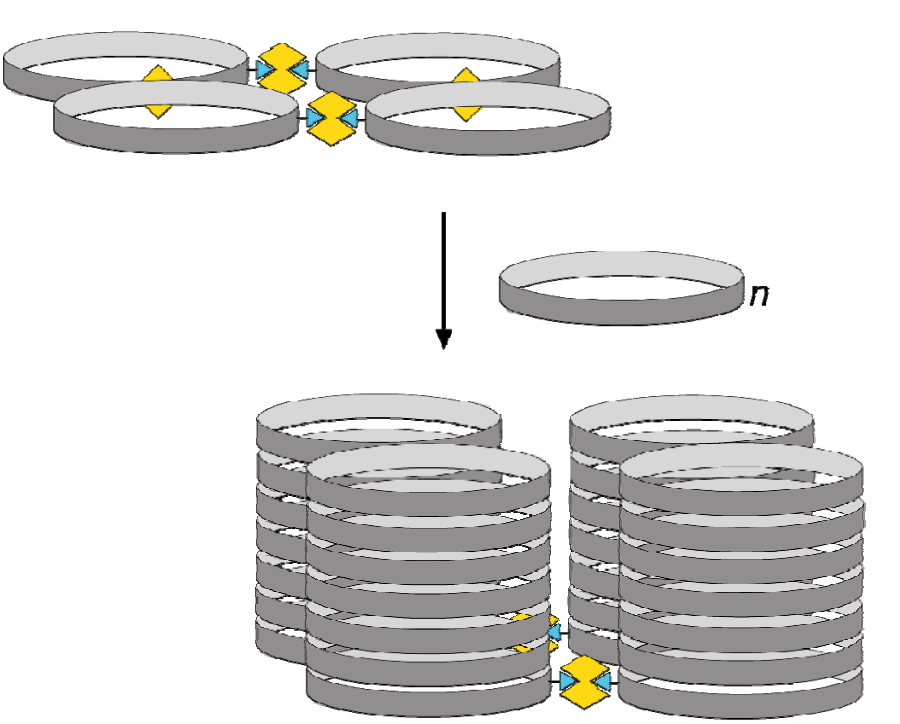

Figure 6.4 Self-assembled tubular arrays grown from a monolayer of pyridyl cyclic peptides with unmethylated non pyridyl cycles.

Efforts to engineer a network similar to the one shown in Figure 6.4 have been attempted in a crystalline solid state with limited success through peripheral side-chain modifications.[37] This new design would facilitate such a system in both the solution and the solid state.

An earlier report of a device fabricated from a peptide nanotube on an alkanethiol covered gold electrode surface acted as a diffusion controlled dynamic biosensor;[38] this system could possibly supplant this earlier device as a high performance system with multiple inputs for analyte detection. By altering the backbone structure of the cycles for interior functionalization,[6, 8] the tubes can be functionalized with a bias creating a selectivity towards different analytes. Shown in Figure 6.5 is a cation selective biosensor with the top cycle internally functionalized with carboxylates.

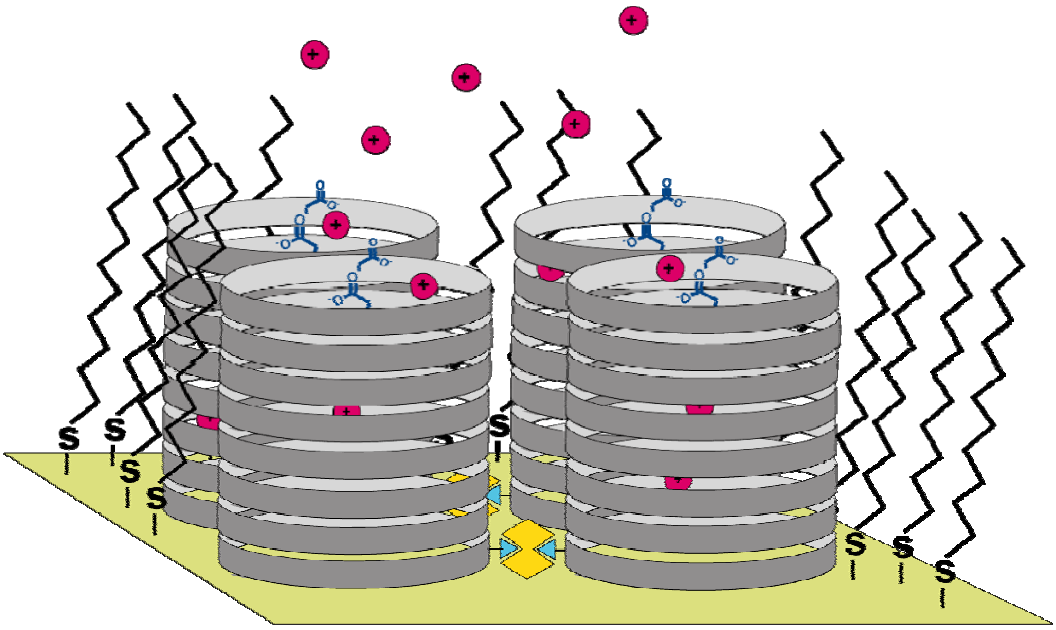

Figure 6.5 Tubular array cationic biosensor embedded in an alkanethiol SAM on a gold electrode.

An early desire of Ghadiri's was to utilize the tubes in molecular electronics.[12] It can be envisaged that coordinating tubular arrays having different internal functionalizations can be used for the growth and insulation of conjugated systems for electro-optical applications.[39-41]

Finally, by functionalizing other side-chains with latent functionalities that can be reacted post self-assembly the final architectures can be covalently captured. The coordination would align and place the components and this architecture could then be covalently glued together. A simple demonstration of this system has already been reported. In this system a cyclic dimer having terminal alkenes off alkyl side-chains was covalently captured using a metathesis catalyst.[36] This same strategy could be employed for larger more sophisticated architectures, giving permanent structures.

Based on the breadth of research provided by numerous groups there is a deep well of novel cyclic peptide systems to draw from. By gleaning and incorporating features from previous reports into our one of a kind system a myriad of new architectures and materials can be imagined.

6.4 References

[1] Ghadiri, M. R., Choi, C. Secondary structure nucleation in peptides. Transition metal ion stabilized a-helices. *J. Am. Chem. Soc.* **1990**, *112*, 1630-1632.

[2] Ghadiri, M. R., Fernholz, A. K. Peptide architecture. Design of stable a-helical metallopeptides via a novel exchange-inert ruthenium(III) complex. *J. Am. Chem. Soc.* **1990**, *112*, 9633-9635.

[3] Handel, T., DeGrado, W. F. De novo design of a Zn2+-binding protein. *J. Am. Chem. Soc.* **1990**, *112*, 6710-6711.

[4] Ruan, F., Chen, Y., Hopkins, P. B. Metal ion-enhanced helicity in synthetic peptides containing unnatural, metal-ligating residues. *J. Am. Chem. Soc.* **1990**, *112*, 9403-9404.

[5] Amorín, M., Brea, R. J., Castedo, L., Granja, J. R. The Smallest α,γ-Peptide Nanotubulet Segments: Cyclic α,γ-Tetrapeptide Dimers. *Org. Lett.* **2005**, *7*, 4681-4684.

[6] Amorín, M., Castedo, L., Granja, J. R. New Cyclic Peptide Assemblies with Hydrophobic Cavities: The Structural and Thermodynamic Basis of a New Class of Peptide Nanotubes. *J. Am. Chem. Soc.* **2003**, *125*, 2844-2845.

[7] Amorín, M., Castedo, L., Granja, J. R. Self-assembled peptide tubelets with 7 Å pores. *Chem. Eur. J* **2005**, *11*, 6543-6551.

[8] Bitta, J., Kubik, S. Cyclic Hexapeptides with Free Caboxylate Groups as New Receptors for Monosaccharides. *Org. Lett.* **2001**, *3*, 2637-2640.

[9] Brea, R. J., Amorín, M., Castedo, L., Granja, J. R. Methyl-blocked dimeric α,γ-peptide nanotube segments: formation of a peptide heterodimer through backbone-backbone interactions. *Angew. Chem. Int. Ed.* **2005**, *44*, 5710-5713.

[10] Clark, T. D., Buehler, L. K., Ghadiri, M. R. Self-Assembling Cyclic β^3-peptides Nanotubes as artificial transmembrabe Ion channels. *J.Am. Chem. Soc.* **1998**, *120*, 651-656.

[11] Fernandez-Lopez, S., Kim, H.-S., Choi, E. C., Delgado, M., Granja, J. R., Khasanov, A., Kraehenbuehl, K., Long, G., Weinberger, D. A., Wilcoxen, K. M., Ghadiri, M. R. Antibacterial agents based on the cyclic D,L-α-peptide architecture. *Nature* **2001**, *414*, 452-455.

[12] Ghadiri, M. R., Granja, J. R., Milligan, R. A., McRee, D. E., Khazanovich, N. Self-assembling organic nanotubes based on a cyclic peptide architecture. *Nature* **1993**, *366*, 324-327.

[13] Horne, W. S., Ashenasy, N., Ghadiri, M. R. Modulating Charge Transfer through Cyclic D,L-α-Peptide Self-Assembly. *Chem. Eur. J* **2005**, *11*, 1137-1144.

[14] Horne, W. S., Stout, C. D., Ghadiri, M. R. A Heterocyclic Peptide Nanotube. *J. Am. Chem. Soc.* **2003**, *125*, 9372-9376.

[15] Pavone, V., Benedetti, E., Di Blasio, B., Lombardi, A., Pedone, C. Regularly Alternating L,D-Peptides. III. Hexacyclic Peptides from Valine or Phenylalanine. *Biopolym.* **1989**, *28*, 215-223.

[16] Sanchez-Quesada, J., Ghadiri, M. R., Bayley, H., Braha, O. Cyclic Peptides as Molecular Adapters for a Pore-Forming Protein. *J. Am. Chem. Soc.* **2000**, *122*, 11757-11766.

[17] van Maarseveen, J. H., Horne, W. S., Ghadiri, M. R. Efficient Route to C_2 Symmetric Heterocyclic Backbone Modified Cyclic Peptides. *Org. Lett.* **2005**, *7*, 4503-4506.

[18] Albrecht, M., van Koten, G. Platinum group organometallics based on "pincer" complexes: sensors, switches, and catalysts. *Angew. Chem. Int. Ed.* **2001**, *40*, 3750-3781

[19] Yount, W. C., Loveless, D. M., Craig, S. L. Strong means slow: Dynamic contributions to the bulk mechanical properties of supramolecular networks. *Angew. Chem. Int. Ed.* **2005**, *44*, 2746-2748

[20] Gerhardt, W. W., Zucchero, A. J., Wilson, J. N., South, C. R., Bunz, U. H. F., Weck, M. Supramolecular cruciforms. *Chem. Commun.* **2006**, 2141-2143.

[21] Gerhardt, W. W., Weck, M. Investigations of Metal-Coordinated Peptides as Supramolecular Synthons. *J. Org. Chem.* **2006**, *71*, 6333-6341.

[22] Guan, X., Gu, L.-Q., Cheley, S., Braha, O., Bayley, H. Stocastic Sensing of TNT with a Genetically Engineered Pore. *Chem. Bio. Chem.* **2005**, *6*, 1875-1881.

[23] Bayley, H., Jayasinghe, L. Functional engineered channels and pores (review). *Mol. Membrane Biol.* **2004**, *21*, 209-220.

[24] Kang, X.-f., Cheley, S., Guan, X., Bayley, H. Stochastic Detection of Enantiomers. *J. Am. Chem. Soc.* **2006**, *128*, 10684-10685.

[25] Gu, L.-Q., Braha, O., Conlan, S., Cheley, S., Bayley, H. Stochastic sensing of organic analytes by a pore-forming protein containing a molecular adapter. *Nature* **1999**, *398*, 686-690.

[26] Bayley, H., Cremer, P. S. Stochastic sensors inspired by biology. *Nature* **2001**, *413*, 226-230.

[27] Wong, D., Jeon, T.-J., Schmidt, J. Single molecule measurements of channel proteins incorporated into biomimetic polymer membranes. *Nanotech.* **2006**, *17*, 3710-3717.

[28] Malmstadt, N., Nash, M. A., Purnell, R. F., Schmidt, J. Automated Formation of Lipid-Bilayer Membranes in a Microfluidic Device. *Nano Lett.* **2006**, *6*, 1961-1965.

[29] Granja, J. R., Ghadiri, M. R. Channel-Mediated Transport of Glucose across Lipid Bilayers. *J. Am. Chem. Soc.* **1994**, *116*, 10785-10786.

[30] Sanchez-Quesada, J., Isler, M. P., Ghadiri, M. R. Modulating Ion Channel Properties of Transmembrane Peptide Nanotubes through Heteromeric Supramolecular Assemblies. *J. Am. Chem. Soc.* **2002**, *124*, 10004-10005.

[31] Kersey, F. R., Yount, W. C., Craig, S. L. Single-Molecule Force Spectroscopy of Bimolecular Reactions: System Homology in the Mechanical Activation of Ligand Substitution Reactions. *J. Am. Chem. Soc.* **2006**, *128*, 3886-3887.

[32] Friggeri, A., van Manen, H.-J., Auletta, T., Li, X.-M., Zapotoczny, S., Schönherr, H., Vancso, G. J., Huskens, J., van Veggel, F. C. J. M., Reinhoudt, D. N. Chemistry on surface-confined molecules: an approach to anchor isolated functional units to surfaces. *J. Am. Chem. Soc.* **2001**, *123*, 6388-6395.

[33] Li, X.-M., Auletta, T., van Veggel, F. C. J. M., Huskens, J., Reinhoudt, D. N. Directed, selective insertion of single molecules into patterned self-assembled monolayers of alkanethiols with different chain lengths. *Org. Biomol. Chem* **2004**, *2*, 296-300.

[34] van Manen, H.-J., Auletta, T., Dordi, B., Schönherr, H., Vancso, G. J., van Veggel, F. C. J. M., Reinhoudt, D. N. Non-covalent chemistry on surface-confined isolated dendrimers. *Adv. Funct. Mater.* **2002**, *12*, 811-818.

[35] Clark, T. D., Buriak, J. M., Kobayashi, K., Isler, M. P., McRee, D. E., Ghadiri, M. R. Cyclindrical β-sheet peptide assemblies. *J. Am. Chem. Soc.* **1998**, *120*, 8949-8962.

[36] Clark, T. D., Ghadiri, M. R. Supramolecular Design by Covalent Capture. Design of a Peptide Cylinder via Hydrogen-Bond-Promoted Intermolecular Olefin Metathesis. *J. Am. Chem. Soc.* **1995**, *117*, 12364-12365.

[37] Hartgerink, J. D., Granja, J. R., Milligan, R. A., Ghadiri, M. R. Self-assembling peptides nanotubes. *J. Am. Chem. Soc.* **1996**, *118*, 43-50.

[38] Motesharei, K., Ghadiri, M. R. Diffucison limited size-selective ion sensing based on SAM supported peptides nanotubes. *J. Am. Chem. Soc.* **1997**, *119*, 11306-11312.

[39] van Nostrum, C. F. Self-assembled wires and channels. *Adv. Mater.* **1996**, *8*, 1027-1030.

[40] van Nostrum, C. F., Nolte, R. J. M. Functional supramolecular materials: self-assembly of phthalocyanines and porphyrazines. *Chem. Commun.* **1996**, 2385-2392.

[41] van Nostrum, C. F., Picken, S. J., Nolte, R. J. M. By self-organization to a multistranded molecular cable with a length of several micrometers. *Angew. Chem., Int. Ed Engl.* **1994**, *33*, 2173-2175.

Chapter 7

Cruciform Supramolecular Architectures: Today and Tomorrow

7.1 Abstract

This chapter recapitulates the objectives and accomplishments, of this research project. The final goal, a rapid optimization methodology for emissive and solution processable polymeric materials via a supramolecular strategy has not been achieved. The challenges and problems with this first generation system are stated and a number of synthetic ideas to overcome them are given. Each idea is critically reviewed and efficient synthetic schemes are provided.

7.2 Current Status of Cruciform Supramolecular Architectures

The objective of the project described in chapter 5 was to create a class of cruciform polymeric materials with tunable physical and photophysical properties that could be rapidly optimized into processable materials. A self-assembly strategy was chosen to accomplish this objective due to the fast and defect free polymerization growth inherent in SPs. The attractive and tunable optical properties of terminal bipyridyl cruciforms make them outstanding candidates for incorporation into supramolecular materials. They can be viewed as ditopic ligands for coordination to a suitable metal complex, such as a bimetallic pincer complex giving cruciform polymers. The supramolecular synthesis of cruciform materials heretofore has not been investigated. It was envisaged that a toolbox of functionally different cruciforms could be used to self-assemble and rapidly optimize a new class of luminescent polymers.

The initial goal of the project was to understand and control the coordination behavior of multiple cruciforms to multiple pincer complexes. The results showed that the physical properties of the polymers in solution were dependent on both the concentration of the solution and the K_a of the metal-ligand interaction.[1] The luminescent intensity of solution and thin film polymeric samples was shown to be inversely dependent on the K_a of the metal-ligand interaction.[1]

These preliminary results demonstrated that bipyridyl cruciform molecules are good ligands for coordination to bismetallated pincer complexes, giving coordination polymers with chain-like polymeric properties in solution. However, for this project to further advance several shortcomings of these materials need to be addressed.

The DP of even our best system, related to the K_a, is still too low to induce a sufficient chain entanglement required for a processable polymer. The only solvents suitable for our materials are DMF and DMSO, the competitive and polar nature of both lowers the K_a of our metal-ligand interaction. The high boiling points of the polar solvents also make them difficult to remove, further complicating polymeric solution processing. Antithetical to this is the decreased luminescence as the K_a increases, an inherent phenomenon that occurs after coordination to pyridyl crucifoms. Based on theses initial results the DP, processability, and luminescence cannot be simultaneously improved in these materials.

7.3 Future Work Towards Cruciform Supramolecular Architectures

The limited solubility of our CPs is most likely due to the rigidness of our final polymeric assemblies in conjuction with a high density of localized charges from the

continuous line of closely spaced metal centers. Synthetically this system may be improved by designing a new metallated pincer complex, which separates the charged metal centers.

Structures **1** and **2**, shown in Figure 7.1, are bimetallic pincer complexes with the metal centers separated by a long alkyl chain. These molecules should improve the flexibility of the polymeric system and also distance the metal center, having a synergistic effect on the solubility in apolar solvents. The spacer of **2** also has ethyl hexyl groups off a central aromatic core to reduce aggregation and improve solubility. Both molecules can be readily prepared from commercially available starting materials. Similar units to **1** have already been used by Craig in cross-linking and main-chain CP systems.[2]

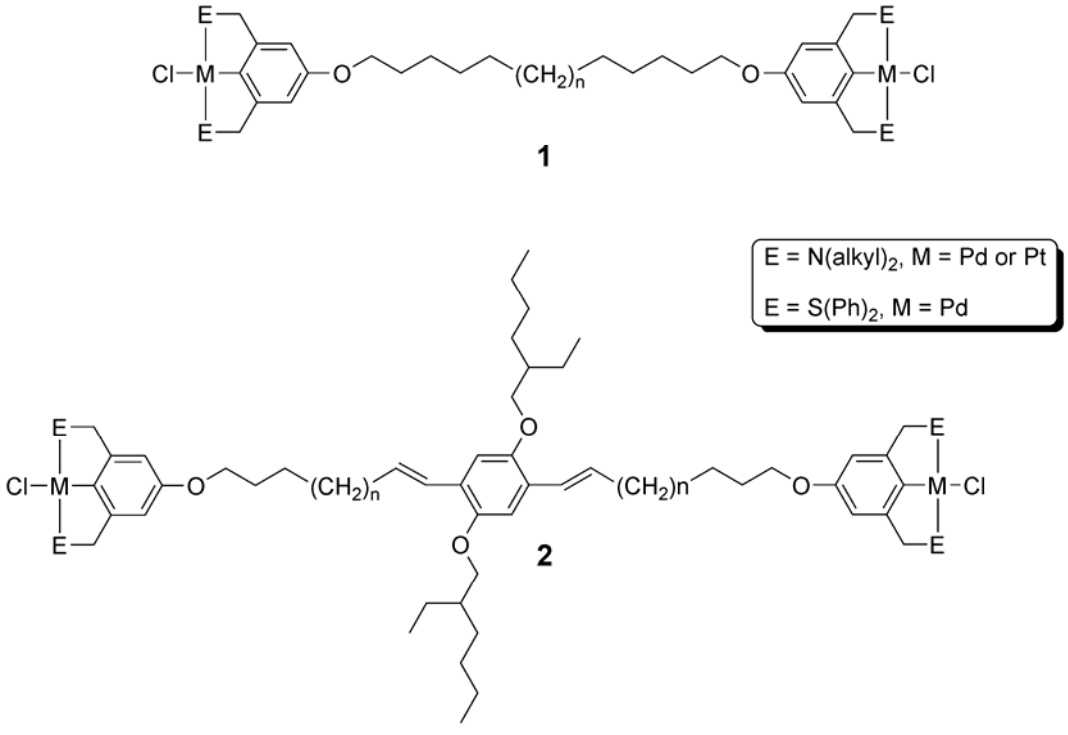

Figure 7.1 Bimetallic pincer complexes with long spacer groups separating the metal centers, and other branched alkyl chains to improve solubility.

Molecules **1** and **2** may improve solubility, but they would not expected to improve or even retain the fluorescence post coordination any more so than the original polymers. We have previously shown that during coordination or protonation, the accumulation of positive charge on the axial pyridyl nitrogens, the LUMO arms, leads to a decrease in fluorescence intensity.[3, 4] To overcome this obstacle I have propose an alternate cruciform supramolecular sython, designed to coordinate to the metallated pincer complex via a phosphine ligand instead of a pyridyl ligand. In a previous report we have shown that metal-coordination along the HOMO arms increases the fluorescence intensity.[4] The HOMO should lie along the diphosphino axis of cruciform **6**, shown in Scheme 7.1, based on the electron donation character of the phosphino groups. Starting material **4** can be synthesized following literature procedures,[5] this synthetic route is the same as previous cruciform syntheses.[6]

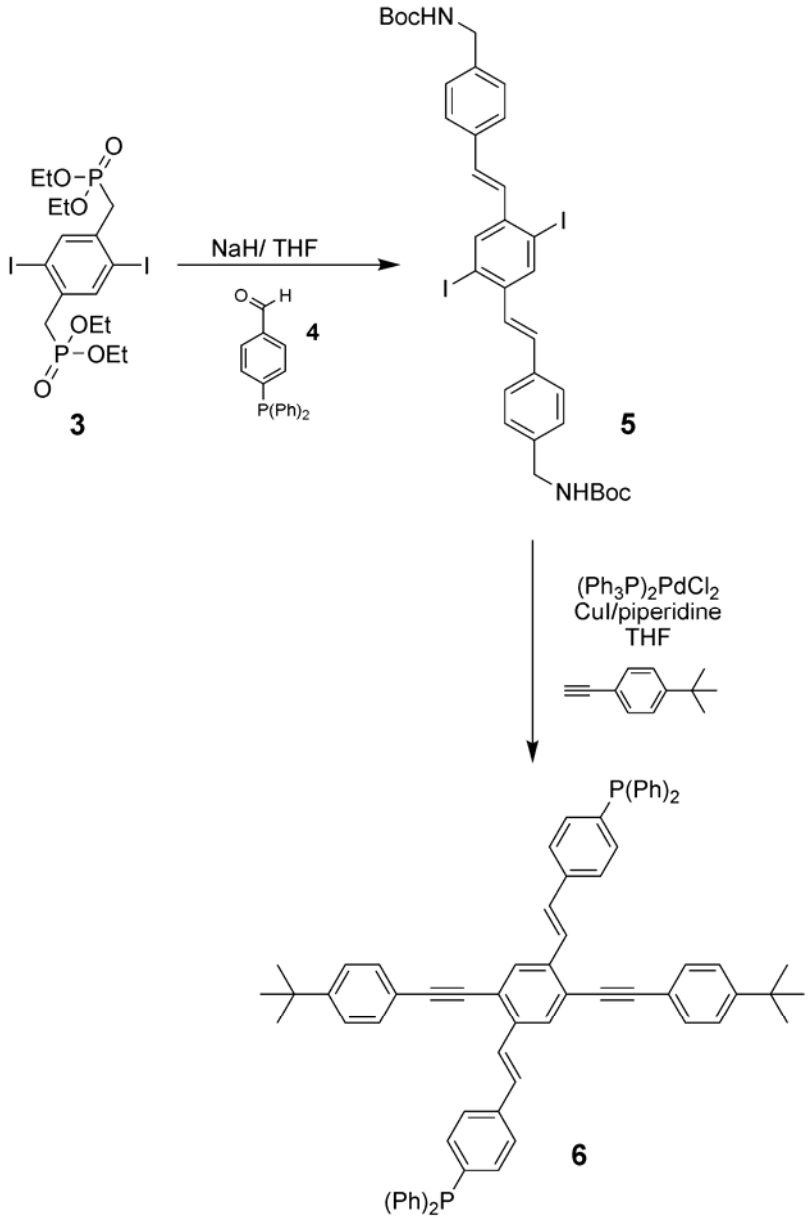

Scheme 7.1 Synthetic route to diphosphino cruciform **6**.

Based on the prior results[4] and empirical observations, cruciform **6** if coordinated to bimetallic pincer complexes **1** or **2** should have improved fluorescence and solubility. Additionally, phosphino ligands have a higher K_a to metallated pincer complexes than

pyridyl ligands.[3, 7] Therefore, the coordination of cruciform **6** through either **1** or **2** is expected to have improved solubility, fluorescence and solution processability.

7.3.1 Cruciform-Pincer Hybrid Complex

A more radical and elaborate cruciform design is a cruciform-pincer hybrid complex, such as **10** shown in Scheme 7.2. Starting material **8**[8] can be synthesized following literature procedures, the remaining steps adhere closely to the standard cruciform synthesis.[6] Metallated pincer complexes are stable under a variety of harsh reaction conditions,[8-10] but their stability under Sonogashira coupling conditions is unknown. Therefore, metallation of the pincer ligand will be carried out after coupling to the cruciform skeleton for the system below.

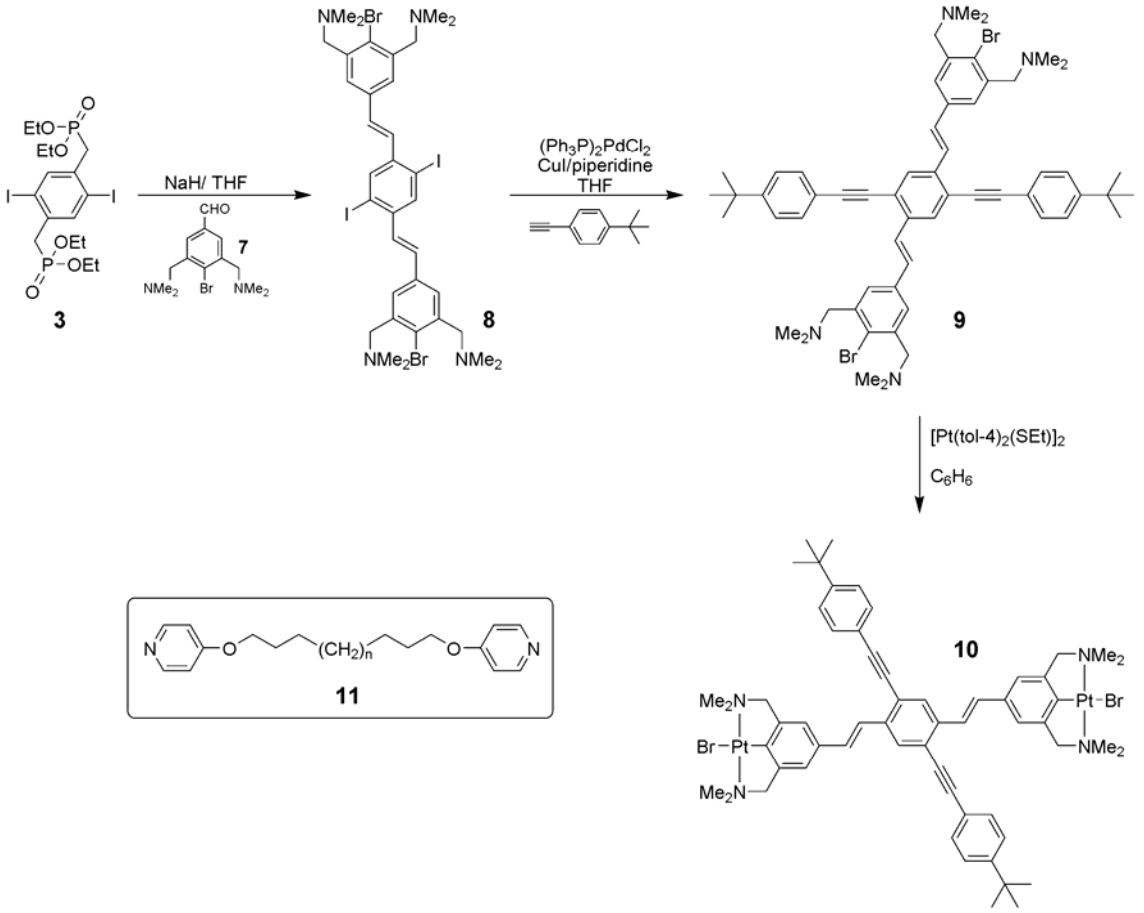

Scheme 7.2 Synthetic route to Pt-pincer cruciform **10**. Ditopic **11** is a proposed ligand to coordinate to **10** giving a novel CP.

By coordinating cruciform **10** to ditopic **11**, or a related molecule, a flexible CP having a reversed coordination can be self-assembled. Owing to the broad molecular similarities, this system is expected to have solubility traits similar to CPs coordinated with spaced pincer complexes **1** or **2**. Scheme 7.2 shows platination of a NCN ligand, this alternatively could also be palladated. Additionally an SCS palladated version of this cruciform could also be designed. I am quite curious to know the luminescent behavior, if any, of this system. It is an attractive and interesting molecule that has no precedence in the literature, and it remains to be seen if this molecule can address our solubility, K_a and luminescent concerns.

7.3.2 Self-associating UPy-Cruciforms

A final modification to the cruciform complex avoids the use of expensive precious metals and may also address the solubility and diminished fluorescence problems of the original system. This systems uses quadruple H-bonded arrays[11, 12] to get high DPs, H-bonded cruciform synthon **17** is shown in Scheme 7.3. Starting materials **12**[13] and **16**[11] can be synthesized following literature procedures.

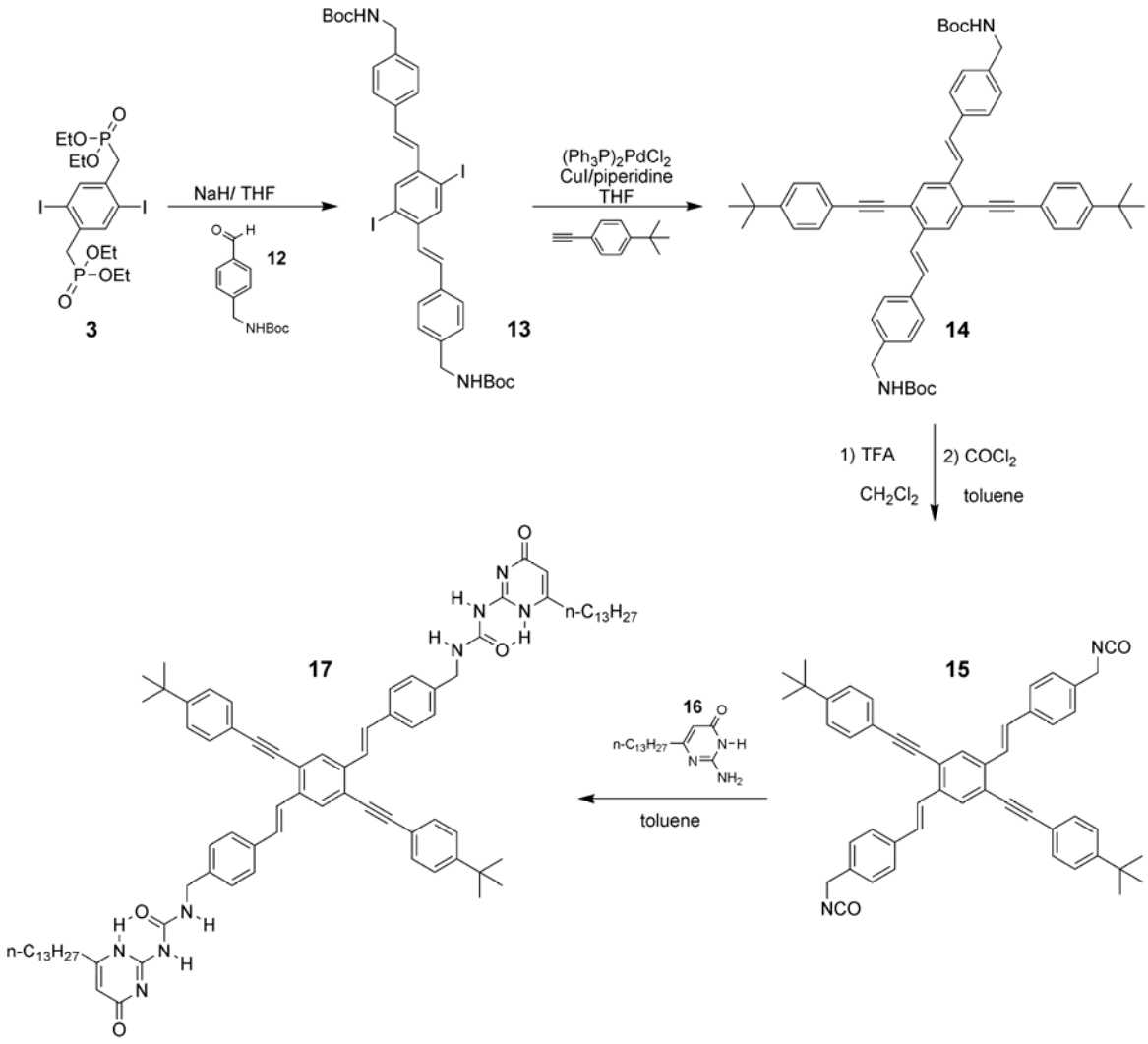

Scheme 7.3 Synthetic route of UPy-cruciform that can form H-bonded SPs.

All components of UPy-cruciform **17** should be soluble in apolar organic solvents, it is expected that **17** would be readily soluble in similar media and should self-associate, dimerizing with a $K_a > 10^8$ M^{-1}.[12]. This strong association would ensure very high molecular weight SPs in dilute solutions. Additionally the UPy H-bonding system is not in conjugation with the cruciform and therefore should not interfere with its fluorescence. If necessary, the UPy moiety could be attached with a longer spacer between the cruciform. Solubility should improve over the original system due to greater flexibility, more alkyl tails, and an overall neutral system after complexation.

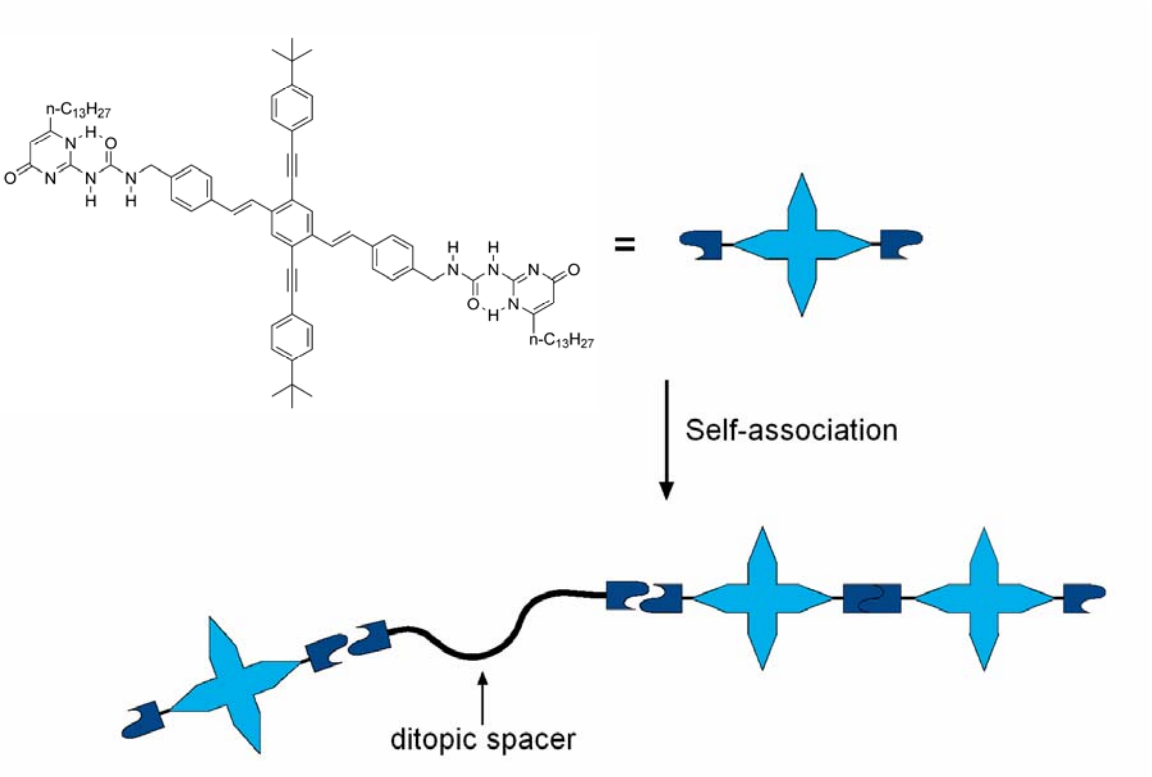

Figure 7.2 Self-association of **17** and supramolecular dilution with a ditopic spacer.

Finally, if this H-bonded system has the cruciforms in to close a proximity, then the system could be supramolecularly diluted by adding a ditopic H-bonded spacer, as shown in Figure 7.2.

Overall to achieve a readily solution processable and fluorescent system, the UPy-cruciform system is based on a large volume of published precedence[11, 12, 14-23] and is synthetically and economically the most viable. However, the pincer complex-cruciform hybrid is the most unique of the proposed structures and has the most mystery surrounding its potential properties and applications.

7.4 Conclusion

To conclude, the accumulation of data and results for chapter 5 was a grueling challenge. Out of respect for those efforts, I hope that all of these novel ideas will be thoroughly investigated by a group of eager and bright young minds.

7.5 References

[1] Gerhardt, W. W., Zucchero, A. J., South, C. R., Bunz, U. H. F., Weck, M. Controlling Polymer Properties through Dynamic Metal-Ligand Interactions: Supramolecular Cruciforms Made Easy. *Chem. Eur. J.* **2007**, in press.

[2] Yount, W. C., Juwarker, H., Craig, S. L. Orthogonal Control of Dissociation Dynamics Relative to Thermodynamics in a Main-Chain Reversible Polymer. *J. Am. Chem. Soc.* **2003**, *125*, 15302-15303.

[3] Gerhardt, W. W., Zucchero, A. J., Wilson, J. N., South, C. R., Bunz, U. H. F., Weck, M. Supramolecular cruciforms. *Chem. Commun.* **2006**, 2141-2143.

[4] Zucchero, A. J., Wilson, J. N., Bunz, U. H. F. Cruciforms as Functional Fluorophores: Response to Protons and Selected Metal Ions. *J. Am. Chem. Soc.* **2006**, *128*, 11872-11881.

[5] Wang, Y., Lai, C. W., Kwong, F. Y., Jia, W., Chan, K. S. Synthesis of aryl phosphines via phosphination with triphenylphosphine by supported palladium catalysts. *Tetrahedron* **2004**, *60*, 9433-9439.

[6] Wilson, J. N., Josowicz, M., Wang, Y., Bunz, U. H. F. Cruciform π-systems: hybrid phenylene-ethynylene/phenylene-vinylene oligomers. *Chem. Commun.* **2003**, 2962-2963.

[7] van Manen, H.-J., Nakashima, K., Shinkai, S., Kooijman, H., Spek, A. L., van Veggel, F. C. J. M., Reinhoudt, D. N. Coordination chemistry of SCS PdII pincer systems. *Eur. J. Inorg. Chem.* **2000**, 2533-2540.

[8] Albrecht, M., Rodríguez, G., Schoenmaker, J., van Koten, G. New Peptide Labels Containing Covalently Bonded Platinum(II) Centers as Diagnostic Biomarkers and Biosensors. *Org. Lett.* **2000**, *2*, 3461-3464.

[9] Albrecht, M., van Koten, G. Platinum group organometallics based on "pincer" complexes: sensors, switches, and catalysts. *Angew. Chem. Int. Ed.* **2001**, *40*, 3750-3781

[10] Guillena, G., Kruithof, C. A., Casado, M. A., Egmond, M. R., van Koten, G. The Suzuki cross-coupling reaction: a powerful tool for the attachment of organometallic 'NCN'-pincer units to biological scaffolds. *J. Organomet. Chem.* **2002**, *668*, 3-7.

[11] Sijbesma, R. P., Beijer, F. H., Brunsveld, L., Folmer, B. J. B., Ky Hirschberg, J. H. K., Lange, R. F. M., Lowe, J. K. L., Meijer, E. W. Reversible polymers formed from self-complementary monomers using quadruple hydrogen bonding. *Science* **1997**, *278*, 1601-1604.

[12] Söntjens, S. H. M., Sijbesma, R. P., van Genderen, M. H. P., Meijer, E. W. Stability and lifetime of quadruply hydrogen bonded 2-ureido-4[1H]-pyrimidinone dimers. *J. Am. Chem. Soc.* **2000**, *122*, 7487-7493.

[13] Far, A. R., Cho, Y. L., Rang, A., Rudkevich, D. M., Rebek, J., Jr. Polymer-bound self-folding cavitands. *Tetrahedron* **2002**, *58*, 741-755.

[14] Scherman, O. A., Ligthart, G. B. W. L., Sijbesma, R. P., Meijer, E. W. A selectivity-driven supramolecular polymerization of an AB monomer. *Angew. Chem. Int. Ed.* **2006**, *45*, 2072-2076.

[15] Dankers, P. Y. W., Harmsen, M. C., Brouwer, L. A., Van Luyn, M. J. A., Meijer, E. W. A modular and supramolecular approach to bioactive scaffolds for tissue engineering. *Nature Mater.* **2005**, *4*, 568-574.

[16] Chang, M. H., Hoeben, F. J. M., Jonkheijm, P., Schenning, A. P. H. J., Meijer, E. W., Silva, C., Herz, L. M. Influence of mesoscopic ordering on the photoexcitation transfer dynamics in supramolecular assemblies of oligo-p-phenylenevinylene. *Chem. Phys. Lett.* **2006**, *418*, 196-201.

[17] Brunsveld, L., Folmer, B. J. B., Meijer, E. W., Sijbesma, R. P. Supramolecular Polymers. *Chem. Rev.* **2001**, *101*, 4071-4097.

[18] Schenning, A. P. H. J., Meijer, E. W. Supramolecular electronics; nanowires from self-assembled p-conjugated systems. *Chem. Commun.* **2005**, 3245-3258.

[19] Hoeben, F. J. M., Jonkheijm, P., Meijer, E. W., Schenning, A. P. H. J. About Supramolecular Assemblies of p-Conjugated Systems. *Chem. Rev.* **2005**, *105*, 1491-1546.

[20] Bosman, A. W., Sijbesma, R. P., Meijer, E. W. Supramolecular polymers at work. *Mater. Today* **2004**, *7*, 34-39.

[21] El-Ghayoury, A., Schenning, A. P. H. J., Meijer, E. W. Synthesis of π-conjugated oligomer that can form metallo polymers. *J. Poly. Sci. Part A.: Polym. Chem.* **2002**, *40*, 4020-4023.

[22] Gohy, J.-F., Lohmeijer, B. G. G., Schubert, U. S. From Supramolecular Block Copolymers to Advanced Nano-Objects. *Chem. Eur. J.* **2003**, *9*, 3472-3479.

[23] Gohy, J.-F., Lohmeijer, B. G. G., Varshney, S. K., Decamps, B., Leroy, E., Boileau, S., Schubert, U. S. Stimuli-Responsive Aqueous Micelles from an ABC Metallo-Supramolecular Triblock Copolymer. *Macromolecules* **2002**, *35*, 9748-9755.

APPENDIX A

X-ray Structural Data for Compound **2** of Chapter 3

Table A1 Crystal data and structure refinement for Compound **2** of Chapter 3.

Identification code	wg4ala_0m	
Empirical formula	C21 H20 N4 O6	
Formula weight	424.41	
Temperature	173(2) K	
Wavelength	1.54178 Å	
Crystal system	Monoclinic	
Space group	P2(1)	
Unit cell dimensions	a = 13.2293(4) Å	α= 90°.
	b = 4.82920(10) Å	β= 100.164(1)°.
	c = 15.8456(4) Å	γ = 90°.
Volume	996.44(4) $Å^3$	
Z	2	
Density (calculated)	1.415 Mg/m^3	
Absorption coefficient	0.887 mm^{-1}	
F(000)	444	
Crystal size	0.60 x 0.09 x 0.06 mm^3	
Theta range for data collection	7.82 to 61.32°.	
Index ranges	-12<=h<=14, -5<=k<=4, -17<=l<=18	
Reflections collected	3859	
Independent reflections	2212 [R(int) = 0.0143]	
Completeness to theta = 61.32°	87.7 %	
Absorption correction	Semi-empirical from equivalents	
Max. and min. transmission	0.9487 and 0.6183	
Refinement method	Full-matrix least-squares on F^2	
Data / restraints / parameters	2212 / 1 / 289	
Goodness-of-fit on F^2	1.049	
Final R indices [I>2sigma(I)]	R1 = 0.0305, wR2 = 0.0702	
R indices (all data)	R1 = 0.0327, wR2 = 0.0714	
Absolute structure parameter	0.1(2)	
Largest diff. peak and hole	0.132 and -0.176 $e.Å^{-3}$	

Table A.2 Atomic coordinates (x 10^4) and equivalent isotropic displacement parameters ($Å^2$x 10^3) for Compound **2** of Chapter 3. U(eq) is defined as one third of the trace of the orthogonalized U^{ij} tensor.

	x	y	z	U(eq)
C(1)	1148(2)	10664(5)	3815(1)	25(1)
C(2)	285(2)	12591(5)	3515(1)	25(1)
C(3)	-241(2)	14293(5)	3976(1)	31(1)
C(4)	-1033(2)	15885(6)	3520(2)	36(1)
C(5)	-1263(2)	15757(6)	2634(2)	37(1)
C(6)	-729(2)	14010(6)	2172(1)	34(1)
C(7)	46(2)	12422(5)	2627(1)	26(1)
C(8)	751(2)	10363(5)	2338(1)	28(1)
C(9)	2228(2)	7526(5)	3075(1)	28(1)
C(10)	3084(2)	8886(5)	2689(1)	24(1)
C(11)	4532(2)	7954(5)	1954(1)	23(1)
C(12)	5577(2)	6791(5)	2373(1)	26(1)
C(13)	5947(2)	7852(5)	3269(1)	27(1)
C(14)	6645(2)	9999(5)	3432(1)	32(1)
C(15)	6962(2)	10916(6)	4266(2)	41(1)
C(16)	5973(2)	7718(6)	4780(2)	43(1)
C(17)	5606(2)	6697(5)	3969(1)	33(1)
C(18)	4239(2)	6838(5)	1047(1)	23(1)
C(19)	3518(2)	7649(5)	-431(1)	30(1)
C(20)	2650(2)	5614(5)	-455(1)	29(1)
C(21)	1233(2)	4293(7)	177(2)	49(1)
N(1)	1382(2)	9411(4)	3082(1)	26(1)
N(2)	3717(2)	7109(4)	2409(1)	24(1)
N(3)	6637(2)	9811(5)	4941(1)	42(1)
N(4)	3923(2)	8642(4)	422(1)	26(1)
O(1)	1577(1)	10214(4)	4540(1)	35(1)
O(2)	804(1)	9579(4)	1622(1)	40(1)
O(3)	3165(2)	11412(3)	2661(1)	40(1)
O(4)	4253(1)	4312(3)	911(1)	28(1)
O(6)	2508(2)	3699(4)	-951(1)	41(1)

Table A.2 (continued)

O(7)	2055(1)	6242(4)	105(1)	35(1)

Table A.3 Bond lengths [Å] and angles [°] for Compound **2** of Chapter 3.

C(1)-O(1)	1.208(2)	C(13)-C(17)	1.385(3)
C(1)-N(1)	1.393(3)	C(14)-C(15)	1.387(3)
C(1)-C(2)	1.484(3)	C(14)-H(14)	0.9500
C(2)-C(3)	1.369(3)	C(15)-N(3)	1.333(4)
C(2)-C(7)	1.389(3)	C(15)-H(15)	0.9500
C(3)-C(4)	1.394(3)	C(16)-N(3)	1.334(4)
C(3)-H(3)	0.9500	C(16)-C(17)	1.382(3)
C(4)-C(5)	1.384(3)	C(16)-H(16)	0.9500
C(4)-H(4)	0.9500	C(17)-H(17)	0.9500
C(5)-C(6)	1.390(4)	C(18)-O(4)	1.239(3)
C(5)-H(5)	0.9500	C(18)-N(4)	1.330(3)
C(6)-C(7)	1.378(3)	C(19)-N(4)	1.445(3)
C(6)-H(6)	0.9500	C(19)-C(20)	1.506(4)
C(7)-C(8)	1.489(3)	C(19)-H(19A)	0.9900
C(8)-O(2)	1.210(3)	C(19)-H(19B)	0.9900
C(8)-N(1)	1.396(3)	C(20)-O(6)	1.207(3)
C(9)-N(1)	1.445(3)	C(20)-O(7)	1.322(3)
C(9)-C(10)	1.528(3)	C(21)-O(7)	1.457(3)
C(9)-H(9A)	0.9900	C(21)-H(21A)	0.9800
C(9)-H(9B)	0.9900	C(21)-H(21B)	0.9800
C(10)-O(3)	1.226(3)	C(21)-H(21C)	0.9800
C(10)-N(2)	1.329(3)	N(2)-H(2N)	0.79(3)
C(11)-N(2)	1.457(3)	N(4)-H(4N)	0.80(3)
C(11)-C(18)	1.520(3)		
C(11)-C(12)	1.531(3)	O(1)-C(1)-N(1)	125.4(2)
C(11)-H(11)	1.0000	O(1)-C(1)-C(2)	128.6(2)
C(12)-C(13)	1.508(3)	N(1)-C(1)-C(2)	106.03(17)
C(12)-H(12A)	0.9900	C(3)-C(2)-C(7)	122.0(2)
C(12)-H(12B)	0.9900	C(3)-C(2)-C(1)	129.78(19)
C(13)-C(14)	1.382(4)	C(7)-C(2)-C(1)	108.2(2)

Table A.3 (continued)

C(2)-C(3)-C(4)	117.4(2)	C(11)-C(12)-H(12A)	108.8
C(2)-C(3)-H(3)	121.3	C(13)-C(12)-H(12B)	108.8
C(4)-C(3)-H(3)	121.3	C(11)-C(12)-H(12B)	108.8
C(5)-C(4)-C(3)	120.8(2)	H(12A)-C(12)-H(12B)	107.7
C(5)-C(4)-H(4)	119.6	C(14)-C(13)-C(17)	117.0(2)
C(3)-C(4)-H(4)	119.6	C(14)-C(13)-C(12)	121.7(2)
C(4)-C(5)-C(6)	121.3(2)	C(17)-C(13)-C(12)	121.3(2)
C(4)-C(5)-H(5)	119.3	C(13)-C(14)-C(15)	119.8(3)
C(6)-C(5)-H(5)	119.3	C(13)-C(14)-H(14)	120.1
C(7)-C(6)-C(5)	117.6(2)	C(15)-C(14)-H(14)	120.1
C(7)-C(6)-H(6)	121.2	N(3)-C(15)-C(14)	123.5(3)
C(5)-C(6)-H(6)	121.2	N(3)-C(15)-H(15)	118.3
C(6)-C(7)-C(2)	120.8(2)	C(14)-C(15)-H(15)	118.3
C(6)-C(7)-C(8)	131.2(2)	N(3)-C(16)-C(17)	124.0(3)
C(2)-C(7)-C(8)	107.9(2)	N(3)-C(16)-H(16)	118.0
O(2)-C(8)-N(1)	124.3(2)	C(17)-C(16)-H(16)	118.0
O(2)-C(8)-C(7)	129.8(2)	C(16)-C(17)-C(13)	119.4(3)
N(1)-C(8)-C(7)	105.86(17)	C(16)-C(17)-H(17)	120.3
N(1)-C(9)-C(10)	111.23(18)	C(13)-C(17)-H(17)	120.3
N(1)-C(9)-H(9A)	109.4	O(4)-C(18)-N(4)	121.9(2)
C(10)-C(9)-H(9A)	109.4	O(4)-C(18)-C(11)	120.28(19)
N(1)-C(9)-H(9B)	109.4	N(4)-C(18)-C(11)	117.8(2)
C(10)-C(9)-H(9B)	109.4	N(4)-C(19)-C(20)	113.30(19)
H(9A)-C(9)-H(9B)	108.0	N(4)-C(19)-H(19A)	108.9
O(3)-C(10)-N(2)	124.5(2)	C(20)-C(19)-H(19A)	108.9
O(3)-C(10)-C(9)	121.2(2)	N(4)-C(19)-H(19B)	108.9
N(2)-C(10)-C(9)	114.27(19)	C(20)-C(19)-H(19B)	108.9
N(2)-C(11)-C(18)	106.28(18)	H(19A)-C(19)-H(19B)	107.7
N(2)-C(11)-C(12)	111.96(17)	O(6)-C(20)-O(7)	124.8(3)
C(18)-C(11)-C(12)	109.85(19)	O(6)-C(20)-C(19)	123.2(2)
N(2)-C(11)-H(11)	109.6	O(7)-C(20)-C(19)	112.0(2)
C(18)-C(11)-H(11)	109.6	O(7)-C(21)-H(21A)	109.5
C(12)-C(11)-H(11)	109.6	O(7)-C(21)-H(21B)	109.5
C(13)-C(12)-C(11)	113.64(19)	H(21A)-C(21)-H(21B)	109.5
C(13)-C(12)-H(12A)	108.8	O(7)-C(21)-H(21C)	109.5

Table A.3 (continued)

H(21A)-C(21)-H(21C)	109.5
H(21B)-C(21)-H(21C)	109.5
C(1)-N(1)-C(8)	111.95(19)
C(1)-N(1)-C(9)	124.50(18)
C(8)-N(1)-C(9)	123.36(18)
C(10)-N(2)-C(11)	123.3(2)
C(10)-N(2)-H(2N)	120(2)
C(11)-N(2)-H(2N)	116(2)
C(15)-N(3)-C(16)	116.4(2)
C(18)-N(4)-C(19)	119.7(2)
C(18)-N(4)-H(4N)	119.6(17)
C(19)-N(4)-H(4N)	120.7(17)
C(20)-O(7)-C(21)	116.4(2)

Symmetry transformations used to generate equivalent atoms:

Table A. 4 Anisotropic displacement parameters ($Å^2 x\ 10^3$) for Compound **2** of Chapter 3. The anisotropic displacement factor exponent takes the form: $-2\pi^2[\ h^2 a^{*2} U^{11} + ... + 2\ h\ k\ a^*\ b^*\ U^{12}\ ]$

	U^{11}	U^{22}	U^{33}	U^{23}	U^{13}	U^{12}
C(1)	22(2)	27(1)	28(1)	4(1)	8(1)	1(1)
C(2)	22(2)	25(1)	27(1)	4(1)	6(1)	-1(1)
C(3)	34(2)	32(1)	29(1)	4(1)	9(1)	3(1)
C(4)	31(2)	35(2)	43(1)	6(1)	12(1)	11(1)
C(5)	29(2)	37(2)	43(1)	10(1)	3(1)	7(1)
C(6)	30(2)	40(2)	30(1)	7(1)	2(1)	-1(1)
C(7)	25(2)	25(1)	28(1)	4(1)	5(1)	-3(1)
C(8)	30(2)	30(1)	26(1)	2(1)	6(1)	-4(1)
C(9)	28(2)	23(1)	35(1)	2(1)	15(1)	5(1)
C(10)	29(2)	20(1)	26(1)	-2(1)	6(1)	2(1)
C(11)	23(2)	19(1)	29(1)	-2(1)	6(1)	-2(1)
C(12)	23(2)	26(1)	31(1)	-6(1)	7(1)	-1(1)
C(13)	21(2)	26(1)	34(1)	-4(1)	3(1)	5(1)
C(14)	27(2)	30(1)	37(1)	-3(1)	1(1)	5(1)
C(15)	35(2)	35(2)	50(2)	-10(1)	-6(1)	0(1)
C(16)	53(2)	39(2)	35(1)	-3(1)	9(1)	4(2)
C(17)	34(2)	32(1)	34(1)	-6(1)	6(1)	-1(1)
C(18)	18(2)	24(1)	29(1)	-2(1)	9(1)	-2(1)
C(19)	36(2)	31(1)	24(1)	2(1)	6(1)	1(1)
C(20)	32(2)	30(1)	24(1)	2(1)	0(1)	6(1)
C(21)	37(2)	58(2)	54(2)	-3(2)	9(1)	-16(2)
N(1)	26(1)	26(1)	27(1)	3(1)	9(1)	4(1)
N(2)	28(1)	15(1)	29(1)	-2(1)	9(1)	-1(1)
N(3)	46(2)	41(1)	36(1)	-11(1)	-1(1)	10(1)
N(4)	31(1)	18(1)	30(1)	-4(1)	6(1)	-2(1)
O(1)	34(1)	45(1)	26(1)	6(1)	5(1)	11(1)
O(2)	47(1)	46(1)	29(1)	-4(1)	11(1)	3(1)
O(3)	44(1)	19(1)	64(1)	0(1)	31(1)	1(1)
O(4)	34(1)	20(1)	31(1)	-4(1)	5(1)	1(1)
O(6)	45(1)	39(1)	37(1)	-14(1)	2(1)	-4(1)

Table A.4 (continued)

O(7)	29(1)	38(1)	40(1)	-5(1)	9(1)	-6(1)

Table A. 5 Hydrogen coordinates (x 10^4) and isotropic displacement parameters ($Å^2$x 10^3) for Compound **2** of Chapter 3.

	x	y	z	U(eq)
H(3)	-74	14384	4584	37
H(4)	-1419	17073	3821	43
H(5)	-1798	16887	2336	44
H(6)	-892	13914	1565	40
H(9A)	1979	5860	2737	33
H(9B)	2503	6929	3669	33
H(11)	4567	10022	1938	28
H(12A)	5531	4747	2391	32
H(12B)	6091	7275	2012	32
H(14)	6907	10844	2973	38
H(15)	7436	12410	4361	49
H(16)	5738	6877	5252	51
H(17)	5125	5218	3892	40
H(19A)	4078	6753	-671	36
H(19B)	3271	9249	-801	36
H(21A)	738	4270	-362	74
H(21B)	887	4861	646	74
H(21C)	1523	2436	293	74
H(4N)	3940(20)	10270(60)	527(14)	27(7)
H(2N)	3630(20)	5510(70)	2438(17)	45(9)

Table A. 6 Torsion angles [°] for Compound **2** of Chapter 3.

O(1)-C(1)-C(2)-C(3)	-0.9(5)
N(1)-C(1)-C(2)-C(3)	179.0(2)
O(1)-C(1)-C(2)-C(7)	179.9(2)
N(1)-C(1)-C(2)-C(7)	-0.3(3)
C(7)-C(2)-C(3)-C(4)	-0.4(4)
C(1)-C(2)-C(3)-C(4)	-179.5(2)
C(2)-C(3)-C(4)-C(5)	-0.7(4)
C(3)-C(4)-C(5)-C(6)	1.2(4)
C(4)-C(5)-C(6)-C(7)	-0.5(4)
C(5)-C(6)-C(7)-C(2)	-0.5(4)
C(5)-C(6)-C(7)-C(8)	179.6(2)
C(3)-C(2)-C(7)-C(6)	1.0(4)
C(1)-C(2)-C(7)-C(6)	-179.7(2)
C(3)-C(2)-C(7)-C(8)	-179.1(2)
C(1)-C(2)-C(7)-C(8)	0.2(3)
C(6)-C(7)-C(8)-O(2)	-0.5(5)
C(2)-C(7)-C(8)-O(2)	179.6(3)
C(6)-C(7)-C(8)-N(1)	179.8(3)
C(2)-C(7)-C(8)-N(1)	-0.1(3)
N(1)-C(9)-C(10)-O(3)	21.5(3)
N(1)-C(9)-C(10)-N(2)	-159.44(18)
N(2)-C(11)-C(12)-C(13)	-63.8(2)
C(18)-C(11)-C(12)-C(13)	178.39(19)
C(11)-C(12)-C(13)-C(14)	-98.7(3)
C(11)-C(12)-C(13)-C(17)	81.9(3)
C(17)-C(13)-C(14)-C(15)	-0.7(4)
C(12)-C(13)-C(14)-C(15)	179.8(2)
C(13)-C(14)-C(15)-N(3)	0.8(4)
N(3)-C(16)-C(17)-C(13)	1.0(4)
C(14)-C(13)-C(17)-C(16)	-0.1(4)
C(12)-C(13)-C(17)-C(16)	179.4(2)
N(2)-C(11)-C(18)-O(4)	-69.1(3)
C(12)-C(11)-C(18)-O(4)	52.2(3)
N(2)-C(11)-C(18)-N(4)	107.7(2)

Table A.6 (continued)

C(12)-C(11)-C(18)-N(4)	-130.9(2)
N(4)-C(19)-C(20)-O(6)	-145.9(2)
N(4)-C(19)-C(20)-O(7)	36.3(3)
O(1)-C(1)-N(1)-C(8)	-179.9(2)
C(2)-C(1)-N(1)-C(8)	0.2(3)
O(1)-C(1)-N(1)-C(9)	-4.8(4)
C(2)-C(1)-N(1)-C(9)	175.3(2)
O(2)-C(8)-N(1)-C(1)	-179.8(2)
C(7)-C(8)-N(1)-C(1)	-0.1(3)
O(2)-C(8)-N(1)-C(9)	5.1(4)
C(7)-C(8)-N(1)-C(9)	-175.2(2)
C(10)-C(9)-N(1)-C(1)	-107.6(2)
C(10)-C(9)-N(1)-C(8)	67.0(3)
O(3)-C(10)-N(2)-C(11)	-6.3(3)
C(9)-C(10)-N(2)-C(11)	174.70(18)
C(18)-C(11)-N(2)-C(10)	-113.5(2)
C(12)-C(11)-N(2)-C(10)	126.6(2)
C(14)-C(15)-N(3)-C(16)	0.0(4)
C(17)-C(16)-N(3)-C(15)	-0.9(4)
O(4)-C(18)-N(4)-C(19)	4.4(4)
C(11)-C(18)-N(4)-C(19)	-172.4(2)
C(20)-C(19)-N(4)-C(18)	54.2(3)
O(6)-C(20)-O(7)-C(21)	6.5(3)
C(19)-C(20)-O(7)-C(21)	-175.8(2)

Symmetry transformations used to generate equivalent atoms:

Table A.7 Hydrogen bonds for Compound **2** of Chapter 3 [Å and °].

D-H...A	d(D-H)	d(H...A)	d(D...A)	<(DHA)
N(4)-H(4N)...O(4)#1	0.80(3)	2.07(3)	2.858(3)	169(3)
N(2)-H(2N)...O(3)#2	0.79(3)	2.12(3)	2.892(3)	169(3)

Symmetry transformations used to generate equivalent atoms: #1 x, y+1, z #2 x, y-1

APPENDIX B

X-ray Structural Data for Compound **3** of Chapter 3

Table B.1 Crystal data and structure refinement for Compound **3** of Chapter 3.

Identification code	wg3gly	
Empirical formula	C20 H18 N4 O6	
Formula weight	410.38	
Temperature	173(2) K	
Wavelength	1.54178 Å	
Crystal system	Orthorhombic	
Space group	P2(1)2(1)2(1)	
Unit cell dimensions	a = 4.7602(3) Å	α= 90°.
	b = 13.4131(9) Å	β= 90°.
	c = 29.517(3) Å	γ = 90°.
Volume	1884.6(2) $Å^3$	
Z	4	
Density (calculated)	1.446 Mg/m^3	
Absorption coefficient	0.918 mm^{-1}	
F(000)	856	
Crystal size	0.40 x 0.08 x 0.04 mm^3	
Theta range for data collection	7.25 to 45.89°.	
Index ranges	-4<=h<=4, -12<=k<=11, -22<=l<=24	
Reflections collected	4179	
Independent reflections	1408 [R(int) = 0.0794]	
Completeness to theta = 45.89°	88.0 %	
Absorption correction	Semi-empirical from equivalents	
Max. and min. transmission	0.9642 and 0.7103	
Refinement method	Full-matrix least-squares on F^2	
Data / restraints / parameters	1408 / 0 / 272	
Goodness-of-fit on F^2	1.020	
Final R indices [I>2sigma(I)]	R1 = 0.0392, wR2 = 0.0620	
R indices (all data)	R1 = 0.0648, wR2 = 0.0666	
Absolute structure parameter	-0.1(5)	
Largest diff. peak and hole	0.122 and -0.195 $e.Å^{-3}$	

Table B.2 Atomic coordinates (x 10^4) and equivalent isotropic displacement parameters ($Å^2$x 10^3)
for Compound **3** of Chapter 3. U(eq) is defined as one third of the trace of the orthogonalized U^{ij} tensor.

	x	y	z	U(eq)
C(1)	4489(12)	6280(4)	1559(3)	31(2)
C(2)	6103(12)	7082(4)	1323(3)	26(2)
C(3)	8062(13)	7731(5)	1496(2)	42(2)
C(4)	9211(12)	8428(4)	1199(3)	48(2)
C(5)	8388(14)	8476(4)	752(3)	49(2)
C(6)	6389(13)	7816(5)	583(2)	39(2)
C(7)	5297(11)	7118(4)	876(3)	29(2)
C(8)	3133(12)	6338(4)	799(3)	30(2)
C(9)	990(10)	5010(3)	1283(2)	27(2)
C(10)	2583(12)	4037(4)	1210(2)	24(2)
C(11)	2104(10)	2222(4)	1183(2)	24(2)
C(12)	1863(12)	1654(4)	740(2)	24(2)
C(13)	20(13)	1907(4)	400(3)	37(2)
C(14)	1595(18)	601(5)	-40(3)	55(2)
C(15)	3434(14)	310(4)	282(3)	37(2)
C(16)	3600(11)	832(5)	668(2)	38(2)
C(17)	588(13)	1623(4)	1556(2)	22(1)
C(18)	1192(11)	536(4)	2208(2)	35(2)
C(19)	3037(14)	-361(5)	2254(3)	37(2)
C(20)	3992(13)	-1780(4)	2700(2)	65(2)
N(1)	2801(9)	5864(3)	1220(2)	23(1)
N(2)	923(8)	3230(3)	1182(1)	26(1)
N(3)	2268(9)	1172(3)	1850(2)	31(1)
O(1)	1875(8)	6118(3)	462(2)	44(1)
O(2)	4520(8)	6017(3)	1949(2)	45(1)
O(3)	5152(8)	4004(2)	1198(1)	31(1)
O(4)	-1974(7)	1581(2)	1565(1)	28(1)
O(5)	5044(10)	-539(3)	2026(2)	52(1)
O(6)	2206(7)	-922(3)	2606(1)	46(1)

Table B.2 (continued)

N(4)	-189(12)	1395(5)	2(2)	63(2)

Table B.3 Bond lengths [Å] and angles [°] for Compound **3** of Chapter 3.

C(1)-O(2)	1.203(6)	C(15)-H(15)	0.9500
C(1)-N(1)	1.400(7)	C(16)-H(16)	0.9500
C(1)-C(2)	1.494(7)	C(17)-O(4)	1.221(6)
C(2)-C(3)	1.375(7)	C(17)-N(3)	1.327(6)
C(2)-C(7)	1.376(6)	C(18)-N(3)	1.452(6)
C(3)-C(4)	1.394(7)	C(18)-C(19)	1.495(7)
C(3)-H(3)	0.9500	C(18)-H(18A)	0.9900
C(4)-C(5)	1.378(7)	C(18)-H(18B)	0.9900
C(4)-H(4)	0.9500	C(19)-O(5)	1.193(7)
C(5)-C(6)	1.392(7)	C(19)-O(6)	1.341(7)
C(5)-H(5)	0.9500	C(20)-O(6)	1.458(6)
C(6)-C(7)	1.376(7)	C(20)-H(20A)	0.9800
C(6)-H(6)	0.9500	C(20)-H(20B)	0.9800
C(7)-C(8)	1.485(7)	C(20)-H(20C)	0.9800
C(8)-O(1)	1.197(6)	N(2)-H(2N)	0.7847
C(8)-N(1)	1.405(7)	N(3)-H(3N)	0.7189
C(9)-N(1)	1.445(6)		
C(9)-C(10)	1.526(6)	O(2)-C(1)-N(1)	125.1(6)
C(9)-H(9A)	0.9900	O(2)-C(1)-C(2)	130.6(7)
C(9)-H(9B)	0.9900	N(1)-C(1)-C(2)	104.4(6)
C(10)-O(3)	1.224(6)	C(3)-C(2)-C(7)	121.5(6)
C(10)-N(2)	1.342(5)	C(3)-C(2)-C(1)	129.2(8)
C(11)-N(2)	1.465(5)	C(7)-C(2)-C(1)	109.3(6)
C(11)-C(12)	1.517(6)	C(2)-C(3)-C(4)	117.2(6)
C(11)-C(17)	1.541(7)	C(2)-C(3)-H(3)	121.4
C(11)-H(11)	1.0995	C(4)-C(3)-H(3)	121.4
C(12)-C(13)	1.376(7)	C(5)-C(4)-C(3)	121.5(6)
C(12)-C(16)	1.394(7)	C(5)-C(4)-H(4)	119.3
C(13)-N(4)	1.363(6)	C(3)-C(4)-H(4)	119.3
C(13)-H(13)	0.9500	C(4)-C(5)-C(6)	120.6(5)
C(14)-C(15)	1.350(8)	C(4)-C(5)-H(5)	119.7
C(14)-N(4)	1.368(7)	C(6)-C(5)-H(5)	119.7
C(14)-H(14)	0.9500	C(7)-C(6)-C(5)	117.7(6)
C(15)-C(16)	1.340(7)	C(7)-C(6)-H(6)	121.1

Table B.3 (continued)

C(5)-C(6)-H(6)	121.1	C(15)-C(16)-H(16)	119.7
C(6)-C(7)-C(2)	121.5(6)	C(12)-C(16)-H(16)	119.7
C(6)-C(7)-C(8)	130.2(8)	O(4)-C(17)-N(3)	124.4(5)
C(2)-C(7)-C(8)	108.3(6)	O(4)-C(17)-C(11)	120.5(5)
O(1)-C(8)-N(1)	124.5(7)	N(3)-C(17)-C(11)	115.0(5)
O(1)-C(8)-C(7)	130.4(8)	N(3)-C(18)-C(19)	109.4(5)
N(1)-C(8)-C(7)	105.2(6)	N(3)-C(18)-H(18A)	109.8
N(1)-C(9)-C(10)	111.3(4)	C(19)-C(18)-H(18A)	109.8
N(1)-C(9)-H(9A)	109.4	N(3)-C(18)-H(18B)	109.8
C(10)-C(9)-H(9A)	109.4	C(19)-C(18)-H(18B)	109.8
N(1)-C(9)-H(9B)	109.4	H(18A)-C(18)-H(18B)	108.2
C(10)-C(9)-H(9B)	109.4	O(5)-C(19)-O(6)	124.1(6)
H(9A)-C(9)-H(9B)	108.0	O(5)-C(19)-C(18)	125.5(7)
O(3)-C(10)-N(2)	123.9(5)	O(6)-C(19)-C(18)	110.4(6)
O(3)-C(10)-C(9)	122.1(5)	O(6)-C(20)-H(20A)	109.5
N(2)-C(10)-C(9)	114.0(5)	O(6)-C(20)-H(20B)	109.5
N(2)-C(11)-C(12)	115.7(5)	H(20A)-C(20)-H(20B)	109.5
N(2)-C(11)-C(17)	107.6(4)	O(6)-C(20)-H(20C)	109.5
C(12)-C(11)-C(17)	108.6(4)	H(20A)-C(20)-H(20C)	109.5
N(2)-C(11)-H(11)	107.3	H(20B)-C(20)-H(20C)	109.5
C(12)-C(11)-H(11)	107.9	C(1)-N(1)-C(8)	112.8(5)
C(17)-C(11)-H(11)	109.7	C(1)-N(1)-C(9)	124.4(5)
C(13)-C(12)-C(16)	117.5(5)	C(8)-N(1)-C(9)	122.7(6)
C(13)-C(12)-C(11)	123.6(6)	C(10)-N(2)-C(11)	121.2(4)
C(16)-C(12)-C(11)	118.9(6)	C(10)-N(2)-H(2N)	120.8
N(4)-C(13)-C(12)	123.4(6)	C(11)-N(2)-H(2N)	117.9
N(4)-C(13)-H(13)	118.3	C(17)-N(3)-C(18)	122.2(4)
C(12)-C(13)-H(13)	118.3	C(17)-N(3)-H(3N)	121.4
C(15)-C(14)-N(4)	124.3(6)	C(18)-N(3)-H(3N)	116.4
C(15)-C(14)-H(14)	117.9	C(19)-O(6)-C(20)	114.8(4)
N(4)-C(14)-H(14)	117.9	C(13)-N(4)-C(14)	115.2(6)
C(16)-C(15)-C(14)	119.1(6)		
C(16)-C(15)-H(15)	120.5	Symmetry transformations used to generate equivalent ato	
C(14)-C(15)-H(15)	120.5		
C(15)-C(16)-C(12)	120.5(6)		

Table B.4 Anisotropic displacement parameters ($Å^2 x\ 10^3$) for Compound **3** of Chapter 3. The anisotropic displacement factor exponent takes the form: $-2\pi^2[\ h^2\ a^{*2}U^{11} + ... + 2\ h\ k\ a^*\ b^*\ U^{12}\ ]$

	U^{11}	U^{22}	U^{33}	U^{23}	U^{13}	U^{12}
C(1)	33(4)	25(5)	36(6)	-2(5)	-1(5)	7(4)
C(2)	23(4)	13(4)	43(7)	-4(4)	1(4)	-3(4)
C(3)	45(4)	31(4)	49(6)	-6(4)	7(4)	3(4)
C(4)	34(4)	30(5)	80(7)	-9(5)	-3(5)	-6(4)
C(5)	43(5)	27(5)	77(8)	10(4)	15(4)	-9(4)
C(6)	46(4)	43(5)	28(6)	10(4)	9(4)	1(4)
C(7)	25(4)	23(5)	37(7)	-1(4)	0(4)	4(4)
C(8)	27(5)	26(4)	37(7)	-3(4)	3(4)	10(4)
C(9)	23(3)	19(4)	40(5)	-4(3)	0(3)	-1(3)
C(10)	34(4)	22(4)	15(4)	5(3)	-1(3)	-11(4)
C(11)	21(3)	21(4)	30(5)	5(4)	4(3)	-1(3)
C(12)	21(4)	22(4)	29(5)	5(4)	1(4)	-2(3)
C(13)	44(4)	29(4)	37(6)	-1(4)	1(5)	4(4)
C(14)	68(6)	50(5)	47(7)	-31(5)	25(5)	-31(4)
C(15)	41(5)	36(4)	35(6)	-13(4)	3(4)	7(4)
C(16)	39(4)	42(4)	33(6)	-2(4)	-3(4)	4(4)
C(17)	29(4)	16(3)	21(5)	-5(3)	0(4)	5(3)
C(18)	27(4)	49(4)	27(5)	14(3)	-1(3)	2(4)
C(19)	42(5)	27(4)	42(6)	1(4)	-14(4)	-12(4)
C(20)	93(5)	44(4)	58(6)	20(4)	15(4)	31(5)
N(1)	28(3)	20(3)	22(4)	0(3)	-4(3)	-4(3)
N(2)	23(3)	18(3)	37(4)	4(2)	-3(3)	8(3)
N(3)	21(3)	46(3)	26(4)	16(3)	-5(3)	-1(3)
O(1)	51(3)	41(3)	39(4)	-2(2)	-14(2)	-3(2)
O(2)	55(3)	42(3)	37(4)	5(3)	-11(3)	-9(2)
O(3)	15(2)	27(2)	50(3)	0(2)	1(2)	-2(2)
O(4)	12(2)	35(2)	37(3)	6(2)	2(2)	1(2)
O(5)	59(3)	39(3)	57(4)	12(2)	27(3)	12(2)
O(6)	49(3)	45(3)	44(4)	22(3)	6(3)	1(3)
N(4)	74(4)	67(4)	48(6)	-1(4)	2(4)	-18(4)

Table B.5 Hydrogen coordinates (x 10^4) and isotropic displacement parameters ($Å^2$x 10^3) for Compound **3** of Chapter 3.

	x	y	z	U(eq)
H(3)	8610	7706	1805	50
H(4)	10592	8881	1307	58
H(5)	9191	8963	557	59
H(6)	5799	7846	276	47
H(9A)	-598	5048	1067	33
H(9B)	209	5022	1594	33
H(11)	4347	2288	1266	29
H(13)	-1168	2468	444	44
H(14)	1537	231	-314	66
H(15)	4594	-257	236	45
H(16)	4912	641	895	46
H(18A)	-750	326	2136	41
H(18B)	1153	908	2498	41
H(20A)	3903	-2248	2445	97
H(20B)	3340	-2112	2976	97
H(20C)	5935	-1557	2742	97
H(2N)	-718	3285	1179	55
H(3N)	3765	1242	1844	55

Table B.6 Torsion angles [°] for Compound **3** of Chapter 3.

O(2)-C(1)-C(2)-C(3)	0.0(9)
N(1)-C(1)-C(2)-C(3)	179.6(5)
O(2)-C(1)-C(2)-C(7)	-178.5(6)
N(1)-C(1)-C(2)-C(7)	1.1(5)
C(7)-C(2)-C(3)-C(4)	-0.2(7)
C(1)-C(2)-C(3)-C(4)	-178.6(5)
C(2)-C(3)-C(4)-C(5)	1.0(8)
C(3)-C(4)-C(5)-C(6)	-0.6(8)
C(4)-C(5)-C(6)-C(7)	-0.5(8)
C(5)-C(6)-C(7)-C(2)	1.2(7)
C(5)-C(6)-C(7)-C(8)	178.8(5)
C(3)-C(2)-C(7)-C(6)	-0.9(8)
C(1)-C(2)-C(7)-C(6)	177.7(4)
C(3)-C(2)-C(7)-C(8)	-179.0(4)
C(1)-C(2)-C(7)-C(8)	-0.3(5)
C(6)-C(7)-C(8)-O(1)	1.9(9)
C(2)-C(7)-C(8)-O(1)	179.7(6)
C(6)-C(7)-C(8)-N(1)	-178.5(5)
C(2)-C(7)-C(8)-N(1)	-0.6(5)
N(1)-C(9)-C(10)-O(3)	14.5(7)
N(1)-C(9)-C(10)-N(2)	-168.5(5)
N(2)-C(11)-C(12)-C(13)	-18.2(7)
C(17)-C(11)-C(12)-C(13)	102.8(6)
N(2)-C(11)-C(12)-C(16)	161.4(4)
C(17)-C(11)-C(12)-C(16)	-77.6(6)
C(16)-C(12)-C(13)-N(4)	0.3(8)
C(11)-C(12)-C(13)-N(4)	180.0(5)
N(4)-C(14)-C(15)-C(16)	-1.4(9)
C(14)-C(15)-C(16)-C(12)	1.2(9)
C(13)-C(12)-C(16)-C(15)	-0.7(8)
C(11)-C(12)-C(16)-C(15)	179.6(5)
N(2)-C(11)-C(17)-O(4)	53.0(6)
C(12)-C(11)-C(17)-O(4)	-72.9(6)
N(2)-C(11)-C(17)-N(3)	-127.5(5)

C(12)-C(11)-C(17)-N(3)	106.7(6)
N(3)-C(18)-C(19)-O(5)	-1.5(8)
N(3)-C(18)-C(19)-O(6)	175.4(4)
O(2)-C(1)-N(1)-C(8)	178.1(5)
C(2)-C(1)-N(1)-C(8)	-1.6(5)
O(2)-C(1)-N(1)-C(9)	-4.5(8)
C(2)-C(1)-N(1)-C(9)	175.8(4)
O(1)-C(8)-N(1)-C(1)	-178.9(5)
C(7)-C(8)-N(1)-C(1)	1.4(5)
O(1)-C(8)-N(1)-C(9)	3.7(8)
C(7)-C(8)-N(1)-C(9)	-176.0(4)
C(10)-C(9)-N(1)-C(1)	-86.4(6)
C(10)-C(9)-N(1)-C(8)	90.7(5)
O(3)-C(10)-N(2)-C(11)	6.6(8)
C(9)-C(10)-N(2)-C(11)	-170.4(5)
C(12)-C(11)-N(2)-C(10)	-111.0(5)
C(17)-C(11)-N(2)-C(10)	127.4(5)
O(4)-C(17)-N(3)-C(18)	2.7(9)
C(11)-C(17)-N(3)-C(18)	-176.8(4)
C(19)-C(18)-N(3)-C(17)	139.1(5)
O(5)-C(19)-O(6)-C(20)	1.1(8)
C(18)-C(19)-O(6)-C(20)	-175.8(4)
C(12)-C(13)-N(4)-C(14)	-0.4(8)
C(15)-C(14)-N(4)-C(13)	0.9(8)

Symmetry transformations used to generate equivalent atoms:

Table B.7 Hydrogen bonds for Compound **3** of Chapter 3 [Å and °].

D-H...A	d(D-H)	d(H...A)	d(D...A)	<(DHA)
N(2)-H(2N)...O(3)#1	0.78	2.19	2.937(5)	159.1
N(3)-H(3N)...O(4)#2	0.72	2.24	2.919(5)	159.2

Symmetry transformations used to generate equivalent atoms:
#1 x-1,y,z #2 x+1,y,z

APPENDIX C

X-ray Structural Data for Compound **4** of Chapter 3

Table C.1 Crystal data and structure refinement for Compound **4** of Chapter 3.

Identification code	WG3pyrAla	
Empirical formula	C21 H20 N4 O6	
Formula weight	424.41	
Temperature	123(2) K	
Wavelength	1.54178 Å	
Crystal system	Orthorhombic	
Space group	P2(1)2(1)2(1)	
Unit cell dimensions	a = 4.7892(2) Å	α= 90°.
	b = 13.5763(4) Å	β= 90°.
	c = 30.7597(10) Å	γ = 90°.
Volume	1999.98(12) $Å^3$	
Z	4	
Density (calculated)	1.410 Mg/m^3	
Absorption coefficient	0.883 mm^{-1}	
F(000)	888	
Crystal size	0.48 x 0.09 x 0.04 mm^3	
Theta range for data collection	8.65 to 51.59°.	
Index ranges	-4<=h<=4, -13<=k<=12, -31<=l<=31	
Reflections collected	7779	
Independent reflections	2153 [R(int) = 0.0299]	
Completeness to theta = 51.59°	98.9 %	
Absorption correction	Semi-empirical from equivalents	
Max. and min. transmission	0.9655 and 0.6765	
Refinement method	Full-matrix least-squares on F^2	
Data / restraints / parameters	2153 / 0 / 285	
Goodness-of-fit on F^2	1.092	
Final R indices [I>2sigma(I)]	R1 = 0.0282, wR2 = 0.0654	
R indices (all data)	R1 = 0.0323, wR2 = 0.0675	
Absolute structure parameter	0.0(2)	
Largest diff. peak and hole	0.152 and -0.165 $e.Å^{-3}$	

Table C.2 Atomic coordinates (x 10^4) and equivalent isotropic displacement parameters ($Å^2$x 10^3) for Compound **4** of Chapter 3. U(eq) is defined as one third of the trace of the orthogonalized U^{ij} tensor.

	x	y	z	U(eq)
C(1)	7063(5)	-2522(2)	1549(1)	21(1)
C(2)	5348(5)	-3070(2)	1230(1)	22(1)
C(3)	3377(5)	-3801(2)	1293(1)	28(1)
C(4)	2110(5)	-4186(2)	927(1)	33(1)
C(5)	2787(6)	-3857(2)	515(1)	35(1)
C(6)	4756(5)	-3116(2)	453(1)	31(1)
C(7)	5984(5)	-2728(2)	817(1)	23(1)
C(8)	8086(5)	-1932(2)	863(1)	26(1)
C(9)	10507(5)	-1130(2)	1488(1)	23(1)
C(10)	9081(6)	-127(2)	1505(1)	21(1)
C(11)	9866(5)	1660(2)	1558(1)	21(1)
C(12)	10776(6)	2118(2)	1990(1)	26(1)
C(13)	9512(5)	3121(2)	2072(1)	22(1)
C(14)	10441(6)	3960(2)	1858(1)	30(1)
C(15)	7341(6)	4955(2)	2204(1)	30(1)
C(16)	6269(6)	4176(2)	2438(1)	29(1)
C(17)	7384(5)	3246(2)	2370(1)	26(1)
C(18)	11211(6)	2185(2)	1176(1)	22(1)
C(19)	10666(6)	3018(2)	488(1)	43(1)
C(20)	8800(6)	3757(2)	284(1)	26(1)
C(21)	8158(7)	4722(2)	-348(1)	43(1)
N(1)	8688(4)	-1869(1)	1305(1)	21(1)
N(2)	10810(4)	634(1)	1533(1)	22(1)
N(3)	9413(5)	4863(2)	1917(1)	33(1)
N(4)	9517(4)	2580(1)	880(1)	27(1)
O(1)	7150(4)	-2582(1)	1942(1)	30(1)
O(2)	9132(4)	-1404(1)	589(1)	36(1)
O(3)	6515(4)	-63(1)	1499(1)	32(1)
O(4)	13774(4)	2221(1)	1143(1)	29(1)
O(5)	6733(4)	4082(2)	443(1)	47(1)

Table C.2 (continued)

O(6)	9799(4)	4010(1)	-106(1)	37(1)

Table C.3 Bond lengths [Å] and angles [°] for Compound **4** of Chapter 3.

C(1)-O(1)	1.211(3)	C(13)-C(17)	1.382(3)
C(1)-N(1)	1.400(3)	C(13)-C(14)	1.388(3)
C(1)-C(2)	1.481(3)	C(14)-N(3)	1.334(3)
C(2)-C(3)	1.382(3)	C(14)-H(14)	0.9500
C(2)-C(7)	1.386(3)	C(15)-N(3)	1.335(3)
C(3)-C(4)	1.381(4)	C(15)-C(16)	1.378(4)
C(3)-H(3)	0.9500	C(15)-H(15)	0.9500
C(4)-C(5)	1.383(3)	C(16)-C(17)	1.387(4)
C(4)-H(4)	0.9500	C(16)-H(16)	1.01(3)
C(5)-C(6)	1.392(4)	C(17)-H(17)	0.9500
C(5)-H(5)	0.9500	C(18)-O(4)	1.232(3)
C(6)-C(7)	1.371(3)	C(18)-N(4)	1.333(3)
C(6)-H(6)	0.9500	C(19)-N(4)	1.450(3)
C(7)-C(8)	1.484(3)	C(19)-C(20)	1.483(4)
C(8)-O(2)	1.216(3)	C(19)-H(19A)	0.9900
C(8)-N(1)	1.392(3)	C(19)-H(19B)	0.9900
C(9)-N(1)	1.443(3)	C(20)-O(5)	1.188(3)
C(9)-C(10)	1.524(3)	C(20)-O(6)	1.335(3)
C(9)-H(9A)	0.9900	C(21)-O(6)	1.452(3)
C(9)-H(9B)	0.9900	C(21)-H(21A)	0.9800
C(10)-O(3)	1.232(3)	C(21)-H(21B)	0.9800
C(10)-N(2)	1.327(3)	C(21)-H(21C)	0.9800
C(11)-N(2)	1.466(3)	N(2)-H(2N)	0.7721
C(11)-C(18)	1.517(3)	N(4)-H(4N)	0.8720
C(11)-C(12)	1.532(3)		
C(11)-H(11)	1.0000	O(1)-C(1)-N(1)	124.0(2)
C(12)-C(13)	1.512(3)	O(1)-C(1)-C(2)	130.3(2)
C(12)-H(12A)	0.9900	N(1)-C(1)-C(2)	105.71(19)
C(12)-H(12B)	0.9900	C(3)-C(2)-C(7)	121.2(2)

Table C.3 (continued)

C(3)-C(2)-C(1)	130.3(2)	C(13)-C(12)-C(11)	113.39(19)
C(7)-C(2)-C(1)	108.5(2)	C(13)-C(12)-H(12A)	108.9
C(4)-C(3)-C(2)	117.2(2)	C(11)-C(12)-H(12A)	108.9
C(4)-C(3)-H(3)	121.4	C(13)-C(12)-H(12B)	108.9
C(2)-C(3)-H(3)	121.4	C(11)-C(12)-H(12B)	108.9
C(3)-C(4)-C(5)	121.5(2)	H(12A)-C(12)-H(12B)	107.7
C(3)-C(4)-H(4)	119.3	C(17)-C(13)-C(14)	116.8(2)
C(5)-C(4)-H(4)	119.3	C(17)-C(13)-C(12)	121.1(2)
C(4)-C(5)-C(6)	121.1(2)	C(14)-C(13)-C(12)	122.1(2)
C(4)-C(5)-H(5)	119.4	N(3)-C(14)-C(13)	124.9(2)
C(6)-C(5)-H(5)	119.4	N(3)-C(14)-H(14)	117.5
C(7)-C(6)-C(5)	117.2(2)	C(13)-C(14)-H(14)	117.5
C(7)-C(6)-H(6)	121.4	N(3)-C(15)-C(16)	123.5(3)
C(5)-C(6)-H(6)	121.4	N(3)-C(15)-H(15)	118.3
C(6)-C(7)-C(2)	121.7(2)	C(16)-C(15)-H(15)	118.3
C(6)-C(7)-C(8)	130.5(2)	C(15)-C(16)-C(17)	118.4(3)
C(2)-C(7)-C(8)	107.8(2)	C(15)-C(16)-H(16)	121.4(15)
O(2)-C(8)-N(1)	123.8(2)	C(17)-C(16)-H(16)	120.1(15)
O(2)-C(8)-C(7)	130.0(2)	C(13)-C(17)-C(16)	119.7(2)
N(1)-C(8)-C(7)	106.2(2)	C(13)-C(17)-H(17)	120.1
N(1)-C(9)-C(10)	111.31(18)	C(16)-C(17)-H(17)	120.1
N(1)-C(9)-H(9A)	109.4	O(4)-C(18)-N(4)	122.3(2)
C(10)-C(9)-H(9A)	109.4	O(4)-C(18)-C(11)	120.3(2)
N(1)-C(9)-H(9B)	109.4	N(4)-C(18)-C(11)	117.4(2)
C(10)-C(9)-H(9B)	109.4	N(4)-C(19)-C(20)	113.6(2)
H(9A)-C(9)-H(9B)	108.0	N(4)-C(19)-H(19A)	108.8
O(3)-C(10)-N(2)	124.6(2)	C(20)-C(19)-H(19A)	108.8
O(3)-C(10)-C(9)	120.6(2)	N(4)-C(19)-H(19B)	108.8
N(2)-C(10)-C(9)	114.7(2)	C(20)-C(19)-H(19B)	108.8
N(2)-C(11)-C(18)	106.04(18)	H(19A)-C(19)-H(19B)	107.7
N(2)-C(11)-C(12)	110.01(18)	O(5)-C(20)-O(6)	124.8(2)
C(18)-C(11)-C(12)	111.11(19)	O(5)-C(20)-C(19)	125.4(2)
N(2)-C(11)-H(11)	109.9	O(6)-C(20)-C(19)	109.8(2)
C(18)-C(11)-H(11)	109.9	O(6)-C(21)-H(21A)	109.5
C(12)-C(11)-H(11)	109.9	O(6)-C(21)-H(21B)	109.5

Table C.3 (continued)

H(21A)-C(21)-H(21B)	109.5
O(6)-C(21)-H(21C)	109.5
H(21A)-C(21)-H(21C)	109.5
H(21B)-C(21)-H(21C)	109.5
C(8)-N(1)-C(1)	111.73(19)
C(8)-N(1)-C(9)	123.31(19)
C(1)-N(1)-C(9)	124.51(18)
C(10)-N(2)-C(11)	123.39(19)
C(10)-N(2)-H(2N)	119.6
C(11)-N(2)-H(2N)	116.8
C(14)-N(3)-C(15)	116.7(2)
C(18)-N(4)-C(19)	120.1(2)
C(18)-N(4)-H(4N)	120.2
C(19)-N(4)-H(4N)	119.6
C(20)-O(6)-C(21)	116.0(2)

Symmetry transformations used to generate equivalent atoms:

Table C.4 Anisotropic displacement parameters ($Å^2 x\ 10^3$) for Compound **4** of Chapter 3. The anisotropic displacement factor exponent takes the form: $-2\pi^2[\ h^2\ a^{*2}U^{11} + ... + 2\ h\ k\ a^*\ b^*\ U^{12}\ ]$

	U^{11}	U^{22}	U^{33}	U^{23}	U^{13}	U^{12}
C(1)	22(1)	20(1)	22(2)	1(1)	5(1)	6(1)
C(2)	18(2)	22(1)	25(2)	-3(1)	0(1)	0(1)
C(3)	25(2)	25(2)	34(2)	2(1)	2(1)	1(1)
C(4)	27(2)	23(1)	49(2)	-5(2)	-5(2)	-7(1)
C(5)	34(2)	32(2)	38(2)	-9(1)	-10(1)	-3(2)
C(6)	33(2)	32(2)	29(2)	-3(1)	-1(1)	2(2)
C(7)	24(1)	20(1)	26(2)	-1(1)	2(1)	0(1)
C(8)	26(2)	27(2)	26(2)	0(1)	1(1)	5(1)
C(9)	18(1)	23(1)	28(2)	-1(1)	-2(1)	1(1)
C(10)	19(2)	26(2)	20(1)	0(1)	-1(1)	0(2)
C(11)	16(1)	19(1)	27(1)	0(1)	-2(1)	1(1)
C(12)	26(2)	26(2)	25(1)	4(1)	-2(1)	1(1)
C(13)	21(2)	23(2)	22(1)	1(1)	-4(1)	-3(1)
C(14)	28(2)	30(2)	32(2)	-4(1)	4(1)	-3(2)
C(15)	33(2)	27(2)	30(2)	-4(1)	-7(1)	6(2)
C(16)	28(2)	33(2)	25(2)	-3(1)	0(1)	3(2)
C(17)	28(2)	28(2)	22(1)	2(1)	-4(1)	-8(1)
C(18)	19(2)	21(1)	25(2)	-2(1)	-2(1)	1(1)
C(19)	32(2)	59(2)	37(2)	21(2)	10(1)	13(2)
C(20)	21(2)	23(2)	33(2)	2(1)	-5(1)	-6(1)
C(21)	55(2)	37(2)	37(2)	12(1)	-15(2)	-5(2)
N(1)	22(1)	21(1)	19(1)	-1(1)	0(1)	-4(1)
N(2)	13(1)	22(1)	31(1)	0(1)	0(1)	-1(1)
N(3)	34(1)	25(1)	40(1)	0(1)	2(1)	0(1)
N(4)	15(1)	38(1)	28(1)	9(1)	2(1)	4(1)
O(1)	36(1)	30(1)	23(1)	1(1)	1(1)	-3(1)
O(2)	42(1)	36(1)	28(1)	3(1)	4(1)	-6(1)
O(3)	17(1)	25(1)	53(1)	1(1)	0(1)	-1(1)
O(4)	15(1)	36(1)	37(1)	11(1)	0(1)	1(1)
O(5)	36(1)	48(1)	58(1)	21(1)	11(1)	15(1)

Table C.4 (continued)

O(6)	42(1)	41(1)	26(1)	10(1)	-2(1)	8(1)

Table C.5 Hydrogen coordinates (x 10^4) and isotropic displacement parameters ($Å^2$x 10^3)
for Compound **4** of Chapter 3.

	x	y	z	U(eq)
H(3)	2914	-4028	1576	33
H(4)	743	-4687	960	40
H(5)	1893	-4142	269	42
H(6)	5228	-2888	170	37
H(9A)	12224	-1082	1310	28
H(9B)	11055	-1329	1786	28
H(11)	7787	1688	1530	25
H(12A)	10236	1671	2230	31
H(12B)	12836	2178	1993	31
H(14)	11921	3885	1655	36
H(15)	6564	5590	2250	36
H(17)	6687	2697	2528	31
H(19A)	11054	2489	275	51
H(19B)	12464	3338	561	51
H(21A)	6307	4447	-409	65
H(21B)	9102	4875	-622	65
H(21C)	7957	5326	-176	65
H(16)	4650(60)	4266(18)	2643(8)	38(8)
H(2N)	12401	548	1519	26
H(4N)	7711	2538	911	33

Table C.6 Torsion angles [°] for Compound **4** of Chapter 3.

O(1)-C(1)-C(2)-C(3)	-0.1(4)
N(1)-C(1)-C(2)-C(3)	-179.8(2)
O(1)-C(1)-C(2)-C(7)	179.4(2)
N(1)-C(1)-C(2)-C(7)	-0.4(2)
C(7)-C(2)-C(3)-C(4)	1.1(3)
C(1)-C(2)-C(3)-C(4)	-179.5(2)
C(2)-C(3)-C(4)-C(5)	0.2(3)
C(3)-C(4)-C(5)-C(6)	-0.7(4)
C(4)-C(5)-C(6)-C(7)	-0.1(4)
C(5)-C(6)-C(7)-C(2)	1.4(4)
C(5)-C(6)-C(7)-C(8)	-178.8(2)
C(3)-C(2)-C(7)-C(6)	-1.9(4)
C(1)-C(2)-C(7)-C(6)	178.6(2)
C(3)-C(2)-C(7)-C(8)	178.2(2)
C(1)-C(2)-C(7)-C(8)	-1.3(3)
C(6)-C(7)-C(8)-O(2)	3.6(4)
C(2)-C(7)-C(8)-O(2)	-176.6(2)
C(6)-C(7)-C(8)-N(1)	-177.4(3)
C(2)-C(7)-C(8)-N(1)	2.5(2)
N(1)-C(9)-C(10)-O(3)	21.9(3)
N(1)-C(9)-C(10)-N(2)	-159.31(19)
N(2)-C(11)-C(12)-C(13)	-171.10(19)
C(18)-C(11)-C(12)-C(13)	71.8(3)
C(11)-C(12)-C(13)-C(17)	105.6(3)
C(11)-C(12)-C(13)-C(14)	-75.3(3)
C(17)-C(13)-C(14)-N(3)	-0.8(4)
C(12)-C(13)-C(14)-N(3)	-180.0(2)
N(3)-C(15)-C(16)-C(17)	-0.5(4)
C(14)-C(13)-C(17)-C(16)	0.8(3)
C(12)-C(13)-C(17)-C(16)	180.0(2)
C(15)-C(16)-C(17)-C(13)	-0.2(4)
N(2)-C(11)-C(18)-O(4)	-60.1(3)
C(12)-C(11)-C(18)-O(4)	59.4(3)
N(2)-C(11)-C(18)-N(4)	118.5(2)

Table C.6 (continued)

C(12)-C(11)-C(18)-N(4)	-121.9(2)
N(4)-C(19)-C(20)-O(5)	10.0(4)
N(4)-C(19)-C(20)-O(6)	-170.4(2)
O(2)-C(8)-N(1)-C(1)	176.3(2)
C(7)-C(8)-N(1)-C(1)	-2.8(2)
O(2)-C(8)-N(1)-C(9)	3.7(3)
C(7)-C(8)-N(1)-C(9)	-175.47(19)
O(1)-C(1)-N(1)-C(8)	-177.7(2)
C(2)-C(1)-N(1)-C(8)	2.0(2)
O(1)-C(1)-N(1)-C(9)	-5.2(3)
C(2)-C(1)-N(1)-C(9)	174.58(19)
C(10)-C(9)-N(1)-C(8)	74.7(3)
C(10)-C(9)-N(1)-C(1)	-97.0(2)
O(3)-C(10)-N(2)-C(11)	-0.6(4)
C(9)-C(10)-N(2)-C(11)	-179.35(19)
C(18)-C(11)-N(2)-C(10)	-122.2(2)
C(12)-C(11)-N(2)-C(10)	117.5(2)
C(13)-C(14)-N(3)-C(15)	0.2(4)
C(16)-C(15)-N(3)-C(14)	0.5(4)
O(4)-C(18)-N(4)-C(19)	3.9(4)
C(11)-C(18)-N(4)-C(19)	-174.7(2)
C(20)-C(19)-N(4)-C(18)	-156.6(2)
O(5)-C(20)-O(6)-C(21)	-1.2(3)
C(19)-C(20)-O(6)-C(21)	179.2(2)

Symmetry transformations used to generate equivalent atoms:

Table C.7 Hydrogen bonds for Compound 4 of Chapter 3 [Å and °].

D-H...A	d(D-H)	d(H...A)	d(D...A)	<(DHA)
N(2)-H(2N)...O(3)#1	0.77	2.14	2.893(3)	165.8
N(4)-H(4N)...O(4)#2	0.87	2.06	2.909(3)	163.4

Symmetry transformations used to generate equivalent atoms:
#1 x+1,y,z #2 x-1,y,z

APPENDIX D

X-ray Structural Data for Compound **5** of Chapter 3

Table D.1 Crystal data and structure refinement for Compound **5** of Chapter 3.

Identification code	WG_PdS	
Empirical formula	C21 H19 Cl O Pd S2	
Formula weight	493.33	
Temperature	173(2) K	
Wavelength	0.71073 Å	
Crystal system	Monoclinic	
Space group	P2(1)/c	
Unit cell dimensions	a = 9.335(4) Å	α= 90°.
	b = 11.521(5) Å	β= 99.614(6)°.
	c = 17.934(8) Å	γ = 90°.
Volume	1901.6(14) $Å^3$	
Z	4	
Density (calculated)	1.723 Mg/m^3	
Absorption coefficient	1.344 mm^{-1}	
F(000)	992	
Crystal size	0.49 x 0.15 x 0.14 mm^3	
Theta range for data collection	2.11 to 28.41°.	
Index ranges	-12<=h<=11, -15<=k<=15, -15<=l<=23	
Reflections collected	12239	
Independent reflections	4692 [R(int) = 0.0318]	
Completeness to theta = 28.41°	98.1 %	
Absorption correction	Semi-empirical from equivalents	
Max. and min. transmission	0.8342 and 0.5589	
Refinement method	Full-matrix least-squares on F^2	
Data / restraints / parameters	4692 / 0 / 236	
Goodness-of-fit on F^2	1.084	
Final R indices [I>2sigma(I)]	R1 = 0.0319, wR2 = 0.0754	
R indices (all data)	R1 = 0.0380, wR2 = 0.0784	
Largest diff. peak and hole	0.797 and -0.537 $e.Å^{-3}$	

Table D.2 Atomic coordinates (x 10^4) and equivalent isotropic displacement parameters ($Å^2$x 10^3)
for Compound **5** of Chapter 3. U(eq) is defined as one third of the trace of the orthogonalized U^{ij} tensor.

	x	y	z	U(eq)
C(1)	3457(3)	2516(2)	11399(1)	20(1)
C(2)	3729(3)	1790(2)	12022(2)	24(1)
C(3)	4974(3)	1958(2)	12555(2)	30(1)
C(4)	5928(3)	2844(3)	12466(2)	32(1)
C(5)	5649(3)	3567(2)	11838(2)	31(1)
C(6)	4423(3)	3403(2)	11301(2)	26(1)
C(7)	975(3)	1103(2)	10911(1)	21(1)
C(8)	1663(3)	79(2)	10595(1)	19(1)
C(9)	1493(3)	-1033(2)	10864(1)	21(1)
C(10)	2083(3)	-1987(2)	10534(2)	23(1)
C(11)	2841(3)	-1819(2)	9938(2)	22(1)
C(12)	3002(2)	-700(2)	9670(1)	19(1)
C(13)	2428(3)	266(2)	9997(1)	18(1)
C(14)	3870(3)	-502(2)	9052(1)	22(1)
C(15)	1980(3)	832(2)	7961(1)	20(1)
C(16)	1106(3)	1806(2)	7822(2)	24(1)
C(17)	-103(3)	1772(2)	7259(2)	28(1)
C(18)	-447(3)	772(2)	6840(2)	30(1)
C(19)	434(3)	-188(2)	6973(2)	32(1)
C(20)	1664(3)	-160(2)	7528(2)	30(1)
C(21)	2325(4)	-4040(2)	10478(2)	44(1)
Cl(1)	3209(1)	3796(1)	9236(1)	31(1)
O(1)	1866(2)	-3039(1)	10848(1)	31(1)
Pd(1)	2762(1)	1861(1)	9645(1)	18(1)
S(1)	1855(1)	2445(1)	10702(1)	20(1)
S(2)	3591(1)	951(1)	8654(1)	21(1)

Table D.3 Bond lengths [Å] and angles [°] for Compound **5** of Chapter 3.

C(1)-C(2)	1.386(4)	C(16)-H(16)	0.9500
C(1)-C(6)	1.393(3)	C(17)-C(18)	1.384(4)
C(1)-S(1)	1.783(3)	C(17)-H(17)	0.9500
C(2)-C(3)	1.389(4)	C(18)-C(19)	1.375(4)
C(2)-H(2)	0.9500	C(18)-H(18)	0.9500
C(3)-C(4)	1.381(4)	C(19)-C(20)	1.389(4)
C(3)-H(3)	0.9500	C(19)-H(19)	0.9500
C(4)-C(5)	1.390(4)	C(20)-H(20)	0.9500
C(4)-H(4)	0.9500	C(21)-O(1)	1.431(3)
C(5)-C(6)	1.379(4)	C(21)-H(21A)	0.9800
C(5)-H(5)	0.9500	C(21)-H(21B)	0.9800
C(6)-H(6)	0.9500	C(21)-H(21C)	0.9800
C(7)-C(8)	1.498(3)	Cl(1)-Pd(1)	2.4040(11)
C(7)-S(1)	1.820(2)	Pd(1)-S(1)	2.3016(10)
C(7)-H(7A)	0.9900	Pd(1)-S(2)	2.3063(9)
C(7)-H(7B)	0.9900		
C(8)-C(9)	1.387(3)	C(2)-C(1)-C(6)	120.6(2)
C(8)-C(13)	1.401(4)	C(2)-C(1)-S(1)	123.9(2)
C(9)-C(10)	1.403(3)	C(6)-C(1)-S(1)	115.47(19)
C(9)-H(9)	0.9500	C(1)-C(2)-C(3)	119.3(2)
C(10)-O(1)	1.366(3)	C(1)-C(2)-H(2)	120.3
C(10)-C(11)	1.391(4)	C(3)-C(2)-H(2)	120.3
C(11)-C(12)	1.393(3)	C(4)-C(3)-C(2)	120.4(3)
C(11)-H(11)	0.9500	C(4)-C(3)-H(3)	119.8
C(12)-C(13)	1.405(3)	C(2)-C(3)-H(3)	119.8
C(12)-C(14)	1.495(3)	C(3)-C(4)-C(5)	119.9(3)
C(13)-Pd(1)	1.985(2)	C(3)-C(4)-H(4)	120.0
C(14)-S(2)	1.821(2)	C(5)-C(4)-H(4)	120.0
C(14)-H(14A)	0.9900	C(6)-C(5)-C(4)	120.3(3)
C(14)-H(14B)	0.9900	C(6)-C(5)-H(5)	119.8
C(15)-C(20)	1.384(3)	C(4)-C(5)-H(5)	119.8
C(15)-C(16)	1.386(3)	C(5)-C(6)-C(1)	119.5(3)
C(15)-S(2)	1.789(3)	C(5)-C(6)-H(6)	120.3
C(16)-C(17)	1.384(4)	C(1)-C(6)-H(6)	120.3

Table D.3 (continued)

C(8)-C(7)-S(1)	110.77(17)	C(15)-C(16)-H(16)	120.3
C(8)-C(7)-H(7A)	109.5	C(16)-C(17)-C(18)	120.5(2)
S(1)-C(7)-H(7A)	109.5	C(16)-C(17)-H(17)	119.8
C(8)-C(7)-H(7B)	109.5	C(18)-C(17)-H(17)	119.8
S(1)-C(7)-H(7B)	109.5	C(19)-C(18)-C(17)	119.8(3)
H(7A)-C(7)-H(7B)	108.1	C(19)-C(18)-H(18)	120.1
C(9)-C(8)-C(13)	120.7(2)	C(17)-C(18)-H(18)	120.1
C(9)-C(8)-C(7)	121.0(2)	C(18)-C(19)-C(20)	120.3(2)
C(13)-C(8)-C(7)	118.3(2)	C(18)-C(19)-H(19)	119.9
C(8)-C(9)-C(10)	120.1(2)	C(20)-C(19)-H(19)	119.9
C(8)-C(9)-H(9)	120.0	C(15)-C(20)-C(19)	119.7(2)
C(10)-C(9)-H(9)	120.0	C(15)-C(20)-H(20)	120.2
O(1)-C(10)-C(11)	124.7(2)	C(19)-C(20)-H(20)	120.2
O(1)-C(10)-C(9)	115.3(2)	O(1)-C(21)-H(21A)	109.5
C(11)-C(10)-C(9)	120.0(2)	O(1)-C(21)-H(21B)	109.5
C(10)-C(11)-C(12)	119.5(2)	H(21A)-C(21)-H(21B)	109.5
C(10)-C(11)-H(11)	120.3	O(1)-C(21)-H(21C)	109.5
C(12)-C(11)-H(11)	120.3	H(21A)-C(21)-H(21C)	109.5
C(11)-C(12)-C(13)	121.2(2)	H(21B)-C(21)-H(21C)	109.5
C(11)-C(12)-C(14)	120.0(2)	C(10)-O(1)-C(21)	116.6(2)
C(13)-C(12)-C(14)	118.7(2)	C(13)-Pd(1)-S(1)	84.83(7)
C(8)-C(13)-C(12)	118.5(2)	C(13)-Pd(1)-S(2)	85.10(8)
C(8)-C(13)-Pd(1)	120.85(16)	S(1)-Pd(1)-S(2)	169.93(2)
C(12)-C(13)-Pd(1)	120.63(18)	C(13)-Pd(1)-Cl(1)	178.89(7)
C(12)-C(14)-S(2)	111.80(16)	S(1)-Pd(1)-Cl(1)	94.98(3)
C(12)-C(14)-H(14A)	109.3	S(2)-Pd(1)-Cl(1)	95.09(3)
S(2)-C(14)-H(14A)	109.3	C(1)-S(1)-C(7)	104.41(12)
C(12)-C(14)-H(14B)	109.3	C(1)-S(1)-Pd(1)	102.10(8)
S(2)-C(14)-H(14B)	109.3	C(7)-S(1)-Pd(1)	99.32(8)
H(14A)-C(14)-H(14B)	107.9	C(15)-S(2)-C(14)	104.51(12)
C(20)-C(15)-C(16)	120.2(2)	C(15)-S(2)-Pd(1)	102.64(9)
C(20)-C(15)-S(2)	121.90(19)	C(14)-S(2)-Pd(1)	99.19(8)
C(16)-C(15)-S(2)	117.65(19)		
C(17)-C(16)-C(15)	119.5(2)		
C(17)-C(16)-H(16)	120.3		

Table D.4 Anisotropic displacement parameters ($Å^2 x\ 10^3$) for Compound **5** of Chapter 3. The anisotropic displacement factor exponent takes the form: $-2\pi^2[\ h^2\ a^{*2}U^{11} + ...\ + 2\ h\ k\ a^*\ b^*\ U^{12}\ ]$

	U^{11}	U^{22}	U^{33}	U^{23}	U^{13}	U^{12}
C(1)	19(1)	22(1)	19(1)	-8(1)	3(1)	4(1)
C(2)	23(1)	31(1)	21(1)	-1(1)	9(1)	1(1)
C(3)	29(2)	43(2)	17(1)	-2(1)	5(1)	8(1)
C(4)	23(1)	45(2)	25(2)	-14(1)	-1(1)	3(1)
C(5)	28(2)	30(1)	36(2)	-9(1)	7(1)	-5(1)
C(6)	25(1)	23(1)	30(2)	-2(1)	5(1)	1(1)
C(7)	18(1)	23(1)	23(1)	-2(1)	6(1)	0(1)
C(8)	15(1)	23(1)	18(1)	-3(1)	1(1)	2(1)
C(9)	22(1)	27(1)	15(1)	1(1)	3(1)	1(1)
C(10)	29(1)	21(1)	20(1)	3(1)	3(1)	3(1)
C(11)	22(1)	22(1)	21(1)	-2(1)	2(1)	6(1)
C(12)	15(1)	24(1)	16(1)	-3(1)	2(1)	3(1)
C(13)	17(1)	19(1)	17(1)	0(1)	2(1)	2(1)
C(14)	22(1)	25(1)	19(1)	-1(1)	6(1)	5(1)
C(15)	23(1)	25(1)	14(1)	2(1)	8(1)	-1(1)
C(16)	28(1)	25(1)	21(1)	-1(1)	7(1)	0(1)
C(17)	27(2)	34(1)	25(2)	3(1)	5(1)	5(1)
C(18)	26(1)	42(2)	21(1)	1(1)	2(1)	-4(1)
C(19)	37(2)	31(1)	28(2)	-7(1)	3(1)	-6(1)
C(20)	30(2)	25(1)	34(2)	-5(1)	5(1)	2(1)
C(21)	72(2)	21(1)	45(2)	4(1)	23(2)	6(1)
Cl(1)	45(1)	21(1)	28(1)	1(1)	9(1)	-3(1)
O(1)	48(1)	20(1)	28(1)	3(1)	14(1)	2(1)
Pd(1)	19(1)	19(1)	17(1)	-1(1)	4(1)	0(1)
S(1)	20(1)	20(1)	20(1)	-2(1)	3(1)	4(1)
S(2)	21(1)	25(1)	20(1)	0(1)	7(1)	-3(1)

Table D.5 Hydrogen coordinates (x 10^4) and isotropic displacement parameters ($Å^2$x 10^3) for Compound **5** of Chapter 3.

	x	y	z	U(eq)
H(2)	3070	1183	12085	29
H(3)	5170	1462	12983	35
H(4)	6774	2959	12834	38
H(5)	6305	4177	11778	37
H(6)	4239	3891	10869	31
H(7A)	1055	1014	11465	25
H(7B)	-69	1135	10689	25
H(9)	977	-1148	11272	25
H(11)	3245	-2463	9715	26
H(14A)	3589	-1082	8647	26
H(14B)	4914	-612	9256	26
H(16)	1334	2492	8112	29
H(17)	-701	2440	7159	34
H(18)	-1290	748	6461	36
H(19)	201	-874	6683	39
H(20)	2284	-817	7611	36
H(21A)	1783	-4086	9962	66
H(21B)	2142	-4740	10758	66
H(21C)	3367	-3981	10461	66